iarigai
print and media research
www.iarigai.org

# Advances in Printing and Media Technology

**Vol. XLI**

*Edited by Nils Enlund and Mladen Lovreček*

Darmstadt
MMXIV

# Advances in Printing and Media Technology

Proceedings of the 41st International Research Conference of iarigai

Swansea, United Kingdom, September 2014

Published by the International Association
of Research Organizations for the Information,
Media and Graphic Arts Industries
Darmstadt, Germany, 2014

Co-edited by

Nils Enlund, Helsinki, Finland
Mladen Lovreček, Zagreb, Croatia





*Printed edition*
ISBN 978-3-9812704-6-4
ISSN 2225-6067

*Online edition*
ISBN 978-3-9870704-0-2
ISSN 2409-4021

Printed in Croatia by Narodne Novine d.d. Zagreb

# Contents

# A time of changes

*Nils Enlund*

Co-editor, Chairman of the iarigai Program and Publishing Committee
E-mail: nilse@kth.se

Things change. This volume of the series *Advances in Printing and Media Technology*, the 41st, is as you have already noticed, different than the earlier ones.

Instead of the familiar, hard-bound printed book, the Management Board of iarigai has decided to publish the proceedings of the 41st annual research conference, held in Swansea, Wales, on September 7-10, 2014, in digital form, available on the internet.

It may seem odd that the proceedings of a scientific conference that to a great extent is focused on printed media are not printed. But unfortunately, although printing in it self is not excessively expensive, distribution and mailing are. Digital publishing saves money for the publisher and thereby also for iarigai members and for all the other readers of the proceedings. In addition, nowadays most readers - researchers and professionals as well as libraries - prefer to access new research findings and technical information online. And if you wish to read the articles on paper, the pdfs can easily be printed locally.

The second major change is that the proceedings are divided into two sections. The first one (*Section A*) contains the full texts of presentations made at the Swansea conference. These presentations were selected by a committee of competent international experts through a double-blind review process based on evaluating extended abstracts. Exactly as in earlier years.

But increasingly, universities and research organizations require scientifically high-ranking contributions to be reviewed as full papers and to be published in established international journals. Therefore, authors of contributions to the research conference were this year given the option of asking for a full-paper review by members of the scientific committee of the peer-reviewed quarterly *Journal of Print and Media Technology Research*. Papers accepted will in due order be published in future issues of the journal. The abstracts of these papers are published in the second part (*Section B*) of these proceedings.

The third change is that this volume is the last one that I have had the pleasure of co-editing. At the end of the year, I am retiring from my position as chairman of the iarigai Program and Publishing Committee and thereby also relinquishing my responsibilities for the yearly conference program and for the proceedings. It is time for younger, eager individuals to take over. I would like to sincerely thank all contributors, readers, reviewers and colleagues, especially my tireless co-editor Mladen Lovreček, for an excellent cooperation over the past years. Thank you!

However, despite these actually very insignificant changes, exciting and inspiring research and innovations in the field of print and media technology continues and will be reported at iarigai conferences, in proceedings and in scientific journals. And this research will bring on further changes in the world of print and media. Editors are therefore convinced that future editions of the *Advances* will uphold their role as a prominent source of information and knowledge, in whatever form they will be published in the years to come.

October 2014

# A1

## *Printing science and technology*

# Halftones images: influence of juxtaposition/superposition of square pattern using digital printing techniques on color rendering

*Maëlle Morgant, Jean-Francis Bloch, Lionel Chagas*

Univ. Grenoble Alpes, LGP2
F-38000 Grenoble, France

CNRS, LGP2
F-38000 Grenoble, France

Agefpi, F-38000 Grenoble, France

E-mails: maelle.morgant@grenoble-inp.org; jean-francis.bloch@pagora.grenoble-inp.fr;
lionel.chagas@pagora.grenoble-inp.fr

**Abstract**

The industrial problem in printing is to set quickly the adjustment of the process for multichromy. Therefore models have to be developed to control efficiently factors affecting halftone colors. The aim of this study is to analyze the influence of juxtaposition/superposition of dots of inks, the pattern printing size, and the percentage of coverage on the colorimetric printing patches, in order to improve colorimetric models efficiency. For this purpose, squares are printed with electrophotographic technique. They are arranged in juxtaposition (one colored square beside the other) and in superposition (one color one top of the other). Primary colors are printed with different nominal percentages of coverage and different nominal sizes. They are printed individually in monochromy, they are then superposed or juxtaposed in the case of polychromy.

The models of Murray-Davies, Yule-Nielsen, and Clapper-Yule are considered. The effective percentages of coverage of each color (percentage of coverage calculated with models) are calculated by two methods (Demichel equations and dot-on-dot screen). The performances of the proposed spectral models are compared in terms of color differences. Models have to be selected according to the resolution of printer, the size of pattern, and the percentage of coverage. Moreover, the juxtaposition or superposition of primary colors influences differently the colorimetric coordinates, and the model efficiency. In the case of polychromy, the models efficiency is improved by the mixture Demichel - dot-on-dot method.

**Keywords** halftone printed, ink superposition, model prediction, electrophotographic technique

## 1. Introduction and background

Halftone images are produced by the juxtaposition or superposition of small colored dots of toner on paper, resulting in a clustered halftone dot. One type of halftone structure is the amplitude modulated (AM). Color modulations on paper are produced by varying the surface coverage of these colored dots and their positions. Different size patterns are used modifying the color rendering. Light beam can incur various interactions with the printed substrate such as reflection, refraction, absorption, and scattering. These effects depend on the nature of the superposed layers, the lighting and observation conditions (Hébert, Hersch, and Becker, 2007). The spatial distribution, the percentage of coverage, and the primary colors have to be considered regarding the colorimetric coordinates of halftone printing.

Models used to predict reflectance and/or transmittance of halftone color printing. The first type of models considers the superposition of layers with homogeneous thickness. The scattering model of Kubelka and Munk (1931) is widely used in paper making industry. It is a two diffuse fluxes approach. The reflection spectrum R(λ) of a printing patch is a function of isotropic scatterings of ink and paper (S(λ)) and their absorption (K(λ)), where λ represents the wavelength. The second type of models is dedicated to predict spectral reflectance of color halftone printing R_h (λ). The Murray-Davies model (1936) predicts the spectral reflectance of halftone color printed by considering the surface of coverage of a single ink:

$$\mathbf{R_h(\lambda) = p_j\, R_{100}(\lambda) + (1 - p_j) R_w(\lambda)} \quad [1]$$

Where $p_j$, $R_{100}(\lambda)$, and $R_w(\lambda)$ represent the surface coverage of the primary color, the reflectance of the full tone of the primary color (100% of percentage of coverage), and the reflectance of the substrate without printing, respectively.

An extension of this model (Neugebauer, 1937) introduced the percentage of coverage of $2^N$ colors, where N is the number of dyes. The predicted spectral reflectance of a patch is considered as a weighted average of the reflectances of the $2^N$ colors. Yule-Nielsen (1951) introduced the optical dot gain effect in the Neugebauer equation:

$$\mathbf{R_h(\lambda) = \left(\sum_{j=1}^{2^N} p_j (R_j(\lambda))^{1/n}\right)^n} \quad [2]$$

Where N; n; $p_j$ and $R_j(\lambda)$ represent the number of primary colors; an empirical parameter which depends on the printer, the substrate, and the period of the frame; the probability of dot surface coverage (assimilated to the percentage of coverage) for one primary color; and the spectral reflectance of full tones and paper, respectively.

The Clapper-Yule model (1953) takes into account surface-reflection, multiple-scattering, internal-reflection, and ink transmittance and may be written for one primary color as:

$$\mathbf{R_h(\lambda) = Kr_s + \left(\frac{r_g(\lambda)(1-r_s)(1-r_i)(1-p_j+p_j t_{100}(\lambda))^2}{1-r_g(\lambda)r_i(1-p_j+p_j t_{100}(\lambda)^2)}\right)} \quad [3]$$

Where K depends on the specular light reflected, $r_s$ and $r_i$ are the Fresnel coefficients of the external and internal reflections for a light with an incident angle of 45°, $r_g(\lambda)$ is the internal reflectance of the substrate, and $t_{100}(\lambda)$ is the factor of transmittance of the light across a solid ink.

These models allow to predict the colors of halftone printed and to determine the effective percentage of coverage. The dot areas of the primary colors are not necessarily linearly related to the digital values sent to the printer (called here nominal ink surface coverage). The effective surface coverage corresponds to light scattering within the paper. This phenomenon, call optical dot gain or Yule-Nielsen effect, increases the size of the dot during printing. It depends on two different factors: the properties of the materials and the geometrical distribution of ink such as location or size (Yang, Lenz and Kruse 2001). Dot gain consists of two contributions, optical and physical dot gains. Both dot gains increase the size of the halftone dot. Physical dot gain is due to the spreading of toner on the paper, depending on ink viscosity or absorption rates by paper. A microscopic images analysis allowed estimating the physical percentage of coverage for each color.

The arrangements of colored dots influence the color rendering in models. Two different alternatives are classically proposed. First, in the Demichel method (1924), the superposed dots localization on the paper is considered as statistically independent. Considering two primary colors (cyan and magenta for example), we obtain four surface coverages: cyan, magenta, blue and white (paper). Secondary, for the superposition cases, each halftone dot combines two dyes one on top of the other (Balasubramanian, 1999). Figure 1 shows an example of the Demichel (dot-off-dot) and the dot-on-dot screen dot localizations.

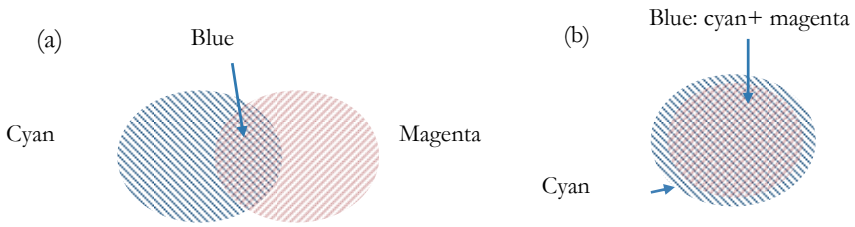


*Figure 1: Dot area coverage for: (a) Demichel method; (b) Dot-on-dot screen*

The Table 1 gives an example of calculation of ink dot coverage for the print of the primary colors cyan and magenta, for the dot-on-dot method.

*Table 1: Area coverage calculated with dot-on-dot method*

| Area coverage | c' ≤ m' | m' ≤ c' |
|---|---|---|
| $p_w$ | (1 - m') | (1 - c') |
| $p_c$ | 0 | (c' - m') |
| $p_m$ | (m' - c') | 0 |
| $p_b$ | c' | m' |

Where c' and m' are the effective surface coverages of cyan and magenta printed on top of a second primary color.

Considering that the prints are not perfect, a weighted mixture of the Demichel and the dot-on-dot methods leads to a modified reflectance model:

$$\mathbf{R_h(\lambda) = (1-\alpha)R_{YN-DOD}(\lambda) + \alpha R_{YN-DEM}(\lambda)} \quad [4]$$

Where $\alpha$, $R_{YN-DOD}(\lambda)$, and $R_{YN-DEM}(\lambda)$ represent the weighting parameter that determines the relative proportions of the two mixing methods, the spectral reflectance predicted by the model of Yule-Nielsen with the dot-on-dot approach, and the spectral reflectance predicted by the model of Yule-Nielsen with the Demichel approach, respectively. Contrary to various studies (Balasubramanian, 1999) or (Xi, 2012), we employed this demarche for both Yule-Nielsen and Clapper-Yule models. This expression is similar to the Murray-Davies model as it is a linear interpolation between spectral reflectances.

In our approach, the $\alpha$ weighting parameter of the mix-models and the effective surfaces of coverage are considered as parameters which are identified by minimizing the color differences. The weighting factor can be studied according to either the percentage of coverage or the size of the pattern.

As the aim of this paper is to predict colors, when particular patterns are printed using electrophotography, squares were printed in both juxtapositions and superpositions. We focus on the influence of two criteria: the size of the printed shape and the percentage of coverage. We considered both monochromic and polychromic configurations. The existing models of color predictions are compared in order to determine the influence of juxtaposition/superposition of inks on the colorimetric rendering. Colorimetric model quality is determined by the differences of color ($\Delta E^*_{ab}$). The limit of acceptability is fixed to $\Delta E^*_{ab}=3$.

## 2. Materials and method

Spectral reflectance predictions of printed patches were calculated with models previously presented, taking into account (i) the spectral reflectances measured of the paper, (ii) the full tone patches, and (iii) the effective percentage of coverage. Then, the difference between the measured color of samples and the predicted color, $\Delta E^*_{ab}$ was calculated fitting the effective surface of coverage, with the generalized reduced gradient method (GRG). This effective percentage of coverage found in monochromatic case was then considered for the polychromic printing calculations.

Electrophotographic printing was made with an Aficio MP C2800 from Ricoh, with a resolution of 600 dpi, on both uncoated and coated papers. Three primary colors were printed (cyan, magenta, and yellow). Test form contained monochromatic square shapes, for different nominal percentages of coverage (25, 50, 75, and 100 %). Nominal sizes of patterns were from 42 μm to 254 μm. In a first-hand, single primary color on the paper (monochromic case) is considered. In a second-hand polychromy is studied, with the juxtaposition and the superposition of inks. In the polychromic case, we considered that primary colors were printed successively on paper. The registration allows arranging the printing squares.

The spectrophotometer Techkon has a geometric measurement of 45/0° (with the detector at 0°). The spectral reflectance factors $R(\lambda)$ were measured from 400 to 700 nm, with a step of 10 nm. The standard illuminant/observer combination was D50-2°. The chromaticity coordinates ($L^*$, $a^*$, $b^*$) were calculated from the spectral data, as well as hue ($h^*$) and chroma ($C^*$).

The physical surface of coverage of toner was determined by microscopic analysis. Printing patches were analyzed with the optical microscope Zeiss, in reflection mode and on black background, with a magnifying power of 10. Then the physical percentage of coverage of each color was determined from the obtained images.

## 3. Results and discussion

### 3.1 Colorimetric coordinates according to monochromic printing conditions

Considering monochromic printing, the quality of the paper does not influence the colorimetric color ($\Delta L^*$ and $\Delta a^*$) as we obtained the same variations for both papers.

For the primary colors cyan and magenta, whatever the paper, the $L^*$ coordinate increased with the square size, as presented in Figure 2. For low percentages of coverage (25 %), the $L^*$ coordinate is mostly affected by the paper, according to a second order polynomial function. This is due to the evolution of the effective percentage

of coverage. For the yellow color, the L* coordinate is neither affected by the evolution of the percentage of coverage nor by the size of the pattern. It remained constant (L* = 90 ± 2). The particularity of the yellow primary color is due to its transparency, more light is scatters as compared to other colors.

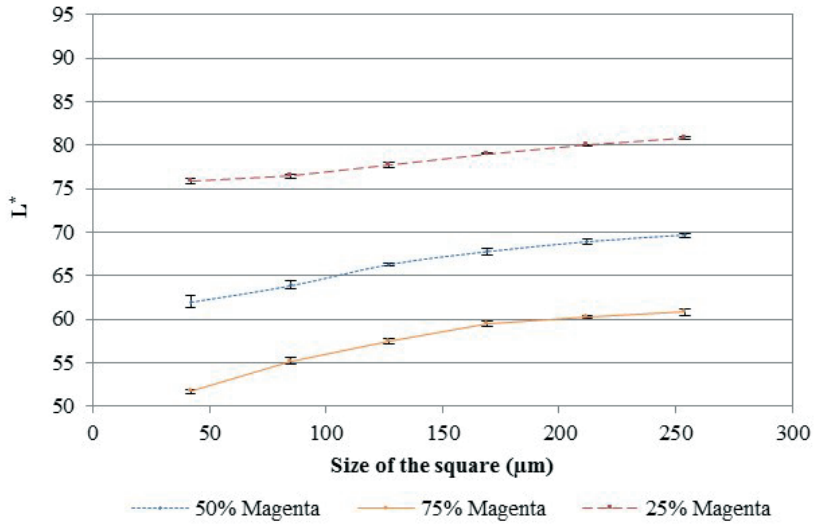


*Figure 2: Evolution of the L* coordinates according to the size of pattern, for 25, 50, and 75% of coverage, for magenta primary color (uncoated paper)*

For both papers, the coordinates b* for yellow and a* for magenta decrease (second order function) when the size of patterns increases, as shown in Figure 3.

This effect can be considered in models prediction to improve the efficiency of color prediction. Visually we note that the difference of colorimetric coordinates is higher between 25 and 50%, than between 50 and 75%: this is not a linear effect. The diminution of percentage of coverage increases a* coordinate for cyan color, whereas b* coordinate for magenta printing remains almost constant. Prints with little patterns present a higher chroma.

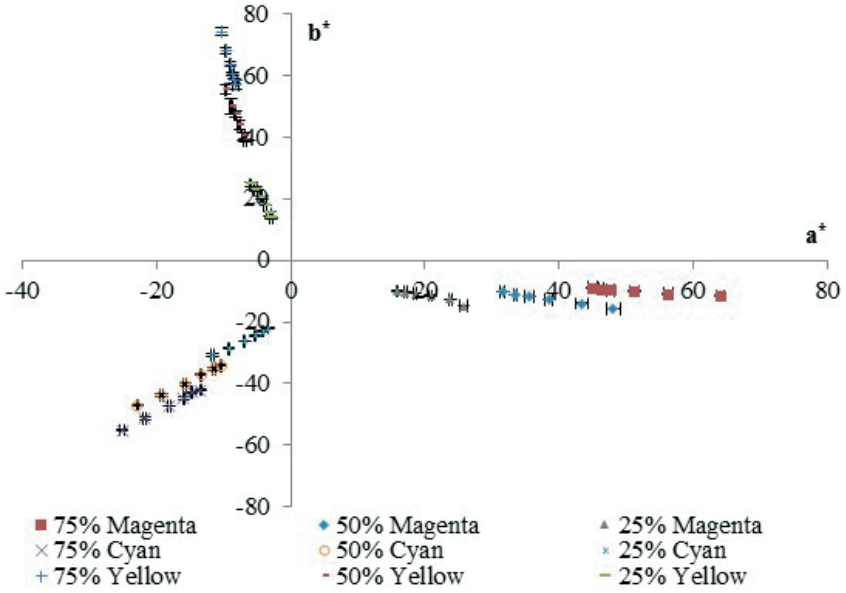


*Figure 3: Evolution of color coordinates b* according to a*, for all sizes of pattern, for 25, 50, and 75% of coverage (uncoated paper)*

Color differences between papers may also be analyzed with hue and chroma, as shown in Figure 4. For both papers, the perception of color difference was higher when the percentage of coverage increased. For uncoated paper, chromaticity was more affected than for coated paper, especially for the magenta primary color ($\Delta C^*=15$ and 22 for coated and uncoated papers, respectively). Chromaticity of yellow is not influenced by the size or the percentage of coverage of patterns.

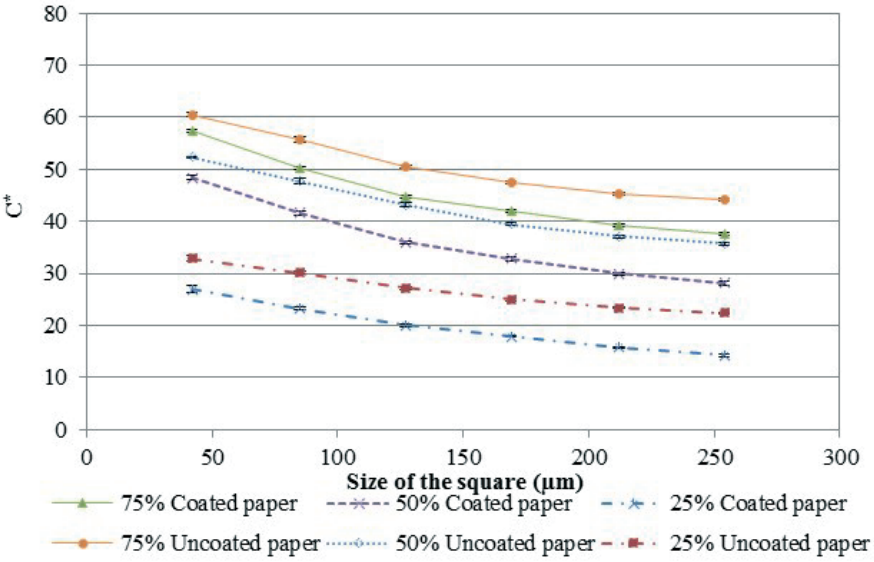


*Figure 4: Evolution of color coordinates C* according to the size of the pattern, for 25, 50, and 75% of coverage, for cyan primary color (both papers)*

Variations of hue are not linear according to the size of the pattern. For coated paper, hue values of cyan and magenta are lower than for uncoated paper.

3.2. Models efficiency in the case of monochromic printing

Considering model efficiency for monochromic printing, for all the printing conditions, the Murray-Davies model is the less efficient considering the minimization of ΔE*ab color difference, as presented in Figure 5. For this model, contrary to others, color prediction follows a polynomial curve according to the size of the pattern, the only parameter considered in equation. Therefore, this model has to be dedicated to the color prediction of quarter/three-quarter of tones with nominal pattern size superior to 127 µm, where the colored interactions between ink layer and paper are less important.

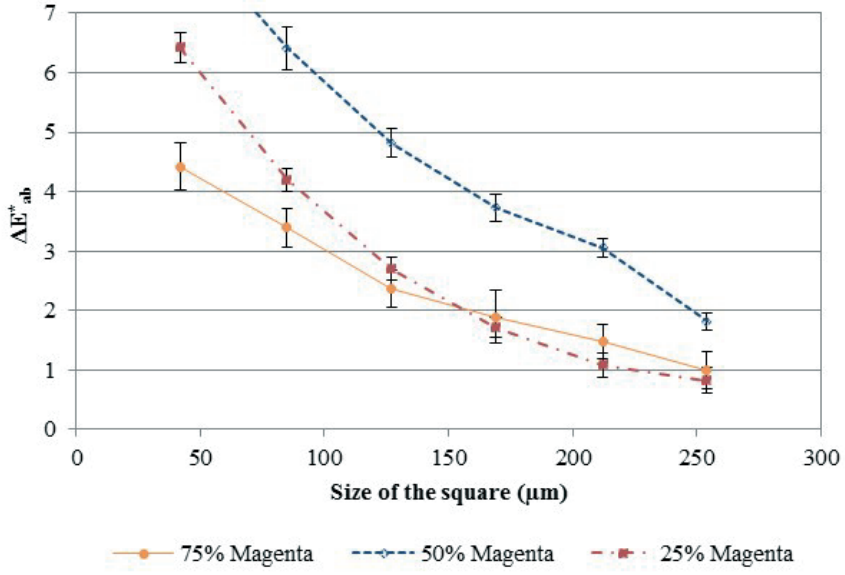


*Figure 5: Color difference according to the size of pattern, for 25, 50, and 75% of coverage, Murray-Davies model, for magenta primary color (uncoated paper)*

For the uncoated paper, the Yule-Nielsen and the Clapper-Yule models, applied for cyan and magenta, present the same evolution of color prediction according to the size of the square (polynomial function), as shown in Figure 6. The size of the pattern influences differently the color prediction according to the models. With both

models, cyan predictions are better for a theoretical size comprised between 85-169 µm. For magenta, the best range is between 85-127 µm. These differences of color predictions according to the size of the pattern restrict the use of amplitude modulated halftone algorithm. Considering the coated paper, for cyan and magenta, color predictions are acceptable for size of patterns superior to 127 µm.

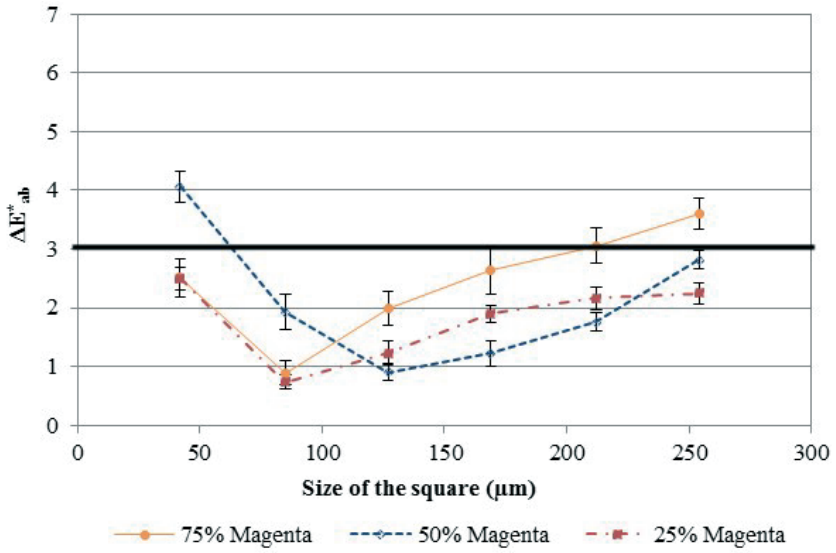


*Figure 6: Color difference according to the size of pattern, for 25, 50, and 75% of coverage, Clapper-Yule model, for magenta primary color (uncoated paper)*

Color prediction for the yellow primary color is always admissible. Considering the effective percentages of coverage (Figure 7), which was calculated to minimize the color prediction, for both papers, little dots give higher effective percentage. The Murray-Davies model overestimates the dot gain as it considers only the incident light: it does not take account the lateral propagation of light within the paper bulk or the internal reflections.

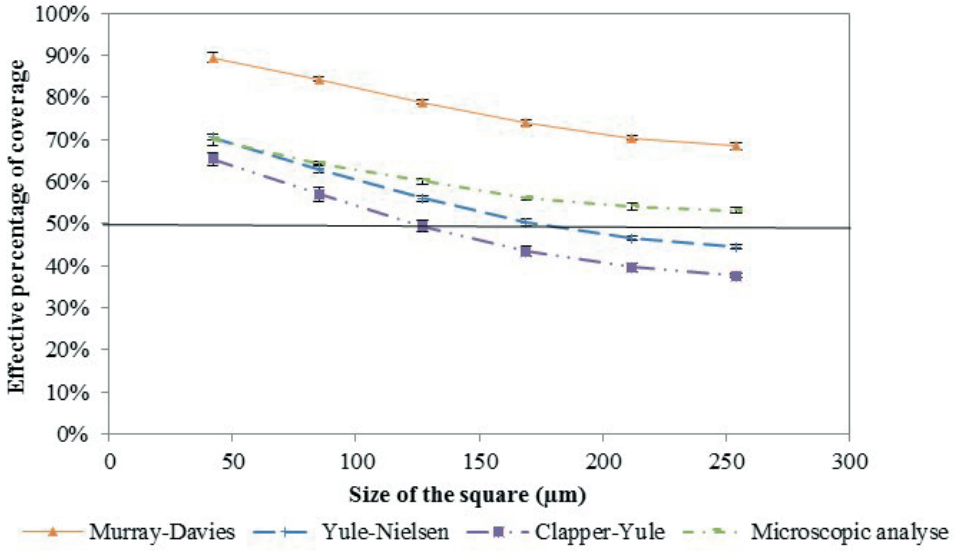


*Figure 7: Effective percentage of coverage for three models, according to the size of pattern, for 50% of coverage, cyan primary color (uncoated paper)*

3.3 Colorimetric coordinates according to polychromic printing conditions

For polychromic printing (cyan and magenta), the ink layer is important enough to mask the optical property of papers. Consequently both papers lead to similar evolutions. In polychromy, lightness is lower than in monochromic printing. The L* variation is more important in the juxtaposition case as ink covers more paper surface.

If yellow is used in polychromic printing, the chroma decreases strongly for high percentages of coverage (75%). Chroma calculated with yellow is superior in juxtaposition case. Therefore, it is advisable to use juxtaposition than superposition dots in order to increase the gamut.

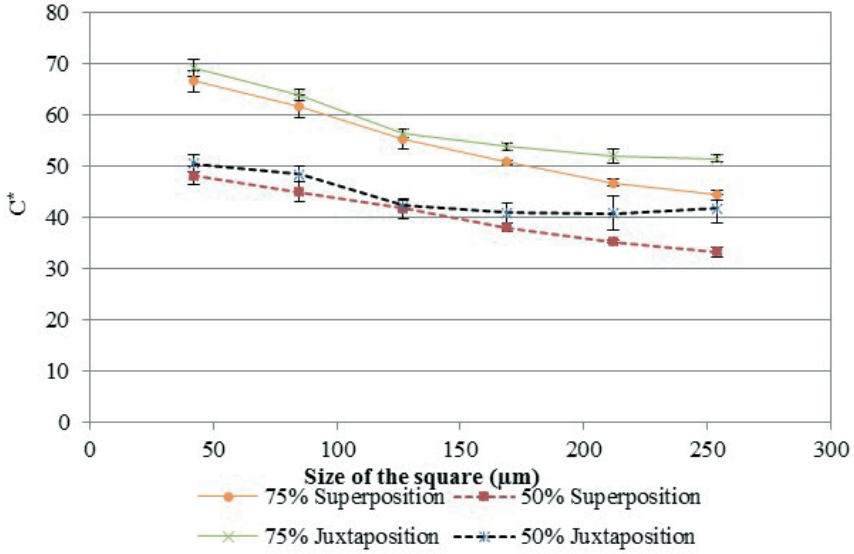


*Figure 8: Evolution of C* color coordinates for juxtaposition/superposition cases, yellow and magenta, according to the size of patterns, for 50 and 75% of coverage (uncoated paper)*

For yellow and magenta, hue shows highest variations according to the paper and the configurations (as presented Figure 9). The evolutions of hue for the superposition and the juxtaposition configurations are opposite for the uncoated paper. This modification is due to the evolution of b*. For the coated paper, hue decreases in the superposition case and stays almost constant for the juxtaposition case (contrary to uncoated paper).

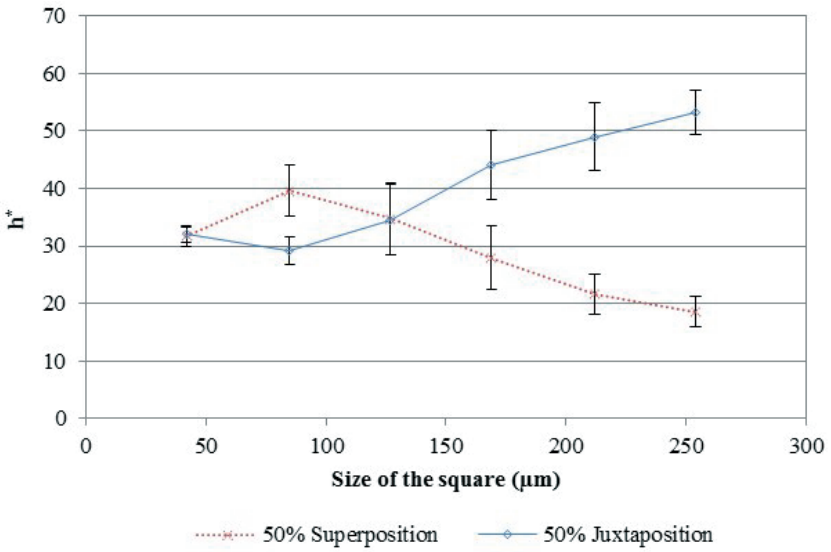


*Figure 9 Evolution of h* color coordinates for juxtaposition/superposition cases, yellow and magenta, according to the size of patterns, for 50 % of coverage (uncoated paper)*

3.4 Efficiency of the different models

Considering polychromic printing, the color prediction with classical models of Yule-Nielsen and Clapper-Yule is not efficient, as ΔE*ab is always higher than 3. Best predictions are obtained with Yule-Nielsen model. As for monochromy, better predictions are obtained for pattern sizes comprised between 85 to 127 µm, because, according to the modulation transfer function (Inoue, Tsumara and Miyake, 1997), light does not travel signifycantly more than 130 µm within paper. As in monochromy, juxtaposition is better predicted than superposition.

The size of pattern and the percentage of coverage have both to be considered in the choice of the polychromic prediction model, because they affect the dot gain, and consequently the effective surface coverage and the color prediction efficiency.

The mixture of Demichel and dot-on-dot used with Yule-Nielsen model improves the predictions, and leads to better predictions than the mixture of Clapper-Yule model.

The evolution of the parameter $\alpha$ of the mixture model [4] allows estimating the register of printer. When the parameter is close to 1, the Demichel method predominates, dots can be considered as juxtaposed.

## 4. Conclusion

For a given primary color, we demonstrated that the size of the pattern and the percentage of coverage are the main factors influencing the color printing. In monochromic printing, colorimetric models are more adapted for a given size of pattern or a percentage of coverage. The Murray-Davies model is adapted for color prediction of quarter/three-quarter of tones with nominal size superior to 127 μm, the Yule-Nielsen or Clapper-Yule models for the sizes comprised between 85 to 169 μm. Smaller sizes are worst predicted due to the influence of dot gain. In polychromic printing, the juxtaposition and the superposition of primary colors influence differently the colorimetric coordinates. The pattern size, as well as the superposition or juxtaposition of the dots, govern the choice of the model of color predictions. To improve the gamut, it is advised to use the juxtaposition case.

The mixture of Demichel and dot-on-dot screen allows estimating the efficiency of the printer register.

The halftoning technique amplitude modulation can be efficiently predicted for theoretical size of pattern comprised between 85 and 169 μm.

The perspectives are to study the influence of the transmittance of the composed dyes formed by the superposition of inks as a function of the ink transmittances. The order of the deposition has also to be introduced in the models. Moreover, the influence of different ditherings as method for reproducing halftone images should be studied.

**References**

Balasubramanian, R. 1999. Optimization of the spectral Neugebauer model for printer characterization. Journal of Electronic Imaging, 8(2), pp. 156-166

Clapper, F. R. and Yule, J. A. C. 1953. The effect of multiple internal reflections on the densities of halftone prints on paper. Journal of Optical Society of America, 43, pp. 600-603

Demichel, E. 1924. Le procedé, 26, pp.17-21, pp. 26-27

Hébert, M., Hersch R. D. and Becker, J. M., 2007. Compositional reflectance and transmittance model for multilayer specimens. Journal of Optical Society of America A, 24(9), pp. 2628-2644

Inoue, S., Tsumara, N. and Miyake, Y., 1997. Measuring MTF of paper by sinusoidal test pattern projection, Journal of Imaging Science and Technology, 41(6), pp. 657-661

Kubelka, P. and Munk, F. 1931. Ein beitrag zur optik der farban-striche. Zeitschrift für technische Physik, 12, pp. 593-601

Murray, D., 1936. Monochrome reproduction in photoengraving. Journal of Franklin Institute, 221, pp. 721-744.

Neugebauer, H. E. J., 1937. Die theoretischen Grundlagen des Mehrfarbenbuchdrucks. Zeitschrift für wissenschaftliche Photographie, 36, pp. 73-89

Xi, S. and Zhang, Y. 2012, The study on physical dot gain of second-order FM halftone based on ink spreading in all ink superposition conditions. 17th Color Imaging Conference, 8292, pp. 1-10

Yang, L., Lenz, R. and Kruse, B., 2001. Light scattering and ink penetration effects on tone reproduction, Journal of Optical Society of America, 18(2), pp. 360-366

Yule, J. and Nielsen, W. 1951. The penetration of light into paper and its effect on halftone reproduction. Technical Association of the Graphic Arts Proceeding, 3, pp. 65-76

# Dot gain analysis from probabilistic spectral modelling of colour halftone

*Ludovic Gustafsson Coppel*

The Norwegian Colour and Visual Computing Laboratory
Gjøvik University College
Norway
E-mails: ludovic.coppel@hig.no

**Abstract**

Perceived ink dot broadening due to light scattering in paper (optical dot gain) is effectively modelled by the empirical Yule-Nielsen model. Another approach is to use probabilistic models whose advantages are linearity and a higher theoretical physical explanation power. In this paper, we compare the performance of the Yang probabilistic model to that of the Yule-Nielsen model in terms of colour prediction of single colorant patches at different ink coverages and study the model parameter dependency on ink, halftone frequency and substrate. The Yang model is tested for substrates with wide range of optical dot gain and different halftone frequencies. The model takes explicitly into account the lateral light scattering in the substrate with a probability for light entering an unprinted area to exit through an ink dot (P_(p-i)). The results show that the model performs as well as the Yule-Nielsen model in predicting the colour of single halftone patches. For multiple coverage prediction, P_(p-i) can be described as a linear function of the apparent coverage but a non-zero offset at zero coverage must be used. Other effects than lateral light propagation are however taken into account by the model parameter P_(p-i). Without further improvements to account for these yet unknown effects, we conclude that the Yang model does not have more explanation power than the Yule-Nielsen model.

**Keywords**: colour prediction model, dot gain, Yule-Nielsen, probabilistic model

## 1. Introduction

Printed dots are generally larger than the nominal dot area, an effect called mechanical dot gain. In addition, lateral light scattering within the substrate leads to what is called the optical dot gain (ODG) or Yule-Nielsen effect. The well-known Yule-Nielsen modified spectral Neugebauer model is one of the most accurate predictive models for the spectral reflectance of printed halftone colours and can also account for different mechanical dot gain depending on ink superposition conditions (Hersch and Crété 2005). The Yule-Nielsen (YN) transform, introducing a non-linear relationship between the reflectance of a halftone and the reflectance of the substrate and solid ink, is however an empirical model whose determined parameters are only valid for one specific printer/ink/substrate and viewing condition combination. Ideally, a spectral colour prediction model should accurately separate mechanical and optical dot gain to allow for predictions without the need for a full model calibration when changing either ink, printing conditions, or substrate. For practical applications, the model parameters should also be determined with fast and affordable measurement methods. While the empirical n-factor in the YN model can account for many different effects, probabilistic models introduced by Huntsman (1987) and further developed by Arney (1997) and later Yang (2010) allows explicit modelling of the optical dot gain. These probabilistic models are also of interest because of their linearity with apparent coverage that may reduce the computational costs for ink separation, especially when using multi-channel printing using more inks than the conventional CMYK.

Both the YN and probabilistic approaches assume homogenously thick and sharply edged dots. Varying ink thickness has been studied by e.g. Arney and Yamaguchi (1999) or Hébert and Hersch (2010). In this work, the YN model is compared to the Yang model for three inks (cyan, magenta, yellow) printed at different resolution with an ink-jet printer on substrates with different extent of lateral light scattering. The aim is to compare the performance of the Yang model to that of the YN model in terms of colour prediction of single colorant patches at different ink coverages and to study the model parameter dependency on ink, halftone frequency and substrate.

## 2. Methods

An inkjet photo paper, an office paper and a tracing paper are chosen in order to vary the degree of lateral light propagation and thereby the extent of ODG. The substrates are printed at 80, 120 and 150 lpi and at 1200 dpi with a HP Designjet 10 PS inkjet printer. The test chart contains 600 patches at 10 different ink coverages for

cyan and magenta and 6 for yellow. Amplitude modulation (AM) halftoning is generated in Matlab with only no ink or full ink dots (1 200 dpi) to avoid unwanted colour management by the printer's RIP.

The Yule-Nielsen (YN) modified spectral Neugebauer model expresses the spectral reflectance raised to the power 1/n as a linear combination of the spectral reflectance of the Neugebauer primaries (NP) raised to the power 1/n as

$$R = \left(\sum_{k=1}^{N} a_k R_k^{1/n}\right)^n \quad [1]$$

where N is the number of NPs, a_k is the coverage of NP k and R_k is the reflectance of the k-th NP. Using a probabilistic approach, the effect of lateral light propagation in the substrate can instead be accounted for as (Yang, 2010)

$$R = \sum_{k=1}^{N} \sum_{l=1}^{N} T_k T_l P_{kl} a_k \quad [2]$$

where P_kl is the probability for light entering an area with NP k to exit through a NP l and T_k=√(R_k/R_1 ), where R_1 is the reflectance of the unprinted paper, is the transmittance of NP k. Using the reciprocity relations P_kl a_k=P_lk a_l, the reflectance of a single colorant patch can we written as (Yang, 2010)

$$R = R_{\mathrm{p}}(1-a) + R_{\mathrm{p}} T_{\mathrm{i}}^2 a - (1-T_{\mathrm{i}})^2 (1-a) P_{\mathrm{p-i}} \quad [3]$$

where P_(p-i) is the probability for light entering an unprinted area to exit through an ink dot, R_p is the reflectance of unprinted paper, a is the apparent ink coverage and T_i=√(R_i/R_p ) is the transmittance of the ink dots, where R_i is the reflectance of ink on paper. The first two terms in Equation 3 correspond to the classical Murray-Davis model. The last term is a correction factor accounting for light propagation within the substrate that makes the reflected light only passing the ink layer once (ink to paper or paper to ink).

Given R_p and R_i, the apparent coverage a and P_(p-i) are determined by minimising the rms difference between calculated spectral reflectance with Eq. (3) and measured spectral reflectance (31 wavelengths between 400 and 700 nm). This results in one P_(p-i) for each apparent coverage a. Once a relationship is established between P_(p-i) and a, P_(p-i) can then be determined for any a. This is similar to the YN model, for which a single n value can be optimised to fit the reflectance of all patches at different apparent coverages.

Two functions are tested to describe the relationship between P_(p-i) and a. The first one assumes proportionality between P_(p-i) and a as suggested by Yang et al. (2001) in an earlier publication. This states that the probability for the light to propagate from paper to ink dot is simply proportional to the ink coverage. Since we show here that the P_(p-i) versus a does not cross the origin we then suggest to use a linear relationship with non-zero offset at zero coverage.

## 3. Results

Figure 1 shows the estimated probability for lateral propagation of the light from unprinted paper to ink dot for cyan ink on the copy, photo and tracing papers at three different halftone resolution (lpi). The results for the magenta inks are shown in Figure 2 and the results for the yellow inks are similar to the results for cyan ink. The relationship between Pp-i and estimated apparent coverage is more or less linear depending on the substrate and halftone resolution.

We notice that the probability for lateral propagation from unprinted paper to ink dot gets in some cases larger than 1, especially for the Copy paper. This is of course not physical and the results of the optimisation that leads to better prediction of the spectral reflectance factor with large correction factors in Equation 3.

The slope of the curves does not vary in a systematic manner. For the copy paper, the slopes are not significantly depending on the halftone resolution, while the shape of the curves are depending on halftone resolution for the photo paper.

The relationship between probability for lateral propagation and ink coverage seems to become less linear with increasing halftone resolution. For the tracing paper, the results are noisier due to lower print quality. Note that the lowest ink coverage at 150 lpi gets zero apparent coverage and a relative high probability for propagation between paper and ink dots. This is also due to the optimisation method and only reflects the fact that the spectral reflectance factor is best predicted with the spectral reflectance obtained for the case where the light only passes the ink layer once.

Overall, the lateral propagation probability curves are shifted upwards, meaning that there is always a high probability for propagation between paper and ink and vice-versa. Most curves do not seem to intercept the y-axis at the origin as it should be expected since no paper to ink dot propagation can actually occur without ink dots.

Figure 3 compares estimated Pp-i of the photo paper and of the tracing paper for the three inks at 80 lpi. As expected, Pp-i is larger for the tracing paper than for the photo paper because more lateral light propagation occurs in the tracing paper. With the YN model, n becomes very high for the tracing paper and any n-value larger than 100 leads to similar prediction results. However, Pp-i is significantly different for the different cyan, magenta and yellow inks. With the YN models, the same effect is observed with ink dependent n values.

In terms of colour prediction, the Yang model performs very well leading to ΔE2000 lower than 1 for nearly all patches, meaning that the spectral reflectance factor can well be modelled by Equation 3 when using the optimised P_(p-i) and apparent coverages for each individual patch. For practical applications it is however necessary to describe P_(p-i) as function of the apparent coverage. This approach is comparable to using one single n value for all coverages in the YN model instead of using specific n for each individual coverage. Figure 4 compares for the magenta ink the performance of the Yang model and the YN model when using single n and a linear relationship between P_(p-i) and coverage, respectively. Similar results are obtained for the other two inks, although ΔE2000 is generally higher for magenta than for cyan and yellow.

For the Yang model, the relationship between P_(p-i) is either assumed to be proportional, i.e. a line crossing the origin (proportional Yang model), or to be linear with an offset at zero coverage (linear Yang model). The linear Yang model performs significantly better than the proportional Yang model. The YN and linear Yang models performs equally in predicting the colour of the 8 magenta halftone patches. The linear Yang model leads more often to lower ΔE than the YN model but for some papers and halftone resolutions (e.g. photo 150 lpi) the YN model performs better.

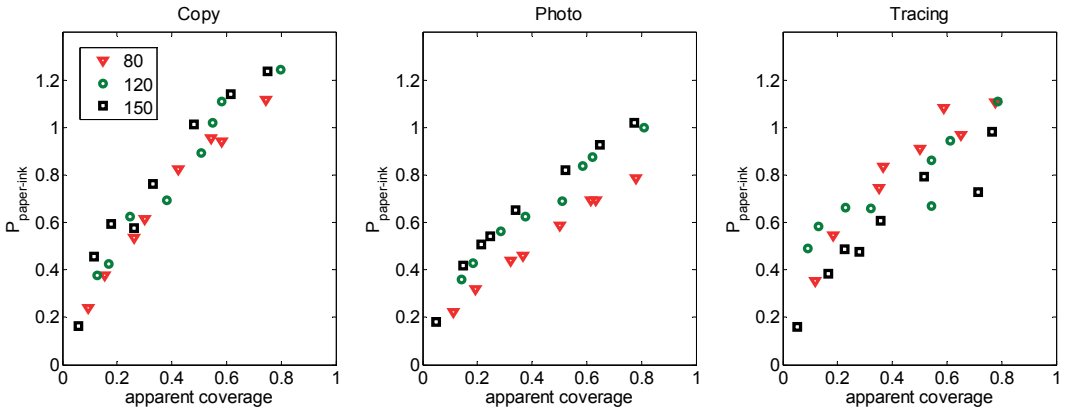


*Figure 1: Estimated probability for light entering an unprinted area to exit through an ink dot versus estimated apparent coverage. Copy paper (left), photo paper (middle) and tracing paper (right) printed with cyan at 80 lpi (triangles), 120 lpi (circles) and 150lpi (square)*

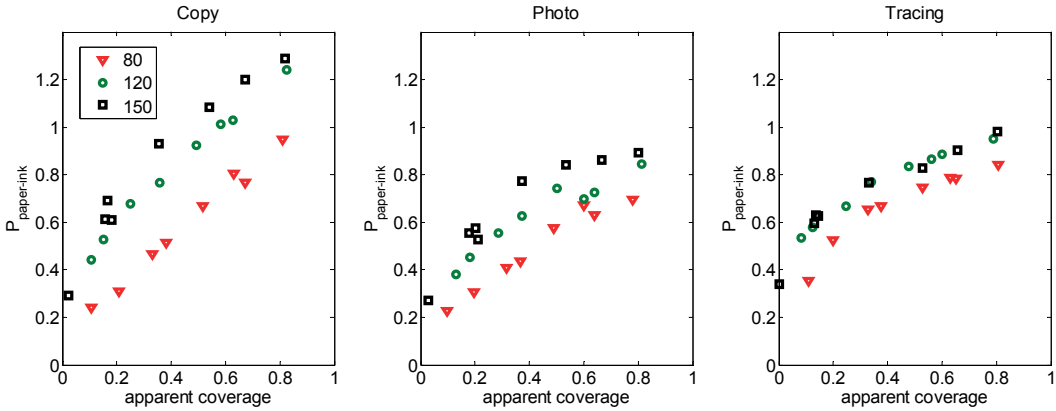


*Figure 2: Estimated probability for light entering an unprinted area to exit through an ink dot versus estimated apparent coverage. Copy paper (left), photo paper (middle) and tracing paper (right) printed with magenta at 80 lpi (triangles), 120 lpi (circles) and 150lpi (square)*

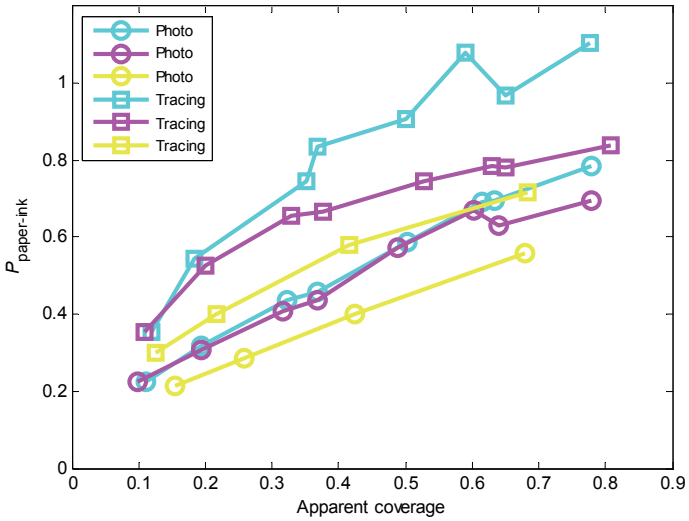


*Figure 3: Estimated probability for light entering an unprinted area to exit through an ink dot versus estimated apparent coverage for photo paper and tracing paper printed with cyan, magenta and yellow at 80 lpi. Pp-i clearly accounts for other effects than ODG when it gets larger than 1*

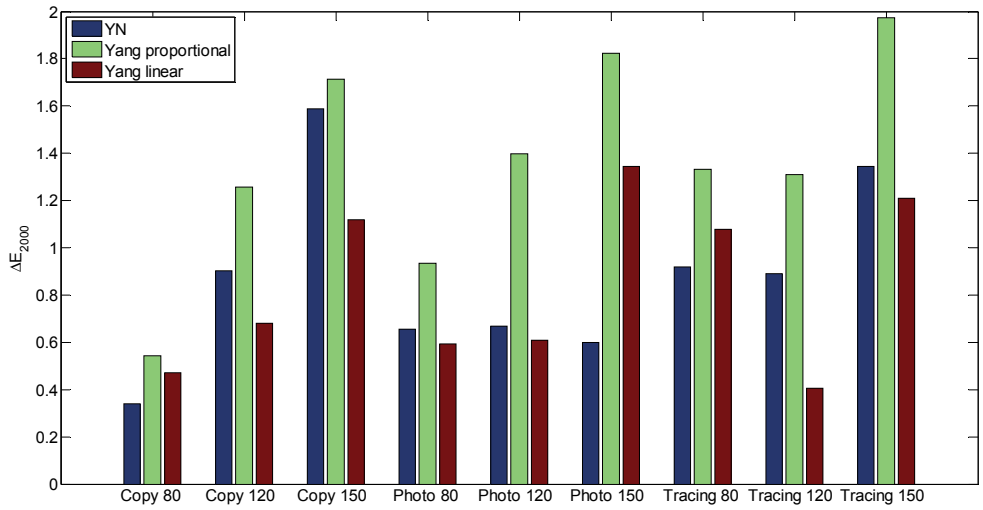


*Figure 4: Mean colour difference of magenta patches (8 different nominal coverages) between predicted and measured reflectance for the three models: Yule-Nielsen with constant n, Yang with proportional Pi-p, and Yang with linear Pi-p, plotted for the different substrates and halftone resolutions*

## 4. Discussion

When it comes to predict the spectral reflectance of single monochrome halftone patches, the tested Yang model performs as well as the Yule-Nielsen model. According to Equation 3, this means that the spectral reflectance of a halftone patch can be model as a weighted sum of the spectral reflectance of ink, paper and the spectral reflectance of light that is propagated within the substrate from unprinted area to ink dots or vice-versa. Since the Yang model is linear with apparent coverage as opposed to the YN model, it should be more easily inverted and may be an alternative to the YN modified Neugebauer model, especially when using more inks than CMYK in multichannel printing.

The main benefit of the Yang probabilistic model lies on the other hand in the fact that it is a physical model for the optical dot gain as opposed to the empirical YN model. However, the results show that the estimated model parameters often lack physical meaning. The probability for propagation from unprinted area to ink dots can exceed 1 and is unexpectedly high even at low ink coverages. Because of that, a linear function with non-zero offset at zero coverage must be used to describe the relationship between propagation probability and coverage.

Although the Yang model explicitly models the lateral light propagation, it is clear that other effects that are not taken into account by the model are modelled as the results of light propagation. In that aspect, the Yang model does not have more explanation power than the YN model and the lateral light propagation parameter (P_(p-i)), as the YN n, differs for cyan, magenta and yellow inks. Attempts were made to account for ink thickness variation as we can expect ink spreading making the smaller dots larger but also thinner. However, although thinner dots result in larger estimated apparent coverages, they also result in larger P_(p-i) thus not affecting significantly the shape of the P_(p-i)-a curves.

## 5. Conclusion

The probabilistic spectral Yang model of colour halftone was tested for a wide range of ODG and different halftone frequencies. The model takes explicitly into account the lateral light scattering in the substrate with a probability for light entering an unprinted area to exit through an ink dot (P_(p-i)). The model performs as well as the Yule-Nielsen (YN) model in predicting the colour of single halftone patches. For multiple coverage prediction, P_(p-i) can be described as a linear function of the apparent coverage but a non-zero offset at zero coverage must be used. Other effects than lateral light propagation are however taken into account by the model parameter P_(p-i). Without further improvements to account for these yet unknown effects, the Yang model does not have more explanation power than the YN model.

**Acknowledgements**

This work was supported by the Marie Curie Initial Training Networks (ITN) CP7.0 N-290154 funding.

**References**

Arney J. S. (1997), "A probability description of the Yule-Nielsen effect, I : Tone reproduction and image quality in the graphic arts", J. Imaging Sci. Technol. 41, 633-636

Arney J. and Yamaguchi S. (1999), "The physics behind the Yule-Nielsen equation," in Proceedings of PICS 1999: Image Processing, Image Quality, Image Capture, Systems Conference, 381-385

Hébert M. and Hersch R. D. (2010), "Analysing halftone dot blurring by extended spectral prediction models," J. Opt. Soc. Am. A 27(1), 6-12

Hersch, R. D. and Crété, F. (2005), "Improving the Yule-Nielsen modified Neugebauer model by dot surface coverages depending on the ink superposition conditions," in SPIE 5667, Color Imaging X: Processing, Hardcopy, and Applications, 4342005, 434-447

Huntsman J. R. (1987), "A new model of dot gain and its application to a multilayer color proof," J. Imaging Sci. Technol. 13, 136-145.

Yang L. (2010), "Probabilistic spectral model of color halftone incorporating substrate fluorescence and interface reflections", J. Opt. Soc. Am. A 27(10), 2115-2121

Yang L., Lenz R. and Kruse B. (2001), "Light scattering and ink penetration effects on tone reproduction," J: Opt. Soc. Am. A 18(2), 360-366

# Next generation printing - Towards spectral proofing

*Ludovic Gustafsson Coppel*[1], *Steven Le Moan*[2], *Paula Žitinski Elías*[3], *Radovan Slavuj*[1], *Jon-Yngve Hardeberg*[1]

[1] The Norwegian Colour and Visual Computing Laboratory
Gjøvik University College, Gjøvik, Norway

[2] Technische Universität Darmstadt, Germany
Darmstadt, Germany

[3] Department of Science and Technology
Linköping University, Norrköping, Sweden

E-mails: ludovic.coppel@hig.no; steven.lemoan@gmail.com; paula.zitinski.elias@liu.se;
radovan.slavuj@hig.no; jon.hardeberg@hig.no

**Abstract**

Different printing systems can produce colours that are perceived as identical under one standard illuminant such as D50. The visual match will however fail in other illuminations if the spectral properties of the inks differs. For soft proofing, this requires the proof to be visualised in the defined illuminant. Using more proofing inks than the conventional CMYK such as RGB increases the colorimetric redundancy, that is the number of different ink combinations that produce a visual match in D50. Using a spectral workflow, the ink separation can be optimised to get a visual match in different illuminations. We test here the feasibility of multi-illuminant (spectral) hard proofing with a multi-channel inkjet printer. We compute the proof of a set of 1269 Munsell patches with an inkjet printer model and compare the performance of a colorimetric and spectral workflow in terms of multi-illuminant proof matches. We show that large colour differences in different illuminants can occur when using a colorimetric workflow only optimising ink separation for D50. Performing a spectral gamut mapping leads to significant improvements as no Munsell targets show a ΔE2000 larger than 3 for all the illuminations tested. The use of additional red, green and blue inks further increases the colorimetric accuracy in different illuminations. Spectral proofing with multichannel inkjet printers opens thus for producing proofs that can be evaluated different visual environments. This can be particularly useful for packagings that make use of several spot colours and are viewed in very different visual environments.

**Keywords**: multi-channel printing, spectral printing, proofing

## 1. Introduction and background

It is possible for two different printing systems to produce colours that are perceived as identical, given a proper calibration. This visual match will however only occur under the illumination and viewing conditions used for calibration due to different spectral properties of the inks and substrates. Only when the print and proof are spectrally matched, they will appear identical in all illuminations.

Multi-channel printers were first introduced to increase the number of reproducible colours (colour gamut), which also led to colorimetric redundancy, i.e. a colour in a specific illumination can be reproduced using several different colorant combinations. This flexibility opens for minimising colour mismatch under more than one illuminant. Spectral proof reproduction can therefore remove the need for viewing booths for proof visualisation and allow comparison of print and proof in different visual environments.

Although a perfect spectral match is very rarely possible, the colorant combination can be chosen so that the difference between production print and proof is minimised for more than one viewing environment (Urban and Berns, 2011). There are a variety of applications that can benefit from considering multiple viewing conditions, such as catalogue or packaging printing, security-driven applications (e.g. watermarking), fine art, material appearance modelling and 3D printing.

Within the ongoing EU Marie-Curie initial training network project Colour Printing CP7.0 - Next Generation Multi-Channel Printing, there have been considerable efforts to understand and overcome the challenge of spectral reproduction workflows: new spectral colour modelling, spectral gamut mapping and halftoning methods with the aim to improve spectral reproduction (www.cp70.org). The purpose of this paper is to address the problem of spectral proofing (i.e. simulating the rendering of a print under various viewing conditions) and to investigate the advantages of using a multi-channel printer for spectral printing. We specifically test the feasibility of multi-illuminant (spectral) hard proofing with a multi-channel inkjet printer.

## 2. Methods

Spectral proofing requires that the target colours are not specified in CIELAB space for one illumination and standard observer (typically D50/2). Instead, the spectral reflectance factor is required as input to the proofing workflow. Once the spectral reflectance of the target colour is known, the task is to find the ink combination on the inkjet printer that gives the lowest colour difference between proof and target in different illuminations. A similar method to the spectral gamut mapping method developed by Urban and Berns (2011) is used here.

In order to test the feasibility of spectral proofing with a 7-inks inkjet printer, a set of reference colour chips with measured spectral reflectance is assumed to be a relevant subset of all printable colours. These spectra are used as target for reproduction with the inkjet printer using its spectral colour reproduction model.

### 2.1 Proofing printer

A Hewlett-Packard HPZ3200 ink-jet printer is used as proofing printer in a CMYKRGB mode. However, the proofs are actually not printed but simulated with the printer model. In order to reduce the number of training samples needed for calibration of the model and limit ink bleeding, the number of colorant overprints is limited to 4, as proposed by Tzeng and Berns (2000). Hence, only 4-ink combinations such as CMYK or CMRB are used, leading to 35 different 4-ink combinations. The printer is modelled with the cellular Yule-Nielsen modified Neugebauer (cYNSN) model, described e.g. by Wyble and Berns (1999), using two cells between 0 and 0.5 apparent ink coverage and between 0.5 and 1 apparent ink coverage. For calibration of the printer model, 35 charts with 625 patches are printed. This set includes all 4-ink combinations at 5 apparent ink coverages (0-100% with 25% step) including training samples (0, 0.5 and 1 apparent coverages) and test samples (0.25 and 0.75 apparent coverage). A highly white non fluorescing paper (200 g/m2 offset proof 9200 semimatt, EFI) is used as substrate and the printed patches are measured with an i1-Pro spectrophotometer (X-rite Inc.).

### 2.2 Proofing targets

The spectral gamut of all printable colours is unknown and will depend on the printing method and inks used. For testing the spectral printing capability of the inkjet printer, the matte Munsell colour chips can however be considered as a relevant subset of all printable colours. The spectral reflectance factor of 1269 matte Munsell chips was obtained from the spectral colour database published online by the University of Eastern Finland, Joensuu (Joensuu, 2014; Kohonen et al., 2006).

### 2.3 Illuminations

The spectral separation used to determine the colorant combination of the proofing system is optimised to get the best colorimetric reproduction in D50 illuminant while reducing the colour mismatch in other illuminants using spectral gamut mapping (Urban and Berns, 2011; Samadzadegan and Urban, 2013). Five illuminations are considered in this experiment: D50, A, and F11 standard illuminants, a Lamina WW-NB light-emitting diode (LED) and a Luxina EXZ-CG-M250 tungsten halogen lamp. These illuminations shown in Figure 1 are chosen to minimise the pairwise similarity of their spectral power distributions (Blahová, 2013; Le Moan and Urban, 2013). The spectral power distribution of the two real illuminations is available from the National Gallery, London (2014).

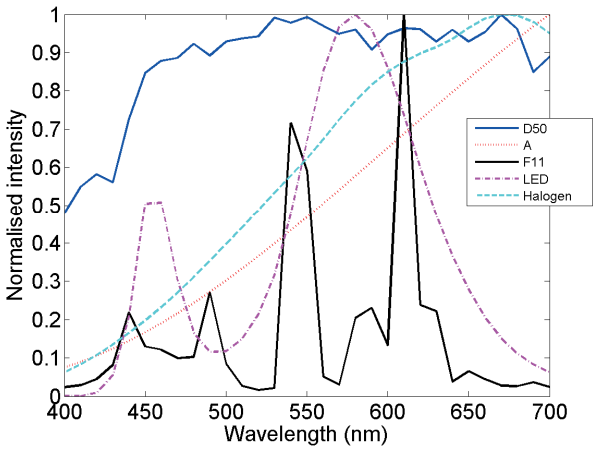


*Figure 1:*
*Normalized spectral power distribution of the used illuminations*

2.4 Calculations and analysis

The spectral separation uses the cYNSN forward model for the inkjet printer and optimises the ink coverages to match the target colour. First, all 4-ink combinations leading to ΔE2000 less than 1 between target and proof in D50 are determined. In order to reduce the number of computations, this is done with an additional constraint on the apparent ink coverages that are only allowed to vary with 0.01 steps. The next step is to select the ink combinations leading to ΔE2000 less than 1 between target and proof in D50 that lead to the lowest ΔE2000 in A. Finally the ΔE2000 in the two other illuminations is computed. This optimisation is performed for all possible 4-ink combinations. The best spectral reproduction is then compared to the "worst case" colorimetric reproduction for which one selects the ink combinations that provide a match in D50 with the largest ΔE2000 in A.

For proofing targets outside the colorimetric gamut of the inkjet printer, ΔE2000 is larger than 1 in D50/2 and the minimum ΔE2000 integer is determined instead. Some targets will be reproducible in D50/2 with CMYKRGB but not with CMYK, due to the smaller colorimetric gamut of CMYK as compared to CMYKRGB. To further investigate the spectral proofing capability of the inkjet printer we therefore select the targets whose reproduction with CMYK for D50/2 does not provide a colorimetric match for the A illuminant and compare the reproduction in the other illuminations for the two CMYK and CMYKRGB modes. From this analysis we can conclude on the improvements in terms of spectral printing when adding the RGB ink channels.

## 3. Results

The result of the colorimetric optimisation in D50/2 with CMYK mode is compared to the results with the CMYKRGB mode in Table 1. Almost all Munsell targets (99%) are reproducible with CMYK with a ΔE lower than 3, which may be acceptable in many applications. On the other hand, the number of Munsell targets reproducible under 1 ΔE increases from 95% to 99% when adding the RGB inks.

*Table 1: Comparison of the estimated colour difference between proof and 1269 Munsell targets under D50 illumination obtained with CMYK and CMYKRGB proof printing. Percentage of Munsell targets in different ⊿E classes*

| | $\Delta E_{2000} < 1$ (%) | $1 < \Delta E_{2000} < 3$ (%) | $\Delta E_{2000} > 3$ (%) |
|---|---|---|---|
| CMYK | 95 | 4 | 1 |
| CMYKRGB | 99 | 1 | 0 |

Figure 2 shows a typical Munsell target whose CMYK colorimetric reproduction for a D50 illumination leads to ΔE less than one but to a large colour difference between proof and target in an A illumination. For this specific sample, using the red and blue inks (YKRB) provides a colorimetric match in both illuminations. Two curves are shown for the CMYK case. These corresponds to the best and worst colorimetric match in D50 for which the colour difference between proof and target in A is the lowest and the largest, respectively.

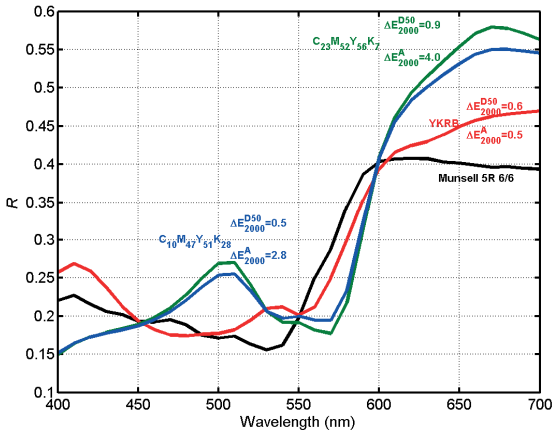


*Figure 2: Original and reproduced spectra of the Munsell 5R 6/6 target. The reproduction are optimised to minimize ⊿E2000 . in both D50 and A illuminations using CMYK inks or the optimal mix of CMYKRGB (red line, YKRB). The green line is the worst CMYK colorimetric match under D50 (leading to the largest ⊿E under A). The blue line is the best CMYK D50 match leading to the lowest ⊿E under A*

Of the 1269 Munsell targets included in this study, 340 can be reproduced in CMYK so that a colorimetric match is made in D50 (ΔE2000 ≤ 1) but not in A (ΔE2000 > 1). This corresponds to the worst case in which a colorimetric optimisation is performed under D50 so that the colour difference between proof and target is maximal under A. For these targets, Table 2 reports the results of the comparison of the spectral reproduction accuracy obtained with the CMYK mode to the one obtained with the CMYKRGB mode. All the reproductions are opti-

mised to get a colorimetric match in D50 illumination. Hence, ΔE between proof and target is less that 1 for all targets irrespective of the printing mode. From all possible reproductions that give a colorimetric match under D50, the two leading to the lowest and largest ΔE between proof and target under A are chosen. Table 2 shows that 85% of the selected targets that do not have a colorimetric match under A with CMYK get a match with CMYKRGB. The colorimetric math is also significantly improved for the LED and halogen illuminations when adding the RGB channels. It can also be noticed that a multi-illuminant workflow in CMYK already can significantly improve the colorimetric match in different illuminants (here D50 and A). Although no targets optimised in CMYK for D50 get a perfect match in A (ΔE ≤ 1), the number of targets with ΔE ≤ 3 in A can increase from 15 to 82% between a (worst case) colorimetric and a multi-illuminant workflow.

## 4. Discussion

The results in Table 1 show that using 7 inks instead of only four overall improves the colorimetric accuracy although CMYK already provides acceptable proofs of the 1269 Munsell chips used in this study (95% are under 1 ΔE2000 and 99 % under 3 ΔE2000). On the other hand, a colorimetric match of a proof target for one single illumination can be achieved with different ink mixtures of the 4 process inks. For production prints, additional goals such as minimizing ink consumption or graininess are utilised in the ink separation. Table 2 shows however that a colorimetric separation (here for D50) can lead to large colour deviations (up to 9 ΔE2000) between proof and target in other illuminations. For almost 50% of the Munsell targets, a colorimetric match in D50 can lead to ΔE2000 larger than 6 under the LED illumination. Performing the spectral gamut mapping described in Section 2.4 allows to choose the colorimetric reproductions that minimise colour difference under A illumination. This leads to significant improvements as no Munsell targets show a ΔE2000 larger than 3 for all the illuminations tested, even without using the extra RGB inks. Our findings show that a spectral workflow can lead to a much better colorimetric match for different illuminants than a D50 colorimetric workflow. This is in contradiction with the findings from Morovic et al. (2012) who concluded that no significant improvement was obtained with a spectral workflow. It should however be emphasised that a colorimetric workflow has several degrees of freedom and will lead to different ink separations depending on its implementation.

The addition of the red, green and blue inks further improve the proof-to-target colour match in different illuminations. This confirms a larger spectral variability and therefore a better suitability of multi-channel printers for spectral colour management. The performance of the spectral gamut mapping algorithm is very dependent on the order of the illuminants for which colorimetric match is optimised for. This is why the results in Table 2 are (after D50) best for the A illuminant. The order of illuminants could be change if a colorimetric match in F11 is for instance weighted higher than a colorimetric match in A. This approach to proofing allows specifying a number of illuminants that are particularly relevant for a given application. When this number becomes large, representative illuminants can then be created by means of a PCA-based approach (Le Moan and Urban, 2013).

*Table 2: Estimated colour difference expressed as ⊿E2000 between proof and Munsell targets in different illuminations for CMYK (D50 worst case colorimetric and multi-illuminant optimisation) and CMYKRGB proof printing, for targets within CMYK gamut (⊿E ≤ 1) under D50 but not under A. The addition of the RGB channels leads to a significant improvement of the colour match in different illumination*

| | | mean ΔE | max ΔE | DE ≤ 1 % | DE ≤ 3 % | DE > 6 % |
|---|---|---|---|---|---|---|
| **D50** | CMYK col | 0.8 | 1 | 100 | 0 | 0 |
| | CMYK | 0.7 | 1 | 100 | 0 | 0 |
| | CMYKRGB | 0.6 | 1 | 100 | 0 | 0 |
| **A** | CMYK col | 4.7 | 8 | 0 | 10 | 15 |
| | CMYK | 2.4 | 3.9 | 0 | 82 | 0 |
| | CMYKRGB | 0.5 | 2.2 | 85 | 15 | 0 |
| **F11** | CMYK col | 3.7 | 8.6 | 4 | 38 | 15 |
| | CMYK | 1.9 | 5.9 | 22 | 60 | 0 |
| | CMYKRGB | 1.7 | 5.9 | 32 | 54 | 0 |
| **LaminaLED** | CMYK col | 5.7 | 9 | 0 | 5 | 46 |
| | CMYK | 3.1 | 6.3 | 0 | 52 | 0 |
| | CMYKRGB | 1.8 | 5.9 | 24 | 69 | 0 |
| **Luxina halogen** | CMYK col | 4.6 | 7.5 | 0 | 10 | 11 |
| | CMYK | 2.4 | 4 | 0 | 81 | 0 |
| | CMYKRGB | 0.5 | 2.2 | 85 | 15 | 0 |

It should be noted that fluorescence, which has so far been neglected in spectral printing, will occur in many commercial prints. This is a main challenge in conventional proofing and becomes even more problematic for spec-

tral proofing since the amount of UV is different for different illuminations. The tested method can however be extended to fluorescing substrates by including fluorescence in the reflectance factor computation (Coppel et al., 2012). This would allow estimating multi-illuminant colour matches for different proofing substrates.

## 5. Conclusions

We tested the feasibility of multi-illuminant (spectral) hard proofing with a multi-channel inkjet printer. Unlike conventional colorimetric reproduction that optimises the proof to match the target in one illumination (typically D50), the proof is optimised to get the best colorimetric reproduction in D50 while reducing the colour mismatch in other illuminants. For conventional printing, colour mismatch between proof and target is more likely to occur for spot colours than for process inks. For a large set of matte Munsell chips, all colours can be proofed under 3 ΔE2000 using multi-illuminant spectral gamut mapping. The use of additional red, green and blue inks further increases the colorimetric accuracy in different illuminations. Spectral proofing with multichannel inkjet printers opens thus for producing proofs that can be evaluated different visual environments. This can be particularly useful for packagings that make use of several spot colours and are viewed in very different visual environments. One of the main challenges in proofing is fluorescence whose impact on multi-illuminant could be evaluated by including fluorescence in the calculations.

**Acknowledgements**

This work was supported by the Marie Curie Initial Training Networks (ITN) CP7.0 N-290154 funding.

**References**

Blahová J., Le Moan S. and Urban P. (2013), "The Impact of Illumination on the Perceived Quality of Spectral Reproductions," in Proc. 19th Workshop Farbbildverarbeitung,1-3

Coppel L. G., Anderson M., Neuman M. and Edström P. (2011), "Fluorescence model for multi-layer papers using conventional spectrophotometers," Nord. Pulp. Pap. Res. J. 27(2), 418-425

Joensuu (2014/06/15), "Spectral database": http://www.uef.fi/fi/spectral/munsell-colors-matt-aotf-measured

Kohonen O., Parkkinen J. and Jääskeläinen T. (2006), "Databases for spectral color science," Col. Res. Appl. 31(5), 381-390

Le Moan S. and Urban P. (2013), "Evaluating the perceived quality of spectral images", in Proc. IEEE International Conference on Image Processing, 2024-2028

Morovic P., Morovic J., Arnabat J. and Garcia-Reyero J. M. (2012), "Revisiting spectral printing: a data driven approach," in Proc. IS&T 20th Color and Imaging Conference, 335-340

National Gallery (2013/06/15), "Spectral power distribution curves", The National Gallery: http://research.ng-london.org.uk/scientific/spd/

Samadzadegan S. and Urban P. (2013), "Spatially Resolved Joint Spectral Gamut Mapping and Separation," in Proc. IS&T 21st Color and Imaging Conference

D.-Y. Tzeng and R. S. Berns (2000), "Spectral-based six-color separation minimizing metamerism," in Proc. IS&T/SID, Scottsdale, AZ, 342–347

Urban P. and Berns R. S. (2011), "Paramer Mismatch-Based Spectral Gamut Mapping," IEEE Transactions on Image Processing 20(6), 1599-1610

Wyble D. R. and Berns R. S. (2000), "A critical review of spectral models applied to binary color printing", Col. Res. Appl. 25(1), 5-19

# Multilevel halftoning applied to achromatic inks in multi-channel printing

*Paula Žitinski Elías*, *Sasan Gooran*, *Daniel Nyström*

Linköping University
Bredgatan 33
S-601 74 Norrköping, Sweden
E-mails: paula.zitinski.elias@liu.se; sasan.gooran@liu.se; daniel.nystrom@liu.se

**Abstract**

Printing using more than four ink channels visually improves the reproduction. Nevertheless, if the ink layer thickness at any given point exceeds a certain limit, ink bleeding and colour accuracy problems would occur. Halftoning algorithms that process channels dependently are one way of dealing with this shortcoming of multi-channel printing. A multilevel halftoning algorithm that processes a channel so that it is printed with multiple inks of same chromatic value was introduced in our research group. Here we implement this multilevel algorithm using three achromatic inks - photo grey, grey, black - in a real paper-ink setup. The challenges lay in determining the thresholds for ink separation and in dot gain compensation. Dot gain results in a darker reproduction and since it originates from the interaction between a specific ink and paper, compensating the original image for multilevel halftone means expressing dot gain of three inks in terms of the nominal coverage of a single ink. Results prove a successful multilevel halftone implementation workflow using multiple inks while avoiding dot-on-dot placement and accounting for dot gain. Results show the multilevel halftoned image is visually improved in terms of graininess and detail enhancement when compared to the bi-level halftoned image.

**Keywords**: multilevel halftoning, multi-channel printing, dot gain compensation, graininess

## 1. Introduction

In order to achieve a colour reproduction, the initial image to be printed is firstly separated into a number of colorant channels. Traditionally, the channels used are cyan (C), magenta (M), yellow (Y) and black (K), but in the interest of reducing graininess and augmenting the colour gamut for high quality colour printing, additional channels are introduced (Jang, et al., 2005). These additional channels can be light cyan (Lc), light magenta (Lm), grey (GY), photo grey (PGY), red (R), green (G), blue (B), orange (O), or a combination of them. Introducing additional channels is a solution to achieve high quality prints in many printing technologies.

After separation, each channel is digitally adapted for the printing process before being sent to the printing device. The reason for this digital adaptation lays in the common nature of the vast majority of printing technologies, where placing ink onto a media substrate is a choice of either depositing or not depositing a drop of ink onto a specific position. The printed image is therefore a result of either printed or not printed spots - duotone impression. In order to achieve a full palette of lighter and darker tones, a digital pre-reproduction step called halftoning is performed. A halftoning algorithm converts each colorant channel of the image into microdots in smaller or greater size and/or concentration that create the illusion of tone gradation. Literature reveals a large number of halftoning algorithms (Wyble and Berns, 2000) that can mainly be categorized in amplitude modulated (AM) and frequency modulated (FM) algorithms (Sharma, 2003). In AM halftoning the size of the dots varies to create the illusion of lighter or darker tones, whereas in FM halftoning, the concentration of dots is the fluctuating factor.

Once the channels are halftoned, the printing system transfers the corresponding channel's ink (C, M, Y, K, etc.) onto the media substrate. In inkjet this means that ink droplets are placed on the paper. A certain ink-paper interaction then happens, known as dot gain or tone value increase. In literature, dot gain is differentiated and even separated as two independent phenomena (Namedanian, et al., 2013). Physical (mechanical) dot gain is the result of ink penetration and ink spreading onto the paper. Because of this spreading, the printed dot will grow in size, resulting in a darker printed image. On the other hand, optical dot gain is the result of light scattering and light absorption. The photons of light that enter the paper through the ink layer scatter in the paper and either get absorbed in it or exit the paper at a further point, possibly at a point with no ink layer. This light exchange between different chromatic areas is the reason for optical dot gain, which also causes the resulted printed dots to appear larger.

Dot gain is the reason there is a differentiation between the ink coverage value sent to the printing system (nominal coverage) and the resulting printed coverage (effective coverage). That is why, before halftoning, the initial

image must be compensated for dot gain so that the printed image has the correct ink coverage values. Dot gain compensation is performed by applying existing mathematical models, such as Murray-Davies model (Murray, 1936), to the initial image, described in Equation 1:

$$\boldsymbol{R = aR_i + (1 - a)R_p} \quad [1]$$

where R is the predicted reflectance, a the fractional ink area coverage, R_i the spectral reflectance of the full coverage ink, and R_p the paper's spectral reflectance. Using this formula, one can calculate the amount of dot gain a printing system will produce (influenced by many factors, as ink, paper, etc.) and adjust the nominal coverage values accordingly. Since dot gain is dependent on the ink, each channel's nominal coverage value needs to be adjusted separately.

It has already been mentioned that multi-channel printing (printing with more than four channels) increases the gamut and improves the overall image quality. Nevertheless, a high number of colorants impose new computational challenges and physical limitations, one of them being a too large number of ink layers printed on top of each other, which causes ink bleeding and colour inaccuracy (Zeng, 2000). Certain halftoning algorithms can help to overcome these issues. For instance, in channel dependent halftoning, the algorithm is applied at two or more channels dependently at the same time, so the halftone dots are placed in a manner that they have minimal overlap between colorants - dot-off-dot halftoning (Gooran, 2004).

Another example is proposed in Gooran (2006) where a multilevel halftoning algorithm combines the channels with the same chromatic values (e.g. magenta and light magenta) by firstly separating the original image into different lightness regions and then halftoning it. One of the advantages of this method is that, in the resulting image channel printed with multiple inks of the same chromatic values, dot-off-dot printing strategy is utilized. This means that only a single ink layer is applied while using multiple inks of same chromatic values, which is an important step in overcoming one of the challenges of multi-channel printing. Meanwhile, using multiple inks with same chromatic values instead of a single ink improves significantly the visual impression of the reproduced image. This is especially obvious in light regions, where using a single ink means placing sparse halftone dots, resulting in a visually obvious graininess in those regions. Meanwhile, the additional colorants used are the washed out versions of the main colorant. Using those inks makes it possible to place the halftone dots in a denser pattern, while maintaining the same lightness value, which results in a less grainy image.

In this paper we implement the proposed multilevel FM halftoning with three achromatic inks - PGY, GY and K, using an inkjet printer. Creating a single channel that will be printed with three different inks proves to be challenging for dot gain compensation, as each ink has a different dot gain curve. In order to perform a successful dot gain compensation, it is necessary to express the dot gain of the three inks used in terms of nominal area coverage of a single, black, ink. In order to do that, correct ink limits for colorant separation must be determined, dependent on the combination of inks, substrate, halftoning algorithm and printing resolution.

This paper is structured as follows. After this introduction the proposed halftoning method workflow is explained in section 2. Section 3, Methodology, describes the experimental setup, how the ink limits for colorant separation were located and how dot gain was compensated. In section 4, Results and discussion, the results of the dot gain compensation are shown. Results of the graininess calculations are also discussed. A conclusion is given in section 5.

## 2. Multilevel algorithm implementation

The multilevel halftoning algorithm was firstly proposed in Gooran (2006). Opposed to the majority of halftoning algorithms that halftone one channel for one ink, multilevel halftoning results in an image channel that can be printed with multiple inks. In one of the steps of multilevel halftoning, any bi-level halftoning algorithm can be applied. This section describes the proposed multilevel halftoning algorithm.

### 2.1 Multilevel halftoning

The workflow of the multilevel algorithm is displayed in Figure 1. For the sake of the argument, the figure created has low resolution so that the halftone dots are visible and the regions are clearly separated.

In the pre-processing step, the original image is separated into a number of regions, each with a range of tone values, where the number of regions depends on the number of inks. One must also set the ink limits, i.e. the thresholds where one ink stops and another one begins, explained in section 3.2. The regions within the thres-

holds represent parts of the image with the same tonal value ranges. For the instance of 3 inks and thresholds of 0.33 and 0.66, three regions exist: tonal values between [0, 0.33], [0.33, 0.66] and [0.66, 1], marked in Figure 1 with numbers 1 through 3. In the same pre-processing step, each of these regions is transformed to values between [0, 1] or [1, 0]; for this instance region 1 has values between [0, 1], region 2 between [1, 0], and region 3 between [0, 1]. Here, 0 means no ink and 1 means fulltone ink.

The reasoning behind setting region 2 between [1, 0] instead of [0, 1] is to avoid neighbouring opposite interval limits, since this could cause a discontinuous image. If region 1 set between [0, 0.33] would be assigned values [0, 1] and region 2 between [0.33, 0.66] would become [0, 1] as well, a problem would appear around 0.33, where there would be a jump in the border between the regions from 1 to 0. This would cause discontinuation around this area that are otherwise easily avoided by assigning values so that neighbouring regions have the same neighbouring interval limit.

In the next step, halftoning, since regions with corresponding assigned values have been separated and scaled between [0, 1], any bi-level halftoning can be applied to the pre-processed image.

In the post-processing step the 0s and 1s in the image are replaced by the limit threshold values, in our example 0, 0.33, 0.66 or 1, depending on the region the pixel belongs to. For example, in those parts corresponding to the region [0, 0.33], 0s remain 0 but 1s are replaced by 0.33. In the region corresponding to [0.33, 0.66], 1s are replaced by 0.33 and 0s by 0.66, and so on (Gooran, 2006). The result is a single image, halftoned for three different inks with the choice of K, GY, PGY or no ink.

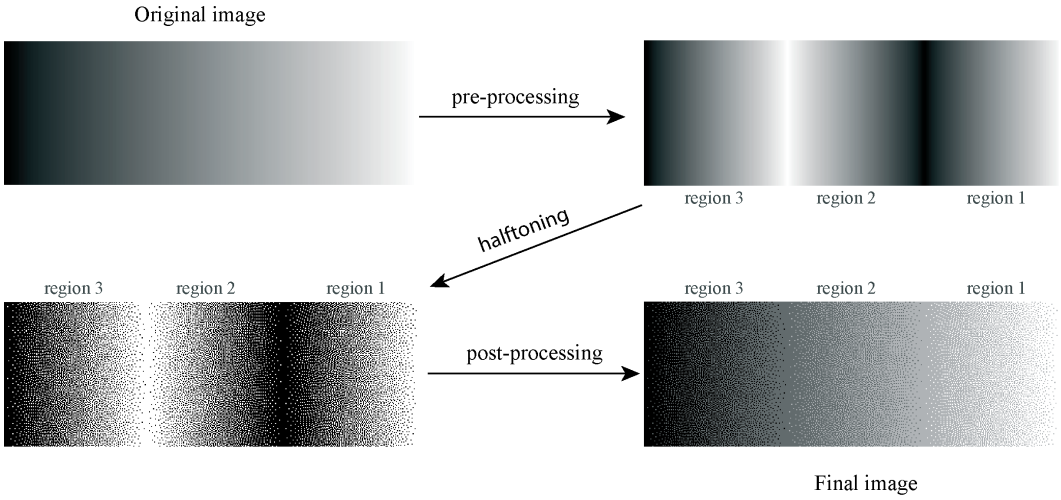


*Figure 1: Multilevel halftoning workflow*

2.2 Iterative Method Controlling the Dot Placement (IMCDP)

As this multilevel halftone workflow can use any bi-level halftoning algorithm, we chose an algorithm developed in our research group to have a better control over the whole process, named Iterative Method Controlling the Dot Placement (IMCDP) (Gooran, 2004). In this halftoning algorithm halftone dots are placed iteratively with the goal of reducing the difference between the original and the halftoned image. The generation of the halftoned image starts with a creation of a blank image with the same size as the original image. The total number of dots to be placed in the halftone image is dependent on the overall original image's lightness/darkness and therefore is known in advance.

Starting with a blank image, in the first step, the algorithm finds the position of the darkest pixel in the original image and places the first dot at that location in the halftoned image. In the next step the low-pass filtered version of the halftoned image is subtracted from the low-pass filtered version of the original image. The low-pass filter used is Gaussian filter with standard deviation 1.3 truncated to 11 x 11 pixels.

This operation is addressed in Gooran (2004: 355) as the feedback process. The location of the maximum pixel value of the created subtracted image is found and at that location on the halftoned image the next dot is placed. The process is continued until the known number of dots is placed, thus achieving the final halftoned image.

## 3. Methodology

This paper deals with the implementation of multilevel FM halftoning as part of a setup for multi-channel inkjet printing. For the purpose of this study the focus is on achromatic inks, i.e. photo grey (PGY), grey (GY) and black (K), aiming for a multilevel dot-off-dot halftoning with three different levels, spanning from no ink to fulltone black.

### 3.1 Experimental setup

The implementation challenges lie in determining the correct threshold levels used for colorant separation and in compensating for dot gain for three different inks. These thresholds are dependent on the ink combination, type of substrate, halftoning method and print resolution.

In order to find proper thresholds for our setup, patches with 0% to 100% nominal ink coverage, in steps of 1%, were printed for all three inks. All prints were made using an inkjet 12-channel printer Canon imagePROGRAF iPF6450. All samples were printed on 90 g/m² uncoated office paper and on 170 g/m² matte coated paper at a resolution of 600 dpi. Nevertheless, the same workflow can be applied to other media substrates and other printing resolutions. The CIEXYZ values of the printed patches were measured using the spectrophotometer BARBIERI electronic Spectro LFP RT, light source D50 with 2° standard observer.

### 3.2 Locating thresholds between inks

Since achromatic inks vary in lightness (correlated with luminance), measured luminance Y values were used to find the thresholds between the inks. The thresholds are the ink coverage values at which the Y value of the black ink matches the Y value at 100% ink coverage of the lighter inks, photo grey and grey (Figure 2).

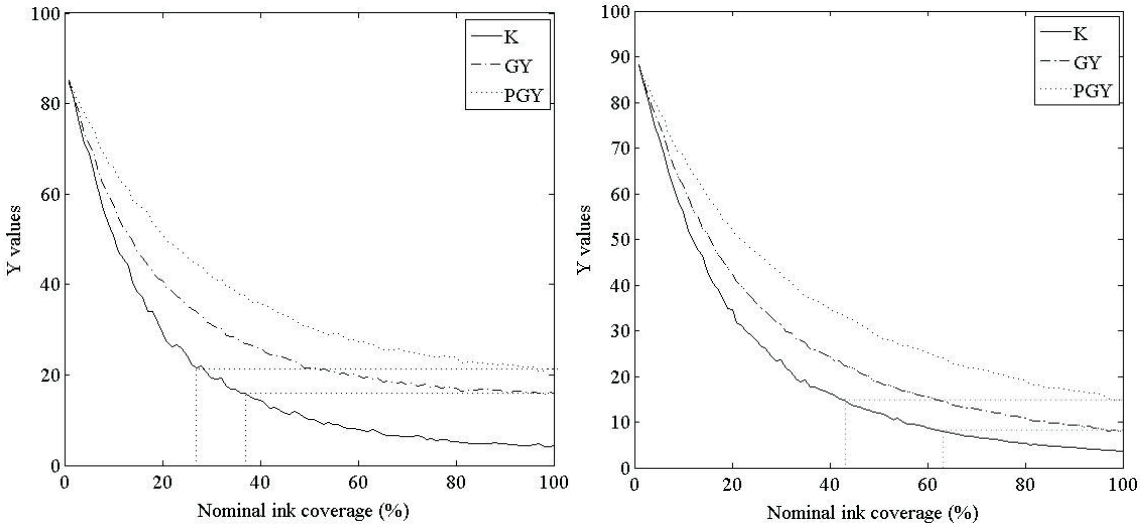


*Figure 2: Y values of the three inks allow locating the thresholds between inks: (left) uncoated 90 g/m² paper, (right) matte coated 170 g/m² paper*

Figure 2 shows the luminance Y values of the three inks - PGY, GY and K, plotted against their nominal ink coverages for the (left) uncoated 90 g/m2 paper and (right) 170 g/m2 matte coated paper. This plot also shows the Y values that match GY and PGY.

For the example of the coated paper, the Y values of fulltone GY match the Y values of 62.5% K, while the Y values of fulltone PGY correspond to the Y values of 42.5% K. Thus for this setup one can conclude that the limits between the regions should be set at 42.5% ad 62.5% ink coverage.

Region 1 would correspond to the light tones up to 42.5% black ink coverage, so [0, 0.425] should be printed with the lightest, PGY ink; region 2 with values from 42.5% to 62.5% black ink coverage, i.e. [0.425, 0.625], should be printed with PGY and GY inks, and region 3, between [0.625, 1], with GY and K. At each of these intervals ([0, 0.425], [0.425, 0.624], [0.625, 1]) the specific ink used spans from 0 to 100% ink coverage at that region.

### 3.3 Dot gain compensation

Paper-ink interaction causes dot gain with the result of ink areas appearing darker and larger once printed. In order to rectify this so that the final result (effective ink coverage) has the tone value intended, the nominal ink coverage for each channel has to be adjusted prior to halftoning and printing. In order to do so, the following methodology was performed.

The calculated thresholds were applied in order to multilevel halftone the patches from 0% to 100% ink coverage, with steps of 1%. The bi-level halftoning algorithm was IMCDP. Afterwards the patches were printed using all three inks simultaneously on the two paper substrates at 600 dpi. The resulting Y values of the printed patches allowed us to adjust the initial image for dot gain compensation using Murray-Davies formula. After printing, measurements were conducted to verify whether successful dot gain compensation has been accomplished.

## 4. Results and discussion

Thresholds were located for each of the inks and paper (Figure 2). For the 90 g/m² uncoated paper, it was found that the Y values of fulltone GY matched K at 38%, while the Y values of fulltone PGY matched K at 28%. Therefore, all tones lighter than 28% are reproduced using the PGY ink ranging from 0% to 100% ink coverage. The range between 28% and 38% is reproduced by a mixture of PGY and GY inks and the nominal ink coverage values between 38% and 100% with a mixture of GY and K inks. For the 170 g/m² matte coated paper the Y values for fulltone PGY and GY inks corresponded to the Y values of K at 42.5% coverage for PGY and 62.5% for GY. This strategy makes the transitions between inks very smooth, which was verified by creating a continuous tone grey ramp image from 0% to 100% coverage, shown in Figure 3. Nevertheless, in order for the grey ramp to appear smooth in the printed proceedings, dot gain compensation must be performed for the specific ink and paper used. Since this information is not available, note that the ramp may not appear smooth in a printed manuscript.

*Figure 3: Multilevel halftoned ramp for three achromatic inks*

The dot gain curves for the three inks individually were plotted against the nominal ink coverage values using the Murray-Davies formula (Figure 4).

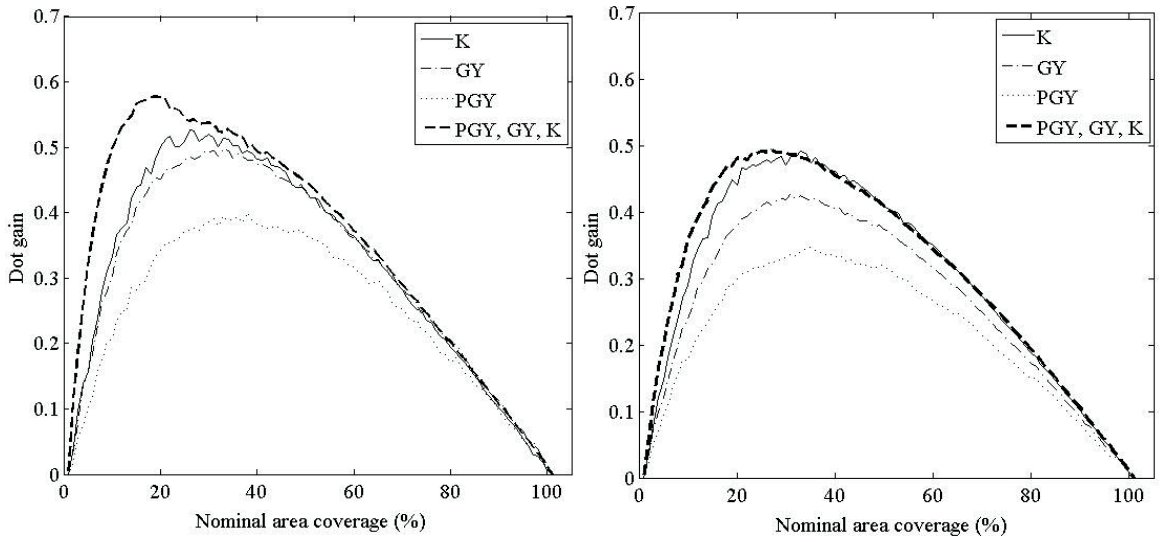


*Figure 4: Dot gain curves for three inks individually and combined, in reference to black, in multilevel halftoning for: (left) uncoated 90 g/m² paper, (right) matte coated 170 g/m² paper*

The calculated thresholds were used to multilevel halftone the patches, print them on both papers and measure them. The dot gain curve of the three inks combined was plotted again and displayed on the same figure.

It can be seen in Figure 4 that the dot gain curves vary from ink to ink and from paper to paper. Each ink has a unique dot gain curve, and it is the three ink combination measurement values that need to be used in order to perform dot gain compensation.

In order to verify the correctness of the dot gain compensation the Y values of the compensated patches were measured. Using Murray-Davies formula the effective area coverages were calculated. If the effective area coverage values are plotted against the nominal area coverage values, the assumption is that they will be the same, thus showing a linear response in the plot. The results are shown in Figure 5 for both papers.

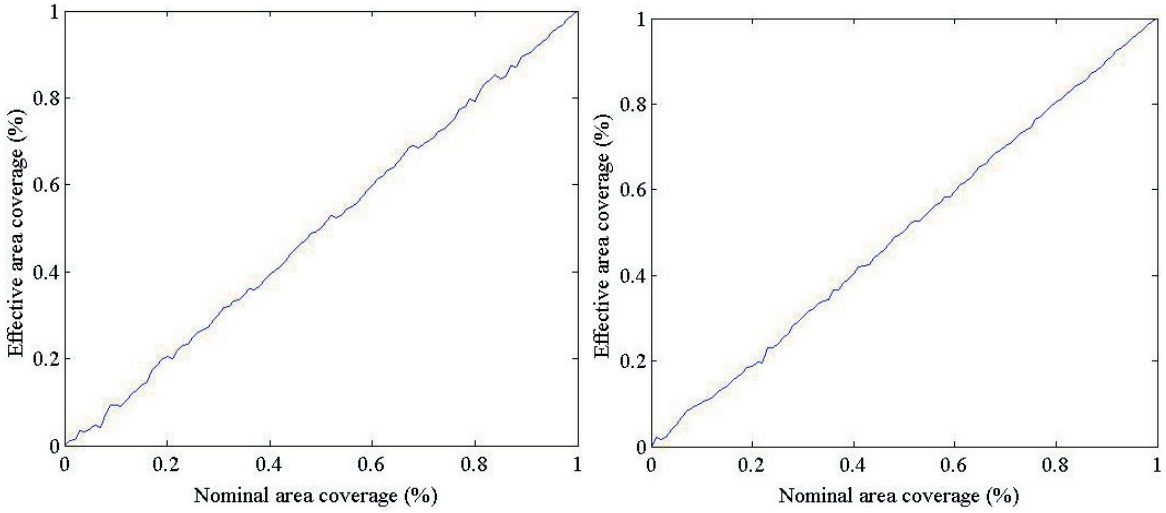


*Figure 5: Effective versus nominal area coverage for the combination of three inks in reference to black in multilevel halftoning, compensated for linear dot gain response for: (left) uncoated 90 g/m2, (right) matte coated 170 g/m2 paper*

As can be seen in Figure 5, the plot of the effective area coverage versus the nominal area coverage is a straight line for both papers, proving a successful dot gain compensation in our workflow.

It has already been mentioned that using three achromatic inks (PGY, GY, K) instead of only one (K) gives the advantage of a less grainy result and therefore visually more pleasant image. In order to illustrate this, a 10% black ink coverage patch was digitally created and halftoned in two different ways - once using only one, black, ink and bi-level halftoning it with IMCDP and the second time using three inks and multilevel halftoning the patch with IMCDP (Figure 6).

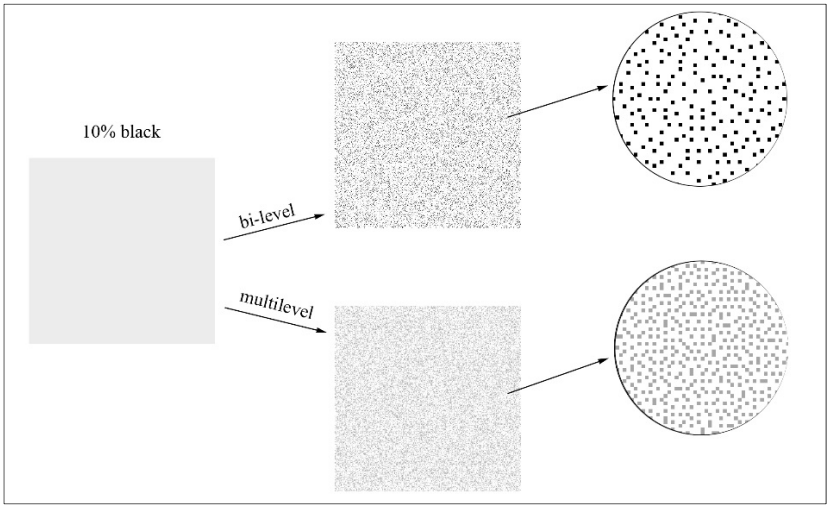


*Figure 6: 10% black ink coverage patch bi-level halftoned (up) and multilevel halftoned (down)*

Note that the patches of Figure 6 are digital representations, not printed results. Therefore, it is likely that on the printed image the overall impression of the halftoned patches differ due to dot gain. Since different inks have different dot gain value, the printed images will most likely appear visually different, since this image has not been compensated for dot gain for any paper-ink setup.

Although both halftoned images have the same mean value of 10% black ink coverage on the digital representation, it can easily be seen that the multilevel halftoned patch (down) shows a less grainy result. This is because while bi-level halftone algorithms default to halftone using a single colorant (in this case K), the multilevel halftone algorithm halftones the patch under the assumption of multiple colorants. For this example, the used setup was three inks and the ink limits found for coated paper, in which 10% black ink coverage corresponds to 10% 1/0.425 = 23.5% PGY ink coverage (Figure 2). The multilevel halftone algorithm then makes use of the PGY ink, with lighter tone than K, and halftones the dots in a denser configuration. Both of these factors account for the fact of a less grainy result, which was also verified by calculating the standard deviation. The standard deviation for the pixel values in the patch bi-level halftoned with IMCDP was 0.3023, while for those of the multilevel halftoning was smaller and equals 0.1815.

Similarly, standard deviation was calculated for digitally produced patches ranging from 1% to 30% black tone value, bi-level halftoned (with IMCDP) and halftoned with the multilevel algorithm. Figure 7 shows the results. It can be seen that the curve indicating the standard deviation of the patches halftoned with the bi-level algorithm is always above the curve of the standard deviation of the multilevel halftoned patches, which proves a less grainy result in the latter case.

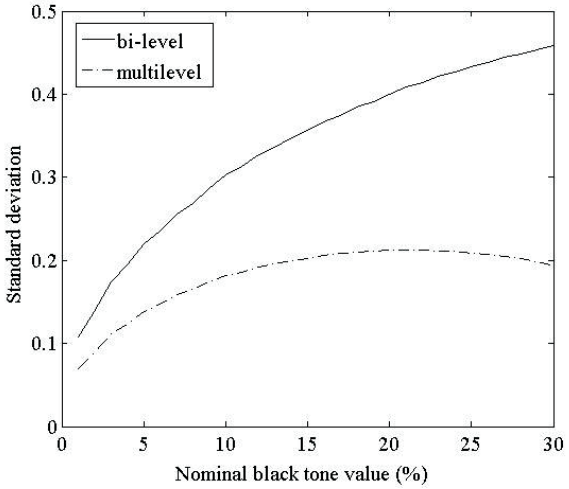


*Figure 7: Standard deviation of pixel values in the patch*

A detail of a digital image was halftoned with the bi-level IMCDP and with the multilevel algorithm at 150 dpi (Figure 8). It is visible not only that the left (bi-level halftoned) image displays more graininess than the right (multilevel halftoned) one, but also that the latter one adds to the level of detail. This higher level of detail can be easily explained by the nature of the multilevel algorithm. Since multiple inks, each ranging from 0% to 100% ink coverage, are to be used to reproduce the image channel, it is obvious that such an image will have a higher detail reproduction than the one being reproduced with only one ink.

*Figure 8: Image detail: (left) bi-level halftoned, (right) multilevel halftoned*

## 5. Conclusions

A multilevel halftoning approach introduced in Gooran (2006) has been implemented in a multi-channel printing setup. The implementation has been done using three different achromatic inks - grey, photo grey and black. Challenges include determining the threshold between each of the ink pairs and achieving a linear dot gain response. Dot gain is ink-specific and it is necessary to calculate a joined dot gain for three different inks in relation to one. Once the initial image has been compensated for a linear dot gain response, the multilevel halftoning algorithm is again applied to the patches, which were then printed and measured. Results of the effective versus nominal area coverage shown in Figure 5 verify that the multilevel halftoning workflow for the printer, inks and substrates used was successfully controlled and can be applied to other frameworks. This means a setup in which multiple inks are used without an ink layer overlap (dot-off-dot impression). In addition, the overall image quality is improved in terms of graininess (verified by measuring the graininess by means of standard deviation) and detail enhancement.

**Acknowledgements**

This work was supported by the Marie Curie Initial Training Networks (ITN) CP7.0 N-290154 funding, which is gratefully acknowledged.

**References**

Gooran, S., 2004. Dependent Color Halftoning, Better Quality with Less Ink. Journal of Imaging Science and Technology, 48(4), pp. 354-362

Gooran, S., 2006. A Novel Hybrid Amplitude Modulated/Frequency Modulated Halftoning Based on Multilevel Halftoning. Journal of Imaging Science and Technology, 50(2), pp. 157-167

Jang I., Son Ch., Park T., Ko K. and Ha Y., 2005. Colorimetric characterization based on color correlation in CMYKGO printer. In: Color Imaging XI: Processing, Hardcopy, and Applications, SPIE-IS&T Electronic Imaging. San Jose, California. Washington: SPIE and Springfield: IS&T

Murray, A., 1936. Monochrome reproduction in photoengraving. Journal of The Franklin Institute-engineering and Applied Mathematics, 221(6), pp. 721-744

Namedanian, M., Coppel, L., Neuman, M., Gooran, S., Edström, P., Kolseth, P., Koh, W., 2013. Analysis of Optical and Physical Dot Gain by Microscale Image Histogram and Modulation Transfer Functions. Journal of Imaging Science and Technology, 57 (2), pp. 20504-1-20504-5(5)

Sharma, G., 2003. Digital Color Imaging Handbook, London et al.: CRC Press

Wyble, D. and Berns, R., 2000. A Critical Review of Spectral Models Applied to Binary Color Printing. Color Research & Application, 25 (1), pp. 4-19

Zeng, H., 2000. Ink limit control for ink-jet printer color calibration. In: Proc. SPIE 4300, Color Imaging: Device-Independent Color, Color Hardcopy, and Graphic Arts VI. San Jose, California, 21 December 2000. Washington: SPIE and Springfield: IS&T

# Colour characheristics of prints printed by oxidative and UV curing inks

*Rozália Szentgyörgyvölgyi*[1], *Erzsébet Novotny*[2], *Pál Görgényi-Tóth*[2]

[1] Óbuda University
Doberdó u. 6.
H-1034 Budapest, Hungary

[2] ANY Security Printing Company
Halom u. 5.
H-1102 Budapest, Hungary

E-mails: szentgyorgyvolgyi.rozsa@rkk.uni-obuda.hu;
novotny@any.hu; jones.gtp@gmail.com

**Abstract**

For prints of stamps, the quality of printing is especially important, so that they represent proper aesthetic value. In addition to their aesthetic value, it is also important that the original colour or colour effect of the printed image or graphics should be retained for the longest possible period of time. Postage stamps are usually printed by using oxidative inks, but because of the special elements that may be present on stamps issued for a special occasions, this type of stamps is printed by using UV technology. However it is important that the two technologies should result in the same print quality.

The purpose of the research work was to examine and assess the aesthetic and usability features of prints printed on stamp papers having different surface properties by using oxidative and UV curing inks. Optical densities and the tone value increase on of the cmyk prints were determined by densitometric measurements. Based on results of spectrophotometric measurements, qualities of cmyk and rgb prints were characterized by colour gamut and ΔEab* colour differences. Furthermore, quality changes that occur by the effect of accelerated aging of prints prepared in stamp papers were also examined. Our goal was to examine which of the two inks systems is better in achieving colour uniformity for longer period after printing and whether there are methods available that are suitable for improving surface uniformity of the ink layers forming the stamp image and can be used in the industrial practice.

**Keywords**: printed stamp, oxidative ink, UV curing ink, accelerated aging

## 1. Introduction

Postage stamps, as means of monetary substitute used for prepaying mails have been part of the mail handling technology for one and a half century. Due to their aesthetic values, their collection started almost simultaneously with their appearances. Meeting the requirements of mail handling and of the stamp-collectors - potential stamp buyers who examines the stamps under magnifier and do not even require any postal service - has a significant role in establishing the methods of issuing postage stamps. Any difference from the proven stamp manufacturing technologies that were applied earlier with good results does occur only if the change provides additional quality improvement for both sides. Stamps are prepared by using different types of printing procedures. Offset printing has also been among these methods for decades.

In the last few years it has been possible to use UV curing inks in addition to the inks fixed by oxidation and penetration processes. Due to their different components and fixation mechanisms, these two types of printing ink provide print images having different colour intensity and surface structure. In spite of the fact that the use of UV curing inks makes it possible to process the prints further almost immediately and by this the time of the manufacturing cycle can be shortened, the too intense colours that are considered as ones not matching this classic product and the unevenness of the print that can be seen under a magnifier causes nowadays some aversion among stamp collectors (Lapin, Lundal, 2011), (Novotny at al., 2011).

The goal of our tests included determining the colour differences between prints prepared by using different types of ink, analysing the topology of printed images and making proposals for reducing the evenness, colour rendition and uniformity problems that occur on the criticized printed image when the new technology is applied in stamp manufacturing. When exposing the prints to accelerated aging, additional information can be gained on the colour changes and the possible changes in the surface features of the prints (Borbély at al., 2012) (Havlinová at al., 2002) (Karlovits at al., 2011).

## 2. Methods

Test prints were prepared on coated (Paper 1) and uncoated (Paper 2) stamp papers (Table 1) under operating conditions. They were printed by using oxidative ink and UV curing ink on small offset printing machines of Heidelberg Printmaster 52-4 and Heidelberg Speedmaster GTO 52-4+L type, respectively. Ink coverage was adjusted in accordance with the recommendation specified in the Standard No ISO 12647-2 (coated stamp paper: DC=1.55, DM=1.5, DY=1.45, DK=1.85; un-coated stamp paper: DC=1.00, DM=0.95, DY=0.95, DK=1.25). Test image was designed by taking into consideration the characteristics of the test chamber used for laboratory accelerated aging of the prints (Figure 1).

In order to compare the quality of the prints, optical properties of the test prints prepared by using the two different technologies were examined. In the next phase of the study, an artificial aging test of the two stamp papers (Paper 2 and Paper 3) was carried out for the purpose of testing their resistance to filtered sunshine. After 144-hour period of artificial aging optical density and color tri-stimulus values were measured. During the artificial aging examination, test prints prepared with oxidative and UV curing inks were irradiated in laboratory equipment designed for artificial aging. Equipment of Atlas Suntest XLS+ type was used by applying Method B6 specified in the Standard ISO 4892-2 without wetting. Radiation intensity was 45 $W m^{-2}$ in the 300 nm - 400 nm range. During the test, temperature of the test chamber was in the range of 24 °C - 65 °C. The test lasted 144 hours during which the samples received a radiation of approximately 23 328 $KJ m^{-2}$.


*Figure 1: Test image 1 - color control patches of CMYK and RGB colours, 2 - 400 patch test chart for gamut sampling, 3 - different lines, 4 - letters in different sizes*

*Table 1: Basic features of the papers*

| *Feature* | *Paper 1* | *Paper 2* |
|---|---|---|
| *Type* | *TROPIMATIC ST SM 110* | *HP. Nr. 157 126* |
| *Grammage, g/m2* | *90±4.5* | *100±2* |
| *Characteristic* | *glossy stamp-paper* | *matt stamp-paper* |

## 3. Results and discussion

During the densitometry measurements it was observed that in spite of the fact that identical ink coverage had been set, density of the prints prepared with oxidative inks were lower (Table 2). This is the result of the different drying mechanisms of the two types of ink. UV curing inks are fixed on the prints almost immediately as opposite to the oxidative offset inks that are drying by penetration, where longer period of time is needed for the final drying.

*Table 2: Measured optical density values of CMYK process colors on substrates printed with both inks*

| Paper | Optical density, D | | | | | | | |
|---|---|---|---|---|---|---|---|---|
| | oxidative ink | | | | UV curing ink | | | |
| | C | M | Y | K | C | M | Y | K |
| 1 | 1.47 | 1.55 | 1.19 | 1.45 | 1.58 | 1.55 | 1.42 | 1.87 |
| 2 | 1.00 | 1.12 | 1.03 | 1.17 | 1.49 | 1.43 | 1.30 | 1.74 |

Determination of colour differences between prints prepared on the same papers by the two different types of ink was based on colour differences. In Figure 2, ΔE*ab was calculated by using the corrected formula of CIE published in 2000. In spite of the fact that this calculation method resulted in lower values, colour differences exceeded the limit values for each colour.

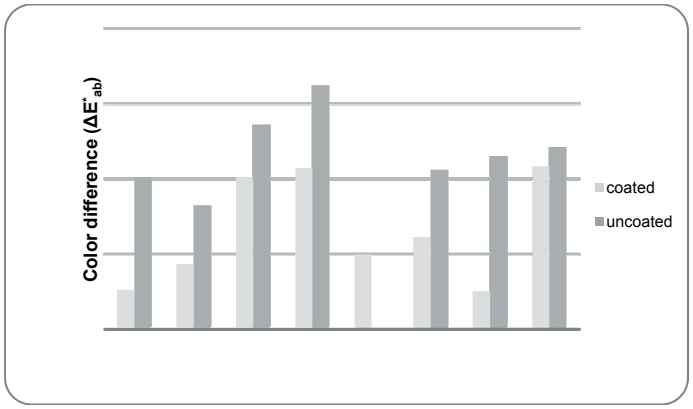


*Figure 2: Colour differences on prints prepared on coated and uncoated stamp papers by using oxidative and UV curing inks*

At these products, colour changes (fading) might be caused by ambient factors, primarily UV radiation that is a part of sunshine. Fading of the prints was characterized by determining colour differences (ΔE*ab) and colour gamuts. The L* a* b* values measured without irradiation were considered as reference standards (Figure 3).

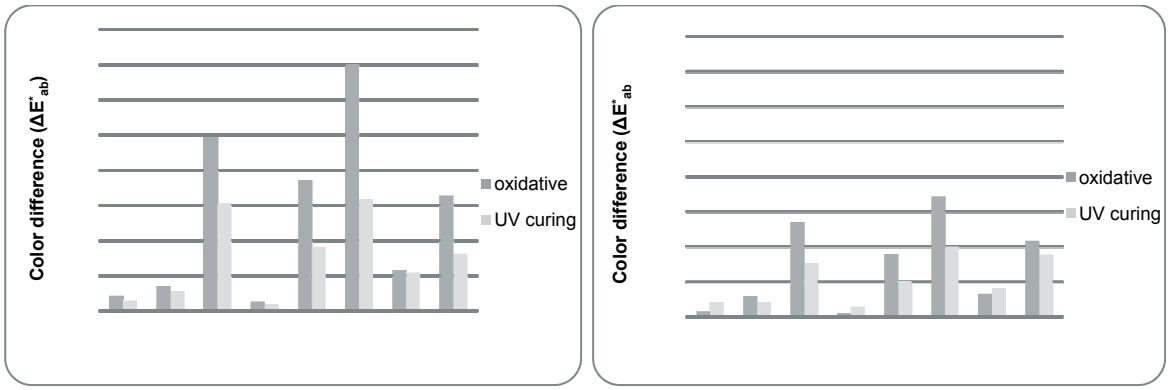


*Figure 3: Colour differences measured on prints by using oxidative and UV curing inks after irradiation lasting 144 hours (left: coated paper; right: uncoated paper)*

When the visual inspection of the prints exposed to radiation was performed, their fading was already observed. Results of the measurements showed that yellow prints were the most sensitive to irradiation (Figure 4). No colour difference was detected during the measurements on black prints even after irradiation lasting 144 hours. The lowest changes were observed on prints prepared on uncoated papers with UV curing inks. Colours that can be detected by human eyes can be depicted in a coordinate system, characterized by three data. The resulted figure is the colour body (gamut) that were depicted in the equipment-independent CIE L* a* b* colour space. An X-Rite Eye-One IO scanning table and software preparing I1 match profiles were used for the measurements. Volumes of colour bodies (gamut) of the prints prepared on coated and uncoated stamp papers by using oxidative and UV curing inks were measured and assessed. The largest and the lowest reproducible colour ranges were measured on prints prepared on coated stamp paper with UV curing ink and on prints prepared on uncoated stamp paper with oxidative ink, respectively (Table 3).

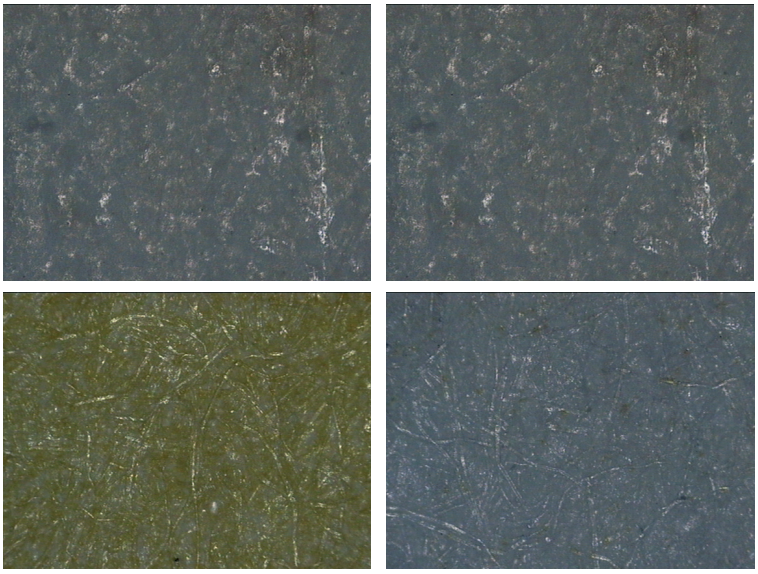

*Figure 4: Magnified 70% yellow sample measured on coated and uncoated paper using oxidative inks (upper: coated paper, lower: uncoated; left: 0 h, right: after 144 h)*

As a result of the 144 h long irradiation, 26-70% gamut reduction was observed on the examined prints (Table 3).

*Table 3: Colour gamut volumes in (rel.) units of measure relative to the maximum value (1)*

| Paper | Colour gamut volumes in (rel.) units | |
|---|---|---|
| | Oxidative ink | UV curing ink |
| Coated paper | 0.95 | 1.00 |
| Uncoated paper | 0.50 | 0.71 |

The largest and the lowest gamut changes were measured on prints prepared on coated stamp paper with oxidative ink and on prints prepared on un-coated stamp paper with UV curing ink, respectively (Figure 5).

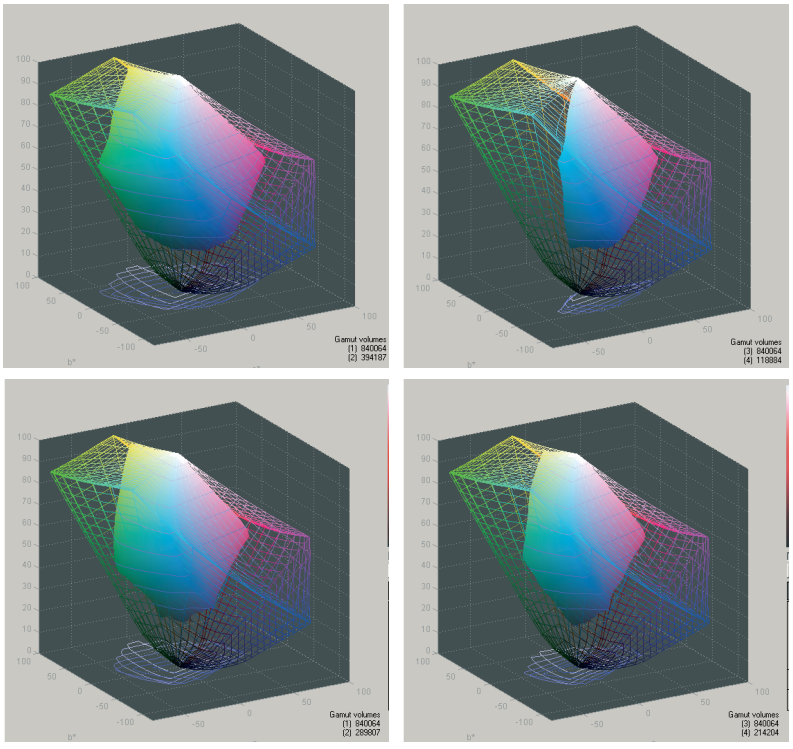

*Figure 5: Colour gamut changes in the CIELAB colour space (upper: the largest decrease, coated paper,oxidative ink, lower: the lowest decrease, uncoated paper, UV curing ink; left: 0 h; right: 144 h)*

*Table 4: Colour gamut changes (⊿) in absolute units of measure*

| Paper | Colour gamut in absolute units of measure | | | | | |
|---|---|---|---|---|---|---|
| | Oxidative ink | | | UV curing ink | | |
| | 0 h | 144 h | Δ | 0 h | 144 h | Δ |
| Coated paper | 394 187 | 118 884 | 70% | 413 373 | 244 494 | 45% |
| Uncoated paper | 205 092 | 106 164 | 48% | 289 807 | 214 204 | 26% |

## 4. Conclusions

Qualities and colour changes occurring after 144 hours of irradiation were examined on prints printed on coated and uncoated stamp papers with two types (oxidative and UV curing) of ink. The largest change that occurred by the effect of 144 hours of irradiation was observed on yellow coloured prints. During the further tests, reproducible colour ranges of the prints and the changes of these ranges that occurred by the effect of 144 hours of irradiation were analysed in an Atlas Suntest XLS+ equipment. Significant gamut volume reduction was measured on the examined prints extent of which was lower on prints prepared by using UV curing inks.

As a result of our examinations, it was established that the uncoated stamp paper used for manufacturing standard stamps being on the market shows less colour changes as a result of aging and this fact partially makes the insistence of the users on this technology reasonable. However, in case of manufacturing special stamps, when stamps printed on coated paper are issued for a specific event or anniversary, it is reasonable to use UV curing inks. In case of coated papers, the colour differences occurring by the effect of the irradiation are the lowest if they stamps are printed with UV curing inks. Aesthetic value of the surface of the UV printed stamp image can be improved by using a thinner ink layer. In this case ink spreads to a lesser extent on the surface during the fixation process and the general colour stimulus gets nearer to the expectations of the users. This can be examined by several test printing and colour management application.

By evaluating the results of the measurements we have gained valuable experience that can be used in the industrial practice and we have made make recommendations for the fields of application of both the oxidative and UV curing inks.

**References**

Borbély, Á., Horváth, Cs., Szentgyörgyvölgyi, R., (2012): Accelerated light aging of digital prints, 39th Research Conference of IARIGAI, Ljubljana, 10-12. 09. 2012, Advances in printing and Media Technology, Vol. XXXIX, pp. 117-122 ISBN 978-3-9812704-5-7

Havlinová, B., Babiaková, D., Brezová, V., Ďurovič, M., Novotná, M., Belányi, F. (2002) The stability of offset inks on paper upon ageing. Dyes and Pigments, Volume 54, Issue 2, Pages 173–188 ISSN: 0143-7208

Karlovits, M., Gregor-Svetec, D. (2011): Comparision of Between UV Inkjet And Conventional Offset Prints Exposed to Accelerated Ageing. Jurnal of Graphic Engineering and Designe, Volume 2. 2011 ISSN 2217-379X, pp.10-15

Lapin, S. C., Lundahl, S. (2011): Dual UV/EB Curing of Printing Inks

http://radtech.org/RTReport_pdfs/dual_uveb_curing_of_printing_inks_summer2011. pdf accessed: 24. 06. 2014.

Novotny, E., Szentgyörgyvölgyi, R., Görgényi-Tóth, P. (2011): Colour effect changes at security graphics due to print media and colour sequence. 38th Research Conference of IARIGAI, Budapest-Debrecen, 11-14 September 2011, pp. 309-317, ISBN978-3-9812704-3-3

# An empirical approach to predict the working-range of contrast-sensors in terms of inline spectral measurement systems

*Daniel Bohn*[1], *Michael Dattner*[2], *Arne Böttger*[2]

[1] Bergische Universität Wuppertal
Rainer Gruenter Straße 21
D-42119 Wuppertal
Germany
E-mails: dbohn@uni-wuppertal.de; a.boettger@uni-wuppertal.de

[2] BST-International GmbH
Heidsieker Heide 53
D-33739 Bielefeld
Germany
E-mail: michael.dattner@bst-international.com

**Abstract**

Contrast-sensors provide the possibility to measure contrast-changes. These measurements result in digital output signal patterns. Typical contrast-sensors for the print-industry can be teached manually to a current color-substrate-combination. This single contrast change can now be recognized with a very high accuracy. In practice, the actual contrast-change can differ to the teached one. Therefore it is important to know how much a teached contrast can differ to the actual one until the searched pattern is not recognized anymore. This is also called working-range of contrast-sensors.

Furthermore, in some cases the sensor is not accessible by the operator. In this case it is necessary to store as less as possible color-substrate-combinations in the sensor (but enough to ensure that all possible contrast-changes are recognized) before installing the system in the machine.

Examining this topic on a spectral scale leads to clear relations and a prediction-approach. Down-sampling this to an RGB-approach utilizes this topic for industrial usage. The narrow-banded (RGB-) illumination of the examined contrast-sensor shows a comparable emission as typical RGB-based camera-systems show in their sensitivity.

Within this paper it is proofed that cyan, magenta and yellow are the three colors that are relevant in terms of practicability. Teaching each color in three different lightness-levels, enables a consistent and reproducible setting of all needed sensor-parameters for the recognition of contrast marks printed in nearly arbitrary colors out of a large color gamut.

Identifying the right (pre-stored) teaching of the sensor is done by analyzing the differences between the absorption of the substrate and the mark-color, or (for the RGB-approach) identifying the lowest value of all three RGB-values to focus on the right storage-range, respectively.

**Keywords**: contrast-sensor, contrast-mark, inline-spectral-measurement, signal-analysis

## 1. Introduction and background

The demand for high quality prints is rising constantly in the print- and media industry. Since the days of new basic printing principles are gone and existing printing technologies such as gravure printing or flexography printing have become easily manageable, the industry is seeking for new ways to further improve print-quality while reducing costs. This development is illustrated in Figure 1.

One key variant for a further improvement of print quality is automation [Huebler11]. Automation enables the possibility to enhance as well as document color stability by using inline spectral measurement systems [Dattner11]. By using this method, it becomes possible to measure and document permanently different positions on a rapport without stopping the printing-press.

Compared to offline spectral measurement devices (handheld spectral photometers), inline spectral measurement systems are far more challenging in their construction. Numerous circumstances need to be taken into account to ensure not only a high measurement frequency, but also a high measurement reproducibility [Dattner11].

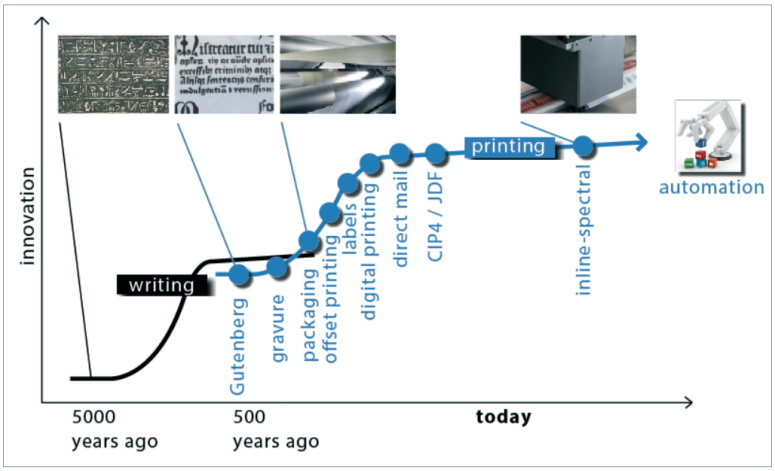


*Figure 1: The past and future evolution of the printing technology*

To outline the basic challenges of inline spectral measurement system in general and to emphasize the purpose of this paper it is important to take the following circumstances into account:

I. Typical color patches on a print control strips are limited to a maximum size of 5x5mm
II. The illumination spot of a typical illumination of a spectral measurement device is 2-4mm in diameter [DIN00]
III. The web moves with a top speed of 1 000 m/min (y-axis).

Figure 2 illustrates that a 4 mm illumination spot barely fits in a 5x5mm patch. The combination of I & II is not a chal-lenge for handheld devices since there is no time limitation to find the right and adequate position for measurement. This also implies that the time to illuminate the sample is virtually not limited (In practice 100 - 500 ms depending on the purpose and the used measurement geometry).

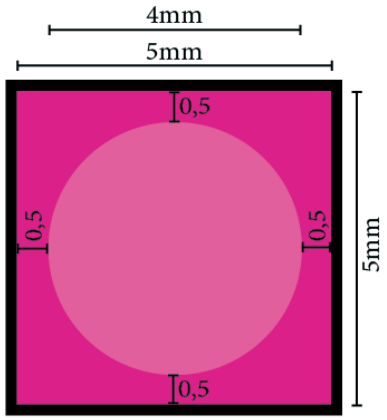


*Figure 2: Illustration of a 5x5mm patch, illuminated by a 4x4mm spot*

III in combination with I and II on the other hand side leads to two serious issues:

1. Because the web moves with a speed of up to 1 000 m/min the exact point of time needs be determined at which the measurement has to be executed
2. Because of I, II and III the available time to illuminate and measure the target is reduced to less than 10 ms.

Additional influences that raise a need for very close-time data about the position to be measured are listed below:

I. The web is moving on the x-axis
II. The web can be stretched

In practice, it is not a solution to ask the customer for different print control strips with a size larger then 5 x 5 mm to overcome these issues. This is especially true for gravure printing because typical printform-cylinders already have 5 x 5 mm patches and a lifecycle that is several years long [Veith08].

Because of these parameters a real-time positioning-solution is required. One option is to make use of an "RGB-Contrast-Sensor". These sensors are able to identify contrast-changes at high frequencies.

This type of sensor in combination with a known contrast-mark-(signal)-pattern on each rapport makes it possible, to precisely identify when a new rapport starts and where the color-patch of interest is located relative to this mark (c.f. Figure 3).

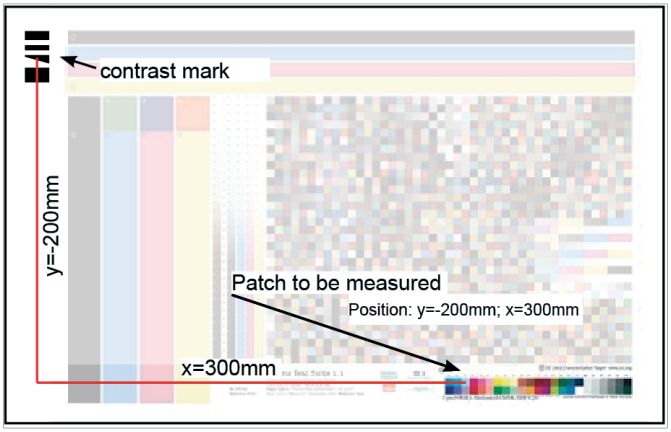


*Figure 3: Example of a typical rapport with a contrast mark and a patch to be measured*

## 2. State of the scientific knowledge

*Remark: Below a simplified contrast-mark is used for simplification reasons. The actual contrast-mark possesses a slanting element to identify the x-movement of the web.*

The relating output signal for the contrast mark shown in figure 3 (left) is illustrated in figure 3 (right). Obviously a perfect contrast is given for black and white. This signal pattern makes it possible to check, if it fits to another known mark pattern.

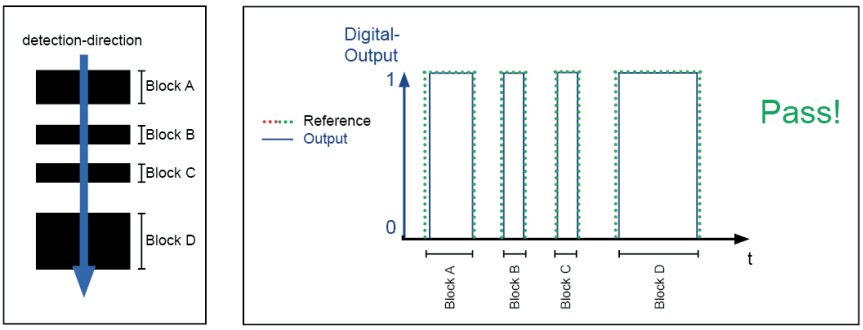


*Figure 4: Illustration of a contrast-mark and the corresponding detection-direction (left). Illustration of the corresponding input-output signals (right)*

Only if the known reference pattern and the actual measured pattern fit together (within predefined tolerances), the mark is recognized and accepted (c.f. Figure 4). If the pattern does not fit the mark, it is not recognized and therefore not accepted (c.f. Figure 5).

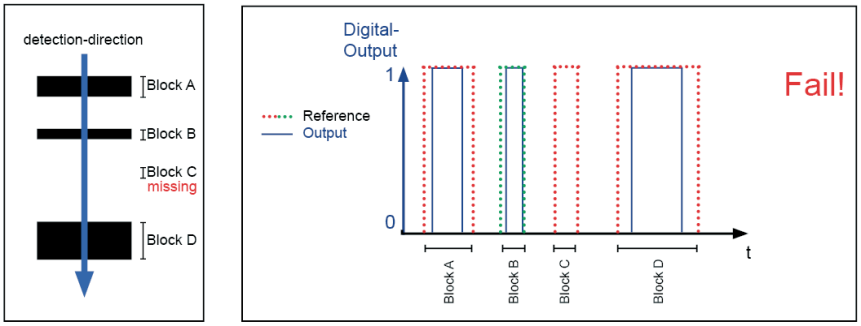


*Figure 5: Inaccurate printed mark-pattern (left). Corresponding, not accepted signal pattern (right)*

On top of that, the intensity of the signal is relevant for the output-pattern: only if the intensity is above the signal-threshold an output-signal is generated. Figure 6 shows the analog signal, the corresponding digital output (concerning the current signal-threshold) and the resulting output signal, which is out of tolerance even if the mark is printed in the correct manner.

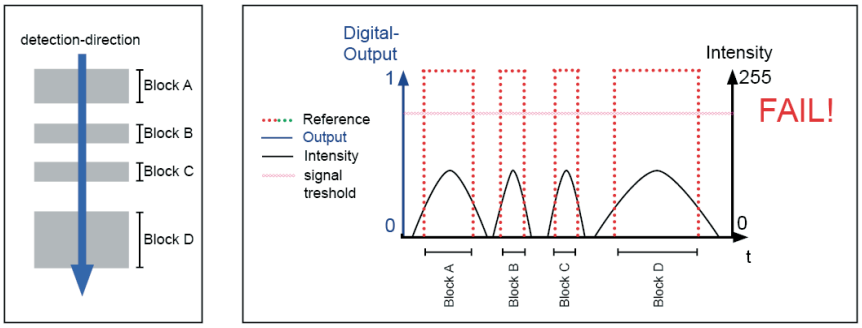


*Figure 1: Contrast-mark with a 30% pigmentation (left). Corresponding, not accepted signal pattern (right)*

In this case the signal-threshold is very high. Even that the contrast-mark in this example is printed correctly in its dimensions, it does not generate an analog signal that is strong enough to get an digital output-signal because of its color (in this example 30% black pigmentation).

Reducing the signal-threshold leads to an accepted output-signal for mark recognition (Figure 7).

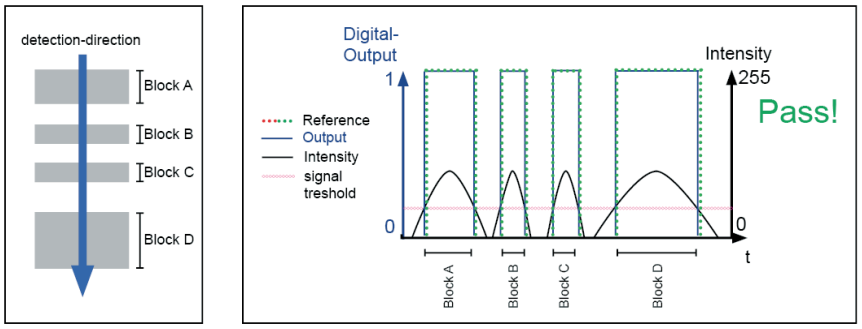


*Figure 7: Contrast-mark pattern with a 30% black pigmentation (left). Corresponding signal pattern with an adjusted signal-threshold-level (right)*

Because of the individual nature of each print-job, it is not possible to fix the color of the mark to e.g. black or gray-tones. It can be printed in any, arbitrary unknown color. Therefore an RGB-contrast-sensor is used, which is very sensitive concerning most colors.

Hence, the purpose of this paper is to build up an (empirical) model that predicts, that teached signal-thresholds (concerning one of the LEDs) enable the recognition of the current, individually colored contrast-mark. The approach starts with contrast-mark-colors with a known spectral response and ends up with a derived RGB-approach that does not rely on spectral measurements anymore.

## 3. Methodology

For the scientific investigation of this paper a special RGB-contrast-sensor of Leuze electronic GmbH + Co. KG is used. This sensor uses three LEDs (Red, Green & Blue) and 127 memory cells for saving individual contrasts (signal-thresholds). If the device is set to "Teach mode" this sensor automatically searches for the maximum contrast (strongest absorption vs. lowest absorption) between the substrate and the mark-color by using the red, green or blue LED. After that the sensor chooses the appro-priate LED with the corresponding signal-threshold. This special RGB-contrast-sensor is illustrated in figure 8.

*Figure 8: RGB-contrast-sensor of the Leuze electronic GmbH + Co. KG*

This sensor is implemented in an (test) inline spectral measurement system of the company BST-International GmbH. The sensor just recognizes if a chosen signal-threshold is reached and accordingly generates a digital-output-signal. Afterwards the generated signal needs to be analyzed and compared with a known signal-pattern. This signal-analysis-software (special version of BST-Internationals QCenter-Spectral) is also provided by BST-International GmbH.

In the first step test specific contrast marks are printed in numerous colors on a white substrate. In the next step tests are conducted to gain information at which point the contrast sensor is not able to recognize a contrast-change anymore. One example for a used test chart is shown in Figure 9. The colors are printed using an EPSON SpectroProof 4900 proof printer with a very high resolution of 2880 x 1440 dpi. This enables the simulation of solid printed contrast marks.

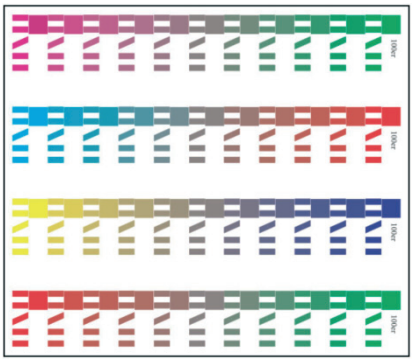

*Figure 9:*
*Testchart featuring a typical contrast-mark and corresponding areas for spectral measurements.*

In a second step the substrate is taken into account. Therefore each of the 500 differently colored contrast-marks is printed upon 16 different substrates (c.f. Figure 11). A brief overview about the used materials by illustrating the individual spectral response concerning black backing (to make sure that transparent and semi-transparent substrates can be distinguished from white substrates) gives figure 10. Figure 11 shows the corresponding full testchart.

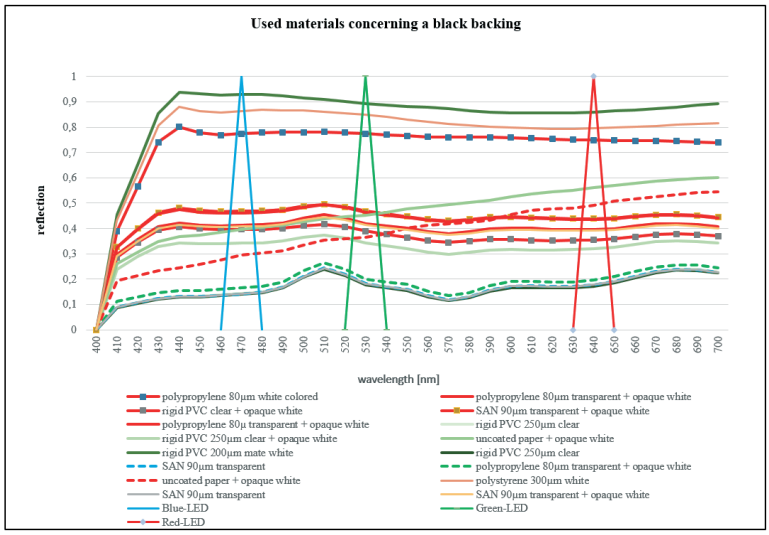


*Figure 10:*
*Spectral response of the used materials concerning a black backing*

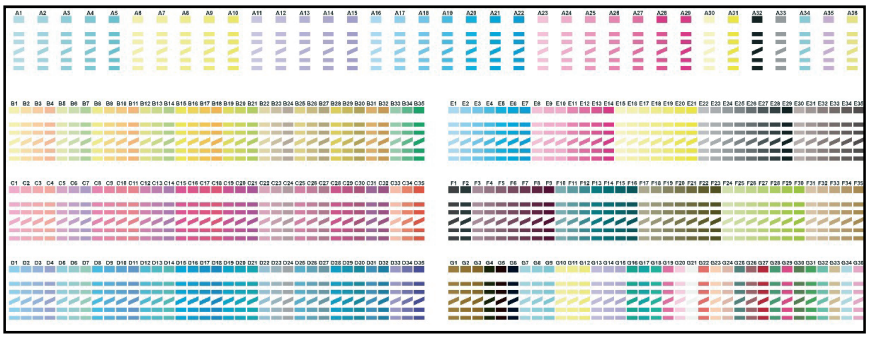

*Figure 11: Overview of the actual test chart that is printed upon each substrate*

## 4. Results

In the first part of this chapter, relevant variables are pointed out and discussed with respect to their influence on the prediction whether a contrast-mark is being recognized or not. This part is required for setting-up the actual model.

The second part of this chapter describes the actual empirical model on a spectral scale.

The third part of this chapter describes a praxis orientated reduction of the spectral model to an RGB-basis.

### 4.1 Variables for setting-up the model

*Emission wavelengths of the used LEDs (RGB)*

LEDs are typically narrowband light sources [Ohno04]. Therefore, it is essential to determine the spectral power-distribution of the used LEDs. An UV-VIS-spectrophotometer, with a very high resolution, (1nm) is used to gain this information. Figure 12 shows the emission behavior of all three LEDs:

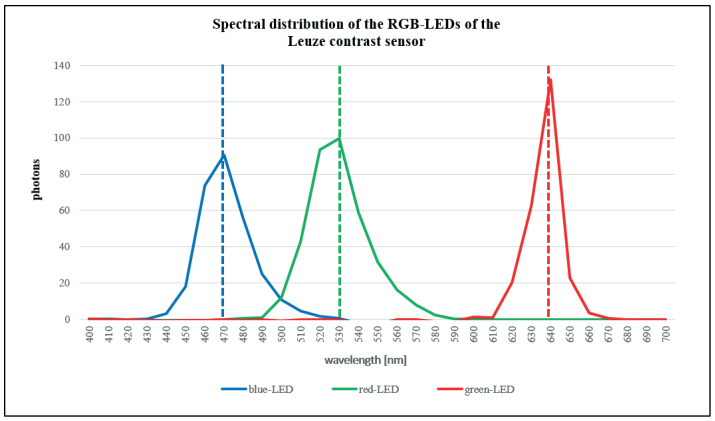


*Figure 12: Spectral distribution of the RGB-LEDs of the Leuze contrast-sensor*

Because of the narrow banded nature of the used LEDs it is not possible to calculate the relative spectral power distribution. Therefore, only the wavelength of the maximum emission of each LED is taken into account:

- Blue LED: 470 nm
- Green LED: 530 nm
- Red LED: 640 nm

Note: Figure 12 gives no absolute information concerning the intensities compared to each other because of unavoidable orientation differences between the LEDs and the measurement aperture. With this information and the spectral response of a contrast-mark, it becomes recognizable why the red, green or blue LED is chosen by the sensor (cf. Figure 13).

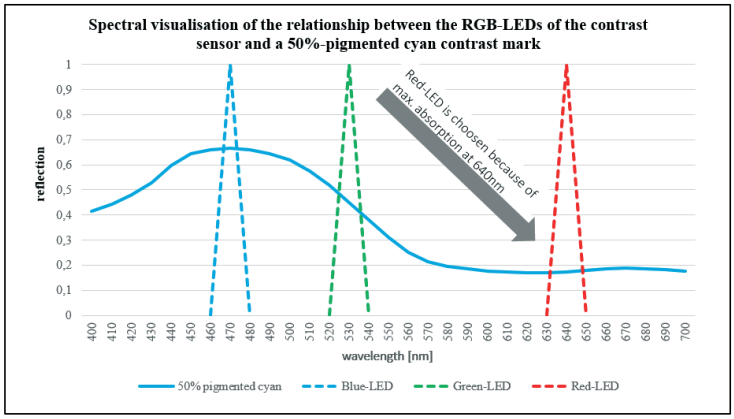


*Figure 13: Spectral visualization of the relationship between the RGB-LEDs and a 50%.pigmented cyan-contrast-mark*

Figure 13 shows the spectral response of a 50% pigmented light cyan. All three LED-peaks are included in this figure (c.f. Figure 12). Because cyan shows for the wavelengths of interest (470 nm, 530 nm and 640 nm) at 640 nm the strongest absorption (compared to a white substrate), the red LED is chosen by the sensor. Further tests prove this relationship also among the other LEDs.

*Teachlimit (Minimum absorption between substrate and contrast-mark)*

It is important to know the minimum absorption difference between the teach-color and the corresponding substrate, which the sensor is able to differentiate with a high certainty. This relationship is illustrated in Figure 14.

Figure 14 shows that a minimum absorption difference of 24% is required to ensure that a specific contrast-level is teachable at all. In this example a 30% pigmented cyan is required to achieve this, whereby a 10% pigmented cyan results in a too low contrast-level difference.

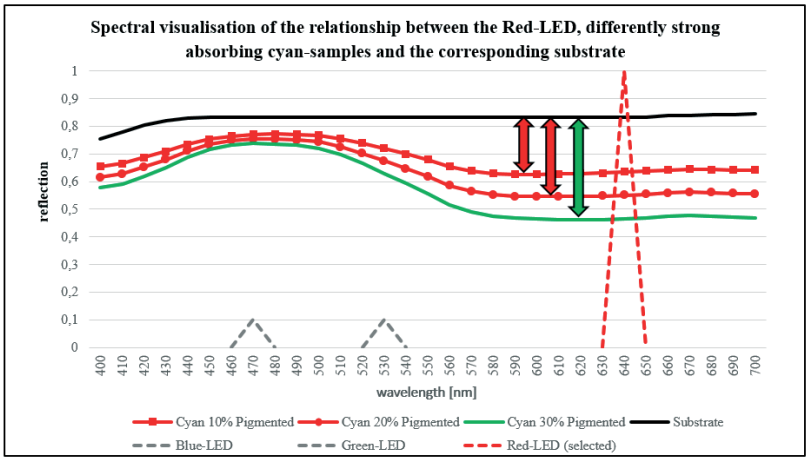


*Figure 14: Spectral visualization between the red-LED, differently strong absorbing cyan-samples and the corresponding substrate*

*Teachconsistency*

For the model as well as for practical purposes it is necessary to exactly know which LED is being chosen by the sensor. Figure 15 shows an example of a teach-color that leads to an uncertainty which LED is chosen by the sensor.

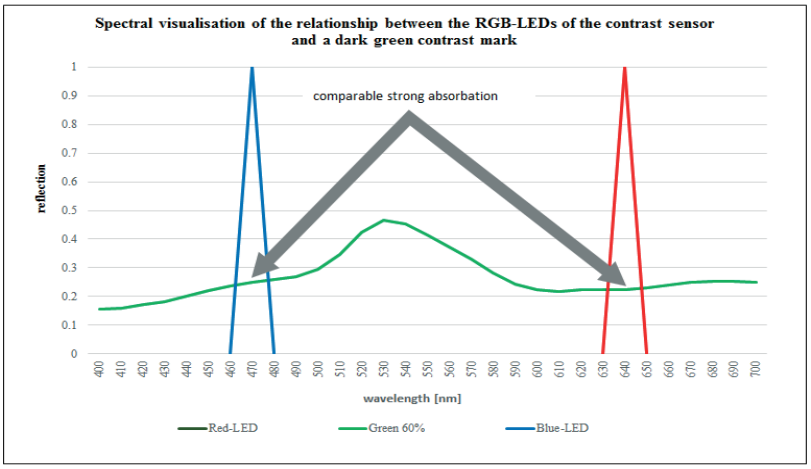


*Figure 15: Spectral visualization of the relationship between the RGB-LEDs (blue and red) of the contrast sensor and a dark green contrast mark*

Figure 15 shows that the spectral response of green is comparable for the wavelengths of the blue and the red LED (470 nm = 0.08 remission, 640 nm = 0.05 remission). A practical test shows that this small absorption difference is not large enough to ensure that the same LED is chosen by the sensor in each case. Hence, it is important to only choose teach-colors that have a definite maximum absorption at one of the above mentioned wavelengths of interest. If this factor is ignored it cannot be ensured that different contrast sensors, that are teached with this teach-color, lead to the same results while using the system in production.

The actual minimum difference to ensure that a definite LED is chosen, is determined by making use of colors that show at a certain area coverage a comparable absorption for two LEDs (c.f. Figure 15). If the lightness of the color is decreased by changing the area coverage, the absorption difference at the wavelength of interest accordingly decreases.


*Figure 16: Example of a typical test chart to test the teachconsistency*

Figure 16 shows a test chart (green) that is used to determine the minimum needed absorption difference for the blue and the red LED. The corresponding spectral response is illustrated in figure 17. In this figure the color "red" indicates that out of ten teach-tests, in one or more cases the LED choosing was not consistent. The right side of figure 17 shows the absorption difference at the wavelengths 470 nm and 640 nm.

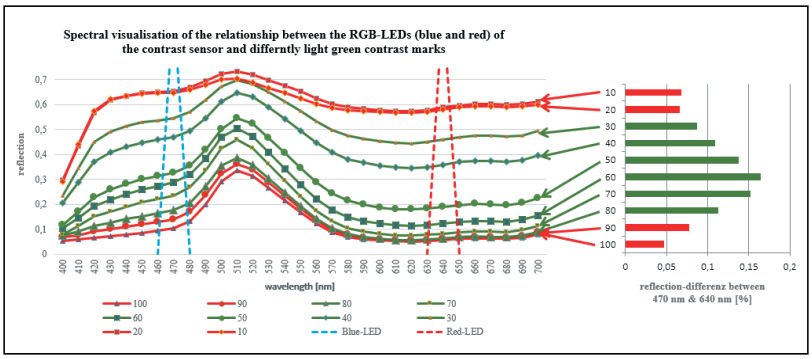


*Figure 17: Spectral visualization of the relationship between the RGB-LEDs of the contrast sensor and a dark green contrast mark (left). Reflection-difference between 470nm & 640nm (right)*

Below an absorption difference of 0.078 an uncertainty whether one and the same LED is selected in each case of not (red marked). Above an absorption difference of 0.011 the LED-selection by the sensor is consistent (green marked). This shows also that a green mark can be recognized in a comparable accuracy by using the blue or the red LED.

*Possible contrast-range below the teach contrast*

Figure 18 and Figure 19 show in combination the capability of the sensor to recognize contrast-changes that are minor than the actual teached contrast. Therefore, several different colors are tested, that show a stronger reflection, and therefore a lower contrast to the white substrate, at 640nm compared to the actual teached color.

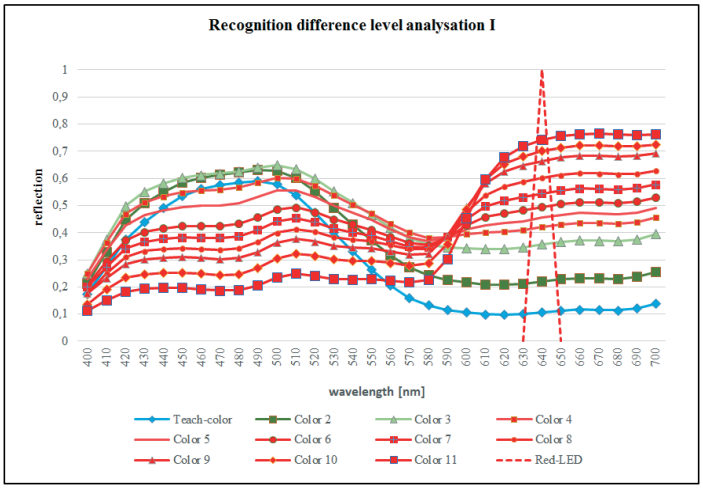


*Figure 18: Visualization of the recognition-range of the red-LED if the actual contrast is lower than the original one I*

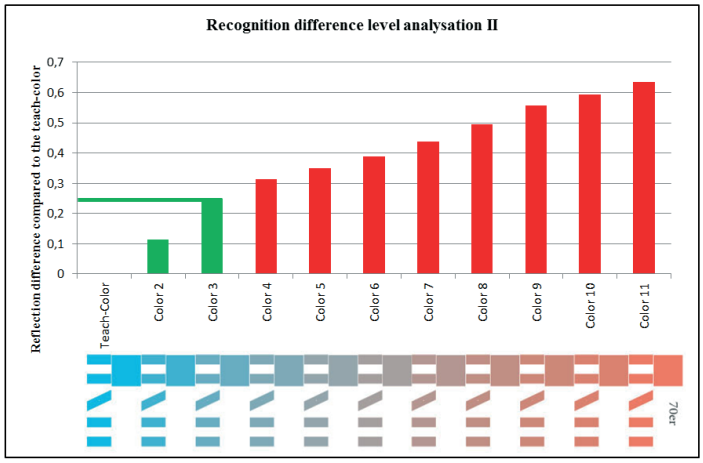


*Figure 19: Visualization of the recognition-range of the red-LED if the actual contrast is lower than the original one II*

In this example contrast-marks with the color "color 2" and "color 3" are recognized by the sensor (up to 28 % absorption difference). The colors 4 to 11, with a higher difference, are not recognized. This way it can be determined how large an absorption difference can get until a corresponding colored contrast-mark is not recognized anymore for each LED.

This test has been carried out for numerous different colored contrast-marks (1 000+). The LED-individual bottom-up reachable absorption difference is shown in table 1.

*Table 1: Possible bottom-up reflection difference [%]*

| LED-color | Possible bottom-up Reflection difference [%] |
|---|---|
| Red | + 24.05 |
| Green | + 20.63 |
| Blue | + 19.88 |

*Possible contrast-range above the teach contrast (less contrast between substrate and mark-color)*

In contrast to the fixed values for the working range of the contrast-sensor for lower absorptions, this limitation is not applicable if the signal threshold is very low right from the start. This variant is illustrated in figure 20.

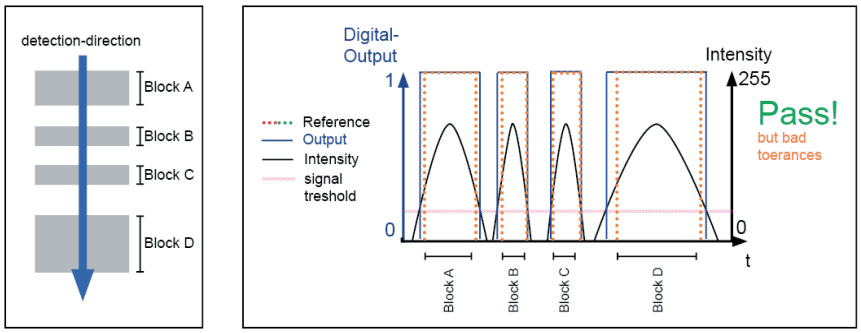


*Figure 20: Illustration of the sensor-behavior if the teached contrast is low and other contrasts are higher in comparison*

As you can see, numerous different signal intensities lead to many different possible digital output signals. The more the teached signal threshold differs to the signal threshold the sensor is teached to (if the current contrast would be actually teached), the more are the occurring tolerances growing (between the reference pattern and the output-signal).

The reason for this behavior is the fact that the sensor integrates across the whole illuminated spot: If a black-white-contrast moves into the illuminated spot, a very low stored signal threshold (for an e.g. gray-white-contrast) is reached far too early. The digital output and therefore the pattern-recognition (with the corresponding tolerances) are affected. In this case there is no maximum acceptable absorption difference for the contrast-identification. The only limitations are the occurring growing tolerances in mark recognition (pattern-size).

## 6. The actual model

The empirical determined limits ΔR for each LED concerning one test substrate are:

ΔR_RED_LED: +24.05
ΔR_GREEN_LED: +20.63
ΔR_BLUE_LED: +19.88

This ΔR is the difference between the absorption of the teachcolor and the current mark-color at the wavelength of interest, as mentioned before. In its most easy variant the possibility if and how well a (from a teached-color different colored) contrast mark can be recognized can be described with formula 1.

$$Prec = (RPW - RTColor) \leq (RTColor + \Delta R) \quad [1]$$

with

Prec = Quality of recognition

(high negative (<-1.0) values indicate a high recognition accuracy, positive values indicate that a recognition is not possible, small negative values (> -1.0 and <-0.001) indicate a recognition but with a lower accuracy)

RPW = Reflection of the current substrate for 470 nm, 530 nm or 640 nm

(depending on the used LED)

RTColor = Reflection of the used teach-color for 470 nm, 530 nm or 640 nm

(depending on the used LED)

ΔR = maximum acceptable difference for 470 nm, 530 nm or 640 nm

(depending on the used LED)

With this approach three teachcolors have been identified which enable a mark-recognition of 90 % of a 1 006 pantone colors large color space. Table 2 shows the teach-colors and the number of Pantone-colors which are acceptable with the individual teach-color. There is a large overlapping, but all three teachings together lead to a recognition value of 90.63 %.

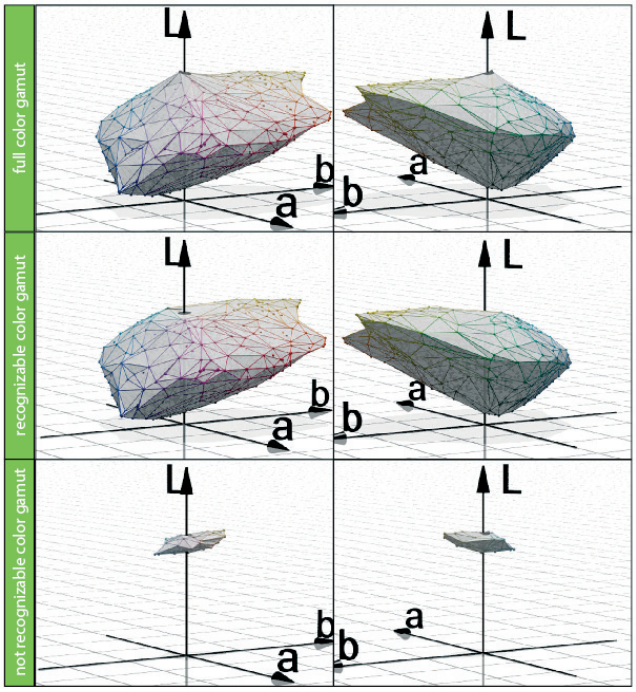


*Figure 21: 1006 Pantone-colors large full color space (top). Recognizable color space with the colors named in table 1 (middle). Not recognizable colors with the colors named in table 1 (top)*

*Table 2: Identified top-three Pantone colors for a maximum recognition of a 1 006 pantone-color large gamut*

| LED | Color name | Recognisable colors [Σ] | Recognisable colors [%] |
|---|---|---|---|
| Red | Pantone 318 C | 661 | 59,49 % |
| Blue | Pantone 100 C | 848 | 76,40 % |
| Green | Pantone 264 C | 745 | 67,12 % |
| Overall | / | 1006 | 90,63 % |

| Color name |
|---|
| Pantone 318 C |
| Pantone 100 C |
| Pantone 264 C |

## 6. Downsampling to an RGB-approach

In practice it is not always possible to get spectral data about the actual used contrast-mark-color. But - especially if inline spectral measurement systems are included in a printing-machine - RGB-based camera systems are at hand. Because the contrast sensor works on an RGB-basis the relevant information can also gathered from images of the contrast-mark.

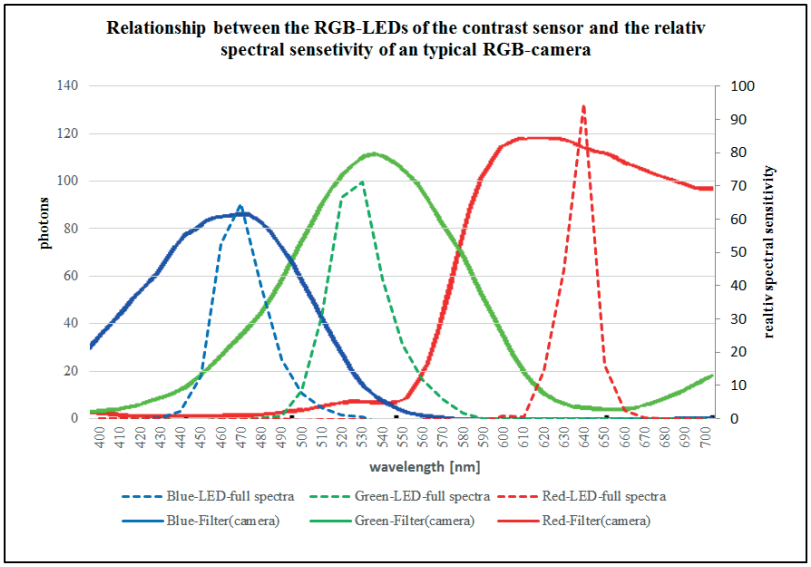


*Figure 22: RGB-camera-sensitivity compared to the emission-behavior of the RGB-LEDs of the investigated contrast-sensor*

Figure 22 shows that the RGB-LEDs of the contrast sensor show a comparable emission to the sensitivity of a typical RGB-based camera system. Taking this as a starting-point, the wavelength at which the current contrast-mark shows the highest absorption (with respect to the LEDs), can also be derived from the RGB-camera-signal. The lowest value of the three camera-RGB values indicates the absorption-maximum of the contrast-mark-color. This enables the possibility to make use of the sensor-store-cells that can be related to the corresponding LED.

## 7. Generalization to arbitrary substrates

Numerous substrates with arbitrary colored contrast-marks (c.f. Figure 10 & Figure 11) have been measured and tested regarding occurring differences with respect to their:

- glossiness
- white-point
- surface-structure
- thickness of the material

In each case the contrast sensor delivers a comparable behavior as pointed out in the chapters before. The absorption-difference between the substrate (or in cases of not completely opaque materials: the substrate in combination with the backing) and the mark-color in the relevant wavelength-ranges is responsible for the related signal-threshold. If this difference is low, the signal-threshold must be low as well and the other way around.

Also here formula 1 holds true by calculating the quality of recognition (Prec) by using the corresponding substrate-information, as mentioned in the chapter concerning white substrate.

## 8. Conclusion

The main result of this research work is the identification of relevant teaching colors: There is no need to teach a contrast sensor concerning black with white. Moreover, black and white reduces the possible recognition-range. Also green with white is not a useful combination for teaching.

Because of the three narrow-banded illumination wavelength-ranges and the requirements for the pattern-recognition the three pantone color mentioned in table 2 can also expressed as cyan, magenta and yellow. Using each in three different lightness-levels enables a consistent and reproducible data-set for all needed and possible signal-thresholds and therefore possible mark-color - substrate variants that can occur.

Overall, this paper provides a basis to use RGB-based contrast sensors with a higher efficiency in production.

## 9. Outlook

While the down-sampling to an RGB-based approach has been proved possible, the next step is to determine a number of contrast-thresholds for each LED. The next step is to determine a smart order in which these thresholds are "tried" weather they recognize a specific mark, printed upon an arbitrary substrate, or not.

Different contrast-sensors from other vendors need to be investigated as well.

**References**

[Huebler11] A. Hübler, 2011, Spektrale Farbmessung in der Druckmaschine -Kerntechnologie zukünftiger Automatisierungsansätz1, 17. Workshop für Farbbildverarbeitung, Konstanz

[Dattner11] M. Dattner, 2011, Inline Spektral Messung - die neue Referenz?, VDI- Seminarreihe: "Inline- vs. Offline-Farbmessung", Darmstadt

[DIN00] DIN. Deutsches Institut für Normung, 2000, ISO 13655 'Spektrale Messung und farbmetrische Berechnung für graphische Objekte', Beuth Verlag, Berlin

[Veith08] S. Veith, S. Barr, Life Cycle Assessment: Flexographic and Rotogravure Printing Comparison & Flexographic Plate Imaging Technologies, E.I. Du Pont de Nemours and Company - DuPont Engineering and Research Technology (DuET), 2008

[Ohno04] Ohno, Y. (2004). "Color rendering and luminous efficacy of white LED spectra". Proc. Of SPIE. Fourth International Conference on Solid State Lighting 5530: 89

# Volume measurement of inkjet droplets

*Michael Schmid, Karl-Heinz Selbmann*

Institute of Print Technology
Bern University of Applied Sciences,
Pestalozzistr. 20, CH-3400 Burgdorf, Switzerland

E-mails: michael.schmid@bfh.ch; karl-heinz.selbmann@bfh.ch

**Abstract**

Obtaining good quality printouts using an inkjet print head depends on good jetting performance. Besides droplet formation and velocity, droplet volume is a critical factor for characterizing this performance. The purpose of this project is the development of an optical method for measuring the volume of single droplets in flight, as well as complementary analysis of statistical data such as droplet volume distribution for the Ricoh Gen5 print head with row spacing of 0.55mm. Waveform designs, unique for each ink and temperature combination, can be improved using this technique. For these reasons, an optical system, using three cameras with varying focal points, was developed to obtain three-dimensional information about droplets in flight. Evaluation of resultant data showed that the chosen method is capable of measuring single droplet volumes within a range of 15%, irrespective of position. Thus, the method is shown to be practicable, and can be integrated into existing drop watchers to allow for the analysis of droplet volume when designing waveforms.

**Keywords**: inkjet, drop watcher, volume measurement, waveform, optical system

## 1. Introduction

Modern ink jet print heads are increasingly being applied in a wide array of technical fields. Ink jet dispensing technology is primarily based on piezo actuator technology, whereby deformations of the piezo elements, in conjunction with system geometry, generate a single droplet of ink. The characteristic deformation of a piezo actuator is defined by a stimulating electrical waveform which varies depending upon the particular print head and ink combination under consideration. A drop watcher system analyses the drop formation performance using an optical system to study the drop immediately following the piezo actuation. The resultant quality of any inkjet printed material is influenced by an array of factors, the most notable of which are drop formation and drop velocity. Another very important factor is the volume of a single ink droplet. A measurement system for ascertaining the volume of a single drop, before it arrives at a substrate material, would be a valuable tool. Measuring drop volume would provide useful statistical data, such as a volume distribution model for single nozzles or for an entire print head. This additional information can then be utilized during development of nozzle excitation waveforms, which are unique for every ink and print head combination. Using a novel optical approach with three cameras viewing the droplet through the same lens system, the Bern University of Applied Science's Institute for Print Technology intends to gather this data, for the Ricoh Gen 5 print head with a nozzle spacing of 0.55 mm.

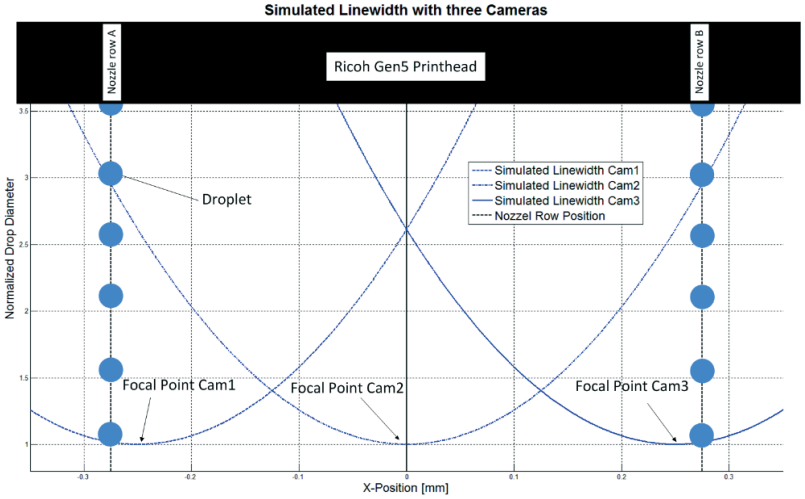


*Figure 1: Influence of the position deviation of a droplet*

Optical systems with large magnification factors have a very narrow depth of focus. This leads to a significant distortion of the depicted droplet if it is not located exactly in in the middle of the focal point, which is the case because the nozzles are arranged into two different rows by the Ricoh Gen5 print head as it can be seen in Figure 1.

To avoid this issue a lens system with two beam splitters and three cameras has been developed, which allows capturing images of a single drop with different depths of focus simultaneously. Using this information the exact position of the droplet can be calculated, as will be explained in the following chapters.

## 2. Methods

Two systems enable the measurement of droplet volume with requisite accuracy using optical techniques. The first system is the physical data acquisition system, composed of a camera-lens combination, a fast illumination system and a trigger electronic unit. This unit, also called trigger-box, is responsible for the synchronization of optical data acquisition and the print controller system. Using a simulated positional encoder signal is, as would be present in an actual print system, so that the print heads will jet at a defined time with the chosen delay time for the illumination.

The second system which is required is a mathematical model for analyzing the image data to calculate droplet volume.

### 2.1 Measurement setup

The goal of the measurement system is the photographic capture of a droplet shortly after ejection from the print head. The quality of the captured image has an enormous influence on the accuracy of the volume calculation. Since the optical system must measure the volume of drops with an average diameter of only 23 µm with an accuracy of 15% it must fulfill certain conditions. The figure 2 shows the setup of test rig. In many typical drop watchers, a number of droplets in series are exposed in a single shutter period to form a composite image showing average droplet formation. Since droplet formation is not perfectly repeatable, the influence of variations in droplet size would falsify volume measurements. Therefore, a bright and fast illumination with a flash duration of 400 ns has been developed, which delivers similar contrast ratios to the typical composite image. The flash generated, using a high power LED, required the use of high currents, which are proportional to the emitted light intensity, as well as fast rise and fall times, to keep the pulse width short.

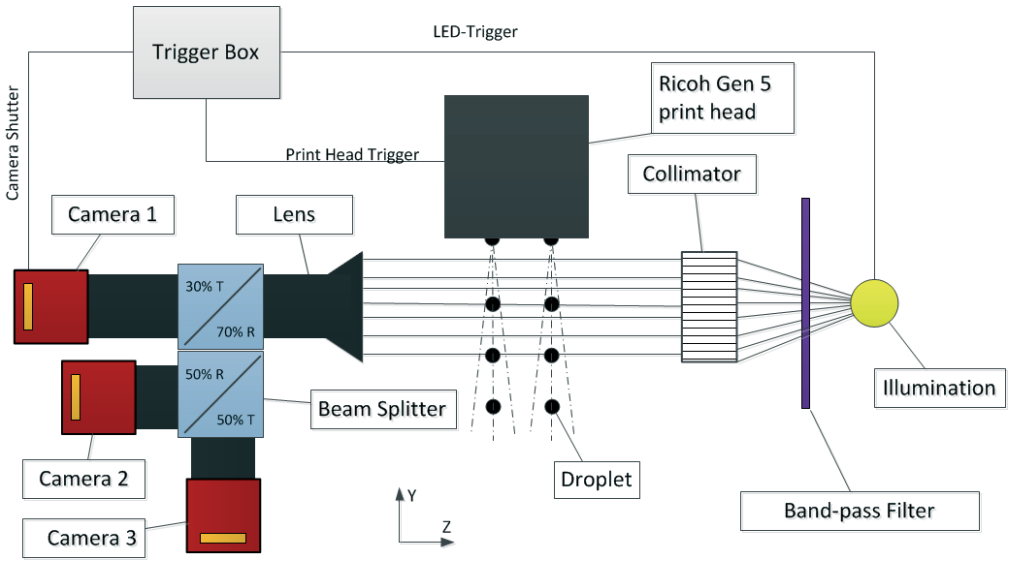


*Figure: 2 Optical configuration of the test rig*

Since the lens of an optical system defines magnification, distortion, maximum optical resolution and an array of other properties, it is a key component for the performance of the measurement assembly. In conjunction with the camera and illumination, it determines the size and resolution of acquired images.

To obtain high repeatability, the print system trigger must be exactly synchronized with the camera and the illumination systems. By simulating a positional encoder signal for the print system, which dictates when droplets

will be jetted, and is controlled by the main computer, the trigger electronic enables this synchronization. The primary running parameters of the trigger electronic are encoder signal frequency and flash delay. The encoder signal frequency is used to simulate the encoder signal of a linear axis, and thus defines the jetting frequency of the print head. The flash delay defines the time of flight of jetted droplets before illumination is provided, determining their position in the resulting photograph.

## 2.2 Calculation of droplet position

An optical system using three cameras enables different focal points by varying the distance between the camera sensor and the lens. A reference grid was measured using various spacing between the lenses and sensor chips. In figure 3, for each camera, the data set of measured line widths as a function of depth of focus, has been plotted.

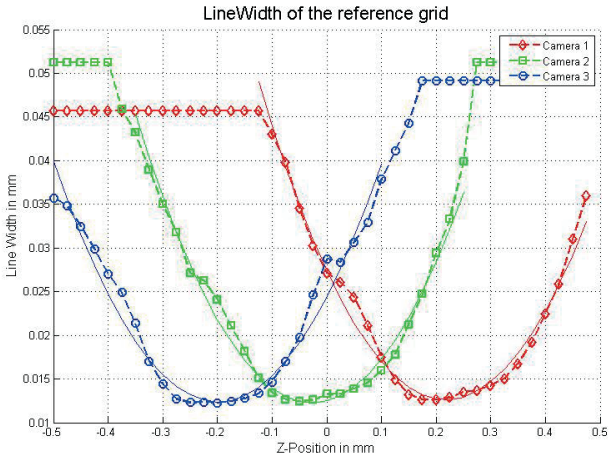


*Figure 3: Measured line width of the reference grid*

Using weighted, third order polynomials, fitted to the data set, the effective z-position of the object can be calculated, by subtraction of the line widths. The influence of this displacement can be used in further volume calculations. An analysis of the calculated z position revealed that the position can be measured within ± 3 µm as long the object is within ± 0.3 mm of the focal point.

## 2.3 Calculation of the droplet volume

Calculating a three dimensional droplet volume out of a two dimensional image requires the use of a mathematical model. Various approaches to this problem were evaluated. It was found that integrating the area along the flight path allows the highest degree of accuracy (Hugli, 2000). As seen in figure three, no assumption of circularity is made, however, rotational symmetry along the flight axis is assumed. The method evaluated in the paper (Thurwo, 2009) was used to calculate volume. However, since the droplet diameter under consideration is more than one hundred times smaller and based on a greyscale image than in that publication, border detection algorithms were completely different.

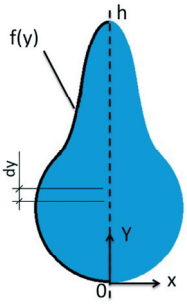


*Figure 4: Rotation model*

$$V_{tot} = \int_0^h f(y^2) * \pi * dy \qquad [1]$$

Since the function f(y) is unknown, it was necessary to find a software implementation for the model in figure 4. Therefore, image processing is used to detect drop border points using a full width at half maximum tresholding approach.

These border points are used to calculate a center line, and a set of sub-areas are then rotated around the center line to obtain a set of sub volumes. The principle is implemented with greyscale images. Figure 5 illustrates the less accurate method with a binary image (Thurwo, 2009).

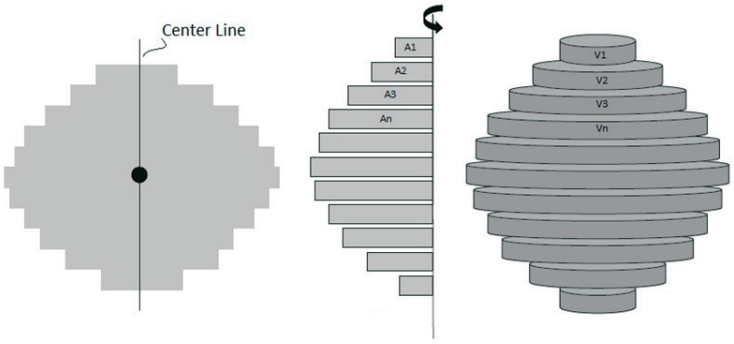


*Figure 5: Implementation of the rotation model (Thurwo, 2009, p. 5)*

As can be seen in figure 6, the cross section of a drop does not have a sharp border. The slope of the border transition, which represents the rate of change of pixel values, is used to determine border sharpness of captured images. If the captured image does not show an abrupt enough transition in greyscale value, then sufficient sharpness has not been acquired, and it will not be considered for statistical evaluation.

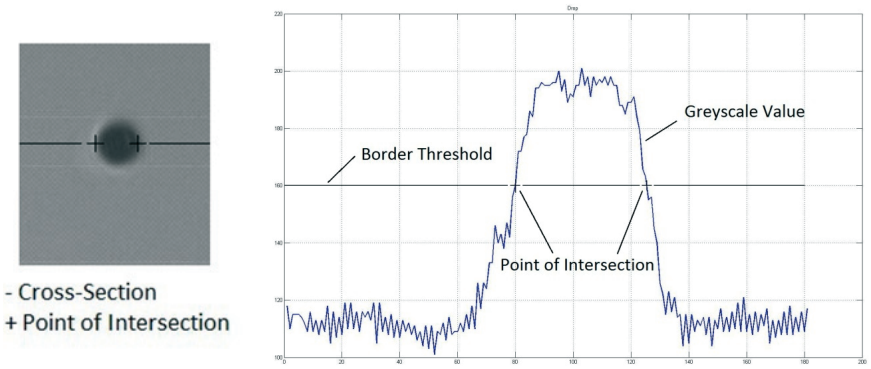


*Figure 6: a) Image of an acquired droplet, b) Cross-section of a droplet*

## 3. Results and discussion

Measurements have shown that the method developed is capable of measuring the volume of a single drop. Figure 7 shows the outline of the evaluated drop from Figure 6a:

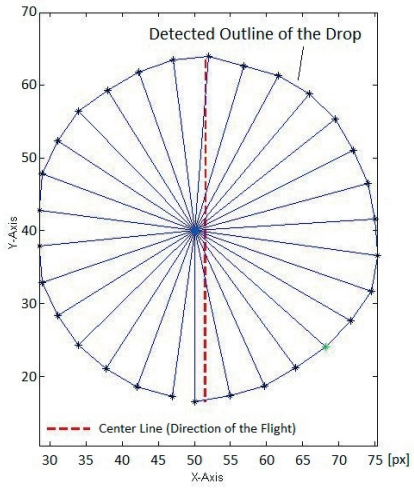


*Figure 7: Measured drop*

The points on the perimeter of the drop represent detected position of the drop boundary as determined by treshholding. The dotted line is the center of rotational symmetry and also shows flight direction.

An analysis of single nozzle volume variation was undertaken at the focal point of the middle camera using 25 images of multiple drops being ejected from the same nozzle. The volumes were then calculated using the method described above. The boxplot in Figure 8 shows the volume distribution of the generated drops. The statistical evaluation of the measured drop volumes has shown that they lie within the required range of values, and that the method has met performance expectations.

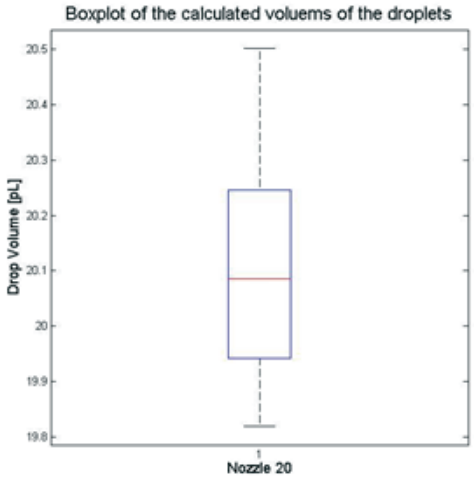


*Figure 8:*
*Volume boxplot of the statistical evaluation*

If the droplet is not located in the focal point it leads to significant estimation errors, because the droplet is depicted with a blurred border. The system with three cameras enables to obtain suitable results even if the drop is beyond the focal point. Based on the measured line width of the reference grid at known positions, as shown in Figure 3, the displacements were considered in further calculations. The results obtained showed that this approach is able to extend the range of z-positions in which volume can be measured to ± 0.3mm, however this improvement is marked by an increase in measurement uncertainty as compared to stationary measurements. An acceptable range of z-position values, with the chosen displacement of the cameras, is visible in Figure 9. In this evaluation is the camera with the closest focal point considered to calculate the volume according the captured images and the measured lens characteristics.

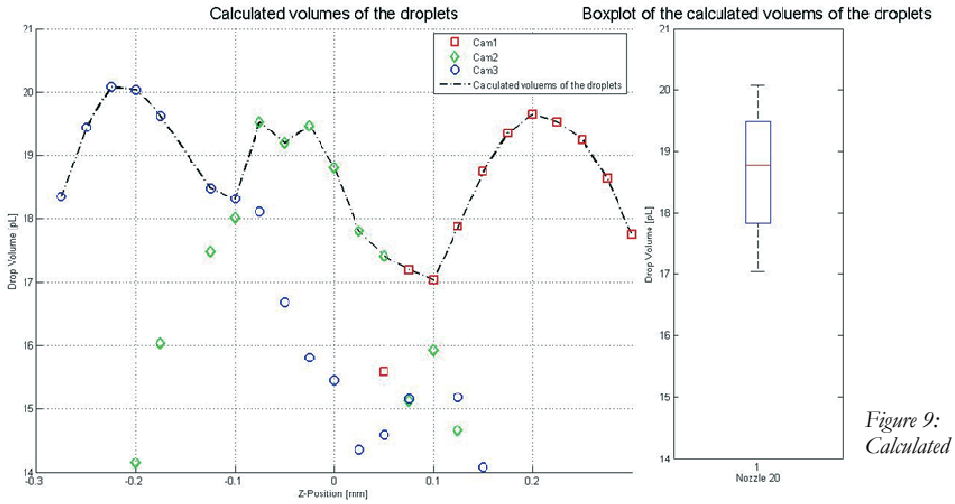


*Figure 9:*
*Calculated volume of one droplet*

Since the displacement of the cameras has a positive influence on measurement range, but conversely a negative influence on measurement distribution, the trade-off must be considered. The particular application will determine which aspect of the measurement is more important. Conceptually, the system would allow the use of even more cameras, although this would necessitate more powerful illumination. Using the developed approach, in conjunction with the mathematical model of drop displacement, the influence of drop position on volume measurements could be reduced, but not eliminated.

## 4. Conslusion

The investigation of the evaluated data has shown that the intended measurement accuracy of 15%, independent of drop position, is feasible. The goal of the project was to develop a tool enabling evaluation of another droplet quality attribute, besides droplet formation and droplet velocity, which could be used for waveform design of the Ricoh Gen5 print head.

The development of the lens system, which enables the photographic capture of the same droplet at three different positions using two beam splitters, became a key element of the system. The additional depth information contained in the image could be used to calculate drop position and, further, drop volume. This extended depth of focus allows to collect data of two nozzles banks of a Ricoh Gen5 print head without a moving the camera or the print head, which can be used by endurance tests.

However promising the results, further research in this field is needed, to increase the independence of z-position and drop volume measurement accuracy. To increase the sharpness of the captured images in the direction of flight a faster and brighter light source is requested. With the magnification of the lens and the pixel size of 2.2 µm, a flash duration of 100 ns would prevent a shift of the droplet during illumination of more than a single pixel on the sensor. Additionally, other features, like the contrast of the image (Abmayr, 1994) or the slope of the drop border, could be considered in the mathematical model to increase the independence of drop position in the z direction on volume measurements.

Nevertheless the approach could be implemented in the existing drop watcher and enable measurement of an additional quality attribute of the droplet, helping to improve waveforms for certain fluids with the Ricoh Gen5 print head.

**Acknowledgements**

Sincere thanks are given to Brian von Gunten, Ramon Felder and Manfred Schär for their support.

**References**

Abmayr, W., 1994. Einführung in die digitale Bildverarbeitung. Stuttgart: B. G. Teubner

Hugli, H., Gonzalez, J., 2000. Drop volume measurements by vision. Imaging 2000, SPIE Electronic Imaging Conference, San Diego, Jan 2000. SPIE Vol 3966-11, pp. 60-66

Maier, C., 2004: Techniken der Hochgeschwindigkeitsmikrokinematographie zur Bewertung von Mikrodosierungssystemen und Mikrotropfen. Düsseldorf: VDI Verlagg, Reihe 8 Nr. 1037.

Thurow, K., et al., 2009. An optical approach for the determination of droplet volumes in nanodispensing, Journal of Automated Methods and Management in Chemistry, Volume 2009, Article ID 198732, Hindawi Publishing Corporation

# Flexographic ink-coating interactions - Effects of kaolin clay/GCC blends in coating layers

*Erik Bohlin*, *Caisa Johansson*, *Magnus Lestelius*

Karlstad University
Faculty of Health, Science and Technology
Department of Engineering and Chemical Sciences
Karlstad, Sweden

E-mails: erik.bohlin@kau.se; caisa.johansson@kau.se; magnus.lestelius@kau.se

**Abstract**

The purpose of this study was to relate print quality aspects, such as print gloss and print density, to ink penetration of water-based flexographic ink into coatings with differently engineered properties. Different amounts of kaolin clay were added to a ground calcium carbonate (GCC) based top coating for pilot coating of cartonboard. The ratio of kaolin/GCC were 0/100, 20/80 and 50/50. Full-tone prints on these coated samples, using water based flexographic ink of two different viscosities, were produced. The ink viscosity was varied by increasing the temperature of the ink from 23° C to 50° C. The three pilot coated samples were printed at a printing force of 25, 50, 75 and 100 N.

Increased printing force increased the print density to a higher degree than did increased ink temperature for coatings with a pure GCC pigment (of lower porosity). For coating layers containing both GCC and kaolin clay (having higher porosity compared to the pure GCC coating), decreased viscosity increased the print density more than increased printing force. Print density was also affected by ink penetration, suggesting that the optical response is sensitive to the ink-substrate interaction layer. The result presented in this work also suggests that the print gloss decreases with increased amount of penetrated ink due to a higher rate of ink vehicle removal and thereby a higher ink surface roughness.

**Keywords**: print, ink penetration, ink viscosity, print gloss, coating structure

## 1. Introduction

The major constituent of a coating colour is the pigment. Calcium carbonate, kaolin clay, talc or a mixture of these are the most commonly used pigments. Calcium carbonate, either ground (GCC) or precipitated (PCC), is a very white mineral consisting of nearly sphere-shaped particles. Kaolin clay, on the other hand, consists of disc-shaped particles having a slightly lower whiteness. For this reason, calcium carbonate is often used when a white surface is given priority, while kaolin clay is used to obtain a good coverage and a smooth and glossy surface. Commercial coating pigments are available in a wide range of particle sizes, particle shapes and particle size distributions. By mixing different pigments, coating layers with broad variations in porosity, structure and surface properties can be created.

Clay particles have negatively charged surfaces and positively charged edges and clay particles tend therefore to attract each other and form aggregates, so-called house-of-cards structures. Alignment of the plate-like particles in a loose house-of-cards structure yields an open and porous dry coating layer (Larsson et al. 2006). Compared to the more closely packed structure formed by spherical GCC pigments, clay particles are more able to reorient themselves and clay coatings are thus considered to be more compressible upon calendering (Larsson et al. 2006; Dean 1997).

Different shapes and sizes of pigments create different particle size distributions and these in turn affect the size and shape of the pores formed in the consolidated coating layer. When the porosity of a surface is explained and calculated, the pores are often modelled as tubes of a fixed diameter that stretch vertically from the surface and downwards through the coating layer. This is of course a rough simplification, but for GCC coatings it is often a sufficient assumption. Nevertheless, clay coatings produce more complex pore structures, where not only the size and shape but also the orientation of the pigment particles must be considered. Chinga et al. (2002) have shown that coatings containing a larger proportion of clay have a lower pore area fraction than a coating containing less clay. It was also shown that a coating layer containing either a high or a low proportion of clay had a more compressed structure at the surface than inside the coating.

The smoother the surface, the higher is the measured gloss. A low print gloss is an indication of a rough print surface, and this often means that the print density is also low, resulting in a poor image and poor colour re-

production (Oittinen and Saarelma 1998). The print gloss and the gloss contrast are thus important factors when a high quality print is desired. The gloss contrast, i.e. the difference between the paper gloss and the print gloss is important for the readability of a printed text or the appearance of a printed image. The gloss contrast can be expressed as (Oittinen and Saarelma 1998):

$$\Delta G = G_{pr} - G_{pa} \quad [1]$$

where ΔG is the gloss contrast, Gpr is the print gloss and Gpa is the gloss of the coated or uncoated paper substrate used for printing.

A printed area should have a high gloss to give an image that is aesthetically attractive to the observer, and the print gloss is related to the rate of ink vehicle removal and to what rate the ink levels before it sets. Both the coating pore diameter and the numbers of pores per unit area, or pore density, of the coating are factors that have a strong influence on the ink setting rate (Cummings & Lyons 1996; Preston et al. 2000; Preston et al. 2001; Olsson et al. 2007). Smaller pores and higher pore density increases the ink setting rates. With ink setting a certain amount of ink penetration also occurs. Due to capillary forces, and also mechanical forces in the printing nip, ink pigments moves down into the substrate together with the ink vehicle where a mixed layer of coating material and ink pigment forms. A higher surface porosity often results in a faster ink setting and this leads to a greater ink penetration in the z-direction and a lower print gloss (Preston et al. 2008; Preston et al. 2002).

Another factor that also has an influence on the ink setting rate is the viscosity of the ink. In general the viscosity of a printing ink decreases with increasing temperature, which needs to be considered in high speed coating and printing processes where the temperature of the fluid may increase considerably due to the heat evolved in the machines (Nordström 2000; Nordström & Johnson 2002).

It has been shown that a substrate with a high surface roughness accepts more ink than a substrate with a smooth surface. However, this is only valid for a certain degree of roughness. Too rough a surface reduces the contact area in the nip, and this reduces the ink transfer (De Grace & Mangin 1983). The authors also concluded that the ink penetration increased to a certain extent with increasing nip pressure. Too high a nip pressure closes part of the surface pores and reduces the ink transfer.

The viscosity also has a great impact on the print density. A high viscosity ink gives a denser print as more ink is transferred (Walker & Fetsko 1955), i.e. a darker tone is achieved than with an ink of lower viscosity. The optical print density, or the reflection density, is a measure of contrast. In other words, the property describes how well the substrate is covered by ink after printing and its appearance in contrast to the surrounding unprinted substrate.

Up to a certain point, the print density increases with increasing amount of ink transferred to the substrate. However, after the point when the surface is completely covered and the ink layer is sufficiently thick, the print density reaches a stable value that is not affected by additional ink (Tollenaar & Ernst 1962).

The purpose of this study was to relate print quality aspects, such as print gloss and print density, to ink penetration of water-based flexographic ink into coatings with differently engineered properties achieved by varying the proportions between kaolin clay and calcium carbonate in the coating colour. Pilot-coated paperboard was printed in a laboratory flexographic printer, using two different printing nip pressures. The ink penetration was determined by means of visual evaluation of microscopic images. Earlier results, by the authors, indicate that ink transfer and distribution is affected by the roughness and the porosity of the substrate. For water-based flexographic ink, a large pore size and a large pore volume appears to increase the pressure driven ink penetration developed in the flexographic printing nip (Bohlin et al. 2013). It has also been found that increased amount of binder in the coating layer decreases both the ink transfer and the print quality, such as print density, print mottle and the occurrence of un-covered areas (Bohlin et al. 2014). In this work, the viscosity of the ink was altered by heating the ink. Full tone prints with ink temperature varied from 23 °C (room temperature) to 50 °C were produced, using printing forces of 25, 50, 75 and 100 N.

## 2. Methods

A three-ply cartonboard (Duplex) with a basis weight of 179 $g m^{-2}$ with a core of unbleached sulphate pulp sandwiched between a bleached top layer and an unbleached bottom layer (Supplied by Billerud Korsnäs AB, Frövi, Sweden) was used as a substrate. The cartonboard was pre-coated with a 95/5 blend of calcium carbonate (GCC)/kaolin pigment at a coat weight of 11 $g m^{-2}$ using a stiff ceramic blade. Three different coating colours,

each containing GCC (Hydrocarb 90, Omya AB, Malmö, Sweden) and styrene-butadiene latex with Tg 24 °C and a particle size of 120 nm (Eka Synthomer Oy, Oulu, Finland) added at 12 pph was used in the top coating formulations. Different amounts of kaolin clay (Capim DG, Imerys) were added to the top coating recipes. The ratio kaolin/GCC for the three coatings were 0/100, 20/80 and 50/50, and these numbers are used for denotation of the samples. An aqueous dispersion of an acrylic copolymer (Sterocoll FD, BASF Paper Chemicals, Ludwigshafen, Germany) was added as thickener at 0.3 parts dry per hundred parts of pigment to all coating dispersions. The dispersions were diluted to a target Brookfield viscosity of 1000 mPas (spindle no. 4, 100 rpm). The resulting solids content were 67 % (0/100), 66 % (20/80) and 65 % (50/50). The coat weight was 12 g m$^{-2}$.

The coating was performed on the pilot machine at Korsnäs AB, Frövi, Sweden at a speed of 500 m min$^{-1}$ using a bent ceramic blade held at a blade angle of 19°. Calendering was done on-line in a customary set-up for this board grade using a soft nip with a rubber roll of hardness 65° Shore D and a steel roll held at a temperature of 100 °C while applying line loads of 30 or 100 kN m$^{-1}$. Gloss measurements of coated and printed surfaces were performed by means of a gloss meter (Zehntner glossmeter, 20°-75°, Shropshire, UK) at 75° (ISO 8254-1). The surface roughness in μm of coated surfaces was determined by a Parker Print Surf (PPS) device operated at a clamping pressure of 1.0 MPa (Testing Machines Inc., New York, USA).For Gloss and PPS characterization a minimum of 8 samples were analyzed. The pore size distribution of coated surfaces was characterized by an Autopore III mercury porosimeter, allowing porosity and tortuosity to be estimated. Pore sizes in the range of 0.05-0.5 μm were used for determination of average pore radius. Scanning Electron Microscopy, SEM (Jeol 6700F cold field emission scanning electron microscope) was used to investigate the structure of the coated cartonboard surfaces.

The coated paperboard was printed with a water-based cyan ink, Sun Chemical Inks A/S, Skovlund, Denmark. The surface tension of the ink was determined to 37 mJ m$^{-2}$ by a Sigma 70 tensiometer (KSV Instruments Ltd. Finland) equipped with a platinum DuNoüy ring. The ink was diluted with de-ionized water to a viscosity of 25 s, as measured with a Zahn cup no 2. Printing was done by a laboratory flexographic printer (IGT-F1 laboratory flexographic printer, IGT Testing Systems, Amsterdam, NL), using an anilox roll (volume 2.7 ml/m2 and screen ruling 235 lines cm$^{-1}$), and a printing plate with hardness 57° Shore A and thickness 1.7 mm (Miller Graphics, Sunne, Sweden). Constant speed (0.3 m s$^{-1}$) and printing force 25, 50, 75 and 100 N, was used to print the full tone areas using printing ink with temperature 23 °C, 32 °C and 50 °C. The surface temperature at various locations was measured by an IR thermometer (optris® MiniSightPlus, Sensotest Electronics & Sensors, Järfälla, Sweden).

The theoretical ink penetration into the different coating layers, or the thickness of the mixed layer of ink and coating material, due to mechanical forces acting in the nip was calculated by means of Equation [2] (Aspler 1993; Zang & Aspler 1995).

$$h^* = \frac{\varepsilon}{\tau} \cdot \left( \sqrt{\frac{r_1^2 \cdot t_1 \cdot P}{4 \cdot \eta}} + \sqrt{\frac{r_2 \cdot \gamma \cdot t_2 \cdot \cos\theta}{2 \cdot \eta}} \right) \qquad [2]$$

where h* is the total ink penetration, ε is the porosity, and τ is the tortuosity. $t_1$ is the time under which the substrate is exposed to pressure in the printing nip, P is the maximum nip pressure and η is the ink viscosity. γ is the surface energy of the fluid, $t_2$ is the time to ink leveling and θ is the contact angle. The typical pore radius r in Equation [2] is divided into $r_1$ and $r_2$, where $r_1$ is the most suitable radius for pressure penetration and $r_2$ for the capillary absorption. It has been suggested that average measured pore radius is not the most relevant one for capillary absorption, and that pores at the finer end behaves under a different dynamic than larger ones (Schoelkopf et al. 2002). However, in this work $r_1$ is considered to be equal to $r_2$ (Bohlin et al. 2013).

Microscopic images of printed surfaces were obtained by an Olympus BX51 microscope (Hamburg, Germany) equipped with a ColorView 111 soft imaging system (Münster, Germany). The average ink penetration depth was evaluated from microscopic analysis of cross-sections of printed surfaces (Leica DMRX, Leica Mikroskopie & Systeme GmbH, Wetzlar, Germany) by a method described previously (Bohlin et al. 2013). The print density was evaluated by a GretagMacbeth densitometer D19C (Regensdorf, Switzerland).

## 3. Results

Mercury porosimetry measurements showed an increased porosity, or void fraction, with an increased amount of kaolin (Figure 1), but the typical pore diameter of 0.08 μm were equal for all the three samples. SEM images clearly showed the structural changes when the amount of disc-shaped kaolin particles increased among the more sphere-shaped GCC particles (Figure 2).

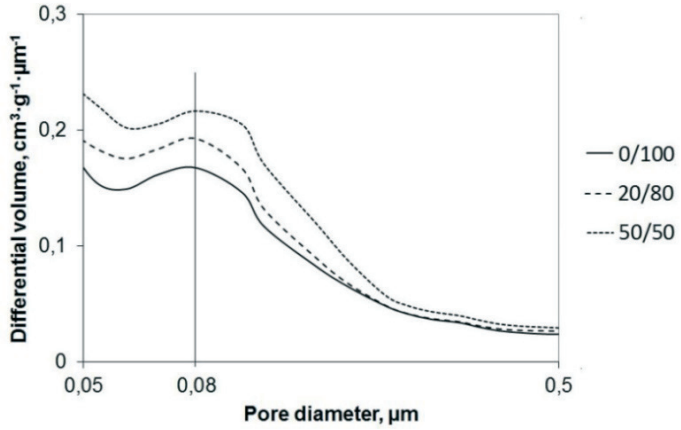


*Figure 1: Mercury porosimetry measurements of the three samples. The porosity increased with increased amount of kaolin in the coating*

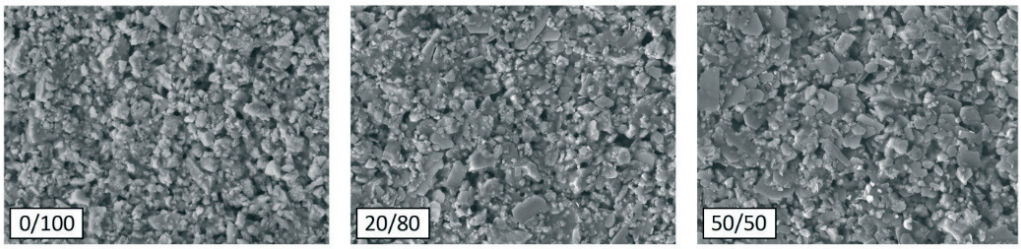


*Figure 2: SEM micrographs showing, from left to right, kaolin/GCC ratio of 0/100, 20/80 and 50/50*

The gloss was found to increase with increased amount of kaolin clay in the coating layer. Figure 3 (left) shows gloss results for the samples, which agrees well with the flatter surface formed by incorporation of clay particles as indicated in Figure 2. The increased roughness with increased amount of kaolin content (Figure 3, right) indicates a more porous surface layer due to the mix of GCC and kaolin particle structures. This mix creates a different particle packing and a more open structure compared to a pure GCC layer (Larsson et al. 2006).

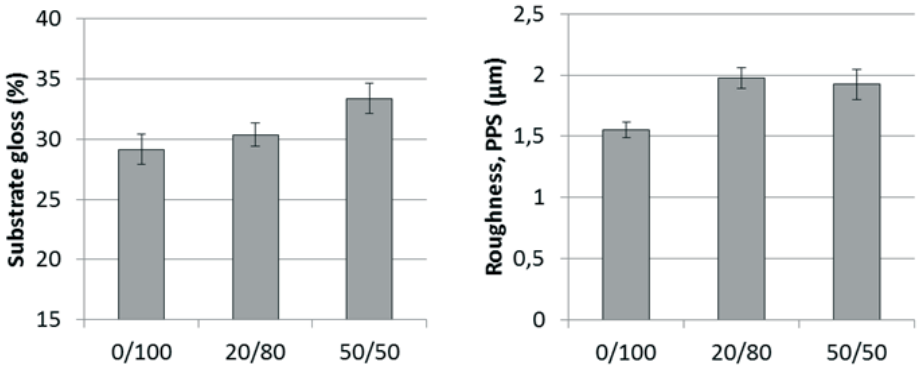


*Figure 3: Gloss as a function of kaolin/GCC ratio. Gloss increased with increased amount of kaolin. Error margins indicate standard deviation*

The tortuosity and porosity of the coating layers are presented in Table 1.

*Table 1: Tortuosity and porosity of the three coatings*

| | **Tortuosity, $\tau$** | **Porosity, $\varepsilon$** |
|---|---|---|
| **0/100** | 1.667 | 0.29 |
| **20/80** | 1.672 | 0.35 |
| **50/50** | 1.669 | 0.45 |

The viscosity of the ink decreased with increased temperature from 23 °C to 50 °C. Figure 4 shows the viscosity of the inks as a function of shear rate from 1 to 1 000 $s^{-1}$.

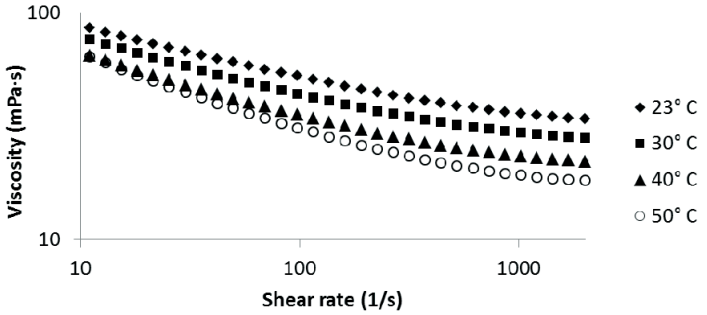


*Figure 4: Viscosity as a function of shear rate for varying ink temperature*

As an approach to further investigate the effects of varying ink temperature on the print transfer, the surface temperature of the printing device at various locations and on the fresh printed surface was recorded during the printing process. Measurements were carried out immediately after manual application of the ink onto the anilox roll; after transfer of the ink to the printing plate (i.e. after one rotation of the printing plate holder) and on the printed cartonboard surface.

The measurement technique has, although it is simple and quick, its limitations and despite the various temperatures of the applied ink, almost identical ink film temperatures were recorded at the various measuring points. The data suggests that there was a very rapid decrease in ink temperature when applied onto the anilox roll (all parts of the printing device as well as the cartonboard substrate initially had the same temperature as prevailing in the room, i.e. 23 °C). However, the temperature of the ink film was, as anticipated, found to decreese slightly with each step, with about 1 °C decrease from the printing plate to the finished print (Figure 5). The surface temperature was also independent of applied print force and on the composition of the coating layer.

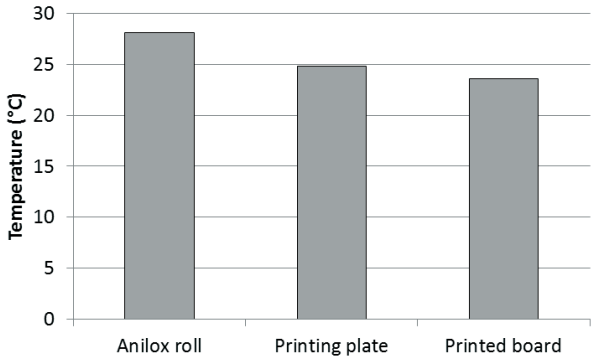


*Figure 5: Temperature drop for the ink, initially heated to 50°C, through the different parts of the printing device*

Based on the outcome of the printing trials at different ink temperatures and printing forces, the three pilot coated samples printed with ink at 23 °C and 50 °C at a printing forces of 25 and 50 N were chosen for further investigation. This resulted in twelve different printed samples. The print density for these samples are shown in Figure 6 where the coatings are placed in three groups on the x-axis, and the different printing conditions are denoted with printing force and ink temperature.

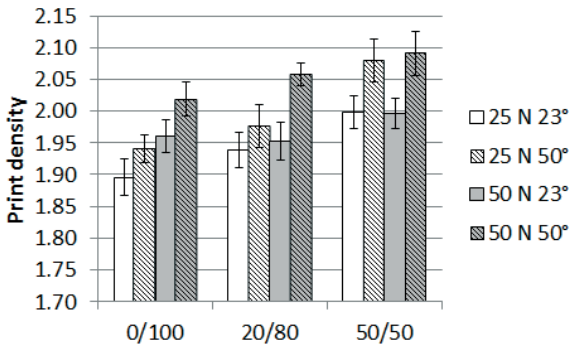


*Figure 6: Print density for the twelve printed samples. Average from 7 measurements. Error bars indicate standard deviation*

The print density increased with increased amount of kaolin clay, increased printing force and with increased ink temperature. For the 0/100 sample, print density increased more when the printing force increased from 25 to 50 N compared to when the temperature increased from 23 °C to 50 °C. The print density for sample 50/50 did not increase to any large extent with increased printing force, but it increased with increased temperature for both printing forces.

Figure 7 shows both thickness of the ink layers (left) and the depth of the penetrated ink (right) that was estimated from cross-section images of the printed samples. When a printing force of 25 N was used both the thickness of the ink layer and the penetrated ink seemed to increase when the kaolin clay/GCC ratio increased from 0/100 to 20/80 and then decreased when the ratio continued to 50/50. For samples printed at 50 N, the values either increased with increased rate of kaolin or remained on approximately the same level. The thickness of the ink layer decreased with increased printing force for samples 0/100 and 20/80.

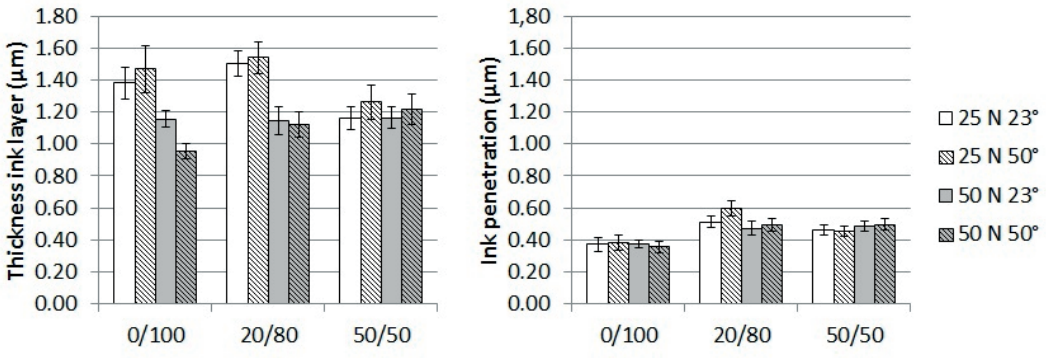


*Figure 7: The thickness of ink layer (left) and the depth of penetrated ink (right). Average from 20 measurements. Error bars indicate standard deviations*

Compared to the evaluated ink penetration, the calculated penetration (Equation [2]) showed roughly the same trend, increased penetration with increased clay content, but with slightly higher values. Figure 8 displays both calculated (gray bars) and evaluated (white bars) penetration for the three samples, printed at 25 N with an ink temperature of 23 °C.

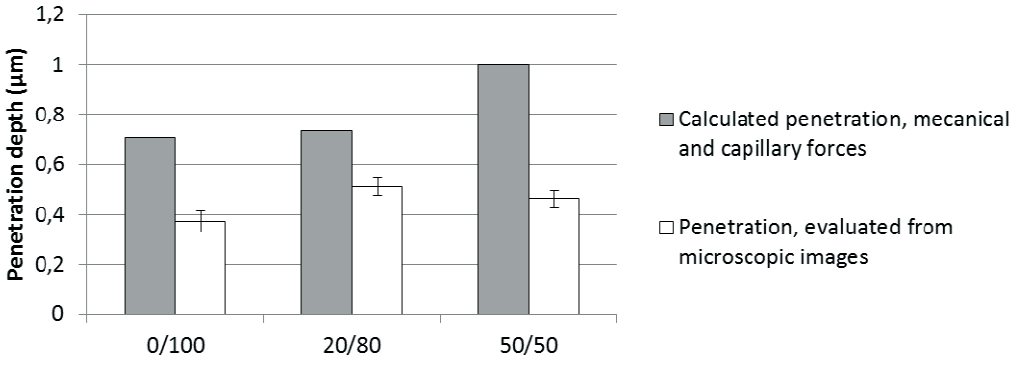


*Figure 8: The calculated (black bars) and evaluated (white bars) penetration for the three samples, printed at 25 N with an ink temperature of 23°C*

Figure 9 shows the fraction of ink penetration depth of the total ink layer. The fraction of penetrated ink increased with increased printing force, and for some of the samples also with increased temperature. However, as with the ink layer thickness (Figure 7), sample 50/50 that contained the highest amount of kaolin clay, differed somewhat from the other two samples, as the fraction of penetrated ink showed more irregular values among the printing conditions. As for the print density (Figure 6), with the exception of printing conditions 25 N 50°C for sample 0/100, the fraction of penetrated ink increased more with increased printing force than with increased temperature when no kaolin clay was present in the coating layer. Sample 20/80 also showed this trend.

Figure 10 shows the print gloss (left) and the gloss contrast (right). The print gloss decreased when kaolin clay was added to the coating. The gloss contrasts (Equation [1]), and to a certain extent also the print gloss, showed opposite values than those for the substrate (Figure 3, left). The gloss contrast decreased while the gloss of the substrate increased with increased amount of kaolin clay. In the same manner as the print density (Figure 6) and the

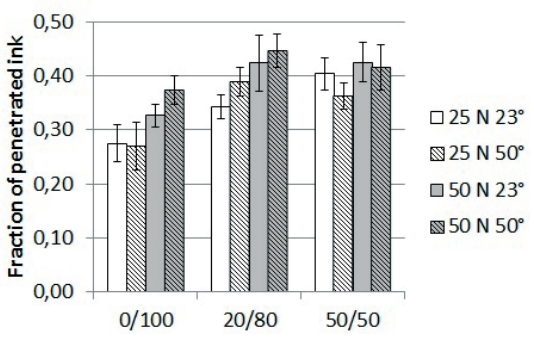


*Figure 9: Fraction of penetrated ink*

the fraction of penetrated ink (Figure 9), the print gloss and the gloss contrast increased more with increased printing force than with increased ink temperature for sample 0/100 while the samples containing kaolin clay did not produce any significant trend. Temperature, and thus viscosity, seems to have an effect on the gloss as the trend is that gloss increases with higher temperature (although error margins overlap).

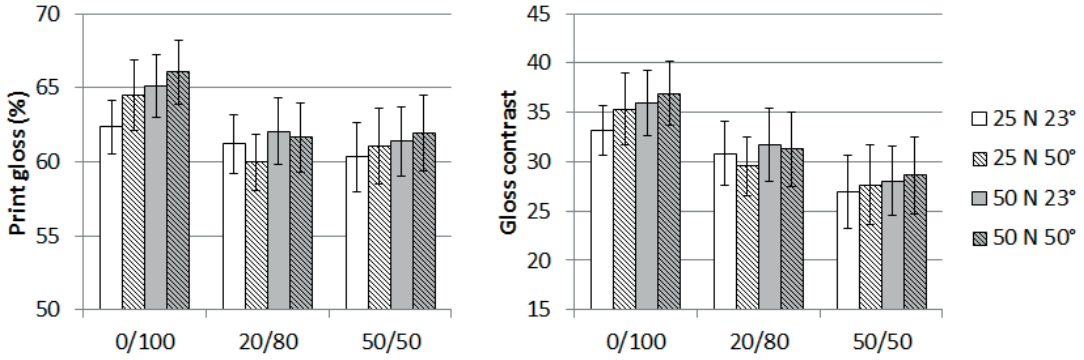


*Figure 10: Print gloss (left) and gloss contrast (right)*

As can be seen in Figure 11, the results described in this work suggest that there is a connection between penetrated ink and print quality parameters, represented here by the print gloss. The black dots in Figure 11 represent all the twelve printed samples used in this work. The print gloss decreased with increased ink penetration depth.

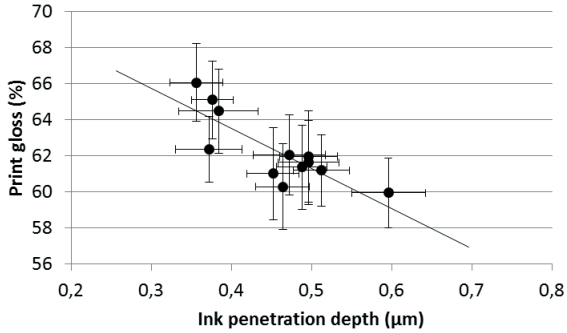


*Figure 11: Print gloss as a function of ink penetration. The print gloss decreased with increased ink penetration depth*

## 4. Discussions

Higher temperature, and thus lower viscosity, appears to affect penetration trend wise. The fraction of penetrated ink appears slightly higher for higher temperatures (Figure 9).

A deeper ink penetration suggests a higher rate of ink vehicle removal which is likely to result in a lesser time for ink to level on the surface. The roughness of the ink surface, which is caused by ink splitting in the printing nip exit and the underlying substrate roughness, remains to a higher degree if the penetration of ink vehicle and ink pigments increases. The difference in ink temperature could also affect the ink vehicle removal as the water

evaporation rate should increase with increased ink temperature. However, measurements of surface temperature of the ink layer on the printing plate and immediately after transfer to the cartonboard showed no significant differences between ink originally heated to 50 °C and the ink having room temperature. Hence, the minor variations in temperature achieved in this manner are believed not to have induced major changes in the evaporation of water from the ink played. Thus, evaporation rate changes are not believed to have influenced ink penetration significantly in this study.

## 5. Conclusions

Studying ink deposition on calcium carbonate and kaolin coating, it was shown that increased printing force increases the print density to a higher degree than increased ink temperature for coatings with a pure GCC pigment. For coating layers containing both GCC and kaolin clay, having a higher porosity compared to the pure GCC coating, increased ink temperature, and thereby decreased viscosity, increases the print density more than increased printing force.

The deposition of the ink film, on top of the substrate surface and penetrated into the coating layers, showed a complex response to commonly used print quality parameters. Print density increased with increasing porosity, generally. This was accompanied by and increased fraction of penetrated ink, suggesting that the optical response for the printed samples was affected by this ink-substrate interaction layer. Also print gloss was affected. Even though gloss increased with increased ratio of kaolin clay to the coating, print gloss decreased with increased ratio of kaolin clay. The result presented in this work suggests that the print gloss decreases with increased amount of penetrated ink, which in turn gives a higher rate of ink vehicle removal and thereby a higher ink surface roughness.

**Acknowledgements**

The Swedish Governmental Agency for Innovation Systems (VINNOVA) and the industry participants in the PaperOpt project are gratefully acknowledged for their financial support. Billerud Korsnäs Frövi is thanked for performing the pilot coating. The authors are indebted to Eka Synthomer and Omya for supplying material, and Stora Enso and Imerys for performing measurements on both coated and printed cartonboard materials, as well as for valuable discussions on the experimental results.

**References**

Aspler, J. S. (1993). Interaction of ink and water with paper surface in printing: A review. Nordic Pulp & Paper Research Journal, Vol 8 no (1), 68-74

Bohlin, E.; Lestelius, M.; Johansson, C. (2013) Flexographic ink-coating interactions - Effects of porous structure variations of coated paperboard. Nordic Pulp & Paper Research Journal, Vol 28 no (4), 573-581

Bohlin, E.; Lestelius, M.; Johansson, C. (2014) Flexographic ink-coating interactions - Effects of latex variations in coating layers. Manuscript in preparation

Chinga, G.; Helle, T.; Forseth, T. (2002). Quantification of structure details of LWC paper coating layers. Nordic Pulp and Paper Research Journal, 17 (3), 313-318

Cummings, D. O.; Lyons, A.V (1996) Influence of Engineered Kaolin on Web Offset Blister Resistance. Proc. TAPPI Coating Conference, Nashville, TAPPI Press, Atlanta, p. 16

Dean, T. W. R. (1997). The Essential Guide to Aqueous Coating of Paper and Board. Leatherhead, United Kingdom: Paper Industry Technical Association

De Grace, J. H.; Mangin, P. J. (1983). A Mechanistic Approach to Ink Transfer Part I: -Effect of Substrate Properties and Press Conditions. London, UK: Banks, W.H., Ed. Pentech Press. 312-332

Kipphan, H. (2001). Handbook of Print Media, Technologies and Production Methods. 1st edition, Berlin, Germany: Springer

Larsson, M.; Engström, G.; Vidal, D.; Zou, X. (2006). Compression of coating structures during calendering. In 2006 TAPPI Advanced Coating Fundamentals Symposium, Turku, Finland, February 8-10, Session 6. 19

Nordström, J. E. P.(2000) Thermal changes in a Waterless Sheet-Fed Offset Inking Station. International Printing & Graphic Arts Conference, Savannah, GA, USA, TAPPI Press, 153-165

Nordström, J. E. P.; Johnson, J. (2002) CSWO (Cold Set Waterless Web Offset) Using Standard Tmp/Dip Newsprint. International Printing & Graphic Arts Conference, Bordeaux, France, pp. 11

Olsson, R.; Yang, L.; Lestelius, M. (2007). Water retention of flexographic inks and its influence on final print gloss. Nordic Pulp and Paper Research Journal, 22 (3), 287-292

Preston, J. S.; Daun M.; Nutbeem C.; Jones A. (2000) Attaining print performance through pigment engineering. Wochenblatt Für Papierfabrikation, vol. 5, pp252-265

Preston, J. S.; Elton, N. J.; Legrix, A.; Nutbeem, C. (2001) The role of pore density in the setting of offset printed ink on coated paper. Proc. TAPPI Advanced Coating Fundamentals Symposium, San Diego

Preston, J. S.; Elton, N. J.; Legrix, A.; Nutbeem, C.; Husband, J. C. (2002). The role of pore density in the setting of offset printing ink on coated paper. Tappi Journal, 1 (5), 3-5

Preston, J.; Hiorns, A.; Parsons, D. J.; Heard, P. (2008). Design of coating structure for flexographic printing. Paper Technology, 49 (3), 27-36

Schoelkopf, J; Gane, P. A. C.; Ridgway, C. J.; Matthews, G. P (2002). Practical observation of deviation from Lucas-Washburn scaling in porous media. Colloids and Surfaces, A: Physicochemical and Engineering Aspects, 206 445-454

Tollenaar, D.; Ernst, P. A. H. (1962). Optical Density and Ink Layer Thickness. In Proceedings of International Conference of Printing Research Institute (IARIGAI). 214-234

Walker, W. C.; Fetsko, J. M. (1955). A Concept of Ink Transfer in Printing. American Ink Maker (December), 38-44, 69-71

Zang, Y. H.; Aspler, J. S.; (1995). Influence of coating structure on the ink receptivity and print gloss of model clay coatings. Tappi Journal, 78 (1), 147-154

# A2

## *Printed functionality and special printing*

# Temperature coefficient of resistance of inkjet printed silver nanoparticles

*Daniele Sette*[1], *Christophe Poulain*[1], *Anne Blayo*[2]

[1] Université Grenoble Alpes, F-38000 Grenoble, France
CEA, LETI, MINATEC Campus
F-38054, Grenoble, France

E-mails: daniele.sette@cea.fr; christophe.poulain@cea.fr;
anne.blayo@pagora.grenoble-inp.fr

**Abstract**

This paper focuses on the experimental investigation of the temperature coefficient of resistance (TCR) of inkjet printed silver nanoparticles on a silicon thermal oxide substrate. The influence of the annealing temperature on the TCR is explored under air and nitrogen. Measurements under Nitrogen allow exploring negative temperatures values without condensation. TCR values as high as 3000 ppm/C, almost 80% of the silver bulk value, have been measured for silver thin films annealed a 350°C during one hour. TCR of inkjet printed films has proven to be constant in the temperature range between -25°C and 75°C. These results point out how to improve the sensitivity of inkjet printed silver for sensing applications such as temperature and vacuum sensors.

**Keywords**: inkjet printing, silver nanoparticles, TCR, annealing temperature.

## 1. Introduction

In the last decade, printing processes experienced a fast development for manufacturing large area electronic components. While printing equipment capabilities such as resolution, repeatability and stability are being improved, advances in chemistry and materials science lead to a whole spectrum of new functional materials befitting to printing processes. Indeed, conductive, dielectric, and semi-conductive inks are commercially available and studies are still undergoing on complex materials with magnetic (Voit, 2003) or piezoelectric properties (Windle, 1999).

After printing, these functional materials usually require post-treatments (annealing, UV-exposure, photonic flash) in order to trigger and improve their functionality. Silver nanoparticle inks are widely employed owing to their high colloidal stability and electrical performance. Studies on the influence of the annealing temperature on both the electrical conductivity and the microstructure evolution of these films have attracted much attention.

In this paper, the temperature coefficient of resistance (TCR) of inkjet printed silver layers is investigated. The TCR is an intrinsic property which relates the resistance R of a conductive material to its temperature and can be extracted from experimental data using equation [1].

$$R(T) = R_0\big(1 + \alpha(T - T_0)\big) \qquad [1]$$

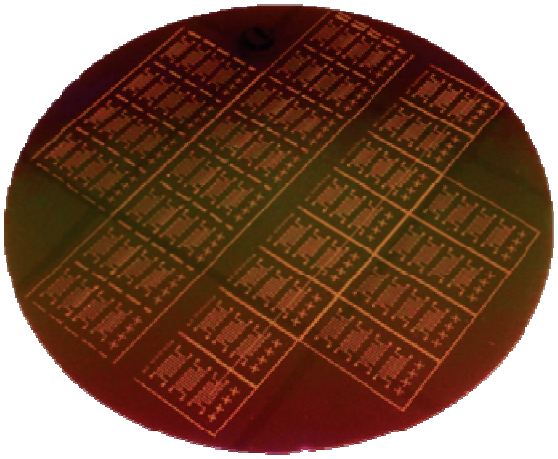

*Figure 1: Inkjet printed planar resistors on 200 mm silicon wafer*

Where $\alpha$ is the TCR, expressed in ppm/°C, $R_0$ the resistance at room temperature $T_0$, and $T$ the resistance temperature. Equation [1] shows that the electrical measurement of the resistance variation allows monitoring environmental variations for sensing applications (temperature, pressure, flux). Because of their high TCR, inkjet printed silver nanoparticles have been used in different sensing components such as temperature sensors (Courbat, 2009; Molina-Lopez, 2012) and vacuum sensors working on the Pirani principle (Sette, 2013). For electrical interconnections or the fabrication of RF components, whose performance are strongly influenced by the electrical conductivity of the material, low TCR values are required; whereas for sensors, increasing the TCR value induces a higher sensitivity.

In this paper, we propose to characterize the TCR of inkjet printed silver nanoparticles. This work is focused on the influence of the annealing temperature on TCR of inkjet printed silver, measured on planar resistors printed with a commercial silver ink on a 200 mm silicon wafer (Figure 1).

## 2. Experimental details

### 2.1 Sample fabrication

In order to achieve an accurate measurement of the TCR of inkjet printed silver layers, the pattern in Figure 2 was printed on a 200 mm silicon wafer with a 2 µm thick thermal silicon oxide. A silicon substrate was chosen because of its high thermal conductivity and low thermal expansion at 350 °C. The 500 nm thick thermal silicon oxide ensures a high quality dielectric layer that cannot interfere with the electrical measurement of the printed silver layer.

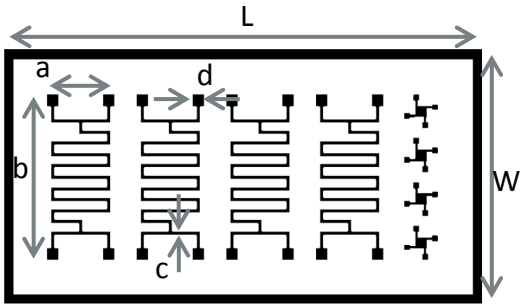


*Figure 2: Test pattern for TCR measurement*

Each pattern is made of four serpentine resistors whose dimensions are detailed in Table 1. There are also four 1 mm² van der Pauw patterns for resistivity measurements, however they are not used in his study.

*Table 1: Dimensions of the test pattern*

| | | | |
|---|---|---|---|
| a | 5.3 mm | d | 1 mm |
| b | 12.7 mm | L | 42 mm |
| c | 0.3 mm | W | 22 mm |

Samples were printed with a Dimatix DMP2800 printer at a resolution of 476 pixels/cm, corresponding to a 21 µm pitch. A commercial ink from SunChemical, with 40 % in weight of silver nanoparticles was used to print the test patterns. After printing 24 patterns (Figure 1), the whole wafer was dried in an oven at 60 °C during one hour. The silver layer thickness is around 1µm. Finally, the printed samples were annealed in an oven during one hour at different temperatures between 150 °C and 350 °C. In Figure 3, a single printed pattern annealed at 200 °C is illustrated.

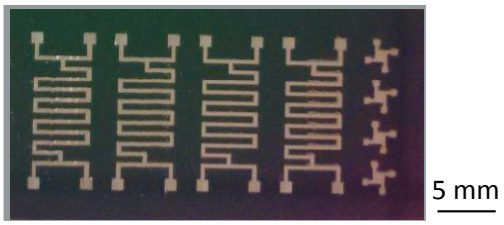


*Figure 3: Printed test pattern annealed at 200°C during 1 hour*

## 2.2 Experimental setup and protocol

The measurement of the TCR requires an accurate measurement of both the resistance variation and the sample temperature. Also, the temperature of the sample has to be homogeneous and stable. The sample temperature was controlled with a programmable benchtop temperature forcing system (Flex TC from Mechanical Devices), allowing temperature variations up to 50 °C/min between -50 °C and 150 °C. The sample under test was held on the thermal module with thermal grease on a contact area of 3 cm², which guarantees a fast thermal equilibrium compared to ovens.

The resistance of the sample was measured with Copper-Beryllium probes, which offer both a low electrical contact resistance and an elastic behavior. The resistance variation was measured by a four point electrical method with a Keithley 2182A nanovoltmeter and a DC current source set at 1 mA (Keithley 2400). The DC current supply at 1 mA prevents the material from self-heating by Joule effect. The temperature at the sample surface was measured by a PT100 temperature probe connected to a Keithley 2700. The experimental setup is illustrated in Figure 4.

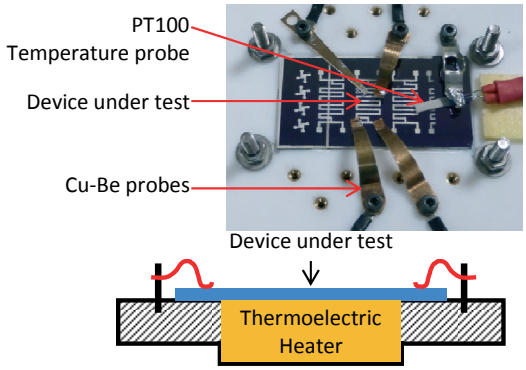


*Figure 4: Experimental setup*

The first measurements were realized in air and condensation phenomena were avoided by applying temperatures higher than 25 °C. Thermal steps of four minutes between 25 °C and 75 °C were applied while the resistance was measured. For temperature higher than 75 °C, a slow decrease of the resistance was observed, and attributed to the gradual sintering of the silver nanoparticles. The TCR was measured on decreasing temperature steps because slight variations of the resistance during increasing temperature steps were observed. Figure 5 illustrates the simultaneous measurement of the resistance and the temperature for a sample annealed at 250 °C during one hour. On this curve, it can be observed that the resistance variation follows the temperature target. The spikes at the beginning of the steps are due to temperature feedback regulation.

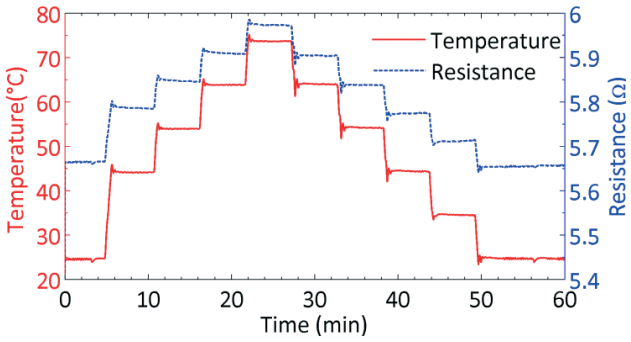


*Figure 5: Temperature and resistance measurement in air of a sample annealed at 250°C during 1 hour*

To extend the temperature measurement range, we have developed a hermetic chamber mounted around the experimental setup that allows realizing the measurement under a nitrogen flux with an over pressure of 100 mbar. A hygrometer placed inside the chamber shows that the relative humidity drops down to 1% in less than 5 minutes. Such configuration of the setup allowed measurements in a temperature range from -25 °C up to 75 °C without any condensation on the samples surface. It was shown that inkjet printed silver layers exhibit a porous structure (Birnbaum, 2007; Sette, 2014) and thus a capacity to absorb water molecules. As a consequence, in the

nitrogen flux configuration, the samples were heated at 75 °C during 30 min in the chamber before the TCR measurement to degas the silver layers. Also, the soaks duration was extended from 4 min in air to 10 minutes in nitrogen because of a longer thermalization period.

## 3. Results

The determination of the TCR of the silver layer is done through the linear fit of the relative resistance variation ΔR/R as a function of the sample temperature, plotted in Figure 6. The TCR value is given by the slope of the linear curve. The curves in Figure 6 have the expected linear behavior predicted by equation (2) both in air and nitrogen, and the coefficient of determination $R^2$ of the linear fit is higher than 0.99.

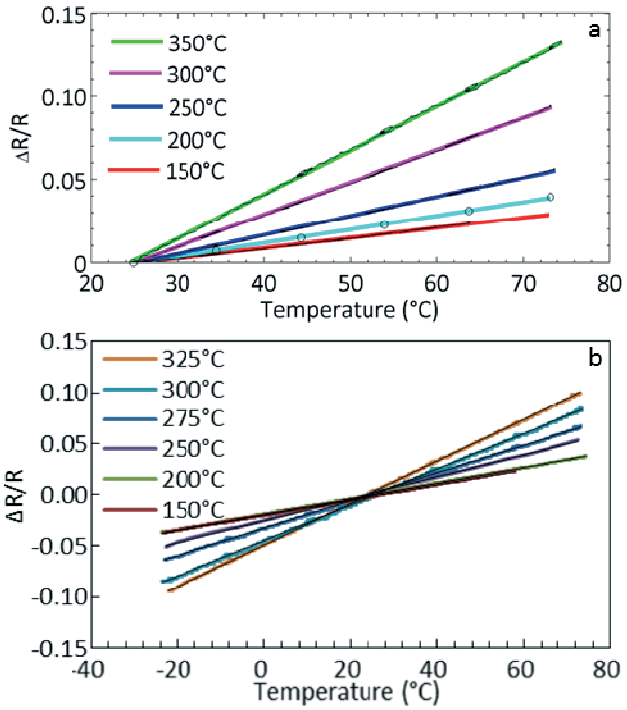


*Figure 6: Relative resistance variation as a function of temperature for different annealing temperatures. Experimental data (black lines and dots) and fitted data (color lines). a) Measurement in air. b) Measurement under nitrogen*

For each annealing temperature, three different resistors were measured. In Figure 7 are reported the Extracted TCR values form the linear fit of the experimental data. Standard deviation is lower than 10 % demonstrating the accuracy and repeatability of the measurements, for the sake of clarity error bars are not traced.

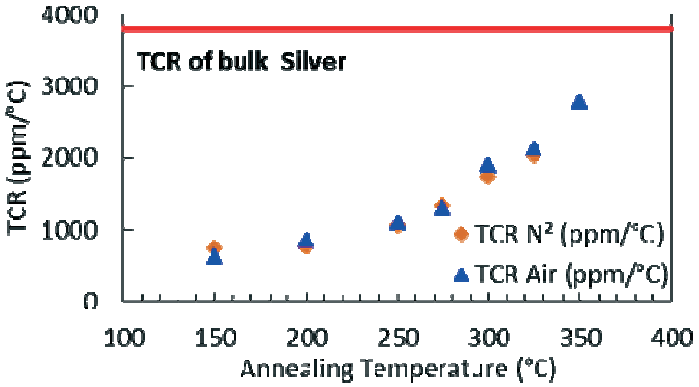


*Figure 7: Evolution of the TCR with annealing temperature*

After thermal cycling, microscopy investigation of the printed layers surface did not reveal any cracks or delamination.

## 4. Discussion

The TCR increases with the annealing temperature and reach 75 % of the silver bulk value for the samples annealed at 350 °C. Also, the measurements performed under the nitrogen flux show that the TCR value is stable in the range -25 °C - 75 °C, with values similar to those measured in air during the cooling process. Further investigations in controlled hygrometry atmospheres should bring major information on the effect of water absorbed by the silver layers.

The measured values are in agreement with measurements of other works, reported in table 2. The comparison to the reported values of TCR shows that variations of the TCR can be attributed to several parameters: silver nanoparticles initial dimensions, annealing time and temperature, substrate, addition of tuning (Ni) or capping materials (parylene).

*Table 2: TCR of inkjet printed silver layers reported from literature (non-exhaustive)*

| Reference | Sample | Substrate | TCR |
|---|---|---|---|
| Slade, 2013 | Bulk silver | - | 3 800 ppm/°C |
| Sette et al., 2013 | Inkjet printed silver (SunChemical EMD5714) annealed at 150 °C, 5h | Kapton HN 75 µm, Dupont | 910 ppm/°C |
| Courbat et al., 2011 | Inkjet printed silver (DGP 40LT-15C , Anapro) with parylene coating annealed at 150 °C, 1h | pe:smart paper type 2, Felix Schoeller | 1 100 ppm°/C |
| Molina-Lopez et al., 2012 | • Inkjet printed silver (DGP 40LT-15C, Anapro) annealed at 150 °C, 30 min<br>• Same sample with Ni electrodeposition | PET, *Melinex ST506, Dupont* | • 630 ppm/°C<br>• 4 300 ppm/°C |
| Felba et al., 2009 | Inkjet printed silver (4-10 nm nanoparticles) annealed at 250 °C, 1h | Microscope glass slides | 2 080ppm/°C |
| Tao et al., 2013 | Organic silver conductive ink (OSC ink annealed at 120 °C, 30s | PET | 700 ppm/°C |

The microstructure of the printed layers depends on the nanoparticles size and their evolution during sintering. Electrical conductivity of thin polycrystalline films is lower than bulk value because of conduction losses due to electrons scattering at grain boundaries and surfaces (Mayadas, 1970). Several studies (Singh, 1974; Pichard, 1983; Zhang, 2006) demonstrated that the TCR also depends on these conduction losses and thus on the layer microstructure. The increase of the annealing temperature of inkjet printed silver layers causes a strong decrease of the electrical resistivity (Lee, 2005) and also a growth of the silver grains (Kim, 2005; Kamishny, 2011); explaining why the TCR of the polycrystalline printed layers also increases with the annealing temperature.

Deschacht and Boyer (1985) have related the TCR of thin films to the mechanical constraints in the thin film generated by the difference of thermal expansion between the substrate and the film itself. Thus, when comparing the TCR values of the printed silver layers, the substrate nature has also to be considered.

The knowledge of the effect of the annealing step of inkjet printed silver layers is required to optimize the process depending on the final application, and there are several parameters that must be considered.

## 5. Conclusion

This study offers a thorough investigation of the TCR of inkjet printed silver nanoparticles dependence on the annealing temperature. We have described a reliable experimental setup for measuring the TCR of thin films both in air and nitrogen. The experimental results show with a remarkable accuracy that the TCR can be increased up to 75 % of the silver bulk value. The results give a reliable evolution of the TCR with the annealing temperature that could help improving the sensitivity of inkjet printed sensors. Finally, this work once more highlights the strong influence of the annealing temperature on the intrinsic physical properties of thin layers made of nanoparticles. The knowledge of such dependence is essential for the development of printed components.

**References**

Birnbaum, A., Wahl, K., Auyeung, R. & Piqué, A. 2010. Nanoporosity-induced effects on Ag-based metallic nano-inks for non-lithographic fabrication. Journal of Micromechanics and Microengineering, 20, 077002

Courbat, J., Kim, Y. B., Briand, D. & de Rooij, N. F. Inkjet printing on paper for the realization of humidity and temperature sensors. Solid-State Sensors, Actuators and Microsystems Conference (TRANSDUCERS), 2011 16th International, 5-9 June 2011 2011. 1356-1359

Deschacht, D. & Boyer, A. 1985. General expression for the temperature coefficient of resistivity of polycrystalline semi-metal films. Journal of materials science, 20, 807-811

Felba, J., Nitsch, K., Piasecki, T., Paluch, P., Moscicki, A. & Kinart, A. The influence of thermal process on electrical conductivity of microstructures: Made by ink-jet painting with the use of ink containing nano sized silver particles. 9th IEEE Conference on Nanotechnology, 2009. IEEE, 408-411

Kamyshny, A., Steinke, J. & Magdassi, S. 2011. Metal-based inkjet inks for printed electronics. Open Applied Physics Journal, 4, 19-36

Lee, H.-H., Chou, K.-S. & Huang, K.-C. 2005. Inkjet printing of nanosized silver colloids. Nanotechnology, 16, 2436

Mayadas, A. & Shatzekes, M. 1970. Electrical-resistivity model for polycrystalline films: the case of arbitrary reflection at external surfaces. Physical Review B, 1, 1382

Molina-Lopez, F., Vasquez Quintero, A., Mattana, G., Briand, D. & de Rooij, N. F. 2012. All-additive Inkjet Printed Humidity and Temperature Sensors Fabricated and Encapsulated at Foil Level. Proceedings of 14th International Meeting on Chemical Sensors-IMCS, 1, 1122-1125

Pichard, C. R., Komnik, Y. F., Belevtsev, B. I. & Tosser, A. J. 1983. Effect of grain boundary scattering on the TCR of thin tin films. Journal of Materials Science Letters, 2, 360-362

Sette, D., Mercier, D., Brunet-Manquat, P., Poulain, C. & Blayo, A. Micro Pirani pressure sensor fabricated by inkjet printing of silver nanoparticles. The 17th International Conference on Solid-State Sensors, Actuators and Microsystems (TRANSDUCERS & EUROSENSORS XXVII): 16-20 June 2013. 1783-1786

Singh, A. 1973. Grain-size dependence of temperature coefficient of resistance of polycrystalline metal films. Proceedings of the IEEE, 61, 1653-1654

Slade, P. G. 2013. Electrical contacts: principles and applications, CRC Press

Tao, Y., Tao, Y., Wang, B., Wang, L. & Tai, Y. 2013. A facile approach to a silver conductive ink with high performance for macroelectronics. Nanoscale research letters, 8, 1-6

Voit, W., Zapka, W., Belova, L. & Rao, K. 2003. Application of inkjet technology for the deposition of magnetic nanoparticles to form micron-scale structures. IEEE Proceedings-Science, Measurement and Technology, 150, 252-256

Windle, J. & Derby, B. 1999. Ink jet printing of PZT aqueous ceramic suspensions. Journal of materials science letters, 18, 87-90

Zhang, Q., Zhang, X., Cao, B., Fujii, M., Takahashi, K. & Ikuta, T. 2006. Influence of grain boundary scattering on the electrical properties of platinum nanofilms. Applied physics letters, 89, 114102

# Effect of polyelectrolytes on conductivity for printed functionality

*Dimitar Valtakari, Roger Bollström, Martti Toivakka, Jarkko J. Saarinen*

Abo Akademi University, Center for Functional Materials
Laboratory of Paper Coating and Converting
Porthansgatan 3, FI-20500 Åbo/Turku, Finlad
E-mail: dimitar.valtakari@abo.fi

**Abstract**

The present work describes the behavior of silver and conductive polymer tracks and films in the presence of an anionic or a cationic polyelectrolyte that are typically used in papermaking. The relative humidity increase was studied with silver electrode tracks on hygroscopic polyelectrolyte films. The effect of silver track uniformity, corrosion and conductivity were susceptible to the electrical current passing through humidity. In this regard, the anionic electrolyte was more inert in comparison to the cationic one. PEDOT:PSS formed nonuniform layers with lowered electrical performance when spin-coated on anionic polyelectrolyte coated glass substrate in comparison to clean, noncoated glass substrate. On the cationic polyelectrolyte coated substrates spin-coated PEDOT:PSS formed uniform and well conducting layers.

**Keywords**: paper electronics, printed electronics, polyelectrolyte, PEDOT:PSS, silver electrodes

## 1. Introduction

Fabrication of electronic devices directly onto paper substrate has caught attention in recent years. Besides printing conductive non-patterned or patterned areas on paper,[1,2] an increasing number of devices and concepts have been demonstrated, such as an all-organic active matrix display,[3] a passive ultra-high frequency RFID tag module embedded in a paper-on-paper structure,[4] moisture or temperature sensors,[5,6] an ethanol sensor,[7] a piezoresistive MEMS force sensor,[8] a $H_2S$ sensor,[9] a low-cost platform for electrochemical analysis,[10] a electrochemical detection device for paper-based microfluidistics[11,12] and a photovoltaic device.[13]

The paper substrate based electronics can be split into two main categories utilizing either bulk or surface conductivity. In the former category, the paper material is treated to become an electrically conductive integral device component. Bulk conductivity can be achieved either by soaking an uncoated paper by immersion or coating with conductive polymers or by *in situ* polymerization in the paper.[14,15,16,17] It can also be produced directly from wood pulp fibers that are coated by multi-sequenced, layer-by-layer method with conductive polymers or particles.[18,19,20,21] Adding silver plated carbon fibers or activated carbon fiber to the pulp or preparing conductive paper out of kraft pulp mixed with metalized polyester fibers provide alternative routes for conductive paper production.[22,23]

Our work concentrates on the surface conductive paper electronics which are typically constructed on coated paper grades.[24,25,26] Coating a base paper improves its performance and compatibility with the intended end-use application. Improved printability and optical characteristics together with well controlled barrier properties can be achieved as well as enhanced surface strength, opacity, surface smoothness and finely tuned porosity.[27,28] Performance of printed functionality, e.g. conductive tracks, is significantly improved through use of optimized coating layers.[29,30] In this study we investigate the impact of polyelectrolytes in direct contact with conductive layers. Polyelectrolytes are widely used as retention agents in the papermaking process. Addition of polyelectrolytes in the wet end of the paper machine improves retention of mineral pigment fillers introduced into the fiber matrix of the pulp as well as retention of starch, gum or rosin sizing during the formation of base paper. Polyelectrolytes are also used as dispersing agents in coating formulations. Since the pigments used in coatings are almost fully coated by the dispersant, this may interfere with the printed conductive layers. An understanding of the impact of the polyelectrolytes on the functionality of conductive layers is crucial for optimized device performance when fabricated on paper substrates.

## 2. Experimental

Two polyelectrolytes were investigated with two conductive materials. The polyelectrolytes consisted of anionic sodium polyacrylate [PA, Polysalz S, Basf, Germany] and cationic poly(dimethyldiallylammonium chloride) [poly-DADMAC]. Silver and homogenized conductive polymer poly(3, 4-ethylenedioxythiophene) poly(styrenesulfonate) [PEDOT:PSS, Clevios PH 500 (Heraeus Holding GmbH, Germany)] were used as conductive materials.

All the samples were prepared on a glass substrate to eliminate additional variables and complexity brought by the coated paper substrate, *i.e.* the wide choice of coating pigment particle mixtures with varying absorption and surface roughness characteristics.

The polyelectrolytes were spin-coated [KW-4A (Chemat Technology Inc., USA)] onto hand cut 2.5 x 2.5 cm glass slides for 60 s at 1050 rpm (Polysalz S) or 1300 rpm (polyDADMAC) using the following concentrations: Polysalz S at 2.5 wt%, 5 wt% and 10 wt%, and PolyDADMAC at 1 wt%, 2.5 wt%, 5 wt% and 10 wt%.

Homogenized standard PEDOT:PSS was spin-coated on top of the polyelectrolyte coated samples and annealed at 130 °C and 15 min according to manufacturer specifications. Resistivity of PEDOT:PSS was measured across two parallel conductive hand painted silver stripes over 10 mm distance with a Keithley 2100 Digital Multimeter at ambient conditions (24 °C and RH 50%). A multimeter is device designed to measure resistivities or voltages within a given range against predefined, constant current levels. This creates voltage potential variations within a given resistivity range or resistivity variations within given voltage range. In general, this will not cause any issues. At very high resistivities, however, the voltage amount becomes significant, ~50 V, causing severe noise or non-conductivity in sensitive polyelectrolyte film measurements.

Resistivity measurements of the polyelectrolyte coatings were performed across 10 mm x 1.2 mm silver electrode pairs oriented in line, short ends pointing at each other 30 μm apart. The electrode tracks on the polyelectrolyte coated samples were fabricated through a mask using a high vacuum evaporation method. Silver (99.999%) tracks were grown at 2-3 nm/min rate up to a total thickness of 150 nm. The samples were stored in nitrogen atmosphere prior to the resistivity measurements at various relative humidities (RH 20%, 50% or 80%).

Since a multimeter device can cause problems when measuring sensitive polyelectrolyte films with high resistivities due to the required high voltages ~50 V, Agilent 4142B Modular DC Source/Monitor mainframe was used for resistivity measurements of the polyelectrolyte base coating layers. This instrument can provide control over both current and potential together with a high sensitivity in the GΩ-range. All the electrical measurements were performed with current flowing from left to right. Current and voltage levels were carefully matched to produce fast and low noise L-shaped current curves as a function of time. This way the current floor was reached quickly ensuring short, 2-3 second measurements, which keeps current induced corrosion of silver to a minimum. PolyDADMAC was typically measured at 5 V and Polysalz S at 10 V.

The magnifying power fiducial camera (100x) of Dimatix materials inkjet printer in combination with an external light source and Dimatix Drop Manager -software were used for silver sample image analysis. This enabled the inspection of 1.4 mm x 1.1 mm image area.

Scanning electron microscope, SEM, was used to inspect the structure and measure the thickness of single and bilayers of polyDADMAC and PEDOT:PSS. The samples were freeze-fractured after dipping them in liquid $N_2$ for a minimum of 5 s to provide clean, unaltered cross sections. With our samples, this specific sample preparation step provided a critical tradeoff and was therefore abandoned. As the frozen sample is removed from liquid $N_2$, moisture from the surrounding air becomes condensed into ice on the cold surface. Some of the condensed ice melts forming water droplets on the > 0°C hygroscopic polyDADMAC layer. The water droplets are absorbed by the polyDADMAC layer making it swell and deformed. Not a good idea from layer thickness determination point of view. In addition, in PEDOT:PSS coated higher concentration polyDADMAC bilayer samples, the PEDOT:PSS layer could suffer and become destabilized by the moisturized polyDADMAC.

Bilayer PA/PEDOT:PSS and polyDADMAC//PEDOT:PSS color shifts from light to dark blue were measured and quantified in terms of print density using an optical densitometer [SpectroDens, Techkon, Germany]. Print density itself is an indirect measure that modern day densitometers determine and calculate virtually based on readouts from a spectral scanning head. Instrument settings were selected in accordance with ISO (Status) E, D50 illuminant, 2° observing angle and CMYK color space. Samples were measured back to front through the glass slide, the PEDOT:PSS film placed face-down against a pile of office paper serving as background. The polarization filter was turned on to avoid possible reflections originating from the glass and polymer film surfaces.

## 3. Results

All studied materials were deposited and measured on pristine glass substrate. The electric performance for silver and the conductive polymer PEDOT:PSS is fairly well known, less so for polyDADMAC and PA. In terms of electrical sheet resistance, silver and PEDOT:PSS belonged to a different segment, Ω respectively kΩ range, in

comparison to the closest polyelectrolyte, polyDADMAC, separated by roughly 1-2 orders of magnitude (Fig. 1). The polyacrylate (PA/Polysalz S) displayed very high sheet resistance in the GΩ range.

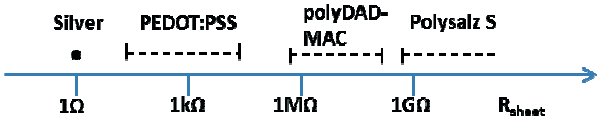


*Figure 1: Generalized snap shot of materials placement on the sheet resistance map*

3. 1 Silver on top of polyelectrolyte coating

Polyelectrolytes are inherently hygroscopic which may cause dimensional instability in the polyelectrolyte coating at higher relative humidity. Therefore, silver electrodes fabricated on top of polyelectrolyte coated samples were stored and measured at a relative humidity of 18%, 50% or 80%. The polyelectrolyte coating concentrations were fairly high in this work.

On anionic Polysalz S coatings silver showed no traces of corrosion beside light oxidation at the silver surface at RH 18% and RH 50% (Figure 2). Under extreme humidity, RH 80%, the gap between right hand and left hand electrode showed a directional, current induced corrosion. This was triggered by the measuring multimeter instrument turning the right hand electrode into an anode and the left hand electrode into a cathode.

Silver electrodes showed a significant corrosion on cationic polyDADMAC. At RH 50% and 80%, the polyelectrolyte coating experienced dimensional instability (swelling) resulting in silver electrode disintegration. Corrosion was enhanced by humidity. The external multimeter source made both electrodes corrode even stronger, especially halfway between the measuring probes (Figure 2).

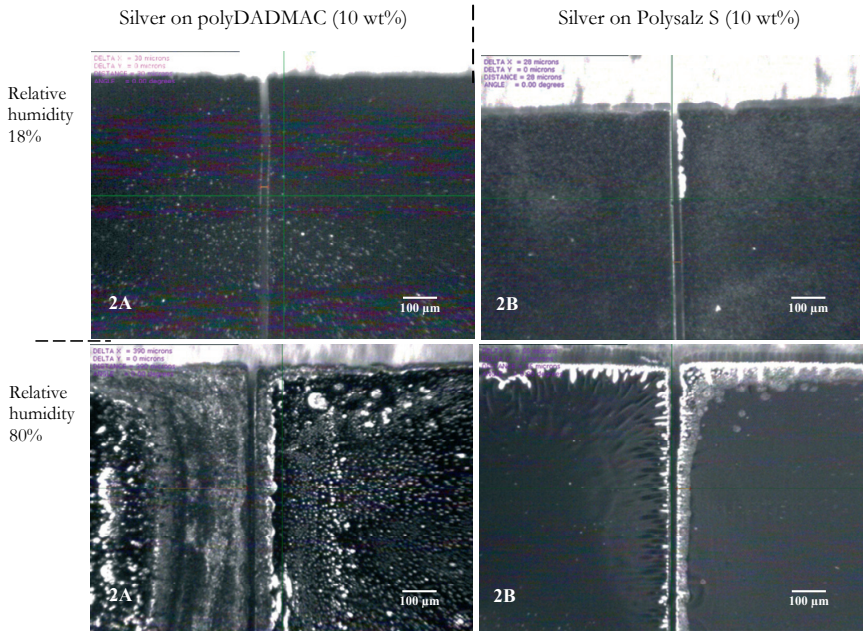


*Figure 2: Behavior of evaporated silver on spin-coated polyelectrolyte at RH 18% and RH 80%. Microscope magnification: 100× Actual image area: 1.4 mm × 1.1 mm*

3.2 PEDOT:PSS on top of polyelectrolyte coating

PEDOT:PSS dispersed in water was deposited on top of the polyelectrolyte coated glass samples by spin-coating. PE-DOT:PSS comprises of highly conductive, hydrophobic cationic PEDOT polymer groups adsorbed on anionic PSS polyelectrolyte chains. This is known as the secondary structure with the primary structure being represented by isolated PEDOT and PSS components (Fig. 3). PSS makes a strong polyelectrolyte, i.e. it is fully charged in solution and dissociates well in water. Mixing the secondary structure with water gives a rise to the formation of colloidal particles (tertiary structure) consist-ing up to 90-95% of water, hydrophobic PEDOT groups being pushed into the center of the particle surrounded by water and anionic PSS. These colloidal particles form the building blocks of conductive PEDOT:PSS films and coatings (quaternary structure).

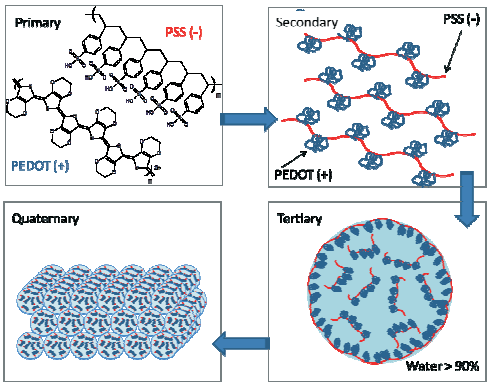


*Figure 3:*
*PEDOT:PSS structures in hierarchal order*

Transfer method, carrier liquid composition, drying method and drying time all contribute to the PEDOT:PSS film structure, packing density and conductivity. Studies show that spin-coating may provoke segregation in the quaternary structure transforming it through into a structure consisting of lentil-like PEDOT clusters separated by very thin PSS lamellas and excess PSS on top.[31,32]

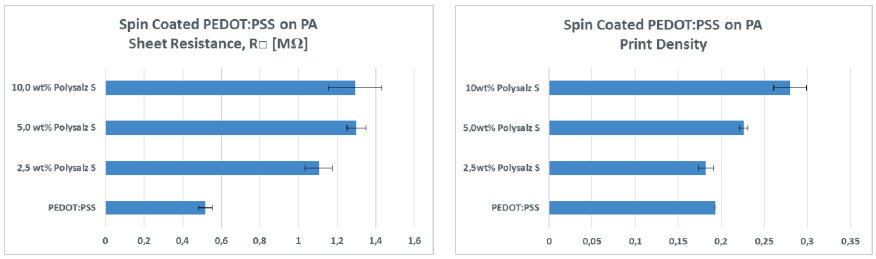


*Figure 4: Sheet resistance (left) and print density (right) values of spin-coated PEDOT:PSS on PA coated glass. Print densities are gross values (print density of glass slide, 0.09-0.10)*

Standard homogenized PEDOT:PSS was spin-coated on top of the polyelectrolyte coated samples. Anionic PA (Polysalz S) is a strong polyelectrolyte. Introduction of PEDOT:PSS made PA effectively dissociate with the PEDOT:PSS water dispersion, resulting in smeared, non-uniform film coverage with strong local color shifts. This caused pronounced sample-to-sample variation observed in terms of increased standard deviation in print density values and sheet resistance values, especially at the strongest PA concentration (Figure 4). Smeared bilayer samples could not produce consistent print density values and neither did they perform very well in comparison to the PEDOT:PSS single layer reference.

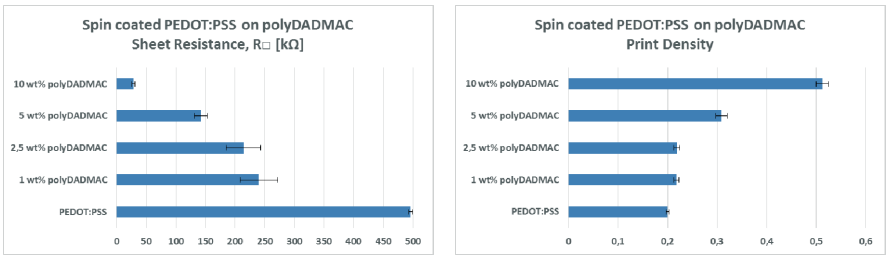


*Figure 5: Sheet resistance (left) and print density (right) values of spin-coated PEDOT:PSS on polyDADMAC coated glass. Print densities are gross values (print density of glass slide, 0.09-0.10)*

Spin-coated PEDOT:PSS performed much better on polyDADMAC as clearly seen in Figure 5. PEDOT:PSS produced dark-er colored samples at higher polyDADMAC coating concentrations due to stronger adsorption of the oppositely charged PE-DOT:PSS at the solid-liquid interface. PEDOT:PSS adsorption caused sheet resistance values drop in all polyDADMAC//PEDOT:PSS bilayer samples. Correctly and accurately produced samples resulted in consistent measurement values with only minor deviations.

In bulk, introduction of polyDADMAC solution into the PEDOT:PSS water dispersion makes it unstable. The dispersion particles collapse as the PEDOT:PSS component becomes separated from the water component. In spin-coating, quick de-position and drying of the adsorbed PEDOT:PSS layer prevented it from becoming destabilized beyond control by the poly-DADMAC underlay, hence the observed significant decrease in sheet resistance.

A series of the standard homogenized PEDOT:PSS was deposited and kept for periods ranging from 20 to 120 seconds on the 10 wt% polyDADMAC before initialization of the spin-coating step (Figure 6). Sheet resistance levels remained close to identical, except for deposition time intervals exceeding 60 seconds. Long deposition periods increase the interaction in the solid-liquid interface for the worse producing bilayers of some higher sheet resistance performance and lower sample reproducibility. At shorter deposition periods, the polyDADMAC concentration forms the predominant factor for PEDOT:PSS adsorption and bilayer homogeneity.

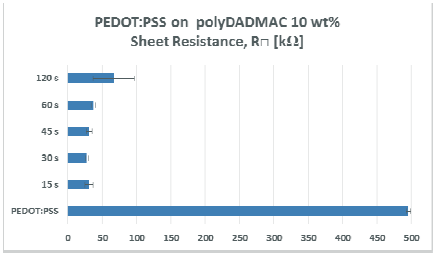


*Figure 6:*
*PEDOT:PSS spin-coated on 10 wt% cationic polyDADMAC. Timespan (in seconds) refers to the time elapsed from the moment of PEDOT:PSS deposition to the spin-coating initialization. Longer bar means higher sheet resistance, R□*

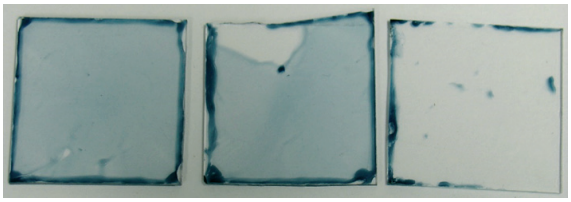

*Figure 7: Spin-coated PEDOT:PSS film defects after extended period (120 s) exposure to 10 wt% polyDADMAC. Left to right: sample with some minor defects (left), sample with local bilayer rip off (in the middle) and a sample with practically no bilayer left (right)*

We assume that prolonged PEDOT:PSS deposition periods enable the hygroscopic solid polyDADMAC layer to absorb moisture from the PEDOT:PSS water dispersion phase causing swelling, aggregation and disorder at the interface at the expense of bilayer uniformity and electrical performance. At worst, bilayers could lose their grip to the glass substrate surface partly or fully under the influence of centrifugal forces during spin-coating (Figure 7).

In the final test, PEDOT:PSS was spin-coated layer-by-layer in one to three steps in the absence of any PA or polyDADMAC electrolyte (Figure 8). The prefix mono-, bi-, tri- refers to number of repeated deposition/spin-coated steps and stacked PEDOT:PSS layers on the glass substrate. The multiple layers of PEDOT:PSS were expected to provide a thicker overall layer thickness, darker color, i.e. higher print density, and lower sheet resistance. This is exactly the case in Figure 8! It might be pure coincidence that the sheet resistance results of the bilayer and the trilayer PEDOT:PSS samples almost coincide with the 5 wt% and 10 wt% polyDADMAC//PEDOT:PSS bilayer results presented in Figure 5. After all, the polyDADMAC concentrations test series could have been picked in some other way. In fact, also their corresponding print densities almost overlap with each other which cannot be considered a coincidence anymore.

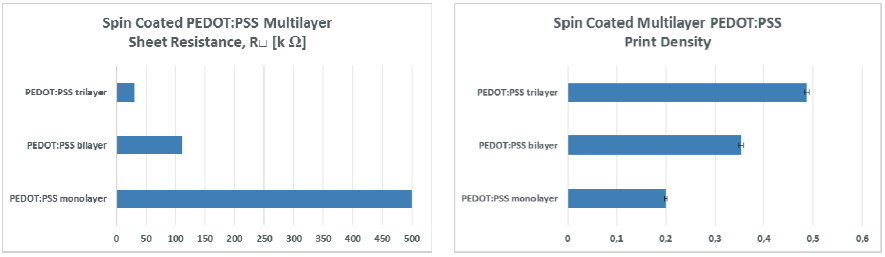


*Figure 8: Sheet resistance and print density values of multilayer (layer-by-layer) PEDOT:PSS only spin-coated samples. Print densities are gross values (print density of glass slide, 0.09-0.10)*

3.3 SEM sample profile analysis

SEM sample profile analysis were performed on single layer polyDADMAC or PEDOT:PSS samples and bilayer polyDADMAC//PEDOT:PSS samples. Beside layer thickness determination, we were interested to get some first-hand confirmation about the structure of these layers.

The reference, spin-coated single layer PEDOT:PSS showed a 90 nm thick quaternary structured layer with two PEDOT:PSS water dispersion particles rows on top of each other (Fig. 9). Dispersion particle diameters ranged from 40 to 65 nm.

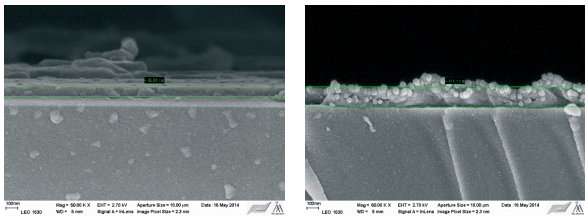

*Figure 9: Spin-coated PEDOT:PSS on glass (left & right). Dispersion particles remain intact on the surface despite the spin-coating. PEDOT:PSS thickness approx. 90 nm*

Spin-coated single layer polyDADMAC samples showed layer thicknesses ranging from 33 nm and 748 nm for respectively 1wt% and 10 wt% polyDADMAC (Table 1.). The increase in polyDADMAC layer thicknesses goes hand in hand with the increase of polyelectrolyte concentration. The layer thickness change does not linearly follow the polyDADMAC concentration change because of the viscosity factor of the solution which is concentration dependent. Stronger polyDADMAC solution show higher viscosity, i.e. it is more resistant to deformation brought by the centrifugal and compression forces during the spin-coating action. This adds some additional thickness portion to the overall layer thickness all other things held constant.

*Table 1: Thickness of single layer polyDADMAC and polyDADMAC/PEDOT:PSS bilayers. Underlined figures refer to layer thicknesses depicted in Fig. 8*

| Single Layer Sample | Thickness [nm] | Bilayer Sample | Thickness [nm] |
|---|---|---|---|
| 1.0 wt% pDADMAC | 33-47 | 1.0 wt% pDADMAC + PEDOT:PSS | 106 |
| 2.5 wt% pDADMAC | 117-124 | 2.5 wt% pDADMAC + PEDOT:PSS | 206-248 |
| 5.0 wt% pDADMAC | 300-307 | 5.0 wt% pDADMAC + PEDOT:PSS | 234-256 |
| 10.0 wt% pDADMAC | 710-748 | 10.0 wt% pDADMAC + PEDOT:PSS | 360 |

According to our results, the layer thickness of the single layer polyDADMAC samples exceed the total thickness of the bilayer samples at higher polyDADMAC concentrations (Table 1). Bilayer sample preparation is a delicate process. Reproducible results require good hand skills and close attention to detail, especially when PEDOT:PSS is deposited on top of 5 wt% and 10 wt% polyDADMAC coated samples. At the time of the bilayer sample preparation for SEM imaging, the sample preparation skills were not yet fully up to the required level. Because of this some of the polyDADMAC became locally thinned out when depositing PEDOT:PSS on top.

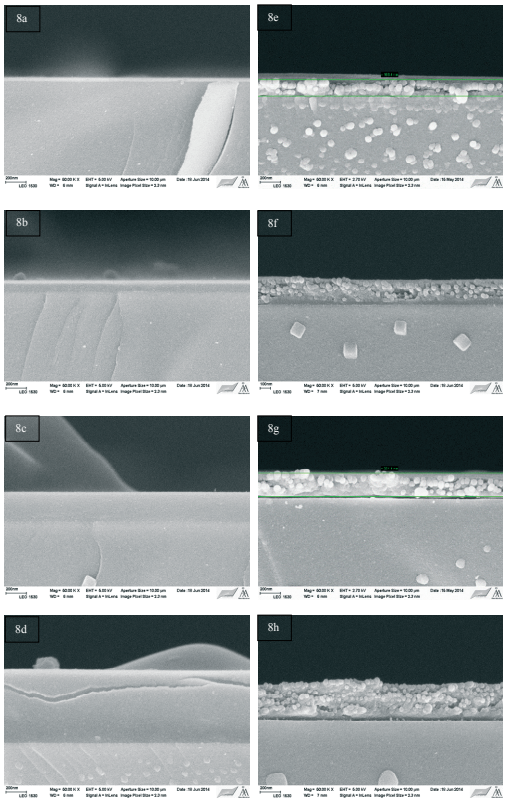


*Figure 10: Left column (8a-8d): 1.0 wt%, 2.5 wt%, 5.0 wt% respectively 10.0 wt% single layer polyDADMAC. Right column (8e-8h): bilayers comprising spin-coated PEDOT:PSS deposited on polyDADMAC of identical concentration as in the left column. Magnification: 50 000 x*

The most important SEM based single observation is that on all samples with bilayers the PEDOT:PSS presserves its quaternary structure. From a SEM sample preparation and study point of view this is not self-evident. A detailed explanation is presented in the experimental section. A higher polyDADMAC concentration cause stronger attraction leading to the formation of a thicker PEDOT:PSS adsorption layer. On closer inspection some of the PEDOT:PSS dispersion particle rows seem to sink into or blended with the polyDADMAC underlay creating a diffuse interface region in between the two layers. Layer blending at the bilayer interface is a common spin-coating associated phenomenon.

## 4 Discussion

In the first half of this work the polyelectrolyte conductivity and compatibility with silver electrodes was studied. Both polyDADMAC and PA coatings showed high sheet resistances in the MΩ respectively GΩ range. At first glance, the given electrical performance range represented by these polyelectrolytes might appear modest. However, from a chemical corrosion point of view, the corrosion rate becomes easily boosted up, if a small external low voltage current is able to pass through the coating. Air humidity together with external current, had a significant impact on the hygroscopic and corrosive polyDAMAC making the silver top electrodes corrode easily. Extreme humidity alone was enough to make the PolyDADMAC swell and the silver top electrodes disintegrate. Neither humidity nor external current caused any serious damage to the PA or the silver electrodes on top.

The polyelectrolyte concentrations used in this work depended on the spin coater's ability to produce repeatable and uniform films. Glass slide samples could not be coated below a certain polyelectrolyte specific concentration readily exceeding the actual concentration found in paper coated surfaces. We can safely state that the PA at the paper coating surface will not have an effect on the function of printed electronics components in direct contact with the coated paper surface. We also assume that the polyDADMAC at the coated paper surface should not cause immediate harm to newly printed electronics components.

In the second half of this work the influence of PA and polyDADMAC on the electrical performance of spin-coated conductive polymer PEDOT:PSS was studied. PEDOT:PSS didn not perform very well on PA, where the two layers blended unfavorably showing weaker electrical performance in comparison to the single layer PEDOT:PSS reference. On polyDADMAC it was the opposite story.

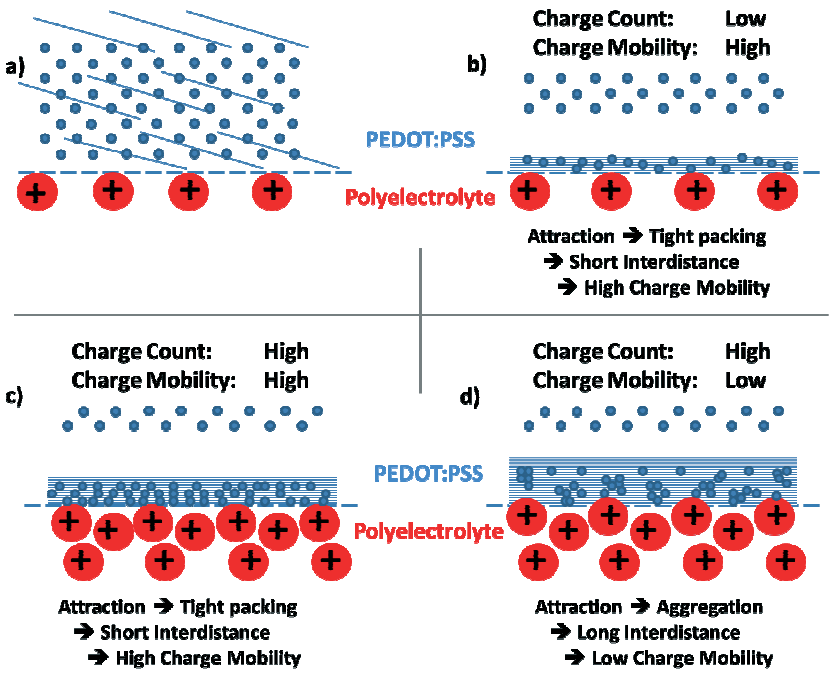


*Figure 11: Deposition of PEDOT:PSS on top of cationic polyDADMAC.*

The PEDOT:PSS deposition step (Fig. 11a) is followed by an attraction step. The oppositely charged PEDOT:PSS water dispersion particles are attracted by the positive polyDADMAC underlay forming an oversaturated adsorption layer of quaternary structure at the liquid solid interface. The thickness of the oversaturated

adsorption layer is determined by the polyDADMAC concentration (Fig. 11b and 11c). The adsorption stops growing, reaching its maximum thickness, by the time PEDOT:PPS particles in the bulk situate too far away to become attracted by the interface.[33,34,35]

According to SEM results much of the PEDOT:PSS quaternary structure is preserved. In general, the macromolecular weight of polyDADMAC is close to 100 kD hindering it from sipping quickly past the PE-DOT:PSS adsorption layer into the bulk phase. Still, prolonged deposition periods (> 60 s) may destabilize the PEDOT:PSS layer structure partly or completely prior to the spin-coating (Fig. 7d). Sample fabrication dif-ficulties also suggest that locally applied external pressure during deposition of PEDOT:PSS may create local defects in the oversaturated adsorbed dispersion particle region by stirring the quaternary layer structure. As a result the electrical performance can drop heavily - an aspect worth noticing when dealing with contact printing method related approaches.

Bringing together data from SEM image analysis in addition to the sheet resistance and print density results we suggest that in the polyDADMAC//PEDOT:PSS based bilayer samples there is a very strong dependency between:

i. the change in the adsorbed PEDOT:PSS layer thickness and the shift in print density
ii. the concentration strength of the polyDADMAC underlay and the attracted oppositely charged PEDOT:PSS layer thickness adsorbed on top
iii. the PEDOT:PSS quaternary coating structure thickness and quality and the sheet resistance level

Based on these assumption, the amount of PEDOT:PSS adsorbed and spin-coated on the 5.0 wt% and 10.0 wt% coated polyDADMAC samples resemble to the PEDOT:PSS amount of the two- and three-times PEDOT:PSS consequently deposited and spin-coated samples. This would mean that the oversaturated PEDOT:PSS adsorption layer alone determines the electrical performance in the polyDADMAC//PEDOT:PSS bilayers.

## 5. Conclusions

The overall amount of anionic and cationic polyelectrolytes in paper coatings might be considered low, but these agents are localized on the surface where it mostly matters. They reside at the surface of single paper coating pigment particles maximizing and exposing the number of polyelectrolytes to conductive materials adhered to the top paper coating.

The sodium polyacrylate (Polysalz S) film remained dimensionally stable and showed only little changes in electrical conductivity at various relative humidities. Besides normal air bound oxidation, silver tracks showed only slight signs of directional, current driven corrosion. Cationic polyDADMAC, on the other hand, was the exact opposite to the polyacrylate. Being more prone to dimensional instability at RH 50% and higher, evaporated silver tracks began disintegrating accompanied by corrosion. The latter was strongly affected by the electrical current.

Spin-coating PEDOT:PSS on top of sodium polyacrylate (Polysalz S) made the polyacrylate dissociate into the PEDOT:PSS resulting in non-uniform films of low reproducibility. These films showed weaker conductivity than single layer PEDOT:PSS reference films. In reality, the polyacrylate stays strongly adsorbed to paper coating pigments.

On top of cationic polyDADMAC, PEDOT:PSS can form a nicely conductive layer. The oppositely charged PE-DOT:PPS water dispersion particles are attracted and arranged against the cationic polyelectrolyte layer at the solid-liquid interface, prior to spin-coating. Under well controlled circumstances this can produce a reproducible conductive bilayer showing up to 16 times lower sheet resistance in comparison to pure PEDOT:PSS spin-coated films at constant rpm.

**Acknowledgements**

The authors would like to thank María Inés Placencia Pena for her hard work in the chemical laboratory as well as Simon Baumgartner for creating the CAD model for the UV-LED lamp.

**References**


[1] Tobjörk, D., Österbacka, R. *Adv. Mater.* 23 (2011), 1935

[2] Mäkelä, T., Jussila, S., Vilkman, M., Kosonen, H., Korhonen, R. *Synth. Met.* 135-136 (2003) 41

[3] Andersson, P., Forchheimer, R., Tehrani, P., Berggren, M. *Adv. Funct. Mater.* 17 (2007) 3074

[4] Yang, L., Rida, R., Vyas, M., Tentzeris, M.M. *IEEE Transactions on Microwave Theory and Techniques 55* (2007) 2894

[5] Unander, T., Nilsson, H.-E. *IEEE Sens. J.* 9 (2009) 922

[6] Courbat J., Kim Y.B., Briand, D., de Rooi, N.F. *Proceedings of 16th International Solid-State Sensors, Actuators and Microsystems Conference, 2011 TRANSDUCERS*, 1356-1359, Beijing, China (2011)

[7] Arena, A., Donato, N., Saitta, G., Bonavita, A., Risso, G., Neri, G. *Sensor Actuat B - Chem* 145 (2010) 488

[8] Liu, X.Y., O'Brian, M., Mwangi, M., Li, X.J., Whitesides, G.M. *Proceedings of 2011 IEEE 24th International Conference on Micro Electro Mechanical Systems (MEMS), 133-136*, Cancun, Mexico (2011)

[9] Sarfraz, J., Määttänen, A., Ihalainen, P., Keppeler, M., Lindén, M., Peltonen, J. *Sensor Actuat B - Chem* 173 (2012) 868

[10] Määttänen, A., Vanamo, U., Ihalainen, P., Pulkkinen, P., Tenhu, H., Bobacka, J., Peltonen, *J. Sensor Actuat B - Chem* 177 (2013) 153

[11] Dungchai, W., Chailapakul, O., Henry, C.S. Anal. Chem. 81 (2009) 5821

[12] Nie, Z., Nijhuis, C. A., Gong, J., Chen, X., Kumachev, A., Martinez, A. W., Narovlyansky, M., Whitesides, G. M. *Lab Chip* 10 (2010) 477

[13] Hübler, A., Trnovek, B., Zillger, T., Ali, M., Wetzold, M., Mingebach, M., Wagenpfahl, A., Deibel, C., Dyakonov, A. *Adv. Energy Mater.* 6 (2011) 1018

[14] Björklund, R.B., Lundström, I. *J. Electron. Mater.* 13 (1984) 211

[15] Montibon, E., Lestelius, M., Järnström, L., J. Appl. Polym. Sci. 117 (2010) 3524

[16] Qian, X. Song, H., Wang, L. *Proceedings from the 3rd International Symposium on Emerging Technologies of Pulp and Papermaking*, Guangzhou, China (2006)

[17] Huang, B., Kang, G.J., Ni, Y. Pulp and Paper Canada 107 (2006) 38

[18] Agarwal, M., Lvov, Y.M., Varahramyan, K. *Nanotechnology* 17 (2006) 5319

[19] Zheng, Z., McDonald, J., Khillan, R., Su, Y., Shutava, T., Grozditz, G., Lvov, Y.M. *J. Nanosci. Nanotechnol.* 6 (2006) 624

[20] Wistrand, I., Lingström, R., Wågberg, L. *Eur. Polym. J.* 43 (2007) 4075

[21] Penn C.Q., Thio, Y.S., Gerhardt, R.A. *Nanotechnology* 19 (2008) 1

[22] Jang, J., Ryu, S.K. *J. Mater. Process. Technol.* 180 (2006) 66

[23] Shinagawa, S., Kumagai, Y., Urabe, K. *J. Porous. Mater.* 6 (1999) 185

[24] Denneulin, A., Blayo, A., Bras, J., Neuman, C., *Prog. Org. Coat.* 63 (2008) 87

[25] Trnovek, B., Stanel, M., Hahn, U., Hübler, A.C., Kempa, H., Sangl, R., Foster, M. *Prof. Papermak.* 6 (2009) 48

[26] Amin, Y., Chen Q., Zheng, L.R., Tenhunen, H. Progress in Electromagnetic Research 130 (2012) 241

[27] Bollström et al., Org. Electron. 10 (2009) 1020

[28] Määttänen, A., Ihalainen, P., Bollström, R., Toivakka, M., Peltonen, J. *Colloids Surf. A* 367 (2010) 76

[29] Ihalainen, P., Määttänen, A., Järnström, J., Tobjörk, D., Österbacka, R., Peltonen, *J. Ind. Chem. Eng. Res.* 51 (2012) 6025

[30] Bollström, R., Tobjörk, D., Dolietis, P., Salminen, P., Preston, J., Österbacka, R., Toivakka, M. *Chem. Eng. Process. Process Intensif.* 68 (2013) 13

[31] Nardes et al., Adv. Mater. 19 (2007) 11961

[32] Fabretto et al., Thin Solid Films 516 (2008) 7828

[33] Ouyang et al.,_Polymer_2004

[34] Lindell et al., Chem. Mater. 18 (2006) 4246

[35] Jönsson_2003_Synth. Mat.

# A direct printed passive RF sensor for content aware drug bottles

*Marco Mazza*[1], *Johannes Renner*[1], *Pierluigi Civera*[2], *Fritz Bircher*[1]

[1] College of Engineering and Architecture Fribourg
Perolles 80, CH-1705 Fribourg, Switzerland

[2] Politecnico di Torino,
Corso Duca degli Abruzzi 24, I-10129 Torino, Italy

E-mails: marco.mazza@hefr.chf; johannes.renner@hefr.ch; pierluigi.civera@polito.it; fritz.bircher@hefr.ch

**Abstract**

Lack of compliance with regard to medical prescriptions has become a major cause of treatment failure, a problem particularly faced in the aging population. In order to aid patients in taking their medication properly, various products for solid drugs like electronic pill organizers have recently appeared on the market whereas there is a lack of effective solutions for liquid drugs. In this paper, a novel direct printed RF sensor for drug bottles is presented as a low-cost solution, which can be used for monitoring liquid medication. The fully-printed, single layer metal sensor has been realized on the top of a polyethylene bottle, acting as a resonant LC tank, which can be read remotely. Resonant frequency drifts proportionally to the liquid content, since the distributed capacitance value is affected by the permitivity of the liquid.

The demonstrator presented in this article shows an impressive sensitivity up to 316 kHz/mL, resulting in a cost-efficient and viable solution to detect content variation in the order of sub - milliliters.

**Keywords**: printed LC resonant tank, monitoring drug bottle, passive liquid sensor, syringe extrusion

## 1. Introduction

According to a recent study (Meera, 2012), more and more patients fail to comply with medical prescriptions resulting in a considerable performance gap between potential treatment success rate and actual results within a population. Different studies have clearly shown that 20 % to 30 % of medical prescriptions are never used and approximately 50 % of medications taken for chronic diseases are not taken as prescribed by the treating physician (Peterson, 2003) (Haynes, 2008). In the United States, this lack of compliance has dramatic effects on patient health, resulting in approximately 125 000 deaths annually and 10 % of hospitalizations as well as extra costs for the U.S. health care system, estimated between $ 100 and $ 289 billion.

One of the main reasons for medical non-compliance lies in the simple fact that patients forget to take the drugs as indicated (Tanke, 1993). Plenty of products, such as pill-organizers have recently appeared on the market, providing visual and/or auditory signals to remind the patient to take the prescribed drugs, with additional availability of online support centers and caregivers.

However, little has been done to verify that the patient has actually consumed the medication appropriately. Optical techniques, while providing good reliability, are not particularly effective for their use in transparent liquids or opaque drug bottles and are generally not low-cost and flexible enough for different applications.

In this paper, a novel concept of a printed sensor, remotely read from an RF system is proposed. The design of the capacitive sensing area is aided by numerical simulation. The functionality of the concept is verified by impedance measurements of printed RF sensors on medical bottles.

## 2. Methods

### 2.1 Sensor design

In an initial step, a co-planar capacitive sensing area for the RF sensor is chosen. Printed vertically on the side of the bottle, the resulting capacitance depends both on the dimensions of the capacitor itself and on the surrounding di-electric constant of the medium, according to the approximate formula:

$$C\left[\frac{pF}{cm}\right] = 0.12\frac{t}{w} + 0.18\,(1+\varepsilon_R)log_{10}\left(1+\frac{w}{s}\right) \quad [1]$$

where t is the thickness of the metallic plates, w is the width, s the spacing between the plates and εR the dielectric constant. The above mentioned formula does not take into account the effect of a non-uniform di-electric medium, which is actually the case in this setting.

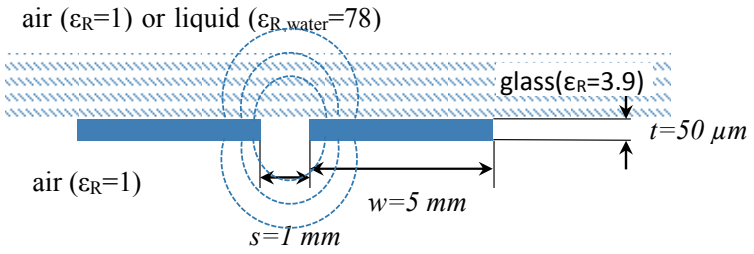


*Figure 1: Co-planar micro strip capacitor principle scheme*

For an estimation of the non-linear capacitive response, the co-planar micro strip on a glass bottle is modeled in COMSOL® Multiphysics and the electric potential distributions are simulated in full and empty bottles. As sketched in Figure 1, the dimensions of the simulated coplanar strips are 100 x 5 x 0.05 mm, with a separation of 1 mm. The diameter of the glass bottle is 60 mm and its average wall thickness approx. 2.2 mm. The simulated co-planar micro strip capacitor is then printed on the glass bottle and its capacitive response in various filling conditions measured.

The proposed design for the RF sensor consists of multiple co-planar strips which are connected by thinner traces to form an open coil. Figure 2 shows a schematic drawing of the sensor design and a picture of the RF sensor printed onto a 250 mL polyethylene (PE) bottle with an outer diameter of 63 mm.

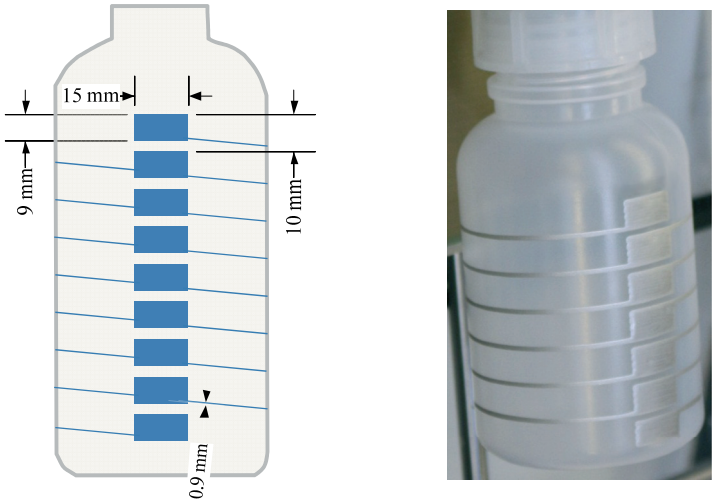


*Figure 2: Schematic design of the RF sensor and picture of the RF sensor printed onto a PE bottle*

As depicted in Figure 2, the chosen dimensions of the coplanar strips are 15x9 mm with a gap of 1 mm. The trace width of the connecting paths of the open coil is 0.9 mm.

2.2 Rapid prototyping of metallic sensors on bottles

In order to prove the concept and to be able to manufacture various sensor geometries in an efficient way, a digital syringe extrusion process was chosen to print a conductive micro particle ink (Chemtronics CW2200) directly onto medical PE bottles without any pretreatment. Polyethylene has been chosen for its optimal characteristics: (i) from a chemical point of view (especially for pharmaceutical applications) (ii) from an electrical point of view (very good performance in the RF domain) and (iii) ink adhesion. The printing platform is realized by a 3D printer (Velleman K8200), equipped with a simple rotational axis for bottles and a syringe extruder (New Era NE-511). All sensors are printed with a 5 mL syringe (B. Braun 8502350N) and a conic dosing needle with 0.41 mm extrusion diameter (OK International- 922125-DUV gauge 22).

In order to maintain a constant standoff between the dosing needle and the bottle surface, the geometries of the bottles are scanned with a touch probe and the Z - levels for the extrusion paths are calculated with linear 3D

interpolation prior to printing. The layer thickness is adjusted by the rate of extrusion in relation to the inner diameter of the dosing needle, the print speed and the line density of the infill pattern.

The electrode geometries as well as printer control are programmed with the technical programming language Matlab®.

2.3 Characterization of printed sensors

For all measurements characterizing sensor responses in different filling conditions, an Agilent 4294A Precision Impedance Analyzer is used. The initial measurements of the capacitive response of the co-planar micro strip have been performed with direct metallic contact to the sensing probes at a frequency of 125 kHz. The chosen frequency matches one of the available ISM (Instrumentation Scientific Medical) frequencies.

For the measurements of the resonance frequencies of the printed RF sensor in different filling conditions, a copper coil wrapped around the bottle holder is connected to the Impedance analyzer. The equivalent electric circuit is depicted in Figure 3.

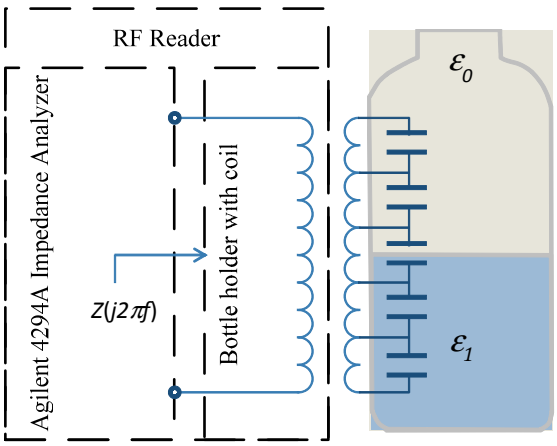


*Figure 3: Equivalent electric circuit for the printed RF sensor and its reader*

As indicated in Figure 3, the RF reader is realized by a coil connected to the impedance analyzer. The RF sensor is equivalent to a distributed LC network alongside the bottle; the capacitor value depends on the surrounding di-electric constant which will be modified by the presence of the liquid inside the bottle.

Due to the inductive coupling between the two coils, the impedance measured on the left hand side of the circuit, will depend both on the primary coil (integrated in the bottle holder) and on the resonating RF sensor.

The resulting LC circuit will then resonate at:

$$\boldsymbol{f_{res} = \frac{1}{2\pi\sqrt{L_{eq}C_{eq}}}} \qquad [2]$$

where $f_{res}$ is the resonating frequency of the passive RF tag, Leq and Ceq are the equivalent lumped inductance and capacitance of the distributed LC network (Figure 3).

Since the presence of a di-electric liquid inside the bottle will increase the di-electric constant and hence the equivalent capacitance, reducing the liquid content of the bottle results in a positive shift in the resonating frequency.

## 3. Results

3.1 Simulation and measurement of the capacitive micro strips

The geometry depicted in Figure 1 is modeled and simulated in COMSOL®, both in 2D and 3D electrostatic stationary analysis. In Figure 4, electric potential distributions are presented. The considerably different electrical potential distributions in the filled and empty case are due to the large difference between the electrostatic constants of air and water. This results in a change of the actual capacitance between the co-planar metallic strips.

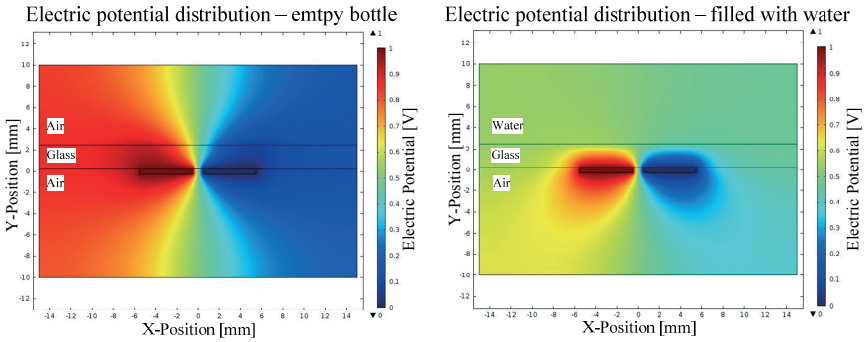


*Figure 4: COMSOL FEM analysis of the electric potential distribution with air (left) or water (right) inside the bottle*

The bottle has been filled with water and its capacity measured with a volume step of 5 mL. The results are presented in Figure 5.

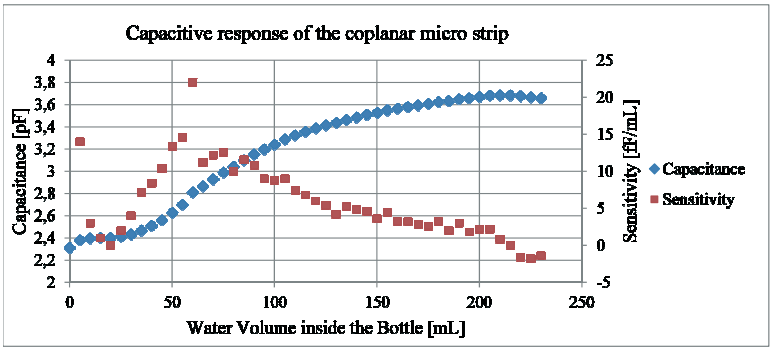


*Figure 5: Capacitance measurements of the co-planar micro strip vs. water volume inside the glass bottle*

The capacitive response is flat up to approximately 40 ml. Up to this level the liquid does not face the printed electrodes and hence does not generate any significant change in the capacitance value. A similar behavior appears at fill volumes of more than approximately 200 ml, as in this case, the water level is higher than the printed strips and, for the same reason, gives no modification in the measurements.

From 40 ml up to 200 ml, the capacitance values clearly relate to the quantity of water poured into the bottle, from 2.3 up to 3.7 pF (in good accordance with simulations), albeit in a non-linear response. Ranging from 4 to 12 fF/mL, the system sensitivity is rather high, considering that in a bottle with a diameter of 60 mm, a variation of 1 ml results in a height variation of only 354 μm.

3.2 Measurements with the proposed RF sensor

Figure 6 shows impedance measurements, performed by sweeping the exciting frequency from 40 up to 100 MHz and modifying the water content in the bottle. As concluded at the end of chapter 2.3, the resonating frequency shifts downward while increasing the liquid level. In the central region of sensing, the RF sensor achieves an average sensitivity of approximately 316 kHz/ml.

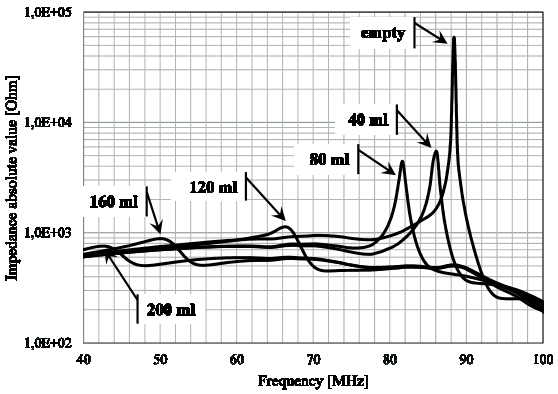


*Figure 6: Impedance measurements of the passive RF sensor detected by the RF reader as a function of the excitation frequency and the water content in the bottle*

As expected, the quality factor of the equivalent circuit and hence the amplitude of the resonance decrease when increasing the liquid level, which is due to the increased losses induced by the presence of water near the distributed coil. It is worth noting that measurements proved to be highly reproducible and almost insensitive to the orientation of the bottle inside the cylinder-reading coil.

Figure 7 shows a plot looking at the resonance frequency vs. the bottle liquid content. In the response curve, two distinct regions with different sensitivity can be seen. The first region has a lower sensitivity of 88.6 kHz/ml and is followed by a second region with a higher sensitivity of 316 kHz/ml. When the bottle is nearly empty or filled beyond the sensor position, the sensitivity is close to zero, as would be expected, considering the capacitive response in Figure 5.

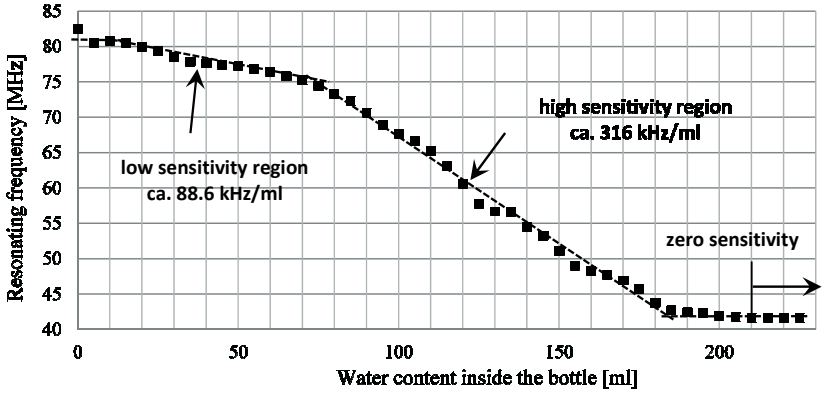


*Figure 7: Resonating frequency response vs. liquid content in the content-aware bottle*

## 4. Discussion

Even when taking into account the low sensitivity region, the performance of the proposed RF sensor is sufficient to allow for a simple and low cost tracking system for a bottle diameter of 63 mm. The sensor's peak detection capability allows to determine the quantity of liquid inside the bottle with a precision in the order of submilliliters. This can be used to monitor liquid content changes and may hence be useful in indirectly determining patient compliance.

As the function measuring liquid level changes per milliliter content is quadratic in relation to the bottle diameter, the precision of the RF sensor decreases quadratically when increasing the bottle diameter. Since drug bottles with diameters significantly larger than 63 mm are unusual for use in home medication - indeed, the majority of drug bottles for home use tend to be smaller in size-, this problem is not likely to be of clinical relevance.

As the rapid prototyping process used to manufacture the first generation sensors is unsuitable for a low cost production in an industrial scale, a different printing process is required. As the proposed sensor design depicted in Figure 2 can be printed in a single pass without any overlapping elements in need of an additional isolation layer, the sensor can be efficiently and effectively produced by various established printing processes such as screen printing or tampon printing. In addition to an increased resolution which enables smaller trace widths for connections, with industrial printing processes, the layer thickness of the printed sensor can be reduced dramatically, resulting in very low ink consumption per printed RF sensor.

## 5. Conclusion

In this paper, a novel direct printable RF sensor for passive measurements of the liquid volume inside drug bottles has been described. Due to its simple design, the sensor can be efficiently printed with established industrial printing processes in a single pass. Its high sensitivity in terms of resonance frequency vs. liquid content in the bottle, (88 kHz/mL - 316 kHz/mL, bottle diameter 63 mm) allows for a simple microcontroller based RF reader to measure the volume content of the bottle, meaning that the reader can be produced at a low costs too.

The precision of the sensor decreases in a quadratic fashion when increasing the bottle diameter. Since significantly larger drug bottles diameters - as used for home medication - are indeed very rare the proposed system may be regarded as a cost-effective solution to monitor the liquid content within sub-milliliter precision.

**References**

Haynes R. B, Ackloo E, Sahota N, McDonald HP, Yao X.,"Interventions for enhancing medication adherence" Cochrane Database Syst Rev. 2008; CD000011

Meera Viswanathan, PhD; Carol E. Golin, M. D; Christine D. Jones, MD, MS; Mahima Ashok, PhD; Susan J. Blalock, MPH, PhD; Roberta C.M. Wines, MPH; Emmanuel J.L. Coker-Schwimmer, MPH; David L. Rosen, MD, PhD; Priyanka Sista, BA; and Kathleen N. Lohr, PhD, "Interventions to Improve Adherence to Self-administered Medications for Chronic Diseases in the United States: A Systematic Review", Annals of Internal Medicine, 4 December 2012, Vol 157, No. 11

Peterson A. M, Takiya L, Finley R., "Meta-analysis of trials of interventions to improve medication adherence" American Journal on Health Syst. Pharm. 2003; 60:657-65

Tanke, E. & Leirer, V., "Use of automated telephone reminders to increase elderly patients' adherence to tuberculosis medication appointments", Proc. Human Factors and Ergonomics Society 193-196, 1993

# Studies on the 3D printing of nanocellulose structures

*David Gethin* [1], *Adam Rees* [1], *Lydia Powell* [2,3], *Gary Chinga-Carassco* [4], *Tim Claypole* [1], *Davide Deganello* [1], *Katja Hill* [3], *David Thomas* [3], *Kristin Syverud* [4]

[1] Swansea University
WCPC, Swansea, UK

[2] Centre for NanoHealth
College of Engineering,
Swansea University
Swansea, UK

[3] Tissue Engineering and Reparative Dentistry
Cardiff University School of Dentistry
Cardiff, UK

[4] Paper and Fibre Research Institute (PFI)
Trondheim, Norway

E-mail: gary.chinga.carrasco@pfi.no

**Abstract**

Nanocellulose has a variety of advantages, which make the material most suitable for use in biomedical devices such as wound dressings. The material is strong, can be used for producing transparent films, can keep a moist environment and form elastic gels with bio-responsive characteristics. In this study we explore the application of nanocellulose as a bioink for use in a bioprinting process. Two different nanocelluloses were used, prepared with TEMPO mediated oxidation and a combination of carboxymethylation and periodate oxidation. The combination of carboxymethylation and periodate oxidation produced a homogeneous material with short nanofibrils. The small dimensions of the nanofibrils reduced the viscosity of the nanocellulose thus yielding a material with good rheological properties for use as a bioink. We also demonstrated that both nanocelluloses inhibited bacterial growth, which is an interesting property of these novel materials.

**Keywords**: bioplotting, wound dressings, nanocellulose, characterization

## 1. Introduction and background

*Wood nanocellulose*

Nanocellulose is a novel material that can be produced from a variety of biodegradable and renewable resources (Turbak et al., 1983; Saito et al., 2006; Pääkkö et al., 2007; Wågberg et al., 2008; Saito et al., 2009; Syverud et al., 2011; Jonoobi et al., 2012; Alila et al., 2013). Nanocellulose may be deposited as a gel to form three-dimensional structures that have potentially diverse applications. The material has various characteristics that make it suitable as a substrate for printing functionality, as well as a component in bioinks. Firstly, well-fibrillated nanocellulose materials are composed of a large fraction of nanofibrils with widths in the nanometer scale and lengths in the micrometer scale. These high aspect ratio nanofibrils are capable of self-assembling and form dense, smooth, transparent and strong structures (Henriksson et al., 2008; Fukuzumi et al., 2009). Based on these characteristics, recent studies have proposed using nanocellulose as the main component in the production of smooth films, which are suitable for subsequent functionalization by printing (Chinga-Carrasco et al., 2012; Orelma et al., 2012).

Secondly, depending on the pre-treatment, different types of nanocellulose can be produced, with a defined morphology and surface chemistry. Recently, it has been demonstrated that oxidized nanofibril gels could act as pH responsive structures (Chinga-Carrasco and Syverud, 2014), which may have applications in dressings for chronic wounds.

The design of tailor-made wound dressings with barrier, absorbent and bio-responsive characteristics may benefit from the structuring of complex porous structures in an effective way. Printing and coating are low-cost processes for surface modification and can facilitate the deposition of specific nanocellulose materials. Provided that nanocellulose can be applied as a bioink, printing can be a most suitable method to form self-standing and high-absorbent porous structures.

*Bioprinting*

The deposition of gelling materials is not a straight forward process. While in a liquid state, traditional volume printing methods are candidate processes. At the onset of gelation, the image transfer process breaks down and alternative technologies that use an extrusion principle are more appropriate. These rely on the ability to maintain constant rheological properties within the gel combined with a preparation process that ensures gel consistency to facilitate volume production.

Deposition of gel materials can be achieved using a Bioplotter (see e.g. Ang et al., 2002; Landers et al., 2007; Wang et al., 2013; Billiet et al., 2014; Inzana et al., 2014). Bioplotting can be considered to be very similar to a variant of rapid prototyping with the exception of the method of deposition. Some variants of rapid prototyping use a mechanical screw and heat source to melt a solid polymer and then extrude it as a highly viscous fluid through a nozzle, whereas the Bioplotter uses air pressure. This is appropriate for low viscosity fluids that can include polymer melts and biopolymers, such as nanocellulose gels. This delivery system has several advantages in that liquids having an appropriate viscosity can be deposited using the Bioplotter. The Bioplotter can also produce complex shapes that would otherwise be unfeasible through traditional manufacturing techniques.

This paper describes how nanocellulose gels may be deposited using a Bioplotter that is capable of extruding the gel to form a predefined 3D structure. The constructs are 'fixed' by freeze-drying, after which their topographical details are explored using microscopy techniques. The study demonstrates that gel structures can be printed to "pattern" surface structures. Additionally, nanocellulose films have potential as wound dressings. With this in mind, we also studied the ability of these prototypical nanocellulose structures to inhibit bacterial growth.

## 2. Methods

*Nanocellulose production*

Two nanocellulose materials have been applied in this study, derived from Pinus radiata bleached kraft pulp fibres. One nanocellulose was pretreated with TEMPO mediated oxidation (Saito et al., 2006; Syverud et al., 2011) and will be denominated as TEMPO nanocellulose in the following. The second nanocellulose material was pretreated with a combination of carboxymethylation and periodate oxidation (Chinga-Carrasco and Syverud, 2014) and will be described as C-Periodate nanocellulose in the following. The nanocelluloses were produced through homogenization using a Rannie 15 type 12.56X homogenizer. The pulp consistency was estimatedby measuring the dry residue with a HR73 Moisture Analyzer. The consistency of the TEMPO and C-Periodate samples was 1.0 % and 0.5 %, respectively.

As an attempt to remove residual fibres from the C-Periodate nanocellulose material, the suspension was additionally filtered through a Sefar 03-140/41 mesh fabric. The filtered nanocellulose was then concentrated by centrifugation for 30 min at 4 000 rpm. The final consistency of the C-Periodate nanocellulose was 3.9 %.

Films (20 g/m²) were made of the TEMPO nanocellulose for use as substrate for printing. The films were made by casting a 0.2 % suspension in petri dishes. The suspensions were allowed to dry for 4-5 days at room temperature (~20 °C).

*Characterisation*

SEM was performed with a Hitachi S-3000 variable pressure SEM, using a secondary electron detector. The acceleration voltage was 5 kV and the working distance was approximately 10 mm. AFM was used for assessing the nanofibril morphology. AFM imaging of the two materials was performed using a Dimension 3100 AFM (Bruker) and RTESPA probes (Bruker). Imaging was performed in tapping-mode operation in air, using a scan rate of 0.7 Hz and an image resolution of 1 024 x 1 024 pixels.

The rheological properties were measured using a Bohlin Gemini HR nano Rheometer (Malvern Instruments Ltd., U.K.), in simple shear mode. The tests were conducted using a plate and cone arrangement. The cone chosen was a 4°, 40 mm diameter cone and the rheometer had a set gap of 0.150 mm. The test was run under ambient conditions varying the strain rate from 1 s-1 to 100 s-1 then back.

*Bacterial growth assessment*

The nanocellulose materials were screened for bacterial contamination. This was performed by incubating the undiluted nanocellulose suspensions at 37 °C and taking hourly optical density measurements at 600 nm (OD600) of the samples over 17 hrs. An MH broth only control was also tested. In addition, the ability of the nanocellulose materials to inhibit or promote bacterial growth in planktonic culture was also examined. Nanocellulose

suspensions (800 µl) were inoculated with 20 µl of overnight culture of Pseudomonas aeruginosa PAO1 and hourly optical density measurements taken as described above. An MH broth control, comprising nanocellulose material (800 µl) with 20 µl MH broth was also included.

*Three-dimensional (3D) bioprinting*

A commercially available 3D Bioplotter (EnvisionTEC GmbH) was used to construct grid structures. The intention was to verify the suitability of the two assessed nanocelluloses for being used as bioinks for 3D printing. The 3D printed constructs were then freeze-dried and assessed by SEM.

## 3. Results and discussion

Figure 1 shows AFM images which reveal the morphology of the nanofibrils. Note the major difference with respect to the length of the individual nanofibrils. Carboxymethylation and periodate oxidation yielded short nanofibrils, compared to the TEMPO quality. The lengths of C-Periodate nanofibrils were in the range of roughly 200 nm.

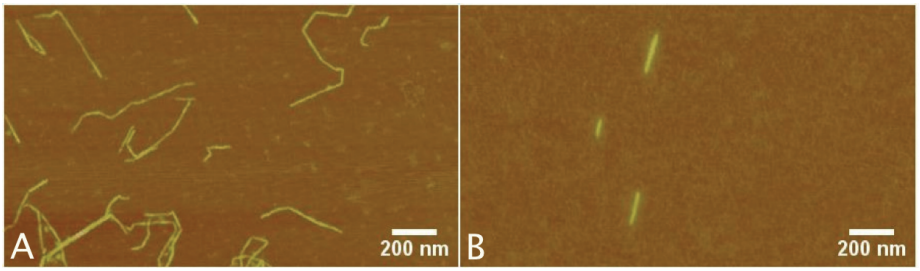


*Figure 1: AFM images of cellulose nanofibrils. A) TEMPO nanofibrils utilized for making the film substrate. B) C-Periodate nanofibrils for application as a bioink*

Additionally, the rheology of the different nanocellulose gels used to deposit 3D constructs was assessed using shear rheology (Figure 2). The nanofibril morphology varied greatly between the two suspensions making it difficult to compare the two data sets, however it can be seen that both suspensions followed the fluid power law with a little hysteresis between shear rate sweeps. This behavior has been previously reported by Iotti et al. (2011) showing a hysteresis loop between those samples similar to those found in this study. However in the literature found, the rheological data showed interesting behavior in strain rates higher than those used in this study (strains up to 1 000 $s^{-1}$). Keep in mind that the concentration of the C-Periodate nanocellulose was roughly 4 times higher than the concentration of the TEMPO nanocellulose. However, the 4x higher concentration was not reflected as 4 x higher viscosity. This was due to the shorter nanofibrils in the C-Periodate sample, which reduced the entanglement of the material.

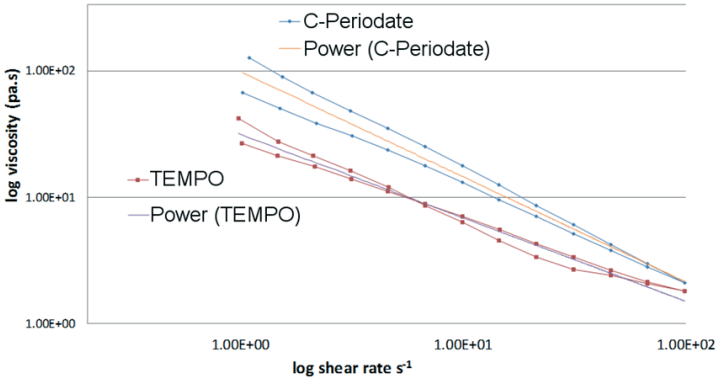


*Figure 2: Rheological properties of the TEMPO and C-Periodate nanocelluloses*

In these experiments, we studied the ability of these prototypical nanocellulose materials to support or inhibit the bacterial growth of the common wound pathogen Pseudomonas aeruginosa. The nanocellulose materials with/without MH broth did not show any significant increases in OD600 which indicated that the suspensions were free from bacterial contamination (Figure 3). This study also revealed that the OD600 measurement of the two nanocelluloses when inoculated with PAO1 did not significantly increase which indicated that the materials inhibited (did not support) bacterial growth (Figure 3), which is an interesting property of these novel materials.

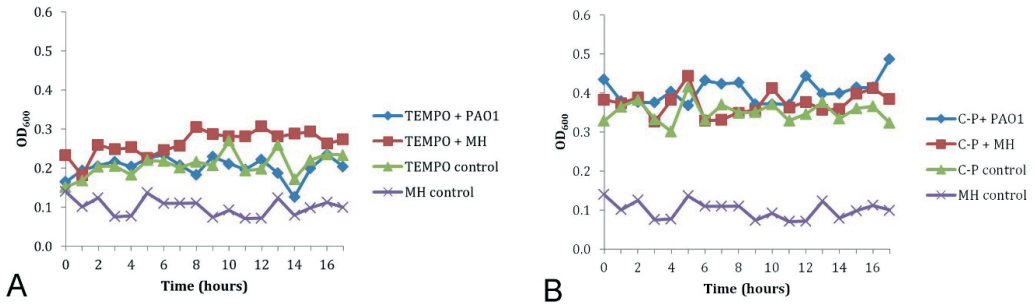


*Figure 3: Optical density measurements for the nanocellulose suspensions with/without Pseudomonas aeruginosa PAO1 to determine whether they support or inhibit bacterial growth. A) TEMPO nanocellulose suspension. B) C-Periodate nanocellulose suspension*

Having clarified the morphology, rheology and the ability of the materials to inhibit PAO1 growth we assessed the suitability of the material to be used as a bioink in 3D printing. Figure 4 demonstrates two grid constructs using the TEMPO and C-Periodate nanocellulose as bioinks. Contrary to the TEMPO nanocellulose, the C-Periodate nanocellulose formed a more solid structure with defined tracks. On the other hand, the TEMPO nanocellulose tended to collapse probably due to the low consistency of the material (0.95%). The C-Periodate nanocellulose had shorter fibrils, higher consistency (3.9%) and an appropriate rheology which was suitable for being used as bioink.

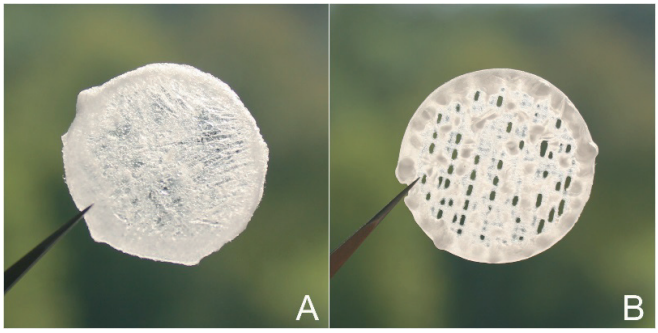


*Figure 4: Grid constructs printed with a Bioplotter unit. A) TEMPO nanocellulose. B) C-Periodate nanocellulose*

Figure 5 shows an SEM image of a simple grid construct where the C-Periodate nanocellulose was deposited on a TEMPO nanocellulose film. The deposited material gave a highly porous structure. Such structures have been reported to be highly absorbent and pH-responsive (Chinga-Carrasco and Syverud, 2014). Hence, similar characteristics can be applied in tailor-made wound dressings with potential to carry and release antimicrobial components.

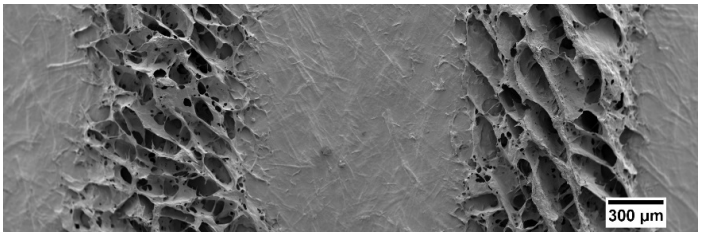


*Figure 5: SEM image of porous 3D tracks printed on the surface of a smooth nanocellulose film. The porous tracks can potentially be applied as bio-responsive structures for the controlled release of integrated components*

## 4. Conclusions

The work shows how nanocellulose may be formulated to manufacture substrates and gels that may be deposited as a bioink through a printing process. Based on the printing of grid structures we conclude that the C-Periodate nanocellulose was suitable for being used as bioink. This was most probably due to the higher consistency and appropriate rheology of the C-Periodate achieved in this study. The nanocelluloses form 3D structures where the tracks have an open porosity and the potential to carry and release antimicrobial components. Importantly, we also demonstrated that the nanocelluloses assessed in this study inhibited bacterial growth. The antimicrobial properties of these materials will be a distinct advantage for healthcare applications.

**Acknowledgements**

This work has been funded by the Research Council of Norway through the NANO2021 program, grant No. 219733 - NanoHeal: Bio-compatible cellulose nanostructures for advanced wound healing applications.

**References**

Alila, S., Besbesa, I., Rei Vilar, M., Mutjé, P., Boufi,S., 2013. Non-woody plants as raw materials for production of microfibrillated cellulose (MFC): A comparative study. Industrial Crops and Products 41, 250-259

Ang, T., Sultana, F. S., Hutmacher, D., Wong, Y., Fuh, J. Y., Mo, X., Teoh, S., 2002. Fabrication of 3D chitosan-hydroxyapatite scaffolds using a robotic dispensing system. Materials Science and Engineering: C, 20(1-2), 35-42. doi:10.1016/S0928-4931(02)00010-3

Billiet, T., Gevaert, E., De Schryver, T., Cornelissen, M., Dubruel, P., 2014. The 3D printing of gelatin methacrylamide cell-laden tissue-engineered constructs with high cell viability. Biomaterials 35 (1), 49-62

Chinga-Carrasco, G. and Syverud, K., 2014. Pretreatment dependent surface chemistry of wood nanocellulose for pH-sensitive hydrogels. J. Biomaterials Applications doi: 10.1177/0885328214531511.

Chinga-Carrasco, G., Tobjörk, D., Österbacka, R., 2012. Inkjet-printed silver-nanoparticles on nano-engineered cellulose films for electrically conducting structures and organic transistors-concept and challenges. J Nanoparticle research 14(213)

Fukuzumi, H., Saito, T., Iwata, T., Kumamoto, Y., Isogai, A., 2009. Transparent and high gas barrier films of cellulose nanofibers prepared by TEMPO-mediated oxidation. Biomac 10, 162-165

Henriksson, M., Berglund, L.A., Isaksson, P., Lindström, T., Nishino, T. 008. Cellulose Nanopaper Structures of High Toughness. Biomac 9(6), 1579-1585

Inzana, J. A., Olvera, D., Fuller, S. M., Kelly, J.P., Graeve, O., Schwarz, E. M., Awad, H.A., 2014. 3D printing of composite calcium phosphate and collagen scaffolds for bone regeneration. Biomaterials 35(13), 4026-34

Iotti, M., Gregersen, W.Ø., Moe, S., Lenes, M. 2011. Rheological Studies of Microfibrillar Cellulose Water Dispersions. J. Polym. Environ. 19, 137-145

Jonoobi, M., Mathew, A. P., Oksman, K., 2012. Producing low-cost cellulose nanofiber from sludge as new source of raw materials. Industrial crops and products 40, 232-238

Landers, R., Hübner, U., Schmelzeisen, R., Mülhaupt, R., 2002. Rapid prototyping of scaffolds derived from thermoreversible hydrogels and tailored for applications in tissue engineering. Biomaterials 23(23), 4437-47

Orelma, H., Filpponen, I., Johansson, L. S., Österberg, M., Rojas, O., Laine, J., 2012. Surface functionalized nanofibrillar cellulose (NFC) film as a platform for immunoassays and diagnostics. Biointerphases 7, 1-12

Pääkkö, M., Ankefors, M., Kosonen, H., Nykänen, A., Ahola, S., Österberg, M., Ruokolainen, J., Laine, J., Larsson, P.T., Ikkala, O., Lindström, T., 2007. Enzymatic hydrolysis combined with mechanical shearing and high-pressure homogenization for nanoscale cellulose fibrils and strong gels. Biomac 8(6), 1934-1941

Saito, T., Nishiyama, Y., Putaux, J. L., Vignon, M., Isogai, A., 2006. Homogeneous Suspensions of Individualized Microfibrils from TEMPO-Catalyzed Oxidation of Native Cellulose. Biomac 7, 1687-1691

Saito, T., Hirota, M., Tamura, N., Kimura, S., Fukuzumi, H., Heux, L., Isogai, A., 2009. Individualization of Nano-Sized Plant Cellulose Fibrils by Direct Surface Carboxylation Using TEMPO Catalyst under Neutral Conditions. Biomac 10(6), 1992-1996

Syverud, K., Chinga-Carrasco, G., Toledo, J., Toledo, P., 2011. A comparative study of Eucalyptus and Pinus radiata pulp fibres as raw materials for production of cellulose nanofibrils. Carbohyd Pol 84(3), 1033-1038

Turbak, A. F., Snyder, F. W., Sandberg, K. R., 1983. Microfibrillated cellulose, a new cellulose product: properties, uses, and commercial potential. J Appl Polym Sci Appl Polym Symp 37, 815-827

Wang, M.-D., Zhai, P., Schreyer, D. J., Zheng, R.-S., Sun, X.-D., Cui, F.-Z., Chen, X.-B., 2013. Novel crosslinked alginate/hyaluronic acid hydrogels for nerve tissue engineering. Frontiers of Materials Science 7 (3), 269-284

Wågberg, L., Decher, G., Norgren, M., Lindström, T., Ankerfors, M., Axnäs, K., 2008. The Build-Up of Polyelectrolyte Multilayers of Microfibrillated Cellulose and Cationic Polyelectrolytes. Langmuir 24(3), 784-795

# Barrier printing of bags for food waste

*Peter Rättö*, *Göran Flodberg*, *Ann-Catrine Hagberg*

INNVENTIA AB
Box 5604
SE-114 86 Stockholm
Sweden
E-mail: peter.ratto@innventia.com

**Abstract**

The grease resistance of paper bags for domestic food waste was improved by a printed barrier. Barrier layers were printed in a full scale flexographic printing press using one, two or three printing nips. Two different substrates were used. The barrier printed sack papers were then converted into sacks and oil and grease resistance of the sacks was tested in a controlled laboratory environment.

The coverage of the substrate depended on the number of nips and the permeability of the substrate. The more permeable substrate showed a high amount of coating penetration and consequently a poor coverage of the barrier coating while conventional sack paper showed a lower penetration of the barrier coating and a better coverage of the substrate.

The barrier printed paper bags showed generally good resistance to water while tests of oil and grease resistance of sacks revealed that the printed barrier layer would not give a complete grease resistance. A barrier layer would only postpone the oil and grease penetration. Grease penetration would generally start at the folds. SEM cross sections of folds revealed that a thicker barrier and a better coverage of the barrier layer would lead to a lower exposure of fibres inside the folds.

**Keywords**: barrier, flexo, folds, permeability, printing

## 1. Introduction

Domestic waste in Sweden is sorted in non-compostable and compostable waste before leaving the household. The waste bags are collected in plastic barrels that are emptied in garbage trucks and transported into compost facilities. Bags for domestic waste have earlier been manufactured from bio-plastics, but are today mostly made from traditional sack paper. None of these two is a good solution. Bags made of bio-plastics tend to create deposits on the mixer arms during industrial composting. Problems with paper bags are of a different character. Grease and water penetrate through the paper causing leakage, odour problems and the bags freeze onto the bottom of the garbage container during the winter.

Paper is a water sensitive material. Water acts as a plasticizer of wood polymers softening the fibres and thus the paper. Additionally, water will interact with the fibre surface and break the hydrogen bonds that bond the wood fibres together. By applying internal or external sizing, the water resistance will improve, but ultimately paper will be sensitive to high and long-time exposure of water. Therefore, leakage will occur even if water resistant paper is used in waste paper bags. Besides, sizing will give no or little improvement in grease resistance.

To improve water resistance of the paper a barrier layer can be applied. Barrier layers are usually applied as plastics during extrusion or by aqueous suspension in a coater. The most common barrier materials are PE and PET. Both of these can provide with excellent barrier properties, and PET can be applied both with extrusion and as a water suspension and will improve grease resistance considerably. Even if traditional plastics will give excellent barrier properties, neither PE nor PET can be used in a waste disposal bag since none of them are compostable. They will also give a too good barrier solution for paper bags for waste disposal where certain permeability is needed for the compostable process to breathe.

The thickness, between 10 and 30 μm, also makes a traditionally coated barrier too expensive as a solution for a waste disposal bag. Even if bio-based alternatives start to emerge, both as extrusion plastics and applied in water suspensions, these alternatives tend to be more expensive than PE and PET with inferior barrier performance.

One way of cutting material costs is with a thinner barrier layer. Both extrusion coating and coating with water suspension require high thicknesses in order to prevent from pin-holes. The printing process might thus be a more cost effective solution for some applications. The thickness of the barrier layer is here controlled roughly by the

number of nips and in order to give a full coverage, two or more nips are likely to be needed. It shall also be emphasized that many thin layers tend to give better barrier properties than one thick layer (Charton et al. 2006, Mesic et al. 2013).

Additional layers are today applied in the printing press on commercial basis. As an example, varnishes are applied by anilox rolls at the end of offset presses to give a shiny surface and to protect the printed surface. There are also a number of commercial barrier coatings for application by printing available today. The application of barriers layers in roll to roll printing is commonly applied in the manufacturing of solar cells and in the electronics industry (Choi et al. 2008, Koidis et al. 2011, Koidis et al. 2013, Krebs 2009, Zhou et al. 2004).

Printing of barriers in packaging applications is an area that has emerged during recent years. Aulin and Ström (2013) compared the barrier properties of alkyd resins applied in a coater and in a laboratory flexographic printing press. They concluded that the substrate has a large impact on the barrier properties of the coated or printed product. The importance of the substrate can also be demonstrated by the results of Rättö and Ålander (2014).

The great barrier performance achieved was most probably attributed to the full coverage and the absence of pinholes due to the smooth nanocellulose films used as substrate. Mesic et al. (2013) compared the coating process with the printing process with latex based suspensions and found that the barrier properties improved with the number of layers. A number of layers were also favourable compared to one thick layer, mostly due to formation of cracks during drying of thick layers.

Even if the substrate and the application process have great impact, it shall be remembered that optimizing the printing ink can improve barrier properties quite considerably. By applying different fillers Zvonkina et al. (2014) were able to improve wetting and barrier performance of a model ink. Super hydrophobic surfaces can also be applied using structures created by ink additives creating lotus like surfaces (Chen et al. 2013).

Application of barriers in a flexographic printing press could thus be a realistic way to improve the performance of paper bags for disposal of compostable domestic waste. Full-scale trials were therefore performed in order to investigate the improvement in grease and water resistance of paper sacks of barrier printed papers. A comer-cial barrier ink was printed on two different substrates using one, two and three nip printing. The papers were then converted to sacks and tested in laboratory tests and field trials. The results were compared to laboratory analysis.

## 2. Materials and method

Two paper substrates with a grammage of 70 $gm^{-2}$ but with different properties were used for the trials. The first substrate was a water resistant unbleached sack paper and the second substrate was a water resistant highly permeable unbleached sack paper. The air permeance of the substrates according to Gurley seconds were 22 and 4 for the first and second substrate respectively. A commercial barrier printing liquid was used for the trials.

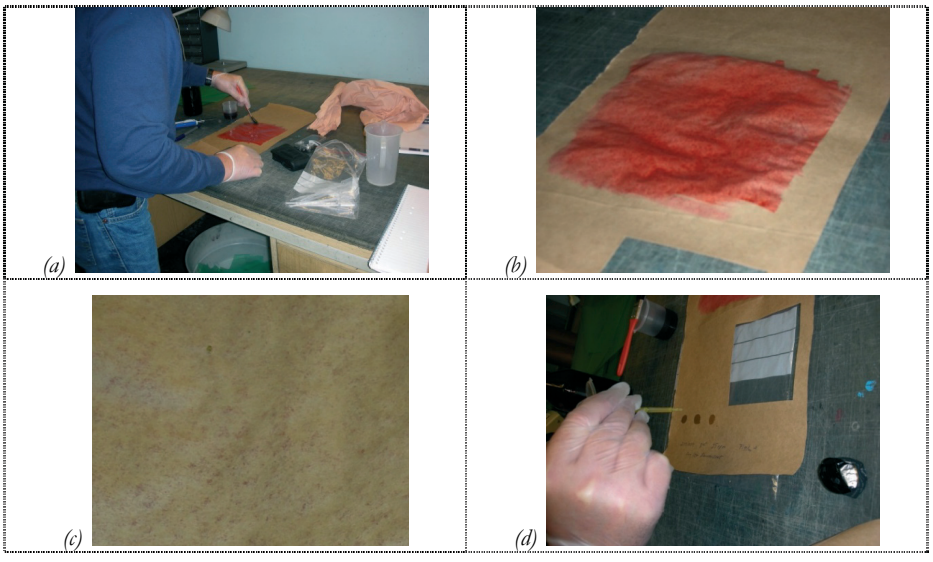


*Figure 1: Illustration of methodology to describe barrier properties. (a) show the application of liquid on the barrier surface, (b) a barrier surface after liquid application, (c) the backside of a barrier printed substrates after ten minutes with stains that has penetrated through the substrate, and (d) illustration of oil drop test with conventional olive oil*

The substrates were printed in a full-scale flexographic printing press using 1, 2 or 3 printing units at a printing speed of 50 m min$^{-1}$. After printing, substrates were cut out from the web tested. Stain tests using a red low surface tension solution were performed on the substrates after printing by applying the solution on the barrier side, see Figures 1(a) and (b), and observing the amount of liquid that had penetrated through the substrate after ten minutes on the backside, see Figure 1(c). Grease testing was performed after printing by dropping conventional olive oil on the barrier side, see Figure 1(d), and then observing the in-plane spreading of the oil drops after 5 minutes.

The samples were later analysed in the laboratories at Innventia. The amount of barrier coating on the substrate was analysed gravimetrically by comparing ten barrier printed rounds of 10 cm in diameter with ten unprinted rounds. Gurley was analysed using a meter from Lorentzen&Wettre AB. The samples were generally too permeable for traditional tests of Water Vapour Transmission rate.

Tests were carried out on 45 litre sacks manufactured from the printed papers. The tests were carried out by placing 500 g margarine and ten pieces of tissue paper bloated in 1 dl of olive oil. Additional tests were performed with ten pieces of tissue paper soaked with 2 dl of water. The sacks were then hung on a stick in a controlled atmosphere, i.e. 23 °C and 50 % RH. The sacks were then observed at intervals during 72 hours.

## 3. Results

### 3.1 Test of materials

The properties of the printed papers are summarized in Table 1. The first substrate, samples 1, 2 and 3 had a lower amount of barrier on the substrate compared to the second substrate, samples 4 and 5. This was due to that a lower amount of printing units was used for the first substrate, but also due to the high liquid absorption of the porous second substrate.

The first substrate (samples 1, 2 and 3) showed less permeable surfaces compared to when the second substrate was printed (samples 4 and 5) despite the lower amount of barrier coating, see Table 1. The Gurley, measured in seconds, also increased at the beginning for the first substrate (samples 1 and 2), with increasing amount of barrier coating from 22 (uncoated) to 29 and 60 sec for 0.83 and 2.54 g m$^{-2}$ of barrier layer respectively. Adding another barrier layer, to 3.87 g m$^{-2}$, did not decrease the permeability according to the Gurley test. The second substrate (samples 4 and 5) showed a highly permeable surface with a Gurley of 4 seconds regardless of the amount of applied coating, i.e. 2.13 and 5.91 g m$^{-2}$.

*Table 1: Summary of measured properties and observations after barrier printing. No. of units refer to the number of printing units*

| Sample | No. of units | g m$^{-2}$ | Gurley seconds | Stain test | Olive oil |
|---|---|---|---|---|---|
| 1 | 1 | 0.83 | 29 | High amounts of liquid penetration | Penetration, low amounts of spreading |
| 2 | 2 | 2.54 | 60 | Low amounts of liquid penetration | Penetration, low amounts of spreading |
| 3 | 3 | 3.87 | 58 | Low amounts of liquid penetration | Low Penetration, low amounts of spreading |
| 4 | 2 | 2.13 | 4 | No penetration | High amounts of penetration and spreading |
| 5 | 3 | 5.91 | 4 | Hardly visible penetration | Stains of penetration |

The liquid penetration test showed slightly different results than the Gurley of the papers suggested. The first substrate (samples 1, 2 and 3) showed a higher amount of liquid penetration than the second substrate (samples 4 and 5). The amount of liquid penetration decreased with the amount of barrier coating for the first substrate. The second substrate showed no significant liquid penetration regardless of the number of printing units used. Stain tests of unprinted samples of the second substrate showed similar results with no significant liquid penetration.

The first substrate showed a larger amount of spreading of oil when printed with one printing unit (sample 1) compared to when printing with two units (sample 2) or three (sample 3). The second substrate (samples 4 and 5) showed a higher amount of oil penetration and spreading compared to the first substrate. Again, a higher amount of barrier on the surface (sample 5) gave a lower amount of oil spreading than the lower amount of barrier (sample 4).

3.2. SEM cross section analysis

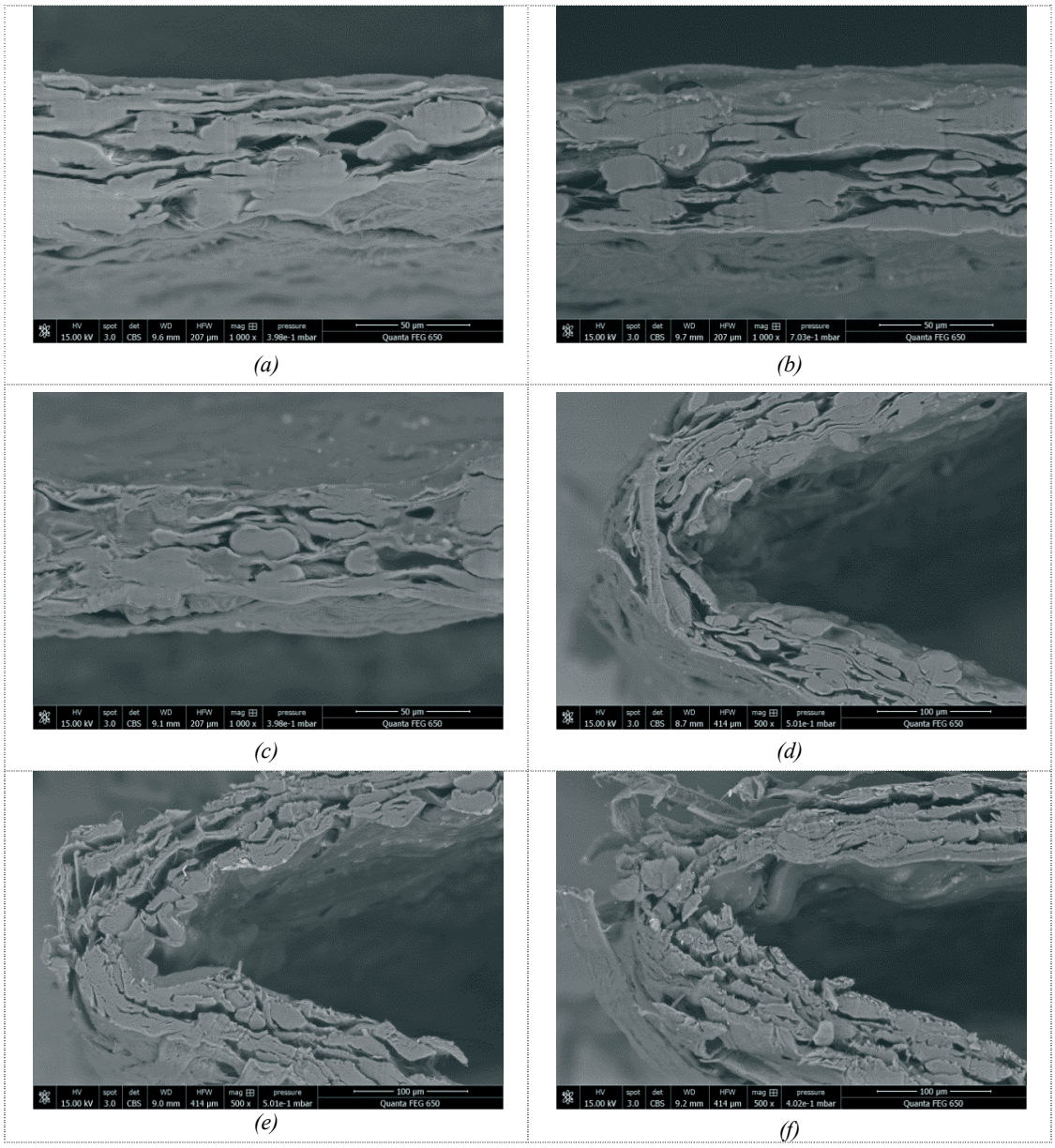


*Figure 2: SEM cross sections of barrier printed papers: (a) sample 2 at a magnification of 1000x, (b) sample 3 at a magnification of 1 000x, (c) sample 5 at a magnification of 1 000x, (d) fold of sample 2 at a magnification of 500x, (d) fold of sample 3 at a magnification of 500x and (f) fold of sample 5 at a magnification of 500x. Note that the barrier layer is on the top of the paper in images (a), (b) and (c) and at the inside of the fold in images (d), (e) and (f)*

The SEM cross sections in *Figures 2(a)* to *(f)* illustrate the coverage of the surface of different papers. It is quite clear that a thicker barrier layer on the normal sack paper was obtained when going from two printing units, *Figure 2(a)*, to three printing units, *Figure 2(b)*. The barrier material also seemed to stay quite well on the top of the surface without too much penetration into the substrate. It is however unlikely that the two unit printing, *Figure 2(a)*, would give a full coverage without any pin-holes. The permeable paper, see *Figure 2(c)*, shows a high amount of penetration of the barrier material. It is therefore plausible that large areas of the fibre surface are uncovered by barrier material.

The thickness of the barrier material also had an impact on the fold. For the normal sack paper, the lower amount of barrier material in sample 2, *Figure 2(d)*, was not enough to cover the surface of the fibres inside the fold, whereas a considerably better coverage inside the fold was obtained with the higher amount of barrier material on sample 3, *Figure 2(e)*. The poor coverage of sample 5, *Figure 2(f)*, led to exposure of the fibres inside the fold of the sack.

### 3.3. Test of sacks

None of the sacks with printed barriers showed problems with the tissue papers soaked with water. Even if the bottom of the sacks had clearly higher moisture contents, the sacks showed no signs of water penetration after 72 hours of exposure. Oil and grease resistance gave different results, see *Figures 3(a)* to *(f)*. The olive oil would generally penetrate the sack paper faster than the margarine, and penetration would generally start at the folds of the sacks. The porous papers, samples 4 and 5, showed immediate oil penetration through the paper material, see *Figure 3(a)*, whereas penetration needed some time for the sacks made from the printed normal sack paper. It shall be mentioned that tests on sacks without a printed barrier showed immediate penetration when exposed to olive oil. After 3.5 hours, the normal sack paper showed stains of oil penetration, *Figures 3(b)* and *(c)*, or hardly no penetration, see *Figure 3(d)*. The treated porous sack paper showed a very large amount of penetration (half the area of the bottom) for sample 4, see *Figure 3(e)*, or a large amount of penetration for sample 5, see *Figure 3(f)*.

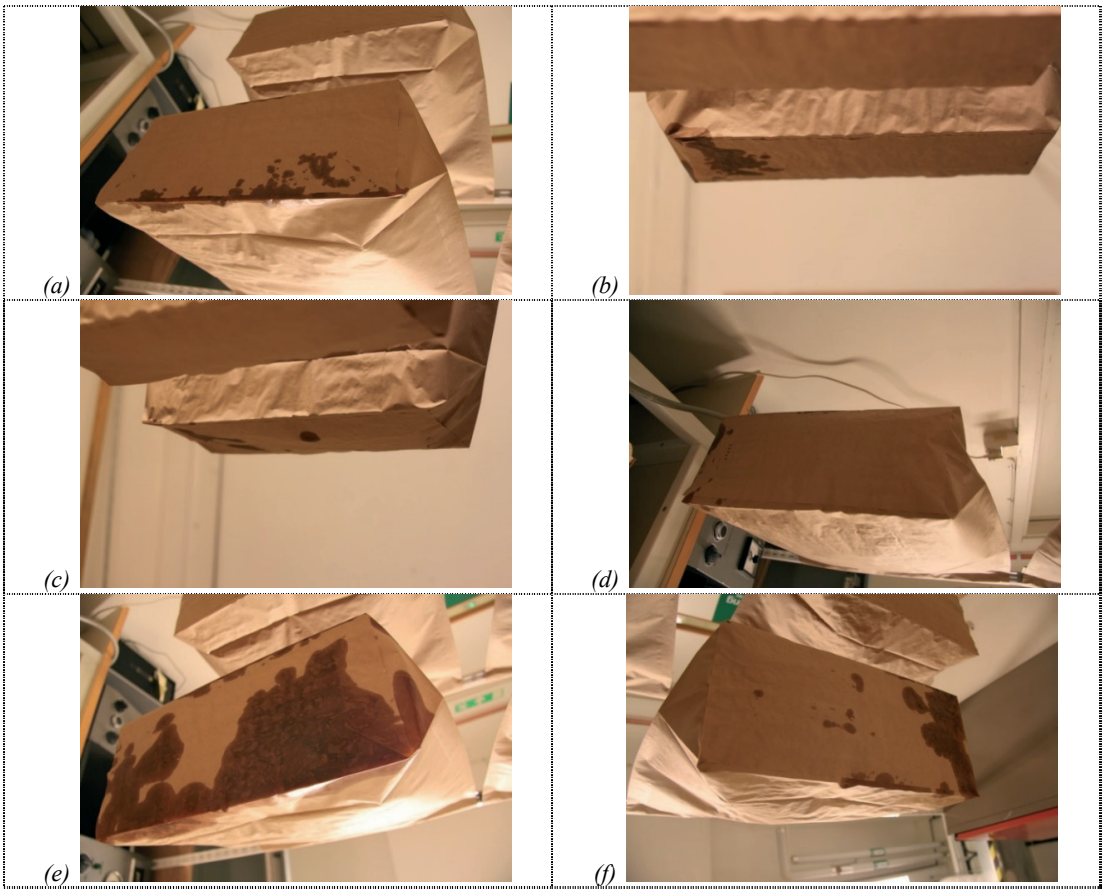


*Figure 3: Laboratory test of sacks with oil and margarine: (a) sample 4 after 10 min, (b) sample 1 after 3.5 h, (c) sample 2 after 3.5 h, (d) sample 3 after 3.5 h, (e) sample 4 after 3.5 h and (f) sample 5 after 3.5 h*

None of the barrier printed sack papers showed complete grease resistance. Samples 1, 2, 4 and 5 showed grease stains over the whole bottom of the sack after 24 hours, while sample 3 showed grease stains over approximately half the area of the bottom of the sack. After 48 hours, all the sacks showed grease stains over the whole area of the bottom of the sack. No leakage could be observed from any of the sacks after 72 hours even if the bottom of the sack was quite greasy.

## 4. Discussion

The full-scale trials showed that the barrier properties depended to a great extent on the substrate. The more permeable substrate showed a higher permeability after barrier printing compared to the normal sack paper, despite a higher amount of barrier coating, 2.13 and 5.91 $g m^{-2}$ compared to 0.83, 2.54 and 3.87 $g m^{-2}$. In fact, the more permeable substrate showed no decrease in permeability with the application of barrier up to almost 6 $g m^{-2}$ which suggest that the printed barrier penetrated instead of creating a film on surface. The poor coverage of the permeable substrate was confirmed by the SEM cross sections, where the coverage of the porous substrate was

illustrated, see *Figures 2(c)* and *(f)*. The normal substrate showed a different pattern where the barrier material stayed on the top and covered the substrate; see *Figures 2(a)*, *(b)*, *(d)* and *(e)*. Consequently, increasing the number of printed layers lead to a thicker barrier layer and thus an improved coverage.

Despite the higher permeability, samples 4 and 5 showed no significant liquid penetration during the stain tests. This was probably due to lateral liquid absorption by the substrate, making penetration in the thickness direction impossible, rather than due to good barrier properties. This was also confirmed when performing the stain test on a non-printed permeable substrate. The oil tests pointed in the direction that a better barrier was achieved with the non-permeable substrate (sample 1, 2 and 3), which showed less oil spreading than the printed permeable substrate (samples 4 and 5) even if a higher amount of barrier material improved the grease resistance of the highly permeable substrate.

Even if the test methods for barrier properties as such, liquid penetration and oil drops, were quite crude, they still described the observations made with SEM micrographs quite well. Another question is how these test methods and properties relate the use in a real product. Even if the lab tests with oil and margarine differ from real conditions during waste disposal, they give a comparison of the performance between different materials. The test showed that none of the barrier materials gave perfect grease resistance: oil and grease would penetrate the substrate completely after three days of exposure. The difference was that a barrier would increase the time of penetration from a few minutes up to hours depending on the substrate and number barrier layers, see *Figures 3(a)* to *(f)*. It was also evident that the folds were the most sensitive areas for oil penetration. Here, the coverage and thickness of the barrier layer seemed to have a great influence. The SEM micrographs, see *Figures 2(d)*, *(e)* and *(f)*, showed exposed fibres inside the fold for the samples 3 and 5, whereas sample 4 showed less exposed fibres due to an intact barrier layer. The intact barrier layer is probably due to a better coverage of the paper surface and a thicker barrier layer which is less sensitive to failure and fibre rising. The consequence was quite well illustrated in the tests with sacks in *Figures 3(c)*, *(d)* and *(f)*.

To draw conclusions from lab tests to performance of products in real conditions is a hard task. The crude test methods of liquid and oil penetrations were of great help during the full scale trials in order to give a quick answer about the coverage of the substrate, while the lab test of the sack papers give a comparison of materials. Since specified conditions were used in the latter, further product improvements can be evaluated at a later stage. On the other hand, the test with the olive oil and margarine were probably tougher on the materials than exposure in real conditions. No problems with leakage have been reported from the field tests with the sacks in real conditions.

## 5. Conclusion

Printed barriers can improve the water and grease resistance of sack papers enough for certain applications. The barrier properties depended to a great extent on the substrate. Application of simple tests (stain tests and oil spreading) can give information during the trials but the validity of these tests also depended on the substrate properties.

There was a clear relationship between grease resistance of the sacks and coverage of the substrate by the barrier layer. The folds were the most sensitive areas for oil penetration where a thicker material with good coverage would show a considerably better barrier performance.

**Acknowledgements**

The authors wish to thank the Swedish Agency of Innovation, Vinnova, for financial support of the project. Björn Andersson and Bror Johansson, both Jonsac are acknowledged for running the full scale printing trials and Joanna Hornatowska, Innventia is greatly acknowledged for performing the SEM analysis.

**References**

Charton C., Schiller N., Fahland M., Holländer A., Wedel, A., Noller K. (2006): "Development of high barrier films on flexible polymer substrates", Thin Solid Films, 502(1 and 2), 99-103

Chen W., Wang X., Tao Q., Wang J., Zheng Z., Wang X. (2013): "Lotus-like paper/paperboard packaging preperade with nanon-modified overprint varnish", Appl. Surface. Sci., 266(1), 319-325

Choi M.-C., Kim Y., Ha C.-S. (2008): "Polymers for flexible displays: From material selection to device applications", Prog. Polym. Sci., 33(6), 581-630

Koidis C., Logothetidis S., Kapnopoulos C., Karagiannidis P.G., Laskarakis A., Hastas N.A. (2011), Mat. Sci. and Eng.: B, 176(19), 1556-1561

Koidis C., Logothetidis S., Kassavetis S., Kapnopoulos C., Karagiannidis P. G., Georgiou D., Laskarakis A. (2013): "Effect of process parameters on the morphology and nanostructure of roll-to-roll printed P3HT:PCBM thin films for organic photovoltaics", Solar Energy Materials & Solar Cells, 112, May, 36-46

Krebs F. C. (2009): "Fabrication and processing of polymer solar cells: A review of printing and coating techniques", Solar Energy Materials & Solar Cells, 93, April, 394-412

Mesic B., Järnström L., Johnston J. (2013): "Multilayering of latex-based barrier dispersion coating on linerboard: Flexography versus conventional coating technology", European Coatings Congress, Session 5, Paper ID 5.2, March 18-19, Nuremberg, Germany

Olsson E., Johansson C., Järnström L. (2014); "Montmorillonite clay for starch-based barrier dispersion coating - Part 1 The influence of citric acid on viscosity and barrier properties", Appl. Clay Sci., accepted for publication

Rättö P., Ålander E. (2014): "Water resistant NFC films", Tappi Proc. PaperCon 2014, Nashville Tennessee, April 27-30, 2014

Zhou Y., Andersson O., Lindberg P, Liedberg B. (2004), Microchim. Acta 146, 193-205

Zvonkina I. J., Gkountara P., Hilt M., Franz M. (2014): "New printing inks with barrier performance for packaging: Design and investigation", Progress in Organic Coatings, 77(3), 646-656

# Flexography as manufacturing method for carbon nanotube based thin film transistors

*Neil Graddage*[1, 2], *Davide Deganello*[2]

National Research Council Canada
Ottawa, Canada

Welsh Centre for Printing and Coating
Swansea University, Swansea UK
E-mail: d.deganello@swansea.ac.uk

**Abstract**

Large volume implementation of printed electronics requires the development of mass-producible and reliable printed transistors. In this work, we present the initial development of field-effect devices printed by flexography using carbon nanotubes (CNTs) as semiconducting material. CNTs offer a number of advantages over commonly adopted organic semiconducting materials, namely high mobility and environmental stability. However their device performance depends on the accurate deposition of the CNT network. Flexography, with its accurate control of thin film deposit, offers the capabilities to address this issue, furthermore as a leading roll-to-roll printing process for packaging, flexography is key to large volume integration.

Devices were produced using Multi Walled CNTs as the active layer. A top gate top contact design device configuration was employed. Flexography was used for printing the source/drain electrodes and CNT layer. Device characterization showed field effect behavior. Two layouts for the electrode, interdigitated and parallel, were tested showing similar ON/OFF ratios. Current device performance was limited by the high off current characteristic of MWCNTs; improvements are expected through refinement of CNT semiconductor layer and scale of the device.

This work has demonstrated the potential of flexography for manufacturing of TFT structures with CNTs as the active layer.

**Keywords**: flexography, CNT, printed transistors, TFT

## 1. Introduction

Production of affordable and reliable printed logic is fundamental for development of large volume printed electronic applications. Large scale adoption of printed transistors is dependent to the integration of large volume roll-to-roll printing processes with high performance, environmentally stable, easy to process semiconducting materials.

Organic semiconductive materials have been the subject of extensive studies, and are commonly used in printed components due to their compatibility with solution processing. However, large volume adoption of these semiconductive organic materials is often limited by major constraints: poor environmental sensitivity, leading to short life span; limited solvent compatibility, leading to use of undesirable solvents; and excessive cost of materials. Carbon Nanotubes (CNTs) can potentially overcome these limitations. CNTs are very stable compounds and have shown to be dispersible into low volatility solvents. Field effect CNT transistors have been achieved in literature showing good performance. Most of the literature is concentrated on inkjet printed CNT devices, which while suitable for laboratory or small scale applications would be less suitable for roll-to-roll printing processes. To obtain high speed roll-to-roll printing with inkjet requires high press complexity and reliable jetting. With regards to upscaling to roll-to-roll processes work has been recently presented on gravure printed CNT transistors (Lau, P.H. et al., 2013), but no work has been presented on flexographic deposition of CNTs.

Integration of printed transistors with flexography over flexible substrates is of particular interest; flexography is the leading roll-to-roll printing process for conventional flexible packaging and it allows accurate thin film deposit with high lateral resolution. The integration with printed transistors would allow a rapid implementation of printed logic into smart packaging, allowing its effective and cost efficient delivery to market.

In this work advances in the integration of CNTs with flexography are discussed. The development of flexographic printed CNT based field effect devices is presented with particular mention of printing manufacturing process and related issues.

## 2. CNTs as semiconductor layer

The ability to create a semiconducting layer with CNTs depends on the ability to control the density of printed CNT network. CNTs can be visualised as one-atom-thick sheets of carbon, or graphene, rolled into cylindrical form. Depending on the rolling angle carbon nanotubes can present semiconducting or metallic properties, with a common manufacturing techniques resulting in a ratio of 2:1 respectively. CNTs can be grown in single-walled (SWCNT) or multi-walled (MWCNT) form. CNTs are also inherently stable structures. Ballistic conductivity has been observed in pristine metallic SWCNTs (Bachtold, A. et al., 2000), while semiconducting CNTs offer theoretical mobilities of >100000cm2/Vs (Durkop, T. et al., 2004).

When using solution deposition techniques it is not possible to deposit individual CNTs accurately, only random networks of CNTs. The macroscopic properties of these networks are dependent upon the nanoscale structure of the material used and the density of the network. While methods for separation of semiconducting and conductive CNTs are now available, these processes are still unsuitable for the volumes required in large scale manufacturing (and extremely expensive). By contrast raw distribution of CNTs can be obtained easily and economically. In order to obtain semiconducting behaviour from networks of raw CNTs, network densities of deposited thin film dispersions need to controlled with the aim of reaching the semiconducting percolation threshold. The semiconducting percolation threshold is defined as the density at which the pathways through the random network are formed by semiconducting tubes alone. At higher densities metallic pathways may form which would short any resulting device resulting in higher off currents. Lower densities may fall below the percolation threshold of the network resulting in no connected pathways at all. In this direction, flexography, with its accurate and variable control of thin film thickness deposit, presents important capabilities for the task.

## 3. CNT Field effect device manufacturing

Figure 1 shows the diagram of the structure of printed CNT field effect devices. First a CNT semiconductive layer was printed by flexography onto a PET substrate. The printing was performed using an IGT F1 flexographic tester. The CNTs were MWCNTs (supplied by Haydale ltd.) and they were deposited as a low concentration liquid dispersion, with NMP as main solvent and PVA as the resin. MWCNTs tend to show semi-metal properties do to the statistical probability of both metallic and semiconducting chiralities being contained within the structure. This results in a reduced dependence upon percolation threshold at the expense of poor device performance. However this was considered acceptable for proof of concept devices. The semiconductor layer image was a square 20 mm per side. The anilox used had a volume of 8 cc $m^{-2}$, leading to an estimated deposited CNT density of 60 mg $m^{-2}$. In the formulation of CNT ink, PVA was added as resin to improve the binding of the nanotubes to themselves and the substrate; this is in major contrast to most of the literature, which rely exclusively on the much weaker Van Der Walls forces in CNTs; a solution that while providing better contacts between nanotubes (hence better performance) is only suitable for laboratory experiments but not (in opinion of authors) for the desired long-term high-wear industrial uses.

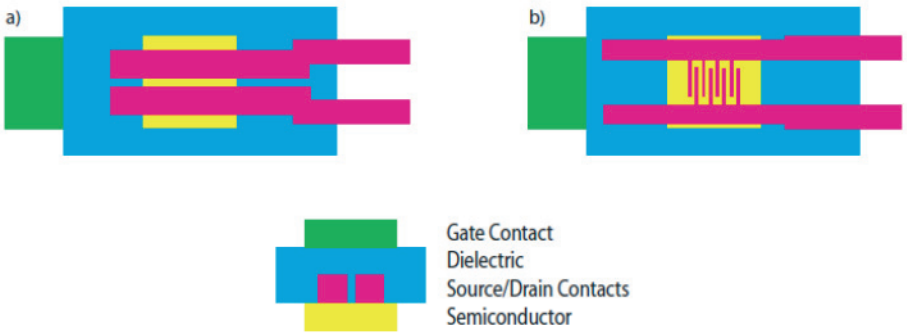


*Figure 1: Structures of manufactured field effect devices*

Following the deposition of CNT layer, the source and drain contacts were flexographically printed. For these contacts, silver nanoparticle ink (Inktec PR-030) was adopted in view of excellent conductivity and feature resolution demonstrated in previous work. Two different designs for source and drain electrodes were selected: an interdigitated design with a channel length of 1 mm and a parallel design with a length of 2 mm. Figure 2 shows example of printed CNT layer with overlapping electrodes. The decision to print silver electrodes over the CNT layer was based on analysis of solvent compatibility. Figure 2 shows also that while the silver flexo-printed layer

was uniform, the CNT deposited layer was characterised by a more fingered/striped pattern. This can be correlated to the commonly-called viscous fingering, non-uniform splitting of ink at the nip due to surface instability, a phenomenon that is amplified by the very low viscosity of the CNT ink (< 20 mPa).

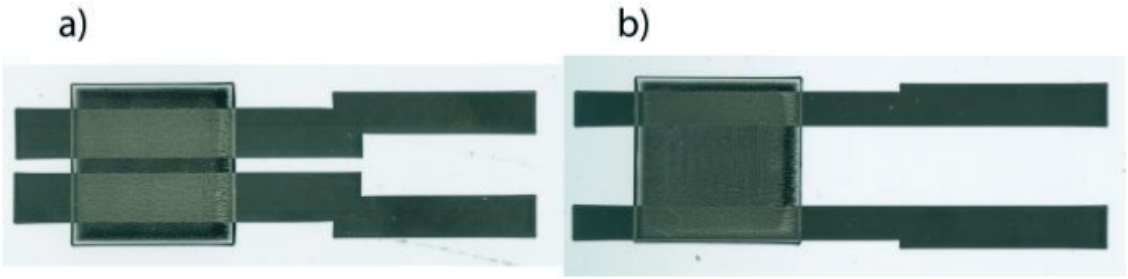


*Figure 2: Optical scans of flexographic printed CNTs layer with source & drain electrodes (interdigitated and parallel)*

Following the deposition of source and drain electrodes by flexography, the dielectric and the gate contact layer were deposited. These layers did not require accurate feature resolution, as for the source and drain electrodes, nor accurate thin layer deposition, such as the CNTs layer. In this first proof of concept, these layers were deposited by bar coating. For the dielectric layer a commercial dielectric screen ink (GEM) was employed. The ink is based upon a thermosetting polymer and scoping experiments showed it to have suitable adhesion and insulating properties. In order to ensure no gate leakage the devices were produced using a total of 4 coatings alternating between bar US20 and US8, with a final thickness of approximately 25 µm. Finally the gate was deposited over the dielectric using a silver micro-particle silver ink (GEM) with bar US20. The silver ink was selected due to its formulated compatibility with the dielectric.

## 4. CNT Field effect device testing

The testing of manufactured CNT Field effect devices was performed on an Agilent E5262A plus Signatone S-116O probe station. As a field effect device, it was expected that by varying the voltage applied to the gate electrode (VGS), the current through the source and drain (ISD) would vary due to the change in conductivity of CNT layer under the electric field of the gate. Measurement of IV performance of the devices is presented in Figure 3. For these measurements, the voltage across source and drain was 0.5V.

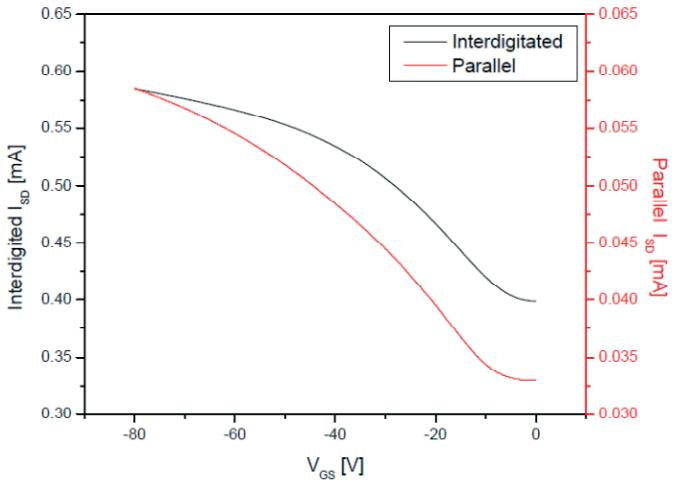


*Figure 3: IV transfer characteristics for interdigitated and parallel devices*

The tests showed successful observation of a field effect. With the change of voltage at the gate, there was a significant variation in current at source and drain (under constant voltage). The CNT layer showed transfer characteristics indicative of p-type behaviour in line with other CNT based devices reported in the literature. The two types of devices, interdigitated and parallel, showed different magnitude in the response but very similar ON/OFF ratios of circa 1.5 and 1.7 respectively. While this ratio is limited, it can be significantly improved through further development and refinement of CNT semiconductor layer and scale of device.

## 5. Conclusions

In conclusion flexography has been shown to be a viable method for deposition of stable field effect devices by using CNTs as the active layer. Significant field effect behaviour was observed in devices despite large device scale in terms of channel length and dielectric thickness. Further performance will be achieved by design and material optimisation. In particular designs should be optimised for the flexographic process given the viscous fingering and layer spreading effects observed.

**References**

Bachtold, A. et al., 2000. Scanned Probe Microscopy of Electronic Transport in Carbon Nanotubes. Physical Review Letters, 84(26), pp.6082-6085

Dürkop, T. et al., 2004. Extraordinary Mobility in Semiconducting Carbon Nanotubes. Nano Letters, 4(1), pp.35-39

Lau, P.H. et al., 2013. Fully Printed, High Performance Carbon Nanotube Thin-Film Transistors on Flexible Substrates. Nano Letters, 13(8), pp.3864-3869

# Printed cathode of rechargeable lithium-ion battery

*Gorazd Golob, Polona Perko, Dejana Javoršek, Marta Klanjšek Gunde, Robert Dominko*

University of Ljubljana
Faculty of Natural Sciences and Engineering
Aškerčeva 12, SI 1000 Ljubljana

E-mails: gorazd.golob@ntf.uni-lj.si; perko.polona@gmail.com; dejana.javorsek@ntf.uni-lj.si; marta.k.gunde@ki.si; robert.dominko@ki.si

**Abstract**

Secondary lithium batteries are efficient source of power supply in many mobile devices and electrical vehicles. They have different technical characteristics based on different materials and production methods used. For the mass production and lab sample preparation of cathode the most common is doctor blade deposition method. Our goal was introduction and investigation of alternative screen-printing technique and optimization of printed cathode layer adhesion to the basic conductive aluminium foil to achieve improved electrical properties. Focus of the experimental part was on the preparation of an effective mixture of cathode material with used NMC composition (LiNi0,5Mn0,3Co0,2O2). Improved contacts between cathode particles and aluminium foil were achieved by increasing of surface free energy of the aluminium foil by using sand paper and KOH treatment. The cathode was covered with electrolyte (1M LiPF6 in a solution of ethylene carbonate and diethylene carbonate) and a glass-fibre separator and a piece of lithium on the top. The cathode, separator and anode - the metal lithium has then been inserted into a vacuum welding device and sealed. Characteristics of the charging and discharging of the cathode material was measured in the potential range between 2.5 and 4.3 V at constant current. The results of electrochemical measurements show us that screen-printed cathode material on aluminium foil for rechargeable lithium batteries is comparable to the same samples prepared using traditional methods. Charging and discharging characteristics and capacity values of the screen-printed cathode material compared to material applied using doctor blade are different and remain as a challenge for future research.

**Keywords**: printed electronics, screen-printing, cathode, Li-ion rechargeable battery, battery performance

## 1. Introduction

Lithium ion batteries are becoming a dominant form of rechargeable (secondary) power source for industrial, transportation, consumer and power storage applications. Conventional production process of Li-ion rechargeable batteries, simulated in lab, includes coating of active cathode layer on the conductive aluminium layer, insertion of separator in a form of thin porous polymer film soaked with electrolyte content and insertion of thin layer of lithium anode. Assembly of the components into final product must be performed in inert moisture-free environment. In the lab a suitable glow-box was used. There are many different forms of final product, based on different chemistry options and different manufacturing techniques (Armond and Tarascon, 2008; Barker et al, 2004; Besenhard, 1999; Gaikwad, 2011; Savastand, 2013; Wendler et al, 2013).

Focus of our research was on the preparation of an effective mixture of cathode material with NMC composition (LiNi0,5Mn0,3Co0,2O2) that was used for printing on the aluminium foil. For the cathode material the particle contact with aluminium foil is of particular importance, since it provides a pathway for electrons and therefore influences the electrochemistry of the battery. Improved contacts between cathode particles and aluminium foil were achieved by an increase of surface free energy of the aluminium foil (Erbil, 2006).

The aim of our research was the analysis of technical possibility for using screen-printing technique instead of conventional doctor blade coating technique for cathode manufacturing in lab conditions while all other materials used and battery assembly process should remain the same (Pflake, 2013).

## 2. Method and research methods

Basic ingredients of cathode layer material used:

NMC (nickel manganese cobaltite) typ 523 - active material,
PVdF (Polyvinylidene fluoride) - vehicle,
NMP (N-Methyl-2-pyrrolidone) - solvent,
Printex or Timcal - conductive carbon black.

For the good properties of the cathode and consequently the entire battery we need homogeneous mixture, which has been obtained by a planetary ball mill (Retsch). Optimizing of formulation was performed using different amounts of ingredients to achieve optimal rheological, adhesion and electrical properties. After several tests we got the final formulation presented in Table 1.

*Table 1:*
*Formulation of cathode layer coating/printing paste*

| Material | Share % | Mass (mg) | Final amount |
|---|---|---|---|
| Printex | 0 | 78.05 | 78.10 mg |
| PVdF (30 mg $ml^{-1}$) | 8 | 62.00 | 2.08 ml |
| NMC | 82 | 640.00 | 640.00 mg |

The NMP was added in quantities necessary to achieve proper rheological properties. The paste was used for coating using conventional doctor blade coater (AFA - III Automatic Thick Film Coater) to get comparable results to previous investigation results. After successfully performed conventional coating we made first tests using manual screen-printing technique with meshes 18 and 62 threads per cm. With additional adjustments of rheological properties we got printed cathode active layer with smooth homogeneous surface without cracks (Figure 1).

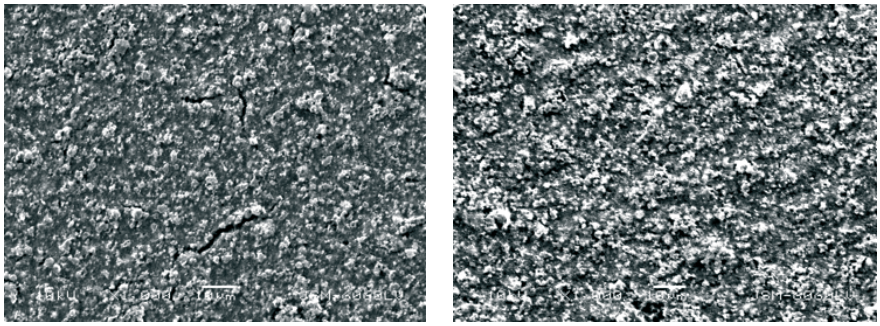

*Figure 1: SEM image of cathode layer applied using conventional doctor blade coating technique (left) with visible cracks and smooth layer achieved using screen printing technique (right)*

We continued our research using semi-automatic screen printing press using 60, 90 and 130 threads per cm meshes. Useful results were only achieved by using the 60 threads per cm mesh. Print with double paste (functional ink) layer was used to obtain a fully printed pattern that was also more uniform. We also had to replace standard polyurethane squeegee with the ethylene propylene diene monomer (EPDM) one, because it is resistant to NMP solvent, present in the PVdF binder (Lyondell).

Conductive substrate used was aluminium foil with treated surface for better adhesion of the paste. We used mechanical treatment with fine sand paper, chemical treatment with 10% solution of KOH and combination of both. Results of achieved surface free energy, calculated using Owens-Wendt and Wu methods from measured contact angles with water and diiodomethane are presented in Table 2. Adhesion of treated surface was significantly improved. Rough surface of treated aluminium foil is shown in Figure 2.

*Table 2:*
*Surface free energy (SFE) of treated aluminium foil*

| | Owens-Wendt | | | Wu | | |
|---|---|---|---|---|---|---|
| Sample | SFE total | Polar | Disperse | SFE total | Polar | Disperse |
| | (mL $m^{-2}$) | | | | | |
| Untreated aluminium | 35.09 | 3.70 | 31.39 | 40.79 | 7.89 | 32.90 |
| Al treated with sand paper P2000 | 56.12 | 19.75 | 36.36. | 60.98 | 23.73 | 37.25 |
| Al treated with KOH (10%) | 67.37 | 27.16 | 40.21 | 71.54 | 30.83 | 40.70 |
| Al treated with sand paper P2000 | 78.32 | 29.54 | 48.78 | 83.48 | 34.68 | 48.80 |

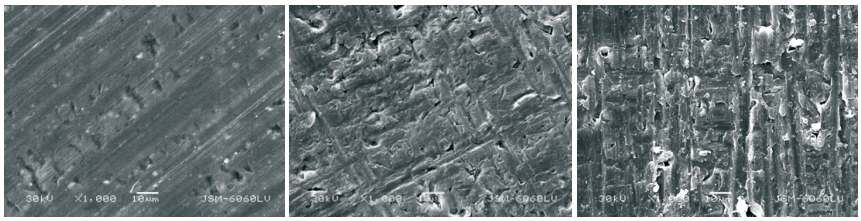

*Figure 2: SEM image of the surface of the untreated aluminium foil (left), aluminium foil, treated with KOH (10%) and the sand paper P2000 (centre), and aluminium foil treated with sand paper only (right) at a magnification of 1 000 x*

Further preparation of the battery takes place in the dry chamber (Labmaster, MBRAUN), as lithium was used for the anode metal, which is air- and water- reactive. When we start with the assembly of the battery, it is first necessary to weigh the cathode, so that we know the weight of the cathode material and, consequently, of the active material later in the process. This is important because the charging current is dependent on the quantity of the material. The cathode was covered with electrolyte (1M LiPF6 in a solution of ethylene carbonate and diethylene carbonate). Then, a glass-fibre separator was placed on the cathode and a piece of lithium, which had first been thinned by rolling, on the top. The cathode, separator and anode - the metal lithium has then been inserted in the "coffee bag". The whole assembly is then inserted into a vacuum-welding device (VG - 017 - P Zepter) and sealed.

## 3. Results of electrical properties and discussion

The constant current, which is necessary to charge and discharge the battery, was calculated using the following equation:

$$I = \frac{m \times F \times c-rate}{M \times t}[\mu A], \qquad [1]$$

where I is the current, m is the mass of the active material, the c - rate = 10 (10 hours of charging, 10 hours discharge), M is the molar mass and t is time.

First results of electrical properties of the battery with screen-printed cathode in comparison with a conventional one, using standard test methods were not very promising. Screen-printed layer is smooth, but also thinner and there are possible changes in formulation caused by filtering of bigger particles and agglomerates in the paste. Cathode material layers on aluminium foil were not usable because they all peeled or were too broken. Response of cathode electrodes was measured in the potential range between 2.5 V and 4.3 V. The value of the constant current of each sample was calculated on the weight of active material. Discharge capacity of samples made by using doctor blade are presented in Figure 3 and charge/discharge characteristics in Figure 4. Discharge capacity of samples made by using screen-printing technique are presented in Figure 5 and charge/discharge characteristics in Figure 6. In the paper, only the most representative results presenting electrical characteristics are shown. From the results the difference between the two presented techniques is clearly discernable. No difference in the voltages shown in Figure 3 and Figure 5 can be seen, from which we conclude that the bad characteristics of the charging and discharging is most likely due to the material chosen. The capacity drops fast in all of the batteries, most likely because of the characteristics of the chosen material.

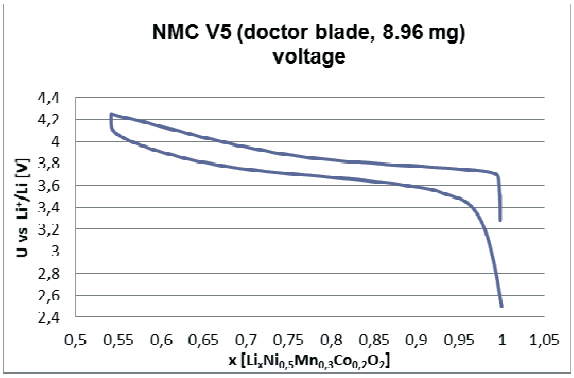


*Figure 3: Characteristics of the charging and discharging of the cathode material made using doctor blade on aluminium foil, treated with KOH (10%) and sandpaper P2000 at room temperature and the flow of 174.285 μA*

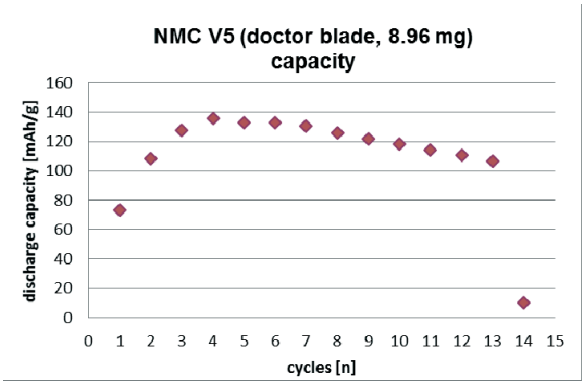


*Figure 4:*
*Capacity of the cathode material made using doctor blade on aluminium foil, treated with KOH (10%) and the sand paper P2000*

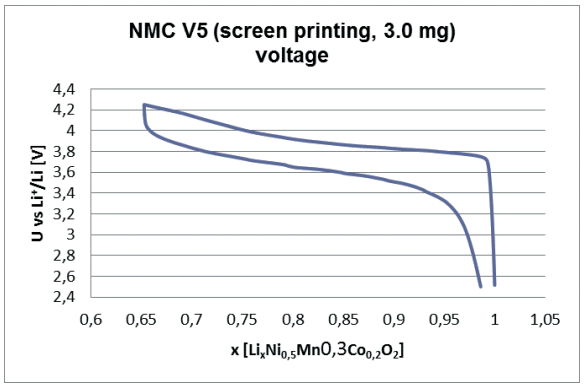


*Figure 5:*
*Characteristics of the charging and discharging of the cathode material, deposited by screen-printing on aluminium foil, treated with KOH (10%) and the sand paper P2000 at room temperature and flow 83.363 μA*

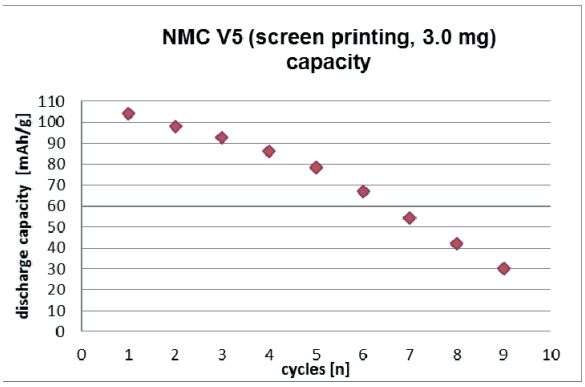


*Figure 6:*
*Capacity of cathode material, deposited by screen-printing on aluminium foil, treated with KOH (10%) and the sand paper P2000*

## 4. Conclusions

Our aims and objectives were achieved with experimental work. We recognized the principle of operation of secondary lithium batteries and we prepared a number of different mixtures of cathode material and determined which gave the best results using screen-printing technique. We have managed to increase the surface free energy of aluminium foil with mechanical and chemical treatment. We managed to improve the contact between the foil and the cathode material to such an extent that the material is no longer peeling and cracking. The results of electrochemical measurements have confirmed that the cathode material for lithium batteries can be screen-printed on aluminium foil and that the results are comparable with the doctor blade application method. The different techniques for applying the cathode material give different characteristics. Further research is needed to explain the differences and to enable improvements.

**References**

Armand, M. in Tarascon, J. M. Building better batteries, Nature, 2008, 451, pp. 625-657

Barker, J., Saidi, M.Y. in Kelley, T. Electrodes comprising mixed active particles, International patent, No. 095607 A2 (2004) 1-4

Besenhard, J. O. Handbook of battery materials. Weinheim, Wiley-VCH, 1999, pp. 1-3

Erbil, Y. Surface Chemistry of Solid and Liquid Interfaces, Oxford, Blackwell Publishing, 2006, pp. 3-7

Gaikwad, A. M., Whiting, G. L., Steingart, D. A. in Arias, A. C. Highly Flexible, Printed Alkaline Batteries Based on Mesh-Embedded Electrodes, Advanced Materials, 2011, vol. 23, no. 29, pp. 3251-3255

Lindsay, M.J. Data analysis and anode materials for lithium ion batteries [cited 7. 5. 2013] Available at: <http://ro.uow.edu.au/theses/359/>

Lyondell: Elastomer Compatibility : Technical data, 2006, pp. 2 [cited 11. 7. 2013]. Available at: <http://www.lyondellbasell.com/techlit/techlit/2688.pdf>

Plafke, J. Screen-printed, flexible zinc battery could pave way for wearable electronics [cited 14. 7. 2013]. Available at: <http://www.geek.com/mobile/screen-printed-flexible-zinc-battery-could-pave-way-for-wearable-electronics-1535131/>

Savastano, D. Advancements in Printed Battery Technology are Driving Growth [cited 14. 7. 2013]. Available at: <http://www.printedelectronicsnow.com/ articles/2011/01/advancements-in-printed-battery-technology-are-dri>

Wendler, M., Hübner, G. in Krebs, M. Development of Printed Thin and Flexible Batteries str. pp. 34 [cited 14. 7. 2013]. Available at: <http://www.hdm-stuttgart.de/international_circle/circular /issues/11_01/ICJ_04_32_wendler_huebner_krebs.pdf>

# A3

## *Media and the consumer*

# Is legibility of typefaces designed for screen use the same for different languages?

*Nace Pušnik*[1], *Dorotea Kovačević*[2], *Maja Brozović*[2], *Klementina Možina*[1]

[1] University of Ljubljana
Faculty of Natural Sciences and Engineering
Snežniška 5, SI-1 000 Ljubljana
E-mails: nace.pusnik@ntf.uni-lj.si; klementina.mozina@ntf.uni-lj.si

[2] University of Zagreb
Faculty of Graphic Arts, Department of Graphic Design and Image Information
Getaldićeva 2, HR-10 000 Zagreb
E-mails: dorotea.kovacevic@grf.hrt; maja.brozovic@grf.hrt

**Abstract**

Large amount of information that we accept is predominantly transmitted through the screens. Communication through the screens is imminent thing, but we try to make it smoother and user-friendlier. The clearance and visibility of typefaces at different viewing conditions is an important aspect when information should impact on people. The use of appropriate typefaces is in consequence undoubtedly important while the design of typefaces differs for print and screen use. There is little attention on which typefaces we choose when we make screen information presentation. Tests on the typefaces performance are for this reason important. Two groups of participants (all together 50 people) took part in the study. Tests were performed in three languages (Slovene, Croatian, English). Tested typefaces (Verdana, Tahoma, Georgia), which were designed for screen use, took part in our testing. The aim of our study was to examine the influence of typefaces on the legibility among students.

**Keywords**: eye tracking, language, legibility, time, typeface and screen

## 1. Introduction and background

Screen reading is without a doubt one of the most common ways of communication in last few years. A wide range of information (documents, advertisements, emails, news etc) is brought to us with the help of the screens (mobile phones, computers, television etc). Therefore, the clearance and visibility of typefaces at different viewing conditions is an important aspect when information should impact people. The quality of screens differs; however, on average, its technology is advanced and there are fewer problems than there were in the past. Nevertheless, the trivia of the area has a strong impact on how the user will read and comprehend certain information (Arditi & Cho, 2007). The use of appropriate typefaces is in consequence undoubtedly important, while the design of typefaces differs for print and screen use (Bernard et al., 2003; Boyarski et al., 1998). It is common that we put little attention to the typefaces used for screen information presentation. Therefore, tests on the typeface performance when broadcasted on screen need to be performed (Bringhurst; 2004, Chaparro, 2010).

The presented typefaces (i.e. Verdana, Tahoma, Georgia) were designed specifically for screen use (Boyarski et al., 1998; Arditi & Cho, 2005). Nevertheless, there are some differences among these typefaces. First of all, the typeface Georgia differs from Verdana and Tahoma in serifs. Secondly, the thickness of strokes differs among all three typefaces. The typeface Georgia has a difference between thick and thin strokes. Thirdly, counter shape is different at all three typefaces. At the Verdana typeface, the counter shape is the biggest. One feature, which is approximately the same at all three typefaces, is the x-height. These factors are important when considering typeface legibility and screen use (Weisenmiller, 1999). We must emphasize that despite one of the three typefaces (i.e. Georgia) being a serif typeface with a difference in stroke width, it was prepared and designed to be used on the screen.

The differences among the typefaces are small. Upper case characters are lightened, the x-height is increased and the ascenders rise above the cap height. Tahoma is mainly ideal for the use in user interfaces and other situations requiring a presentation of information on the screen. Verdana was designed to be legible at small sizes on the (computer) screen (Chaparro, 2010). The lack of serifs, large x-height, wide proportions, loose letter spacing, large counter shape and emphasized distinction between similarly shaped characters are chosen to increase legibility.

Some studies (Josephson, 2003) of typeface legibility by means of reading efficiency resulted in no significant typeface effect. The typefaces Verdana and Georgia were perceived as more legible than Tahoma (Josephson, 2003).

Other studies (Tai et al., 2006; Cooke, 2005) show that (when Verdana, Georgia and Tahoma were compared) Verdana and Tahoma were better accepted than Georgia. The latter turned out similarly at the results of our research (for all the languages).

When measuring reading, fixation points have high importance. The fixations are important to control that the focus of viewers is evenly distributed on the area where the text is presented. More important while observing the reading is time (Dyson & Kipping, 1998, Zhou et al., 2011). The shapes of letters, sizes of the x-height and counter shape are the factors, which largely affect the time spent for reading and comprehension (Leckner, 2012).

The aim of our study was to examine the influence of typefaces on the legibility among students, which are part of different language areas, Croatian and Slovenian. Three different tests were performed according to language, Slovenian, Croatian and English.

## 2. Methods

Three typefaces designed specifically for screen use were shown on a screen in text, the length of which was as recommended (Legge & Bigelow, 2011) 11 lines and included 200 words. Each test person performed two tests, one in a native language (Croatian or Slovenian) and one in the foreign English language. Moreover, the time limitation was included in tests (Chapman, 2005, Gasser et al., 2005). Each text was presented on screen for three minutes and disappeared after that time.

Two groups of participants, each constituting of 25 people (students), took part in the study, which means that overall, 50 persons were involved in the experiment. The Croatian language is a native language of a half and the Slovenian language is a native language for the other half of the tested group. The average age of participants was 22.40 (22.52 Croatians and 22.28 Slovenians). Participants' task was to perform the testing twice, first in their native and then in a foreign language or vice versa. In this case, the sequence was randomly mixed; consequently, the typeface customization can be excluded from the results, this sequence leading to objective results.

The coverage area for each typeface was the same. The distance from the screen to the reader was the same for all testees (i.e. 65 cm) and the viewing angle remained unchanged (Wheildon, 2005). The extent of the visible area was hence almost the same and can be excluded as a variable, which can affect results. The content of text referred to everyday science, mainly covering nature and is considered as popular science material. After each reading of the presented text, the person had to answer (Erdogan, 2008, Peck, 2003) the question connected to the text content.

The time and fixation measuring presented a part of the observation. The eye-tracking device Tobii X120 was used to measure the reading time and to count the number of fixations for each reader. The texts were presented in black colour on a light grey screen (Ojanpää & Näsänen, 2003) with 1 920 × 1 200 px in size (LCD screen).

Comparisons that are a part of our study can be divided into four groups as follows:

a) English: English
b) Croatian: Slovenian
c) English: Croatian
d) English: Slovenian

The useful data of research is a comparison of the results for the English texts. Both nations are a part of the Slavic language group with few differences in their native language (Croatian and Slovenian). Hence, we wanted to perform a comparison between the Croatian and Slovenian language. A comparison between the English and Croatian or Slovenian language, respectively, is probably the least interesting while the language differentiation is enormous and it is difficult to draw conclusions, much more effort being needed to compare two different language groups.

Nevertheless, the focus of our research is based on typeface comparisons among the same language tests (English) and the same language group tests (Croatian, Slovenian).

## 3. Results and discussion

The comparison of English tests (Figure 1) shows that on average, the shortest reading and comprehension time was required for the typeface Verdana (77.12 s). The typeface Georgia turns out as the least successful typeface since the average reading time was the longest (84.30 s). The reason for this can probably be found in the fact

that the typeface Georgia has a difference in stroke width and consists of serifs, which are helpful when reading books but probably less helpful when reading text from the screen. A detailed overlook of results shows that on average, the Slovenian readers needed the less time to read the typeface Verdana (73.99 s), while for the Croatian readers, the shortest time is noticed at the typeface Tahoma (76.76 s). Both groups of participants needed the most time to read the typeface Georgia (Figure 1).

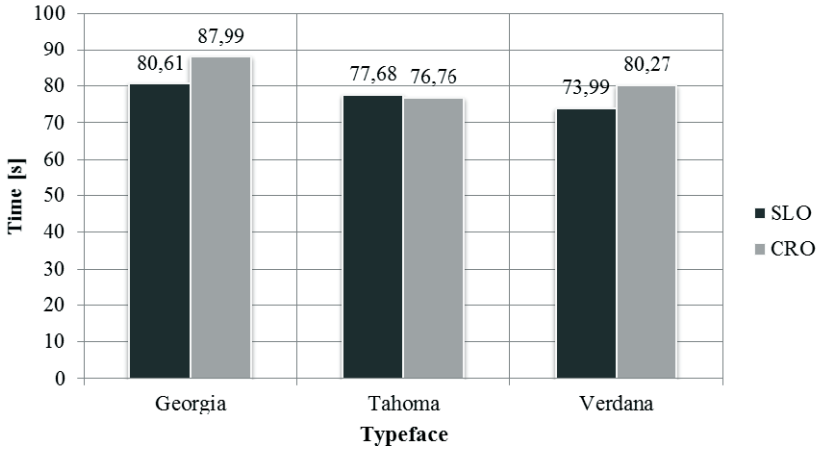


*Figure 1: Comparisons of average reading time for English language*

Observation of Slovenian and Croatian texts is also interesting, while both languages belong to the same language group. It is normal that reading times for the native languages are shorter for between 10 to 20 seconds. The shortest times are noticed at the typeface Verdana (Figure 2) for both nations. A little more time was needed to read texts that were presented in typeface Tahoma. Interesting observation in this aspect is that Slovenian readers needed less than one second more time to read and comprehend texts written in Tahoma while Croatian readers needed almost 4 more seconds to read texts in the same typeface. Typeface Georgia was again the worst accepted. Average reading time of typeface Georgia was the highest (63.96 s). There is noticed turnaround. Slovenian readers needed from 5 to 6 more seconds to read typeface Georgia while differences of reading time for Croatians were not so big. Parallels can be seen among English and native texts. In both comparisons Verdana was read the quickest, followed by Tahoma and Georgia (Figure 2).

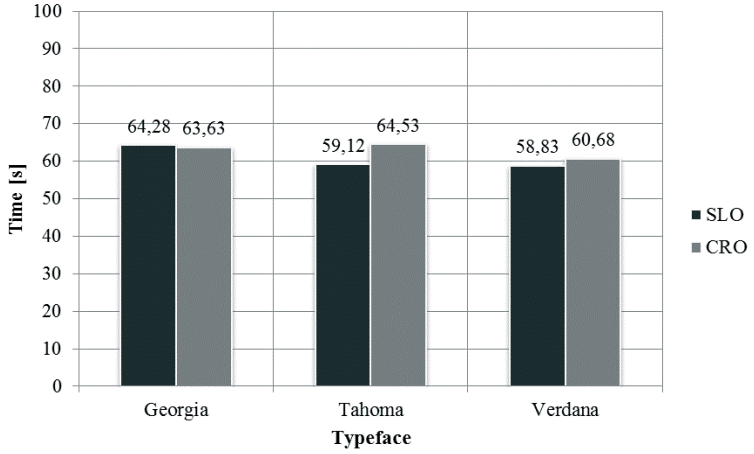


*Figure 2: Comparisons of average reading times for Slovenian and Croatian language*

A constant priority of the typeface Verdana compared to Georgia (Verdana > Tahoma > Georgia) is noticed according to time needed to read each typeface (Figure 1 and 2). Results of our research are comparable to some past studies (Erdogan, 2008, Peck, 2003).

The correctness of answers was very high (merely one or two mistakes in the whole pool of answers). Surprising fact is that there were more correct answers (for both groups of participants) when English tests were performed (Figure 3). In two cases (Georgia and Verdana) participants correctly answered all the questions. When typeface Tahoma was part of examination, the correctness did not reach correctness of hundred percent (Figure 3).

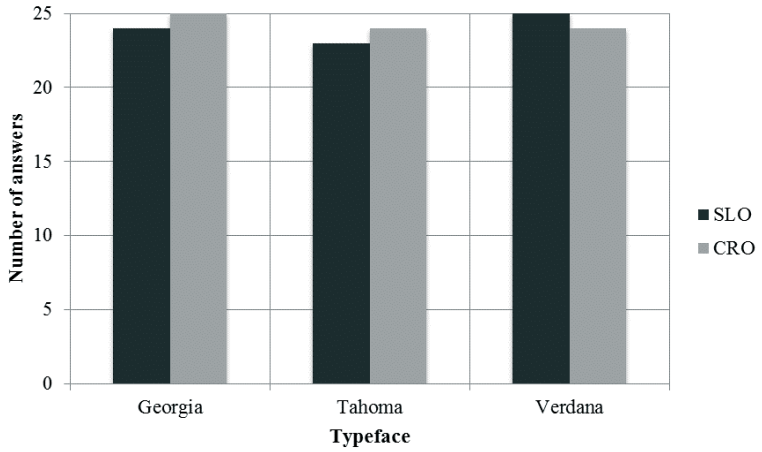


*Figure 3: Comparisons of answers correctness for English texts*

Correctness of answers for native languages did not reach as high percentage as expected. Not in one case there are all correct answers. Perhaps in this case is interesting to highlight only the fact that the correctness of the answers when typefaces Tahoma was observed is the same for both groups (Figure 4).

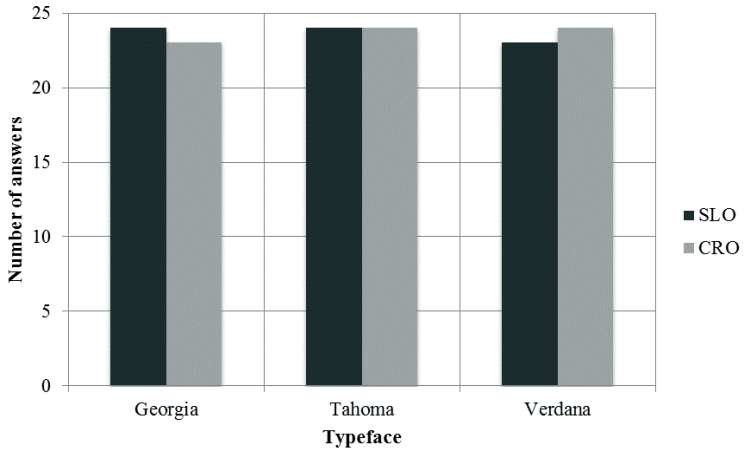


*Figure 4: Comparisons of answers correctness for Slovenian and Croatian texts*

Slovenian tests takers were the most successful at answering when typeface Verdana was presented and Croatians when typeface Georgia was used (Figure 3). Answers about content when text was presented in Verdana were hundred percent correct while there is one mistake when texts in typeface Verdana were presented to Croatian test takers.

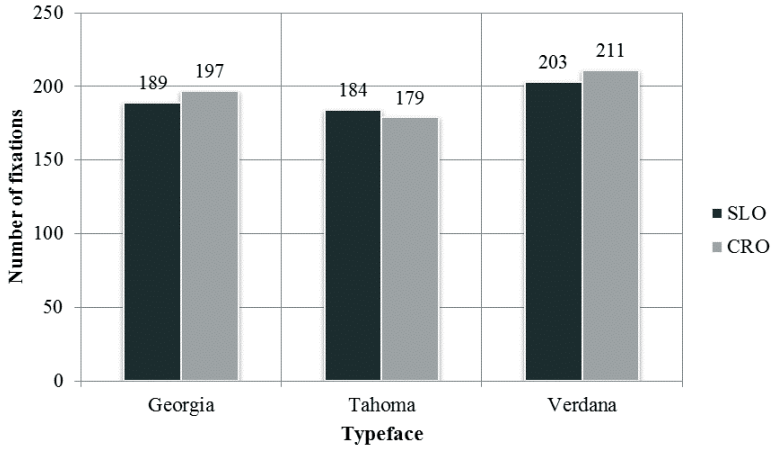


*Figure 5: Number of fixations for English texts*

The reverse situation is noticed when comparison for typeface Georgia was made (Figure 3). Nevertheless, typeface Tahoma shows better acceptability (based on correct answers) for Croatians compared to Slovenians (both for English language test). Differences in answer correctness are small but details that have been exposed previously have a strong impact on how fast the text is read and how high comprehension is.

Parallels among answer correctness and fixation numbers can be seen. Number of fixations is higher for typefaces Verdana and Georgia (Figure 5). From this information we can assume that number of fixation points affects correctness of answers. More fixation points means higher answer correctness. Number of fixations is the smallest at typeface Tahoma; consequently correctness of answers decreases (Figure 3). It is difficult to state with certainty that higher number of fixation points consequently impact on higher answer correctness. In our case this is true, but with reservation.

When number of fixations is observed for native languages, it is seen that Croatian readers needed more fixation points compared to Slovenian readers. Surprising observation is noticed with the typeface Georgia where number of fixations for both nations was the smallest (Figure 6).

The strongest difference is when typeface Tahoma was observed. Croatians needed 200 fixation points (which was the highest number of all fixations for native languages) while Slovenians needed the least fixation points (173). This is somehow interesting while if we take a look of fixation results for English language (Figure 5), typeface Tahoma did not turn out similarly. Slovenian readers needed more fixation points for typeface Tahoma compared to Croatians (English texts). Reverse situation is noticed when comparing native texts to English texts (Figures 5 and 6).

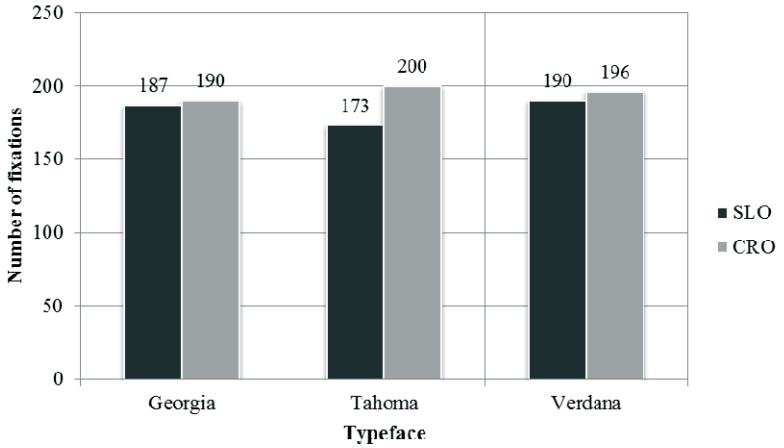


*Figure 6: Number of fixations for Slovenian and Croatian texts*

An overall comparison (English with Croatian and Slovenian) is as mentioned before questionable. The differences among the language groups are too big and for this reason, objectiveness of data can be questionable. Nevertheless, a rough comparison shows the same trend of typeface appropriateness (Verdana > Tahoma > Georgia).

## 4. Conclusions

The counter shape of the typeface Verdana is in comparison with the typeface Tahoma and Georgia bigger. This difference plays an important role when comparing the visibility and comprehension of presented texts. The width at Verdana letters is when compared to Tahoma letters greater, which results in better text visibility on the screen and consequently better comprehension (correctness of answers).

Nevertheless that Georgia is in one part of research better accepted by Croatian test takers, the differences are too small to be safely argued that typeface Georgia is among all tested typefaces less appropriate for screen use. Maybe more appropriate is to say that other tested typefaces in comparison with Georgia were better accepted. Problem of this typeface is probably that it contains serifs, which are not the most practical for on-screen reading.

It is of the essence to choose letters appropriately in order to give clear information, especially since we are on a daily basis exposed to an enormous amount of information brought to us by different media. A correct comprehension of the read text undoubtedly affects our opinion and in consequence, the objective understanding of daily served information. Beside this, testing at various screens (phone, tablet, notebook) should be performed

while screen size differentiations are significant. Rapidly growing technology development lead us to think about screen quality and consequently display quality.

**References**

Arditi, A., Cho, J. Letter case and text legibility in normal and low vision. Vision research, 2007, vol. 47, no. 19, pp. 2499-2505.

Arditi, A., Cho, J. Serifs and font legibility. Vision research, 2005, vol. 45, no. 23, pp. 2926-2933.

Benard, M. L., Chaparro, B. S., Mills, M. M., Halcomb, C. G. Comparing the effects of text size and format on the readability of computer-displayed Times New Roman and Arial text. International Journal of Human-Computer Studies, 2003, vol. 59, no. 6, pp. 823-835.

Boyarski, D., Neuwirth, C., Forlizzi, J., Regli, S. H. A study of fonts designed for screen display. In CHI '98: book of proceedings, Edited by Karat, C. M.,

Lund, A., Coutaz, J., Karat, J. New York: Addison-Wesley Publishing Co., 1998, pp. 87-94.

Bringhurst, R. The elements of typographic style, third ed, 2004. Vancouver: Hartley & Marks.

Chaparro, B. S. Comparing the legibility of six ClearType typefaces to Verdana and Times New Roman. Information Design Journal, 2010, vol. 18, no. 1, pp. 36-94.

Chapman, P. Remembering what we've seen: predicting recollective experiences from eye movements when viewing everyday scenes. In: G. Underwood (Ed.), Cognitive

Processes in Eye Guidance, 2005, pp. 237-258. UK: Oxford University Press. Cooke, L. Information Acceleration and Visual Trends in Print, Television, and Web News Sources. Technology communication quarterly, 2005, vol. 12, no. 2, pp. 155-182.

Dyson, M. C., Kipping, G. J. The effects of line length and method of movement on patterns of reading from screen. Visual language, 1998, vol. 32, no. 2, pp. 150-181.

Erdogan, Y. Legibility of websites which are designed for instructional purposes. World Applied Sciences Journal, 2008, vol. 3, no. 1, pp. 73-78.

Gasser, M., Boeke, J., Haffernan, M., Tan, R. The influence of the font type on information recall. North American Journal of Psychology, 2005, vol. 7, no. 2, p. 181-188.

Josephson, S. Keeping your readers' eyes on the screen: An eye-tracking study comparing sans serif and serif typefaces. Visual communication quarterly, 2003, vol. 15, no. 1, pp. 67-79.

Leckner, S. Presentation factors affecting reading behaviour in readers of newspaper media: an eye tracking perspective. Visual Communications, 2012, vol. 11, no. 2, pp. 163-184.

Legge, G. E., Bigelow, C. A. Does print size matter for reading? A review of findings from vision science and typography. Vision research, 2011, vol. 11, no. 5, pp. 1-22.

Ojanpä, H., Näsänen, R. Effects of luminance and colour contrast on the search of the information on display devices. Displays, 2003, vol. 24, no. 4-5, pp.167-178.

Peck, W. Great web typography. Indiana: Wiley Publishing, 2003.

Weissenmiller, E. M. A study of readability of on-screen text: PhD thesis, Virginia, Polytechnic Institute and State University, Blacksburg, 1999.

Wheildon, C. Type and layout, how typography and design can get your message across - or get in the way. Berkeley : Strathmore Press, 2005.

Tai, Y. C., Sheedy, J., Hayes, J. Effect of letter spacing on legibility, eye movement and reading speed. Journal of Vision, 2006, vol. 6, no. 6, pp. 994.

Zhou, F., QU, X., Helander, M. G., Jiao, J. R. Affect prediction from psychological measures via visual stimuli. International Journal of Human-Computer Studies, 2011, vol. 69, no. 12, pp. 801-819.

# End user views on the environmental sustainability of print media

*Anu Seisto*, *Maiju Aikala*, *Maija Federley*

VTT Technical Research Centre of Finland
P.O. Box 1000, FIN-02044 VTT
E-mails: anu.seisto@vtt.fi; maiju.aikala@vtt.fi; maija.federley@vtt.fi

**Abstract**

Media business environment has gone through changes, which will in the long term affect and guide changes in magazine business. One of the very topical issues relating to the changing media use habits is the environmental effects of both print and digital media. In this study, our interest was mainly in how a paper producer and a media house may work together towards a common goal of sustainable print products and how the consumers respond to the co-operation. The consumer views on the environmental sustainability were collected utilizing an on-line co-creation platform. The participants were invited to the on-line workspace to share ideas, discuss and give feedback about the concepts of ethical partnership and different ways to communicate about it that were presented as narratives. The participants found the ethical partnership between paper producer and media house a desirable concept. The prerequisites for credible ethical partnership include: true impact, noble motivation and extensive definition of company responsibility. The participants were most satisfied with the concept which required active participation of readers/consumers and increased their knowledge and understanding on a well-defined case concerning sustainability. The result indicates that in successful sustainable actions the readers would like to be identified as active partners instead of treating them as passive audience. In addition, they appreciate the increase of knowledge in the area of the action. Journalistic content is found as a trustworthy source of knowledge.

**Keywords**: sustainability, print media, magazine business, consumers

## 1. Introduction and background

Media business environment has gone through changes, which will in the long term affect and guide changes in magazine business. The fundamental topics are related to changing media use habits and the effects on print media, media selection habits, and changing customer expectations (Bilton, 2005; Miles, 2009; Crumby, 2010). In addition to the changes in media use habits, the challenges in magazines' distribution to readers either as subscriptions or as single copies have increased the interest to utilize digital channels also in magazine publishing. Especially tablets and the possibilities they bring along have been of interest lately. For example, tablet editions combine print's ability to engross readers with digital media's interactivity (Ives, 2011; Kaplan, 2011; Crumby, 2010). One of the very topical issues relating to the changing media use habits is the environmental effects of both print and digital media. Environmental impacts occurring during the life cycle of print products and presentation of the results in a manner that is understandable to non-expert stakeholders has been previously studied at VTT (Pihkola et al., 2010; Pihkola et al., 2014).

Forest industry is a pioneer of sustainability development in Finnish industry. A lot of effort has been put in improving existing products and developing new sustainable products and renewable solutions. However, recently, the decreased profitability of the forest industry and massive layouts have made corporate responsibility a much discussed topic in the media. Different stakeholders have started to question companies' ethics and responsibility toward society and local communities. As a solution, paper companies have started to build relationships and cooperation with non-governmental organizations (NGOs). The cooperation between Finnish paper companies and environmental non-governmental organizations has been reviewed from both social and business perspective in the thesis by Mervi Örs (Örs, 2013). In this study, our interest was mainly in how a paper producer and a media house may work together towards a common goal of sustainable print products and how the consumers respond to the co-operation. The study is part of a larger project "The Future Magazine", in which the future of magazines was looked at from the viewpoint of the so-called service-dominant logic. This means that the customer value (value in use) is the starting point of service development.

## 2. Methods

The consumer views on the environmental sustainability were collected utilizing VTT's on-line co-creation platform Owela, which enables early stage user participation in design (Friedrich 2013). The participants were invited to the on-line workspace to share ideas, discuss and give feedback about the concepts of ethical partnership and different ways to communicate about it. The concepts were presented as narratives. 'Ethicality'

included mainly actions targeting to environmental sustainability, but also actions concerning social responsibility. 'Partnership' was specified as co-operation between paper company and media house. The core messages of the narratives are presented below and their English translations as a whole are gathered in Appendix A:

i) Eco-label: Ecological values and especially biodiversity were underlined. The producer of magazine paper has committed to protection of certain species, which is informed with a particular eco-label and short information text.
ii) Common event: Newspaper publisher owns a woodlot in a forest owned by a paper company. The companies arrange informative reader excursions to the woodlot together.
iii) Symbolic eco-act: Small acts targeted to improve our own environment: a paper company donated plants for a magazine, which planted the trees with the readers in order to diminish CO2-load.
iv) Information channel: Acts of company's social responsibility included in a journal article: Main theme in the magazine issue is travelling in Brazil. A portrait presents a teacher, who started his studies in a Brazilian school founded by a paper company.
v) Common campaign: Tour for collecting electronic waste: information about the environmental load of electronic devices available in publisher's magazines, also lot of information about the tour.

The participants were recruited from the community of Finnish users that have earlier participated development projects utilizing the Owela platform. 37 persons had registered to the project, 19 of them took actively part to the discussion. The demographic information of the active participants is presented in Table 1.

*Table 1: Background information of the 19 active participants*

| | Number of participants |
|---|---|
| **Gender** | |
| Female | 10 |
| Male | 9 |
| **Age** | |
| < 30 | 1 |
| 30-40 | 2 |
| 40-50 | 5 |
| 50-60 | 4 |
| > 60 | 7 |
| **Residential area** | |
| Helsinki area | 5 |
| Other parts of Finland | 14 |

## 3. Results

The narratives can be divided into three partly overlapping groups based on their core concepts, which are i) active participation of readers, ii) information delivery and iii) communicating sustainable acts of partner company, as shown in Table 2.

*Table 2: Grouping of the narratives based on their core messages*

| | Active participation of readers | Delivering information | Sustainable acts of partner |
|---|---|---|---|
| Eco-label | | ■ | ■ |
| Common event | ■ | | |
| Symbolic eco-act | ■ | | |
| Information channel | | ■ | ■ |
| Common campaign | ■ | ■ | |

The participants gave the most positive feedback on the narrative describing common campaign for collecting electronic waste. The narrative combined the elements of active participation of consumers and delivering information. The participants found the campaign as "believable and feasible. Story combines the ability to inform, to promote recycling and, thus, to truly influence." They also appreciated the element of locality and noted that magazines are important channels for changing attitudes towards recycling.

*"Magazine articles encourage people to participate and bring their electronic waste to recycling."*

The narratives common event and symbolic eco-act concentrated on activating the consumers to participate. The participants found the described concepts rather positive, but also some questions were raised. In the comments, the power of journalistic content in informing and shaping attitudes was identified:

*"Magazines could write articles about other possible acts, for example collecting the cones and giving possibility to sell the excess seeds to other countries."*

The participants were concerned of the benefits for the environment and motivation behind the partnership:

*"Excursion is a nice idea, but why should the newspaper publisher participate? Newspaper publisher seems only to sponsor the paper company."*

*"Great idea, but doesn't seem to work. Where would the trees be planted, who would take care of them and ensure the growth? The results would be visible after a very long time."*

The narratives eco-label and information channel combined elements of delivering information and communicating sustainable acts of partner company. The participants were the most skeptical with these narratives. Although they identified some positive elements of responsibility behind the narratives, the credibility of both the partnership and its description was questioned.

For example, the Eco-label was commented as follows:

*"I support the idea, I would rather buy a magazine printed on this kind of paper." "Not credible, the active partner is not the company but its supplier. Does the company ensure that paper producer really protects woodpeckers?"*

Also comments about the actions described in Information channel were twofold:

*"Acts of a paper company in developing the local school system can be supported."*

*"Companies (especially global paper companies) are not trustworthy actors in this area."*

## 4. Discussion

The participants were most satisfied with the concept which required active participation of readers/consumers and increased their knowledge and understanding on a well-defined case concerning sustainability. The result indicates that in successful sustainable actions the readers would like to be identified as active partners instead of treating them as passive audience. This attitude of "user in control" and interest in active participation is well in line with other studies of user behaviour related to media use (e.g. Ollikainen et al., 2012) and with the great success of social media services enabling people to actively express themselves. In addition, they appreciate the increase of knowledge in the area of the action. Journalistic content is found as a trustworthy source of knowledge.

One of the major challenges in building an ethical partnership is the bad reputation of paper companies in social and environmental responsibility. Especially their actions in developing countries arouse suspicion. Even though the narratives presented in the study were imaginary and not based on any existing co-operation between paper company and media house, this kind of approach would be recommended to improve the image of sustainability of print media. As this study is based on one discussion conducted in Finland, it would be very interesting to carry out similar studies in other countries to compare the results and receive a wider perspective on the topic.

In general terms, the attitudes of consumers towards media products and services, whether physical and printed on paper or digital, may have important effects on their purchasing behavior and hence should be well understood. Based on the study by Gilg et al. (2005) on sustainable consumption, consumers are likely to purchase in a more sustainable way if they perceive that what they are buying is actually going to impact on the environment and influence future policy. Similarly, personalization of environmental issues and trust in the information provided on the environment is also more likely to engage citizens. Gilg et al. (2005) continue that one of the challenges for policy makers wishing to engage in this move is to incorporate activities that do not necessarily have green credentials, but rather a greater focus on who does what. Our study is very well in line with this in encouraging the print media value chain to pay more attention to activities that increase consumer awareness on sustainability issues related to print products in a way that is trustworthy.

## 5. Conclusions

The participants found the ethical partnership between paper producer and media house a desirable concept, although they were somewhat sceptic about the included elements described in the study. The prerequisites for credible ethical partnership include:

- True impact: The actions for sustainability and social responsibility should have a real impact; no green washing is accepted.
- Noble motivation: Both partners should have a clear role in their own strong areas for advancing sustainability; sponsorship is not enough.
- Extensive definition of company responsibility: Credibility is required in all areas of company responsibility.

**Acknowledgements**

The original idea for this study came from "The Future Magazine" project and the work was carried out as part of the Fortune project. Financial support from Tekes is gratefully acknowledged.

**References**

Bilton, J. (2005) Why did they do that? Understanding consumer purchasing. InCirculation Magazine Jul/Aug 2005. URL: http://www.inpublishing.co.uk/kb/articles/why_did_they_do_that_understanding_consumer_purchasing.aspx

Crumby, R. (2010) How customer behaviours are driving change. InPublishing Magazine May/Jun 2010. URL: http://www.inpublishing.co.uk/kb/articles/how_customer_behaviours_are_driving_cchang.aspx

Friedrich, P. (2013) Web-based co-design. Social media tools to enhance user-centre design and innovation processes. Doctoral dissertation. VTT Science 34

Gilg, A., Barr, S. and Ford, N. (2005) Green consumption or sustainable lifestyles? Identifying the sustainable consumer. Futures 37(2005)6, pp. 481-504

Ives, N. (2011) iPad editions combine print's ability to engross readers with digital media's interactivity. URL: http://adage.com/article/media/magazines-ipad-editions-struggle-attention/149307/

Kaplan, D. (2011) Hearst's Carey: Tablets will provide 25 percent of magazines' circulation. URL: http://paidcontent.org/2011/03/10/419-media-summit-hearsts-carey-tablets-will-provide-25-percent-of-circ/

Miles, M. (2009) What is the future of print? InPublishing Magazine Sep/Oct 2009. URL: http://www.inpublishing.co.uk/kb/articles/what_is_the_future_of_print.aspx

Ollikainen, V., Aalto, E., Kivelä, J., Kuula, T., Liinasuo, M., Lindqvist, U., Lugmayr, A., Maho, H., Norros, L., Seisto, A. and Zheng, H. (2012) New electronic media (NELME) 2016 foresight. VTT Technology 31. 75p

Pihkola, H., Federley, M., Nors, M., Dahlbo, H., Koskela, S. and Jouttijärvi, T. (2010) Communicating environmental impacts of print products. Results from the LEADER project (Part 2). VTT Research Notes 2561. URL: http://www.vtt.fi/inf/pdf/tiedotteet/2010/T2561.pdf

Pihkola, H., Nors, M., Federley, M., Behm, K. (2014) Ympäristötietoisuus ja muuttuva median käyttö. Näkökulmia kuluttajien median käytön ympäristövaikutusten arviointiin ja viestintään. VTT Technology 159. URL: http://www.vtt.fi/inf/pdf/technology/2014/T159.pdfÖrs, M. (2013) Cooperation as a form of corporate responsibility engagement. Case: Finnish Forest Industry and Environmental NGOs. Bachelor's Thesis, JAMK University of Applied Sciences

URL: http://www.theseus.fi/bitstream/handle/10024/69499/Oers.Mervi.pdf?sequence=1

## Appendix A. Narratives on ethical partnership

*Eco-label*

Company wants to communicate to its readers that they take the environmental issues into account in all of their actions. The company is especially active in maintaining the nature's biodiversity. Customer magazine of the company is delivered to almost all households in Finland. The paper used in the customer magazine is produced by a paper company, who plans and conducts its forestry work considering protecting white-backed woodpecker. White-backed wood-peckers are becoming rather rare in Finland, but the above-mentioned paper company has been able to protect the species and even increase its population due to its forestry decisions. The customer magazine supports this protection work of the paper company and informs about it by using a white-backed woodpecker logo with a short information text.

*Common event*

Newspaper publisher owns a woodlot in a forest owned by paper company. The companies arrange informative reader excursions to the woodlot together. The newspaper has arranged, for example, a family excursion on the woodlot, where forestry professionals have delivered information about forests and forestry. The participants were able to walk around the woodlot and study the forest, and at the end of the visit the organizers offered a small picnic by a camp fire. Newspaper has also arranged a "Well-being from the nature" - events, where the participants are provided with information about the functional properties of plants and their use in well-being and beauty care. The participants have also the possibility to collect their own package of well-being with them.

*Symbolic eco-act*

Magazine wants to show that also small acts targeted to improve our own environment can make a difference. Magazine organizes happenings with their readers a couple of times per year. The aims of the happenings are making small good deeds. For example, the magazine wants to take responsibility and be an active player in protecting the environment. Editorial staff and the magazine readers planted trees in order to diminish $CO_2$-load. The plants were donated by a paper company.

*Information channel*

The theme of the magazine issue is travelling in Brazil. Major part of articles gives different kinds of hints for independent travelers, from adventures in rain forest to night life in big cities. Lot of space, both text and pictures, has been given for presenting the attractions that are worth visiting. There are also articles about Brazilian nature and people. In a portrait is presented a teacher, who started his studies in a Brazilian school founded by a Finnish paper company, and who is nowadays actively involved in developing the Brazilian school system.

*Common campaign*

Magazine publisher and a waste collection company organizes a campaign for collecting electronic waste (mobile phones, tablets, laptops) around Finland. All magazine titles of the publisher contain articles about the tour in their issues published during the campaign. Magazines give information about the environmental load of electronic devices, recycling and renewable energy, with which the environmental load from consuming digital media can be decreased.

# The development of media use habits - from childhood to adults

*Timo Kuula, Olli Kuusisto, Anu Seisto*

VTT Technical Research Centre of Finland
P.O. Box 1000, FIN-02044 VTT
E-mail: olli.kuusisto@vtt.fi

**Abstract**

In 2004 a study was carried out with young university students in the greater Helsinki metropolitan area of their media use habits. Eight years later, a new study was conducted with the same group. The methods for data collection were media diaries and semi-structured theme interviews. Based on the results, media use habits adopted at young age evolve and become stronger quite logically when growing up. Readiness to pay for content at young age seems to increase the willingness to pay for services in later phases of life as well. Work is time-consuming, thus time for leisure media use has decreased. Relationship and hobbies are affecting the media use as well. Mobile and easy-to-use services, such as Spotify, fit well in the life of the target group. Individuals want to maintain their habits and express their personality in the changing media environment. Refusing to use Facebook or favouring print media may be counter reactions, which are part of people's media use strategies. Understanding the motives for media usage is vital for generating interesting content that the consumers are ready to pay for.

**Keywords**: media consumption, media use, user groups, media environment

## 1. Introduction

Digitalization is making media to undergo the biggest change in its history. New media services, devices and possible ways to use different kind of media are born and consumers also expect them. Technological development has made it possible for consumers to change their media consumption habits and to prefer new services and new platforms over traditional ones. Business models and audience research are experiencing a transfer from provider-centricity to customer-centricity as firms enter into service business and adopt new value creation perspectives (Viljakainen, 2013). The customer-centric approach means that motivations behind the media usage need to be studied and understood in order to be able to offer the customers content that they wish to consume and utilize, and to do it in a profitable way.

Even though media use habits are changing, some general attitudes and values towards media use evolve in a much slower pace. These attitudes and values are learned in childhood but they can change and evolve when people grow up, move from home to live on their own, start building a career and have a family. People in these life changing situations are described as highly involved and they search for information actively and selectively. Highly involved information seeking persons could be very important to media companies and advertisers (Leopold & Diehl, 2011).

In 2004, a study was carried out with young university students (aged 20-24) in the greater Helsinki metropolitan area of their media use habits (Kuula et al., 2005). Eight years later (2012), a new study was conducted with the same group. The group had graduated and started working. Studying how media use and lifestyles of the original target group had been evolved during the years provided new insights of how media usage is changing among young adults. The focus of this paper is on the results of the follow-up study conducted in 2012.

## 2. Summary of the 2004 study

As a result of the 2004 study, the students were divided into three user groups based on their use of print media (Kuula et al., 2005):

- "The Users" subscribed newspapers and read them regularly. Their appreciation towards print media was high, and print was valued in their childhood homes as well.
- "The Likers" did value newspapers but were not subscribers. They valued print media but didn't use it as much as they wanted. In their childhood homes print media was often highly valued.
- "The Refusers" were not subscribers of newspapers and didn't value print at all. Some of them mentioned the lack of encouraging print tradition in their childhood home, for some print was just an uninteresting and outdated media.

The most important media environment of the target group was also studied (Kuula et al., 2005). Mobile phone and email were mostly used and described as most important media in the whole target group. In the groups "The Users" and "The Likers", both printed newspapers and books were included in the most important media environment.

Generally, the media use of the students was seen as quite homogeneous: It was versatile and communication played an important role in it. However, the attitudes and actions towards print media (especially newspapers) were distinctive factors in the data. As a conclusion it was suggested, that "The Users" will most probably continue valuing and using print media in their future phases of life. On the other hand, most of "The Refusers" will probably not start using print media. "The Likers" were seen as the most interesting group - what will they choose to do? (Kuula et al., 2005.)

## 3. Methods

In both phases (2004 and 2012) of the study, the methods for data collection were media diaries and semi-structured theme interviews. In 2004, every student filled in the media diary during a period of four days including two weekdays and a weekend. A specified diary-structure and a list of media were given to the interviewees. In the follow-up study, the media diary was less formal: the interviewees were asked to write down their media use during the period of approximately one week. The form of the diary was free and no complete list of media was given to the target group. In both phases the media diary was a supplementary method to the interviews. The main purpose of the diary was to activate the interviewees to think and observe their media use before the interview. The media environment in both phases of the study included all media from traditional media of mass communication (books, newspapers, radio, television etc.) to novel electronic and communication media (mobile phones, chat, email etc.).

The semi-structured theme interviews included the following themes in both phases:

- Current media use (description in own words)
- Description of media environment
- Daily routines
- Media contents
- Media use contexts: studying, working, leisure time, social relationships etc.
- Childhood media experiences; family, significant others, and do they play a role today

The method followed the tradition of ethnographic interviewing, since questions about everyday life and daily routines were included. Furthermore, the biographical approach added the aspect of life history (childhood media experiences), which fits well in the ethnographic tradition (Plummer, 2001). Additional theme related to media use changes 2004-2012 was included in the follow-up study. The goal of the follow-up study was to understand the developing media use habits of well-educated people who have become adults in 2000s. The study aimed at providing answers to following questions:

- What are the most important changes in the target group's media environment?
- How have the media use habits of the target group evolved since 2004?
- How does the target group see the role of their childhood media use habits in their media use today?

### 3.1 Target group

The original target group in 2004 included 13 students (aged 20-24; 5 male and 8 female), all studying in the universities of greater Helsinki metropolitan area. Nine out of thirteen (9/13) persons were studied in the follow-up study (aged 28-31; 5 male and 4 female), the rest of the original group members were not reached. All of the interviewees worked and lived in greater Helsinki metropolitan area in 2012, two of the interviewees had children.

## 4. Results

The world had changed during the eight year period that was in between the original study and the follow-up study. From the variety of changes in media environment the most important ones among the target group included Facebook, Spotify, mobile internet and watching of non-linear television.

### 4.1 Important changes in the media environment

Facebook is crucially important media for the group and it has partly replaced private emails and chatting (messenger). Many claimed that they are passive users, meaning that they don't write status updates but read them. However, the use might be active in limited groups related to events and hobbies. There was also criticism towards Facebook: it is time-consuming and too shallow for profound communication. Some thought it as the most irritating media as well. In 2004, mobile phone was seen as the most irritating media as well as crucial media, thus from this viewpoint Facebook has replaced the phone.

Spotify is very popular for listening and buying music and it was used in all three groups. The service fits in well in the everyday life of the target group. An easy-to-use service also motivates the listening of music, as described by an interviewee: "Spotify made it possible to bring music into my everyday life." For mobile internet, smart phone is especially important for groups "Users" and "Likers". It is used for many purposes, including leisure, information and work. News and email are often read via phone, for example while commuting, and it sometimes replaces printed newspapers. It is notable, that tablets were not widely used among the target group.

Watching of non-linear television content has decreased the use of linear television. In the group "Refusers", watching recordings, use of free internet TV-services (public and commercial broadcasters) and downloading content is popular. Groups "Users" and "Likers" additionally use pay-tv channels, IPTV-services and game consoles for buying content. Time for consuming TV content has decreased due to work and children in all groups. It has become more irregular as well.

### 4.2 Changes in media use habits

Generally, free time has decreased within the whole target group since they started in working life and some of them started families. Thus, there is less time for leisure media use. The importance of communication has diminished and pragmatic approach to media use is more emphasized among the target group. Table 1 summarizes how the three user groups and their print media use evolved from the original study in 2004 to the follow-up study eight years later. For the "Refusers" the change was small, they had not become users of print media, but a clear trend was observed towards preferring free contents and services in comparison with the other groups. Only one group member was paying for Spotify. However, one person expressed interest towards printed magazines due to her situation in life as a mother of a small child. The group didn't appear as a forerunner of digital services, as they did in 2004.

The "Likers" were not just likers anymore, but their fondness towards printed newspapers had realized into actual subscriptions. However, one group member had ended the subscription just before the interview, because she wasn't happy with the quality of content anymore. The "Likers" were also willing to pay for other services, such as Spotify, pay-tv channels and magazines.

Interestingly, the "Users" were not subscribers of printed newspapers anymore, because the paper was seen as impractical and not fitting in the daily rhythm. One group member subscribed digital newspaper. Generally, they favoured things that fit well in the daily routines, emphasizing the use of smart phone. However, they still valued print and described printed newspapers sometimes as more pleasant than digital versions. They were willing to pay for content and services, such as Spotify and magazines.

*Table 1: Summary of how the three user groups evolved from the original study to follow-up study*

| | Original study 2004 | Follow-up study 2012 |
|---|---|---|
| "The Refusers" | Did not subscribe newspapers, and didn't like print in general. (4 persons) | Still not subscribers of newspapers. They don't want to pay for content or services. (3 persons) |
| "The Likers" | Did not subscribe newspapers, but did value them. (6 persons) | Subscribe printed newspapers, and are willing to pay for other content and services. The group has logically evolved and become subscribers of printed newspapers. (4 persons) |
| "The Users" | Subscribers of newspapers. (3 persons) | Not anymore subscribers of printed newspapers, but still value print. They are willing to pay for other content and services, one person subscribes digital newspaper. (2 persons) |

The important contexts that affect the media use are work, relationship (family) and hobbies. Work decreases leisure media use, such as watching television and communication with friends. It activates the use of work-related services and contents, such as LinkedIn and professional blogs. Work also motivates the use of digital

media and mobile internet, since workplace usually provides devices (phones, laptops etc.) and requires that they must be used. Relationship and family affects the use of television content ("should we take pay-tv channels?"), newspapers and magazines. It also activates "traditional" phone calls and use of services like Skype. Finally, personal hobbies seem to activate the use of Facebook groups, magazines and hobby-related online services.

The target group members seemed to have different ways of maintaining habits and expressing personality in the changing media environment. According to interviewees, the changing media includes many "irritating" elements. Thus, counter reactions to new services and trends are a part of people's media use strategies. For example, refusing to use Facebook, favouring face-to-face service instead of online shopping, or favouring print media instead of digital can be interpreted as counter reactions to major trends. Also photography was seen as a counter reaction to "hectic" media, as described by an interviewee.

4.3 Childhood media experiences

The interviewees generally felt that childhood media experiences still have an effect on their media use as adults. Childhood media experiences mainly have an effect on

- the use of print media; especially newspapers and books,
- the attitude and habits related to television and movies,
- the readiness and motivation of using new technology,
- the attitude towards media content.

## 5. Conclusion

Media use habits adopted at young age evolve and become stronger quite logically when growing up. Positive attitude towards printed media and an overall readiness to pay for content at a young age seems to increase the willingness to pay for content and services in later phases of life as well.

Work is time-consuming in the life of the target group, thus time for leisure media use has decreased and media use has become more pragmatic. Work together with relationship (family) and hobbies are important contexts and life changing situations in target group's life including high involvement and active information searching. Mobile and easy-to-use services, such as Spotify, fit in well in the life of the target group.

Counter reactions to new services and trends are a part of people's media use strategies. Although major trends in media use are important to follow, the ones who choose not to follow the trends may be interesting from the viewpoint of content and service providers as well. These people might know well what they want, and what they want to pay for.

From the media business viewpoint, understanding the motives for media usage is vital for generating interesting content that the consumers are ready to pay for. Examining the significant phases, contexts and situations of life in the long-term is important, since people affected by life changing situations are actively searching for useful information on products and services which help them (Leopold & Diehl, 2011). The multiplication of media content providers and media channels also leads to smaller and more focused user groups that don't fit into traditional classification criteria. It is possible to engage users during the whole day and week if the content is relevant and context-sensitive, and the users find the content useful and valuable for them, such as Spotify. Further user research is needed in order to develop business models which will enable media industry to cope with in changing media environment.

**References**

Kuula, T., Seisto, A. & Nieminen, S. (2005). Media Use of Young University Students in Helsinki Area. In proceedings of 32nd International IARIGAI Research Conference, Porvoo, Finland, 4-7 September, 2005. pp. 373-378

Leopold, A. & Diehl, S. (2011). The Relevance of Life Changing Situations for Media Usage and their Relevance as a Segmentation Strategy for Media Companies and Advertisers. In Okazaki, S. (Ed.). Advances in Advertising Research (Vol. 2). Breaking New Ground in Theory and Practice. Gabler. pp. 161-175

Plummer, K. (2001). The Call of Life Stories in Ethnographic Research. In Atkinson, P., Coffey, A., Delamont, S., Lofland, J. & Lofland, L. (Eds.). Handbook of Ethnography. Sage. pp. 395-404

Viljakainen, A. (2013). From product to service categories and the transformation of audience research. International Media Management Academic Association IMMAA Conference, Lisbon, Portugal, 3-4 May, 2013

# AudioCanvas: interactive audio photos

*Simon Robinson, Jennifer Pearson, Matt Jones*

Swansea University
Swansea, United Kingdom
E-mails: s.n.w.robinson@swansea.ac.uk; j.pearson@swansea.ac.uk; matt.jones@swansea.ac.uk

**Abstract**

We present a novel interaction technique that helps to make printed information more accessible to those with low or no textual literacy skills. AudioCanvas allows cameraphone users to interact directly with their own photos of media items to receive audio feedback or narration on demand.

**Keywords**: QR codes; camera phones; audio

## 1. Introduction

AudioCanvas is a fusion of Interactive Voice Response (IVR) services and physical objects, as illustrated in Fig. 1. Our design allows users to take a photograph of printed media and use the picture as a canvas for interaction with related audio. The system automatically dials a remote telephone-based voice service, and allows users to touch areas of interest on their own photo titles, captions, adverts or images, for example to hear audio narration for their selection. Our novel design uses precisely-placed QR codes as reference points, allowing it to transmit the user's touch coordinates via DTMF tones over a standard phone line, and ensuring that the service can be used without the need for an internet connection

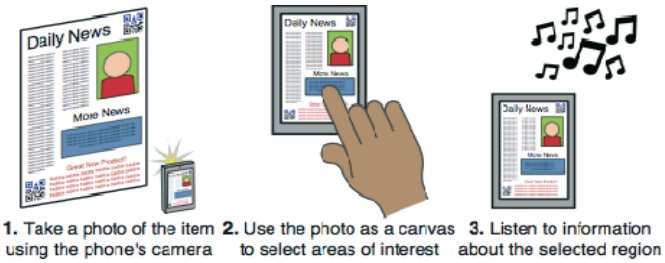


*Figure 1: Interacting with the AudioCanvas system. From left to right: (1) the user takes a photo of an item, which then (2) becomes a canvas to interact with audio content related to the object. (3) audio content is provided over the telephone system; no data connection is required*

## 2. Background

Previous work has augmented physical artefacts with digital media. DigitalDesk (Wellner, 1993), for example, used precisely positioned projectors and cameras to retain paper's affordances but allow documents to be manipulated digitally. Other designs, such as Audio d-touch (Costanza et al., 2010) used custom markers to create user-friendly tangible interfaces. Unlike AudioCanvas, these examples focus on direct interactions with objects; e.g., manipulating physical items to control digital interactions. Our approach differs, letting people use their own photos of items to act as canvases to interact with audio. Other augmentation designs, such as Listen Reader (Back et al., 2001), OCR methods, or commercial options, have required either a client-side metadata database or realtime internet access for their functionality. A major advantage of our design, then, is that the client is completely independent of the media used. This independence means that updates or internet access are not required to support future media items.

### 2.1 Interactive photos

Our design turns photographs into interactive touch canvases for communicating with telephone-based services. Frohlich's related technique (Frohlich, 2004) allowed interaction with paper photos to request audio. The design supported only one track per image, however, and also required a separate projector. Suzuki et al. (Suzuki et al., 2005) demonstrated the use of photos of physical objects as interaction tools, but required a marker on each

object (cf. Parikh et al., 2006). More similar to our design is Seifert et al.'s technique (Seifert et al., 2011), which turns hand-drawn sketches into interactive prototypes. However, our approach focuses on audio interaction, rather than a conversion of photos into digital facsimiles.

Many mobile augmented reality applications are able to add overlays or web links to physical artefacts. Daqri, 2 for example, uses QR codes for tracking; others, such as Blippar 3 or Shortcut, 4 have used image recognition. However, these approaches require a data connection and a large download for every scan. Furthermore, they focus entirely on augmenting a photo or camera preview with visual content. Our system uses QR codes to encode a coordinate grid and phone number on a photographed object, instead. The aim is to add audio to the experience, rather than just providing a different way to enter a website address.

## 3. AudioCanvas

AudioCanvas affords rich experiences with physical objects, allowing any marked-up item to become a touch panel to interact with remote audio resources (see Fig. 1).

Our approach uses two precisely placed QR codes on printed media to support detection of the position of the user's selections on their photo of an item. To interact with the system, the user first positions their phone to take a photo of an item. When both codes are detected, a photo is taken automatically, and the phone dials a voice service in the background. Selecting any region on the photo (with fingers on touchscreens or the joypad on a feature phone) passes the coordinates to the voice service, which plays back the appropriate audio immediately.


*Figure 2: Example AudioCanvas media. Clockwise, from top left: curry packet; newspaper; box of tea; movie poster*

Figure 2 shows several example media items that we have tested for use with AudioCanvas. The system was designed specifically for use where internet access is sparse or unaffordable, and where low textual literacy levels prevent people from reading printed media. AudioCanvas is not meant to be a competitor to automatic translation systems, however. This is partially because such services can require extensive online interaction. More importantly, though, the aim here is to provide a technique through which the content provider or community members can produce appropriate interpretations or comments to supplement the media item in both textual and visual elements. For example, touching on form fields might explain in useful terms the reason this information is required and what it might be used for, in the same way a proximate might guide in person.

### 3.1 Implementation

AudioCanvas has two components: a standard remote voice service (not covered in this paper) and a local client. The client is a mobile phone application that is used to take a photo of an object, allow panning, zooming and selection, and help the user interact with the remote service. The voice service is a standard IVR system, where DTMF (i.e., phone keypad) tones over a standard phone line control the interaction.

Our novel client design uses two separate QR codes on printed media to detect the position of the interactive area within a photo taken by the user. The codes are positioned at opposite corners of the item - one at the bottom left and another at the top right. The bottom left code contains the telephone number of the interactive voice service, and an identifier for the item (e.g., the issue and page number of a newspaper). The top right code is used for coordinate calibration and image alignment (we automatically straighten and skew correct the image).

Figure 3 shows the layout of marked-up objects, and illustrates how touch coordinates are interpreted. Based on the sizes and positions of the two QR codes, the exact position of a touch on the photo can be converted to a location on the physical object without the client application requiring any knowledge about the object itself. This design allows almost any object to be used for interaction, with the system able to calculate exact coordinates within the media automatically. When a user touches the picture they have taken, the coordinate of the current touch point is sent as DTMF tones to the remote telephone service indicated by the lower left QR code. The voice service then plays the relevant audio in response.


*Figure 3: The AudioCanvas coordinate system. Touch point coordinates on the user's photo of an object are calculated based on the distance between and relative sizes of the two QR codes detected on the item. The resolution of the coordinate grid is high enough to allow zooming in to the image and very precise selections, if necessary. Touching a point causes a six-digit DTMF-encoded request for the relevant audio to be sent to the voice site. The audio is played over the phone line in response. The grid is not visible during usage*

## 4. Discussion and conslusions

In this paper we have presented AudioCanvas - a novel photo interaction method that pairs audio with printed media. The design allows interaction directly with self-taken photos of physical items by touching regions on-screen. A remote voice service provides audio content, accessed via a standard phone line to ensure it can be used without a potentially costly network data connection. We believe, as illustrated by our experiments detailed elsewhere (e.g., Robinson et al., 2014), that the technique could be particularly beneficial to those in impoverished areas where low-literacy is common, and where data connections are not yet available or attractive.

**Acknowledgements**

This work was funded by EPSRC grant EP/J000604/2.

**References**

M. Back, J. Cohen, R. Gold, S. Harrison and S. Minneman (2001). 'Listen reader: an electronically augmented paper-based book'. In: Proc. CHI '01, ACM, pp. 23-29

E. Costanza, M. Giaccone, O. Kueng, S. Shelley and J. Huang (2010). 'Ubicomp to the masses: a large-scale study of two tangible interfaces'. In: Proc. UbiComp '10, pp. 173-182

Frohlich, D. (2004). Audiophotography. Springer

T. Parikh, P. Javid, S. K, K. Ghosh and K. Toyama (2006). 'Mobile phones and paper documents: evaluating a new approach for capturing microfinance data in rural India'. In: Proc. CHI '06, ACM, pp. 551-560

S. Robinson, J. Pearson and M. Jones (2014). 'AudioCanvas: Internet-free Interactive Audio Photos'. In: Proc. CHI '14. CHI '14, ACM, pp. 3735-3738

J. Seifert, B. Pfleging, M. Hermes, E. Rukzio and A. Schmidt (2011). 'Mobidev: a tool for creating apps on mobile phones'. In: Proc. MobileHCI '11, ACM, pp. 109-112

G. Suzuki, S. Aoki, T. Iwamoto, D. Maruyama, T. Koda, N. Kohtake, K. Takashio and H. Tokuda (2005). 'u-Photo: Interacting with Pervasive Services Using Digital Still Images'. In: LNCS. Vol. 3468. Springer, pp. 190-207

P. Wellner (1993). 'Interacting with paper on the DigitalDesk'. In: Communications of the ACM 36.7, pp. 87-96

# B1

## *Printing science and technology*

# Formulation of sustainable soy inks

*Alexandra Pekarovicova, Zahra Mashhadi Khodabakhsh, Paul D. Fleming III*

Western Michigan University
Center for Ink and Printability
4601 Campus Drive, A-213 Parkview
Kalamazoo, MI 49008-5462, USA

Email: a.pekarovicova@wmich.edu

**Abstract**

The ink industry is systematically going away from ink formulations that release of volatile organic components from evaporating solvents. Water based ink formulations are definitely more environmentally friendly. Most of the resins found in water based inks are based on acrylic chemistry, synthetized on the base of petroleum, which is not a sustainable raw material. Thus, there is an urgent need to come up with renewable, green polymers for ink manufacture. In this work, soy protein was used to formulate water based digital inks. Preliminary soy ink formulations were made, and based on these results a design of experiments (DOE) was carried out to optimize ink formulations. The DOE was executed comparing soy and acrylic based chemistry. The Z number, a dimensionless combination measure of density, surface tension and viscosity, was employed to predict ink jettability. Several successful inkjet inks based on soy polymer chemistry were formulated.

**Keywords:** soy polymer, acrylic, ink jet, ink formulation, jetting, Z number

# Setting behaviour of inkjet inks studied by high-speed-camera measurements and modelling

*Daniel Weinzierl, Gert Keller, Dirk Fiedler*

Papiertechnische Stiftung
Pirnaer Str. 37
D-01809 Heidenau, Germany
E-mails: daniel.weinzierl@ptspaper.de; gert.keller@ptspaper.de; dirk.fiedler@ptspaper.de

**Abstract**

In this article the dynamics of droplet absorption and penetration into papers are discussed. The experimental penetration data used in this study are derived from a measurement device consisting of a high-speed-camera, suitable microscope objectives and a piezoelectric droplet generator. This device allows studying the penetration of small, single ink droplets with realistic volumes in the range of few picoliters. The working principle of this unit is presented and it is shown that the resulting data can be used to investigate influences of different paper and ink properties on ink penetration. Both dye and pigment based aqueous inkjet inks as well as other fluids are included in this study.

Furthermore, a model based on the Bosanquet differential equation is proposed to calculate ink penetration using structural parameters and properties of the materials used. The model also takes into account real and practical conditions, only limited fluid volumes relevant to the respective printing process are considered. Additionally, several coating layers and transitions between them can be analyzed. Model results are discussed and a comparison of the model and experimental observations is given. The model based on the Bosanquet equation is in good agreement with the measured penetration times which underlines the applicability of both the model and the measurement technique.

**Keywords:** inkjet printing, fluid penetration, modelling

# Study of the effect of the ink layer on selected properties of multilayer packaging films

*Joanna Izdebska, Zuzanna Żołek-Tryznowska, Magdalena Makowska*

Warsaw University of Technology
Faculty of Production Engineering
Institute of Mechanics and Printing, Department of Printing Technology
Konwiktorska 2, PL-00-217 Warsaw, Poland
E-mail: j.izdebska@wip.pw.edu.pl

**Abstract**

Application of multilayer films in packaging allow the reduction of the average weight of packaging and selection of its optimal barrier properties. The review of literatures leads to the conclusion the significance of subjects and its importance for the development of packaging. The aim of the research was to determine the effect of ink and the influence of the ink layer thickness on the mechanical properties of laminates. Studies were performed for the double layer film (PET/glue/OPP) prepared by adhesive method with using a two-component, solvent-free adhesive. Bond strength of laminates and the thickness of each layer were measured. It was found that the thickness of the adhesive layer and the fixed ink has a significant influence on the mechanical properties of laminates. The ink composition, the type of the pigment determines the binding strength of the laminates. Regardless of the thickness of the ink layer the values of bond strength of printed laminate are significantly reduced.

**Keywords:** laminates, double-layer films, multilayer printing, tensile strength

# Dynamics of ink absorption of packaging paper

*Li Yang* [1] *Jianghao Liu* [2], *Xin Li* [2]

[1] Innventia AB
P.O. Box 5604
S-11 486 Stockholm, Sweden

[2] Beijing Institute of Graphic Communication
Beijing, China

E-mails: li.yang@innventia.com; arisliu@bigc.edu.cn; lixinxioanei@126.com

**Abstract**

Liquid absorption dynamics of the packaging papers has been studied with Emtec PDA device, using water-based flexographic ink and water as testing liquids. While the liquid is penetrating into the paper structure, the measured ultrasonic transmittance values change with the absorption time and form two time regimes. The transmittance increases with time in the first regime and decreases in the second. Being internally sized of all of the papers, paper making parameters, e.g. refining and calendaring have strong impacts on the absorption behaviour of the papers, for instance the maximal transmittance and transition time from regime 1 to regime 2; while different fibre blends exhibit only marginal effects. Comparative studies with cloth made of synthesised fibres suggested that it is modifications of wood fibres by the liquids that are responsible for the two-regime structure. Responding to liquid absorption, wood fibres expand in length and width, regain their lumens and change in surface energy etc. These are probably the origins that cause the decreasing transmittance in the second time regime.

**Keywords:** liquid absorption, ink-paper interaction, inkjet, package printing

# Lubrication theory of ink hydrodynamics in the flexographic printing nip

*Hans Martin Sauer, Dominik Daume, Edgar Dörsam*

Institute of Printing Science and Technology (IDD)
Technische Universität Darmstadt
Magdalenenstraße 2
D-64289 Darmstadt, Germany

E-mails: sauer@idd.tu-darmstadt.de; daume@idd.tu-darmstadt.de, doersam@idd.tu-darmstadt.de

**Abstract**

On the base of hydrodynamical lubrication theory we develop a mathematical model for the ink transfer in a flexographic printing process. Using the specific parameter ranges the model may also be applicable to the offset process. Specifically we show how our model can be applied to viscous ink flows in the printing nip in presence of elastic printing plates, and how this sets limits to the possible resolution of the printing image. We also discuss the structure of the contact zone between printing plate and substrate and derive estimates for the dynamic pressure profile in the ink during the transfer process. Finally we discuss the phenomenon of ghost image formation in the printing process and show how the viscous fingering instability can be modeled for curved and elastic plates.

**Keywords:** flexography, lubrication theory, ink viscosity, ink splitting, viscous fingering

# Improvement of water-based varnishing on abrasion resistance in flexographic printing

*Marta Gajadhur, Agnieszka Chrzanowska*

Warsaw University of Technology
Faculty of Production Engineering
Institute of Mechanics and Printing
Department of Printing Technology
2 Konwiktorska Street, PL-00-217 Warsaw, Poland

E-mails: m.gajadhur@wip.pw.edu.pl; a.m.chrzanowskaa@gmail.com

**Abstract**

The objective of the research is to analyse the abrasion resistance in flexographic printing with water-based inks. The article is concerned with the analysis of the impact of different water-based varnishes on the abrasion resistance in flexographic printing with water-based inks. Only water based inks and varnishes were used in the research.

Print rub-off tests were performed for one water-based ink and three different water-based varnishes used in flexographic printing. Tests were performed in the Ink Rub Tester. The rub-off resistance was evaluated by spectrophotometric and visual observations. The ΔEab* parameter was used in evaluation.

**Keywords:** flexographic printing, abrasion resistance, water-based inks, water-based varnishes, spectrophotometric measurements, ΔEab* colour difference

# Improvement of the reproduction accuracy of spot colours in security printing by modifying the ink formula

*Csaba Horváth*[1], *Erzsébet Novotny*[2], *Pál Görgényi-Tóth*[2]

[1] Óbuda University
Institute of Media Technology and Light Industry Engineering
Doberdó u. 6. H-1034 Budapest, Hungary

[2] ANY Security Printing Company
Halom u. 5. H-1102 Budapest, Hungary

E-mails: horvath.csaba@rkk.uni-obuda.hu; novotny@any.hu; gorgenyi@any.hu

**Abstract**

There may occur serious difficulties with the mixing of spot colours for security production, and then the accurate reproduction of the same colours in any subsequent round of repeated production. There are several underlying reasons: on the one hand, the print medium does not contain any optical brightener unlike the ones that are taken into consideration in the formulas that are specified for the Pantone colour chart designed for general use in the printing industry, whole on the other hand problems may be caused by those colours applied in security printing that are hard to copy or scan. Towards the optimization of the costs of manufacturing, it is necessary to be aware of these deviations, and use correction factors in the course of the pre-mixing of colours. In our studies, we examined to what an extent we were to deviate from the formula determined for any specific colour when the spot colours for securities were mixed. We chose colours that could be blended from two basic colours, and consequently we could observe the direction of changes without ambiguities. After a number of iterative steps, it was determined to what extent formulas were to be changed for the examined colours when the individual types of security papers were used, and it was also established that even from the same manufacturer subsequent supplies of inks can considerably differ from each other in terms of the process colours, and therefore this colour difference needs to be taken into account when modifying the formula.

**Keywords:** printing of securities, printing inks, spot colours, ink mixing, Pantone Formula Guide, colour difference

# Security offset printing with twin colors by means of CMYF separation

*Branka Morić Kolarić* [1], *Ivana Žiljak Stanimirović* [2], *Ivana Bak* [3]

[1] Narodne novine d.d.
Printing Operations
Savski gaj XIII put 13, HR-10020 Zagreb, Croatia

[2] Faculty of Graphic Arts
University of Zagreb
Getaldićeva 2, HR-10000 Zagreb, Croatia

E-mails: bmoric@nn.hr; ivana.ziljak@grf.hr; ibak@nn.hr

**Abstract**

A new method of security printing is introduced in this work, thus creating highly protected documents by ink management in three spectrally separated ranges. A numerical experimental color setting has been developed, respecting the ink properties in three wave ranges: 200-400 nm, 400-700 nm and 700-1000 nm. Separation is carried out with process and spot inks, aiming at concealing the graphic in visible spectrum. Such a graphic can be recognized instrumentally in the ultraviolet (F) and infrared (Z) spectra. Extending the Infraredesign method, the ultraviolet spectrum is included through the properties of the dark brown UV ink, thus giving fluorescent green in UV spectrum, while the absorption value is 38% for parameter Z in the NIR spectrum. A separate, third image is visible by the naked eye. By algorithmic mixing of F-ink, having absorption properties in UV and IR ranges, a unique solution for the security printing of documents and valuables is accomplished. CMYF method differs from the CMYKIR method, since the K ink does not have the same properties, while their Z factor is completely different under the same printing conditions. With this new method - CMYF separation - formulations and standards are set for determining the differences between the original and the forgery.

**Keywords:** CMYF separation, offset security printing, UV, V and NIR range, barrier scanning

# The effect of substrate correction on printing conformity

*Robert Chung* [1] *and Li Wu* [2]

[1] RIT - School of Media Sciences
69 Lomb Memorial Drive
Rochester, NY 14623, USA

[2] Shenzhen Polytechnic
Shenzhen, China

E-mails: rycppr@rit.edu; wuli@szpt.edu.cn

**Abstract**

Printing has become more and more of a manufacturing process. As a manufacturing process, the goal is to meet specifications. When printing on nonconforming papers, printing conformity is jeopardized. The use of the substrate-corrected colorimetric aims (SCCA), as specified in ISO 13655, represents a solution. But benefits of SCCA are not fully understood and the solution not widely adopted in the printing industry. A research question arises, "What is the effect of substrate correction on dataset conformity for a large number of offset, digital printing, and proofing jobs?" To answer the question, this research uses a database of 60 jobs to study the effect of substrate correction on printing conformity where the white points of the dataset and the color of the printing paper vary. The results show that substrate-corrected color aims (SCCA) enables more job conformance and reduces failed jobs for both conforming and non-conforming papers.

**Keywords:** printing standards, substrate correction, printing conformity

# Modeling optically induced halftone mottle from variability of lateral light scattering of unprinted paper surface

*Abhijit Bhattacharya* [1], *Swati Bandhyopadhyay* [2], *Phil Green* [3]

[1] ITC LIMITED
Paperboards & Specialty Papers Division
Unit: Bhadrachalam, Sarapaka,
Khammam District, A.P -507128, INDIA

[2] Printing Engineering Department,
Jadavpur University
Salt Lake Campus, Block-LB
Plot-8, Sector-III, Salt Lake, Kolkata - IN-700098, West Bengal, INDIA

[3] The Norwegian Colour and Visual Computing Laboratory
Gjøvik University College
Teknologivn. 22, 2815, N-2802 Gjøvik, Norway

E-mails: abhijit.bhattacharya@itc.in; abhijit.bhattacharya.80@gmail.com;
swatib1@yahoo.com; philip.green@hig.no

**Abstract**

Mottle in halftone prints reduces the perceived quality of printed images. One of the sources of mottle in halftone print is the variation in apparent area of printed dots. Inhomogeneous lateral light scattering within the paper surface in between the printed dots leads to optical dot gain variation which is perceived as halftone mottle. Absence of a reliable model that can predict the paper surface's susceptibility to halftone mottle before printing poses serious challenges in controlling factors in papermaking that contributes to lateral light scattering variability and hence optically induced halftone mottle. In this work the variability in paper surface's lateral light scattering is modeled from the variability in spatial distances between colorimetric coordinates obtained from high resolution microscopic image of a knife edge shadow projection on the unprinted paper surface. We present a new model based upon multivariate paired T2 statistic for characterizing the variability in knife edge shadow response of the paper surface in order to estimate its lateral light scattering variability. The proposed model has been found to effectively predict the visual perception of halftone mottle that arises from inhomogeneous optical interactions between the printed dots and the paper surface.

**Keywords:** halftone mottle, optical dot gain, light scattering, multivariate paired $T^2$

# Characterization of a printed 2D code developing Visual Basic tools for task automation

*Nadège Reverdy-Bruas, Lionel Chagas, Jean-Pascal Poletti, Raphaël Passas*

Univ. Grenoble Alpes, LGP2, F-38000 Grenoble, France

CNRS, LGP2, F-38000 Grenoble, France

E-mails: nadege.reverdy@pagora.grenoble-inp.fr; lionel.chagas@pagora.grenoble-inp.fr; jean-pascal.poletti@hotmail.fr; raphael.passas@pagora.grenoble-inp.fr

**Abstract**

The general context of this study is to establish recommendations for the development of digital models in the framework of counterfeiting. To achieve this goal, printed 2D codes were investigated. Visual Basic tools have been developed in order to automate tasks. Therefore, the present paper allows characterizing the printing process used (conventional and waterless offset); sensitive results were also obtained regarding the kind of printed substrate (coated and uncoated paper). Histograms of area classes were plotted and they revealed that the printing process induced the raise of a new class of small dots not present on the digital file. In addition, two types of counterfeiting methods were carried out and they pointed out that the histograms of the counterfeit codes were different from the original printed code, whatever the attempt of counterfeiting. Furthermore, in these cases, small dots tend to agglomerate and form new area classes of bigger size. The method developed in this study thus allows the identification of the printing process as well as the distinction of true and counterfeit 2D codes.

**Keywords:** 2D codes, security, automation, image analysis, counterfeiting

# B2

## *Printed functionality and special printing*

# New printing structure for lighting single-pixel electroluminescent elements based on non-transparent microelectrodes

*Ardeshir Hakimi-Tehrani*[1], *Jann Neumann*[1], *Martin Schmitt-Lewen*[2], *Thorsten Euler*[1], *Edgar Dörsam*[1]

[1] Institute of Printing Science and Technology (IDD)
Technische Universität Darmstadt
Magdalenenstraße. 2, D-64289 Darmstadt, Germany

[2] Heidelberger Druckmaschinen AG, R&D Department
Kurfürsten-Anlage 52-60, D-69115 Heidelberg , Germany

E-mails: hakimi@idd.tu-darmstadt.de; neumann@idd.tu-darmstadt.de; martin.schmitt-lewen@heidelberg.com; euler@idd.tu-darmstadt.de; doersam@idd.tu-darmstadt.de

**Abstract**

The conventional structure of printed electroluminescent (EL) panels mostly contains a transparent conductive material on the light emitting top side. Regarding the relatively high costs for these materials and their deposition, a research was done on the feasibility of a new structure for printed ELs by segmentation of large EL areas to some smaller separated ones. By screen-printing of microelectrodes in different patterns and line widths and gap sizes of 30 µm, 50 µm and 100 µm with conductive inks, and deposition of phosphor on the upper layer, the light is appearing between the lines.

**Keywords:** electroluminescence (EL), functional printing, printed microelectrodes, screen-printing, side-by-side area segmentation

# Performance optimization of fully printed primary ($ZnMnO_2$) and secondary (NiMH) batteries

*Michael Wendler*[1,2,3], *Tim Claypole*[1], *Erich Steiner*[2], *Martin Krebs*[3]

[1] Welsh Centre for Printing and Coating, Swansea University
Singleton Park, Swansea SA2 8PP, United Kingdom

[2] Media University Stuttgart
Nobelstraße 10, D-70569 Stuttgart, Germany

[3] VARTA Microbattery GmbH
Daimlerstraße 1, D-73479 Ellwangen, Germany

E-mails: 675333@swansea.ac.uk; t.c.claypole@swansea.ac.uk;
steiner@hdm-stuttgart.de; martin.krebs@varta-microbattery.com

**Abstract**

Printed batteries, based on nickel/metal hydride and traditional zinc/manganese dioxide chemistry, were manufactured as single cells in stacked configuration by screen-printing. To identify the performance-limiting element of the printed rechargeable battery, a printed Ni/MH battery equipped with a Zn-probe was assembled. The printed batteries were electrochemically analysed by means of electrochemical impedance spectroscopy in two-electrode configuration and chronopotentiometry. It has been demonstrated that the cathode is responsible for the limitation of the battery performance. The influences of the limitation of the cathode inks were examined and newly water-based electrode inks were developed. The improvement of the electrode inks decreased the overall impedance and raised the value for the open circuit voltage as well as the operating voltage for the primary battery chemistry. In addition to the electrode optimizations, a printable electrolyte/separator-paste, equal to a conventional electrolyte saturated polymer-fleece in its performance, was developed and enables a fully printed battery system.

**Keywords:** printed battery, electrochemical impedance spectroscopy, probe-cell, printable electrolyte

# Cold foil transfer technology for functional printing

*Duy Linh Nguyen*[1], *Alexandra Lyashenko*[1], *Meliksah Ucuncu*[1], *Martin Schmitt-Lewen*[2], *Alexander Weber*[2], *Andreas Henn*[2], *Simon Loeprich*[1], *Edgar Dörsam*[1]

[1] Institute of Printing Science and Technology (IDD)
Technische Universität Darmstadt
Magdalenenstraße 2, D-64289 Darmstadt, Germany

[2] Heidelberger Druckmaschinen AG, R&D Department
Kurfürstenanlage 52-60, D-69115 Heidelberg, Germany

E-mails: nguyen@idd.tu-darmstadt, lyashenko@idd.tu-darmstadt.de;
meliksah.uecue@stud.tu-darmstadt.de; martin.schmitt-lewen@heidelberg.com;
alexander.weber@heidelberg.com; loeprich@idd.tu-darmstadt.de; doersam@idd.tu-darmstadt.de

**Abstract**

Since some years, several research institutes, institutions and companies are working on the realization of electronic components by innovative methods, which can lead to cost-effective, simplified and flexible production of such products. Among other low-cost technologies such as coating and vapor deposition printing as an additive structuring process is one focus of research.

Another interesting additive printing-related method is cold foil transfer technology or also so-called cold foil stamping. The cold foil transfer technology is conventionally used in the finishing step for various, mostly decorative, printing products. For a real metal effect to be obtained in graphic arts printing so-called cold foils are used, which in most cases have an aluminum layer [Kur11]. The metal is applied by vapor deposition with high demands on the polyester foil, so that the metal particles are close together and thus set up a thin homogeneous conductive aluminum layer in the nanometer range.

The fact that the cold foils have a metal layer has led to the idea of using this printing method for electronic applications using its conductivity. The following criteria are important for using cold foil transfer processes for printed electronics: electrical conductivity, reproducibility and reliability of such metal layers, especially depending on different printing process settings. The objective of this research was to investigate the cold foil transfer technology and its process boundaries for the use in the electronics field.

**Keywords:** cold foil transfer, hot stamping, sheet-to-sheet process, mass production, electric conductivity, functional printing, printed electronics.

# On the development of substrate coatings for microfluidics devices: target-enhanced resolution

*Eveliina Jutila*[1], *Risto Koivunen*[1], *Patrick A. C. Gane*[1,2]

[1] School of Chemical Technology
Department of Forest Products Technology
Aalto University, PL 16400
FI-00076 Aalto, Finland

[2] Omya International AG
Baslerstrasse 42
CH-4665 Oftringen, Switzerland

E-mails: eveliina.jutila@aalto.fi; risto.koivunen@aalto.fi; patrick.gane@omya.com

**Abstract**

This study focuses on the development of highly wicking coated substrates for microfluidic devices with enhanced resolution compared to current filter paper-based devices. Four highly absorbing pigments, fumed silica (FM), modified calcium carbonate (MCC), natural diatomite (ND) and flux-calcined diatomite (FCD), as well as three binders, styrene-acrylate (SA) latex, polyvinyl alcohol (PVOH) and carboxymethyl cellulose (CMC), were used to form coating structures with different wicking properties. Studies include characterisation of the pigment particles and thin layer wicking (TLW) experiments, in which wicking height of liquid in coatings is measured as a function of time. The results show that the choice of coating pigment and binder as well as the binder amount has a significant effect on wicking characteristics of a coating. The introduction of diatomite pigments into blends with MCC improved the wicking capabilities of the coating, especially in the case of ND. Latex was found to inhibit wicking of liquid the least, followed by PVOH and CMC. Increased binder amounts reduce wicking due to reduced pore connectivity and binder-filled pores. It was found that the wicking resistance of pigment alone is too high for rapid analysis over long distances in thick coatings. On the other hand, these coating structures could be utilised as high resolution analysis points incorporated into a wicking channel matrix created, say, on a filter paper or placed at junctions of microfluidic channels derived from controlled hydrophobic/oleophobic printing or designed shrinkage fracture geometries.

**Keywords:** microfluidic devices, analytical printed test kits, absorbent coatings, liquid wicking, microdiagnostics, hydrophilic channels, printed functionality

# Inkjet-printed hydrophobic microfluidic channeling on porous substrates

*Risto Koivunen*[1], *Eveliina Jutila*[1], *Patrick A. C. Gane*[1,2]

[1] School of Chemical Technology
Department of Forest Products Technology
Aalto University, PL 16400
FI-00076 Aalto, Finland

[2] Omya International AG
Baslerstrasse 42
CH-4665 Oftringen, Switzerland

E-mails: risto.koivunen@aalto.fi; eveliina.jutila@aalto.fi; patrick.gane@omya.com

**Abstract**

Paperfluidic devices are microfluidic devices patterned out of highly porous paper or paper-like material. Liquid transport in paperfluidic devices is propelled either by surface wetting or interior capillary wicking. The direction of aqueous liquid flow on such devices is controlled by selective patterning of hydrophobic barriers on an otherwise hydrophilic base substrate. A variety of hydrophobic materials and functional printing methods have been lately demonstrated as feasible for producing such patterns. Unlike conventional graphic printing, hydrophobising ink has to penetrate the whole depth of the substrate layer utilised for wicking, in order to produce properly functioning leak-free barriers.

One major expected application area for paperfluidics is in the field of lab-on-a-chip devices, intended to provide simple, transportable, disposable and self-sufficient analytical tools for medical diagnostics and environmental monitoring. On such devices, polar, usually aqueous, fluid samples flow along hydrophilic channels through assay zones, where they chemically interact with pre-applied reagents.

This study focuses on the development of simple solvent-based hydrophobic inks for inkjet printing of microfluidic patterning on paper substrates. Hydrophobic inks were produced by dissolving alkyl ketene dimer (AKD) and low molecular weight polystyrene in p-xylene. Hydrophobic test patterns featuring lines, barriers and channels were inkjet-printed with these inks on two highly porous filter papers. Studied aspects include ink properties and jettability; physical dimensions and functionality of the printed patterns; and relationships between printed patterns and inks, substrates and print settings.

AKD ink was found to produce effective hydrophobic barriers but with poorly defined borders. Polystyrene ink produced well defined borders, but could only penetrate the full depth of the substrate on one paper. Reliable channels $680 \pm 80$ µm wide and barriers $883 \pm 91$ µm wide could be produced with it. Adding polystyrene as a rheological modifier to AKD ink improved jettability, but did not significantly affect end product properties.

Hydrophobic ink penetration into filter paper was found to take place as film flow rather than through complete filling of pores. Paper properties and ink viscosity were considered to play a role in providing ink with a quick access to the reverse side. Differences in border definition might be due to the well-known coffee stain effect and different interaction with the cellulose fibre surfaces.

**Keywords:** functional printing, hydrophobic ink, polystyrene, alkyl ketene dimer, paperfluidics

# B 3

## *Media and the consumer*

# Narrative engagement and reading performance on digital and printed platform

*Olli Nurmi, Janne Laine, Timo Kuula*

VTT Technical Research Centre of Finland
P.O. Box 1000, FIN-02044 VTT
Espoo, Finland
E-mails: olli.nurmi@vtt.fi; janne.laine@vtt.fi; timo.kuula@vtt.fi

**Abstract**

Narrative transportation theory proposes that when people lose themselves in a story, their attitudes and intentions change to reflect that story. Travel can be used as a metaphor for reading to conceptualize narrative transportation as a state of detachment from the world of origin that the story receiver experiences because of his or her engrossment in the story. The state of narrative transportation makes the world of origin partially inaccessible to the story receiver, thus marking a clear separation in terms of here/there and now/before, or narrative world/world of origin.

Narrative engagement is part of narrative transportation and it consists of four dimensions: narrative understanding, attentional focus, emotional engagement and narrative presence.

This study compares the narrative engagement that reading novel-type texts evokes using either a printed book or ebook as reading platform. A reading test in controlled laboratory conditions was conducted and the results show that there were no statistically significant differences of narrative engagement. This result was verified in more natural reading environments with qualitative study.

**Keywords:** eBooks and printed books, narrative engagement, reading speed, comprehension

# Investigating the effects of publishing approaches using print, electronic and augmented reality media on user experience

*Elena Fedorovskaya, Lufei Yu*

Rochester Institute of Technology, Rochester, NY 14623, USA
E-mails: eafppr@rit.edu; lxy4140@rit.edu

**Abstract**

To evaluate the potential role of modern augmented reality (AR) technology in publishing and its usefulness for interactive print, we conducted a study where we investigated the influence of different methods of presenting content on the users' story reading experience. The stories were produced in print and electronic media, with and without augmented reality component, using a multi-media setup consisting of a computer with the monitor display, a smartphone, and a printed material. A 2x2 within-subjects experimental design was implemented (2 levels of medium: print and electronic; and 2 levels of augmentation with video clips: yes or no), wherein 32 participants aged 18-29 years old were asked to read short stories produced with different publishing methods and evaluate their preferences for the presentation and the content, as well as interestingness, comprehension and overall experience with the stories on a 7 point scale using a questionnaire. AR and the medium-AR interaction were found to be significant in determining the preference for the publishing method. The paper-AR combination had the highest score among all the methods and was rated statistically different from the paper only version, which, in turn, had the lowest score. Only the medium-AR interaction was significant for the overall experience judgments, with the trend, similar to the publishing preference data. Overall experience was linked to the users' ratings for the publishing methods, interestingness and enjoyment of the stories, and the ease of understanding the story line. The results indicate that AR enhances user experience, particularly with the print media, making it on par or even higher valued than commonly used electronic media. In contrast, the traditional print version without augmentation was least preferred.

**Keywords:** publishing, augmented reality, print, digital media, storytelling, preferences, user experience

# Visual perception and recollection of pictures in packaging design

*Ulrich Nikolaus and Sandra Bendlin*

Leipzig University of Applied Sciences (HTWK Leipzig)
Faculty of Media
Gustav-Freytag-Straße 42,
D-04277 Leipzig, Germany
E-mail: ulrich.nikolaus@htwk-leipzig.de

**Abstract**

Continuing an ongoing study to analyze consumer reactions to packaging design, test results that explore the visual perception and recollection of pictures in packaging design are presented. Particularly, the extent and reliability of human recollection of pictorial elements on packages that were seen only for a short period of time is discussed in detail. These results help to better understand the visual impact pictures in packaging design have on consumers. The results suggest that consumers discern a great deal of graphical detail in pictures within a very short period of time, but that this recollection varies among users and is sometimes inaccurate. Furthermore, it could be shown that viewers in general describe coherent (albeit sometimes inaccurate) interpretations of visual stimuli instead of isolated details of visual design.

**Keywords:** packaging design; eye tracking; qualitative content analysis; visual perception; pictures

# Novel services for the publishing sector through co-creation with users

*Aino Mensonen, Katri Grenman, Anu Seisto, Kaisa Vehmas*

VTT Technical Research Centre of Finland
P.O. Box 1000, FIN-02044 VTT
Espoo, Finland
E-mails: aino.mensonen@vtt.fi; katri.grenman@vtt.fi; anu.seisto@vtt.fi; kaisa.vehmas@vtt.fi

**Abstract**

The traditional goods dominant logic is very much provider-centric. In case of publishers, the journalists produce content for a product such as newspaper. The product is delivered to consumers, who experience a newspaper service by reading the product. The service dominant logic shifts the focus from provider-centric to customer-centric. Hence companies need to focus in gathering and sustaining audiences, and developing their services not just for their readers but together with them. In this study we present three case studies, in which the publishers want to understand their readers expectations and needs towards new news services and develop the services together with the readers. Two of the case studies, show how to involve the users from the very beginning of the development all the way to the prototyping. Owela co-development platform was utilized in all cases.

The study shows the importance of co-creation with users when developing new services. The loyalty and commitment to publishers brand increases, when the readers feel that their opinions are valued. The process increases the publishers understanding of readers expectations and needs and thus emphasize the users voice in the novel service under the development. Although the cases focus on publishers' digital news services, the same approach may be utilized in the development of physical products as well.

**Keywords:** co-creation, digital services, newspaper publisher

# Index of authors

## Section **A**



## Section **B**